Active Galactic Nuclei

Jörn Wilms

Dr. Karl Remeis-Sternwarte, Bamberg

email: joern.wilms@sternwarte.uni-erlangen.de

Tel.: (0951) 95222-13

Long Version:

http://pulsar.sternwarte.uni-erlangen.de/wilms/teach/agn

ERLANGEN CENTRE
FOR ASTROPARTICLE
PHYSICS

Friedrich–Alexander–Universität
Erlangen–Nürnberg

What are AGN?

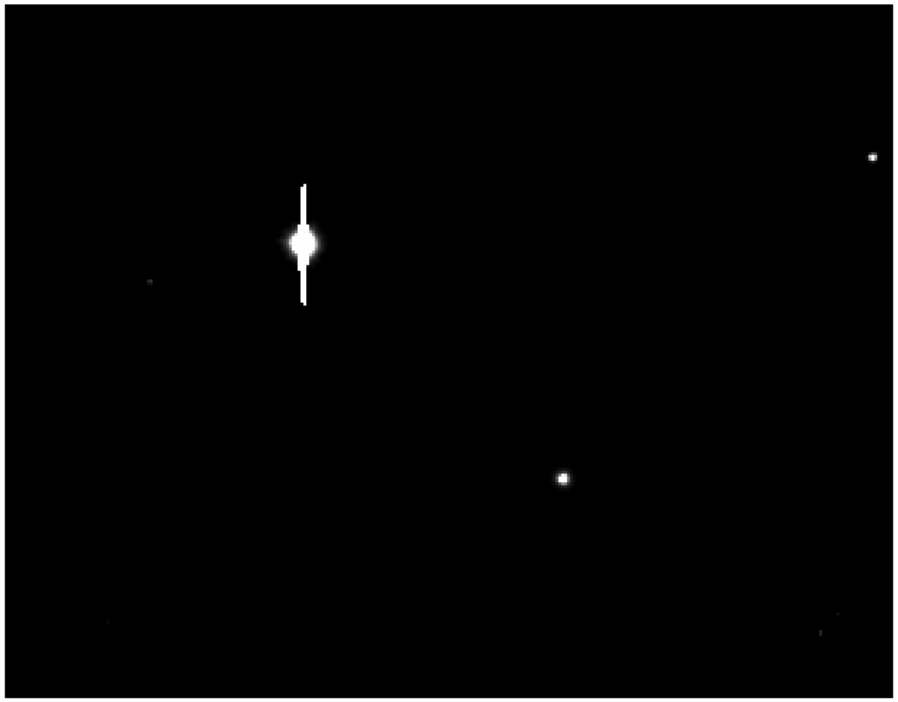

NGC 3783: *linear* intensity scale

What are AGN?

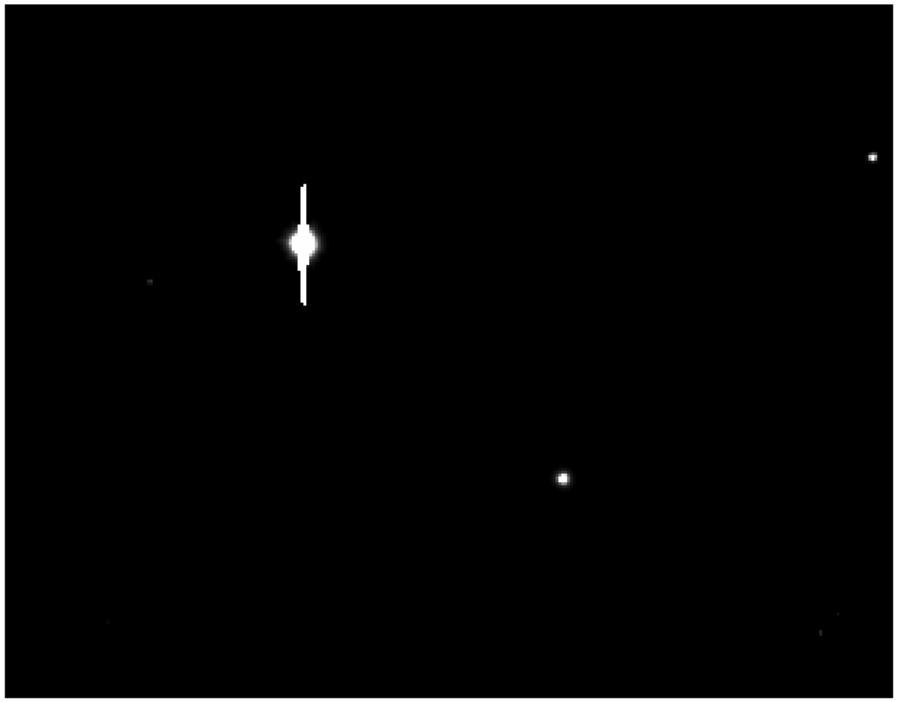

NGC 3783: *linear* intensity scale

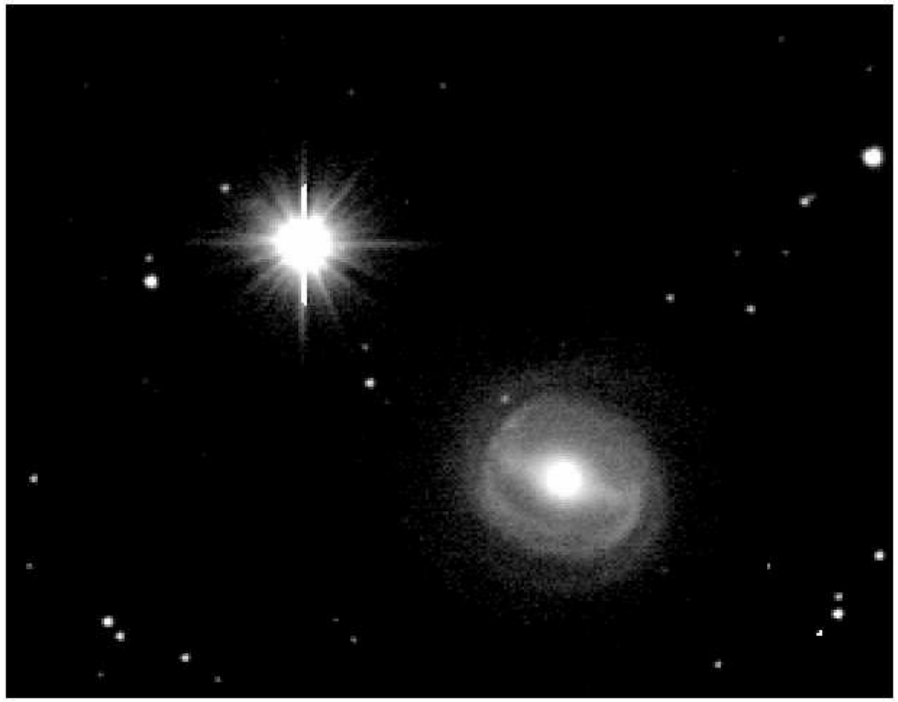

logarithmic intensity scale

What are AGN?

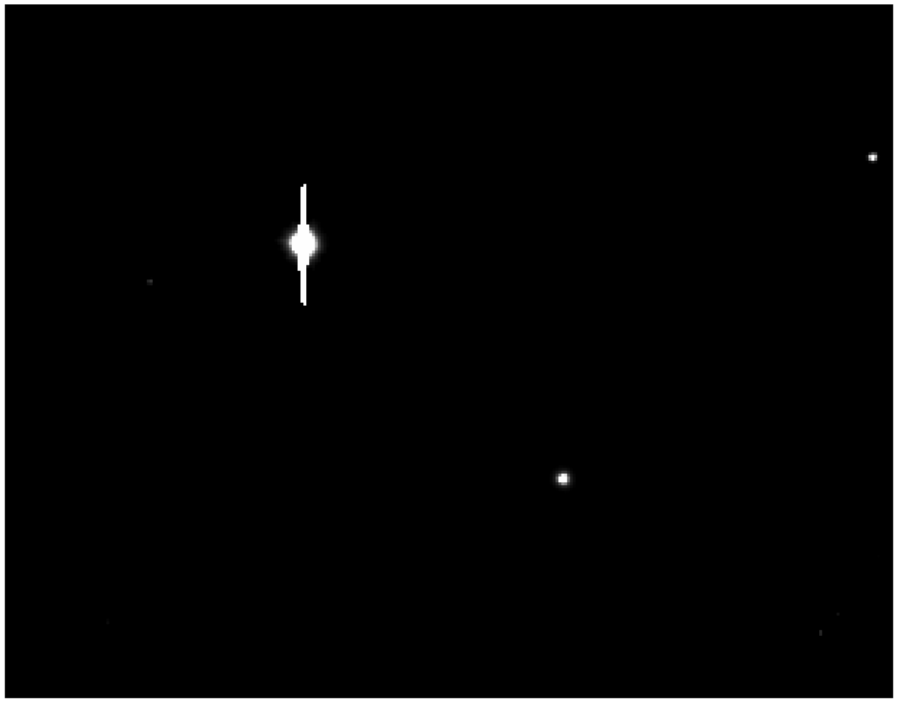

NGC 3783: *linear* intensity scale

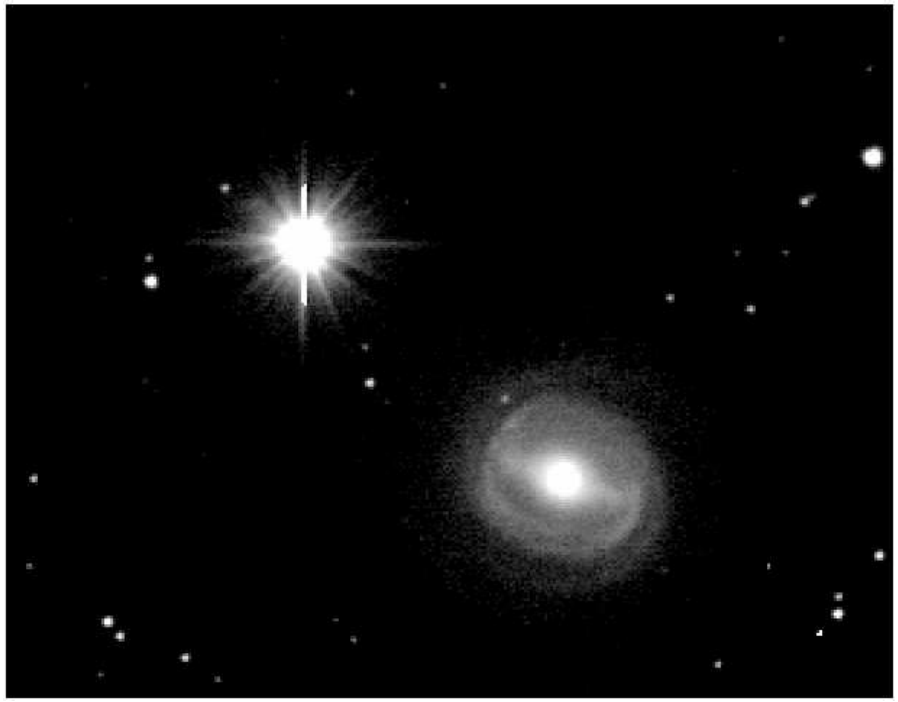

logarithmic intensity scale

Active Galactic Nuclei (AGN): supermassive black holes ($M \sim 10^{6\ldots8}\, M_\odot$), accreting $1 \ldots 2\, M_\odot/\mathrm{yr}$

$\Longrightarrow$ luminosity $\sim 10^{10}\, L_\odot$ (comparable to galaxy luminosity)

M87 – R. Gendler

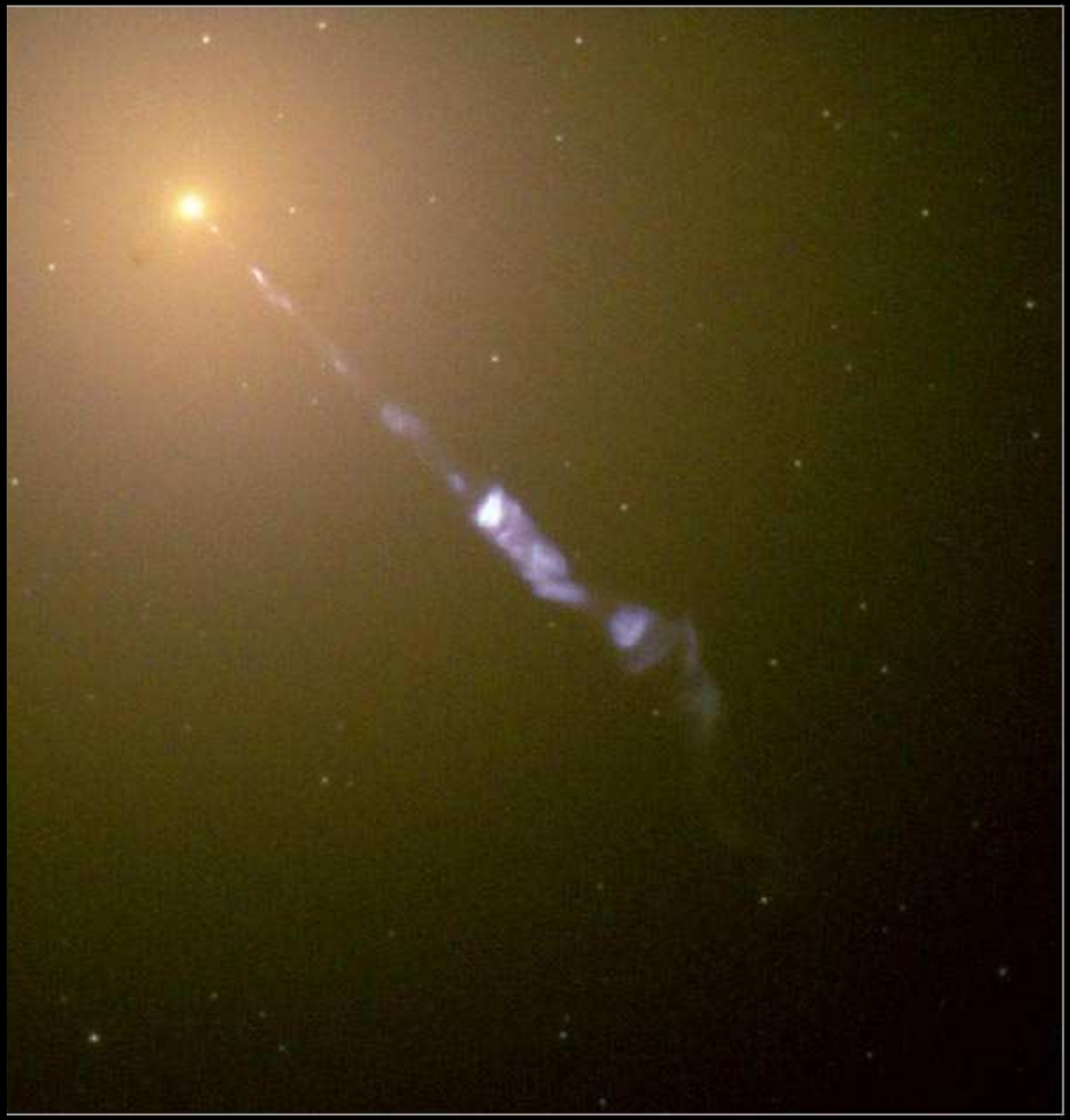

Hubble Heritage

PRC00-20 • Space Telescope Science Institute • NASA and The Hubble Heritage Team (STScI/AURA)

What are AGN?

Observational characteristics of AGN:

- (Normally) high luminosity
- Emission throughout the electromagnetic spectrum (radio to keV, MeV, TeV)

  $\Longrightarrow$ spectrum is "nonthermal"
- strong variability (days to years)
- radio loud sources: relativistic jets, which can be superluminous ($v_{\text{app}} \gg c$)
- broad optical lines ($v_{\text{characteristic}} \sim$ several 1000 km s^{-1})

Outline of the next 3 days:

- Wednesday: History, Unified Model
- Thursday: Accretion, Black Hole paradigm
- Friday: Jets, radio loud AGN

Textbooks on AGN

PETERSON, B.M., 1997, An Introduction to Active Galactic Nuclei, Cambridge: Cambridge Univ. Press, 254pp., $45

Undergraduate level introduction to Active Galactic Nuclei, level is slightly lower than here.

KROLIK, J., 1999, Active Galactic Nuclei: From the Central Black Hole to the Galactic Environment, Princeton: Princeton Univ. Press, 632pp., $57.50

The most comprehensive textbook on AGN available, covers much more material than what is possible here.

KEMBHAVI, A.J. & NARLIKAR, J.V., 1999, Quasars and Active Galactic Nuclei: An Introduction, Cambridge: Cambridge Univ. Press, 476pp., $50

Graduate level textbook, similar to Krolik, but often explains things from a somewhat different point of view.

Other Textbooks

BRADT, H., 2003, Astronomy Methods: A Physical Approach to Astronomical Observations, Cambridge: Cambridge Univ. Press, 458pp., €57.50

Summary of many technical details that are useful to know if you want to become a professional astronomer. Detectors, radiation processes, etc.

PADMANABHAN, T., 2000, Theoretical Astrophysics: Volumes 1–3, Cambridge: Cambridge Univ. Press, ∼ 500pp. each, ∼€60 per volume

Introduction to the (theoretical) physics of astrophysics. Short, concise, great. Graduate level, but understandable, although not for the faint hearted. . .

FRANK, J., KING, A., RAINE, D., 2002, Accretion Power in Astrophysics, 3rd edition, Cambridge: Cambridge Univ. Press, 398pp., €55.90

The standard textbook on accretion, covering all relevant areas of the field, including AGN.

History of AGN research

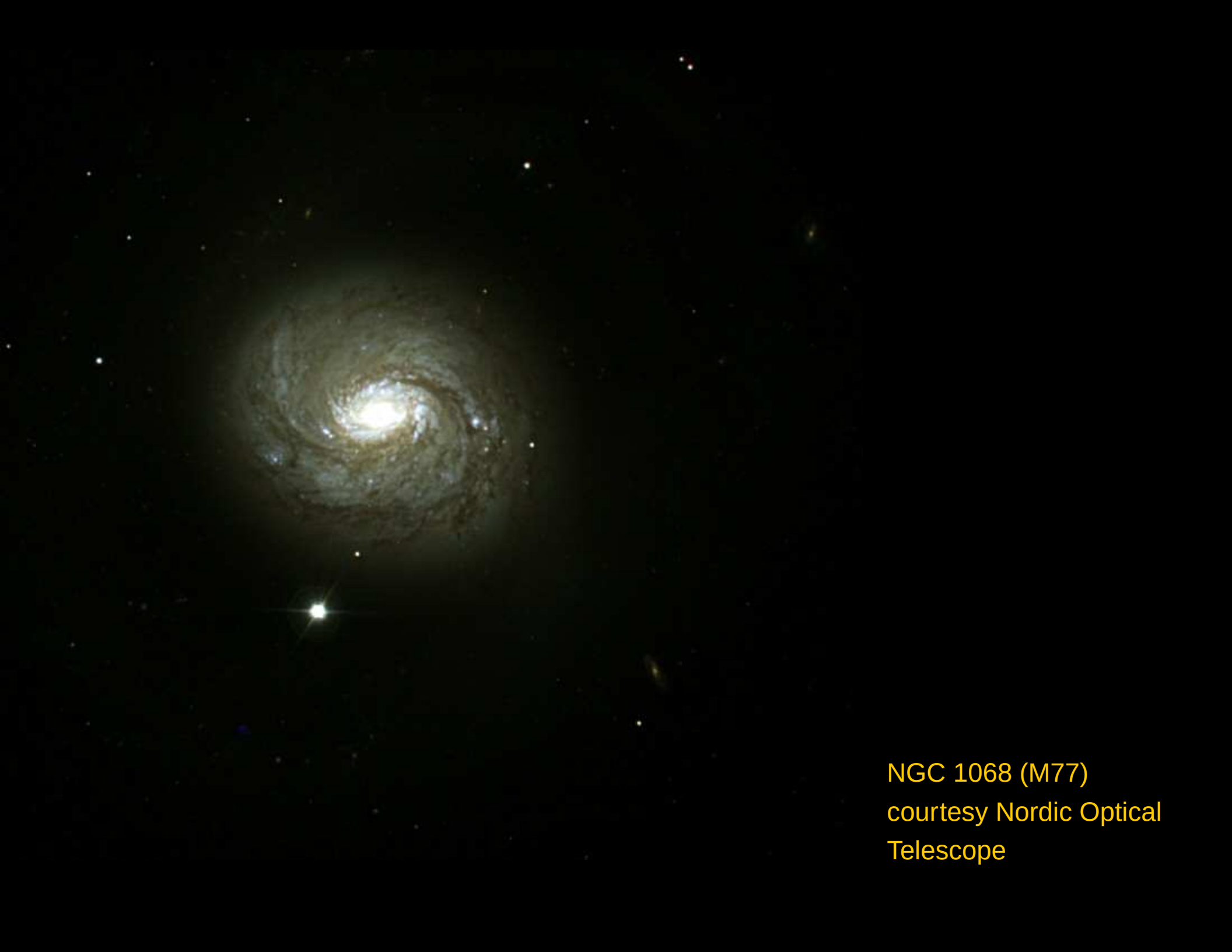

NGC 1068 (M77)
courtesy Nordic Optical Telescope

1908: E. Fath

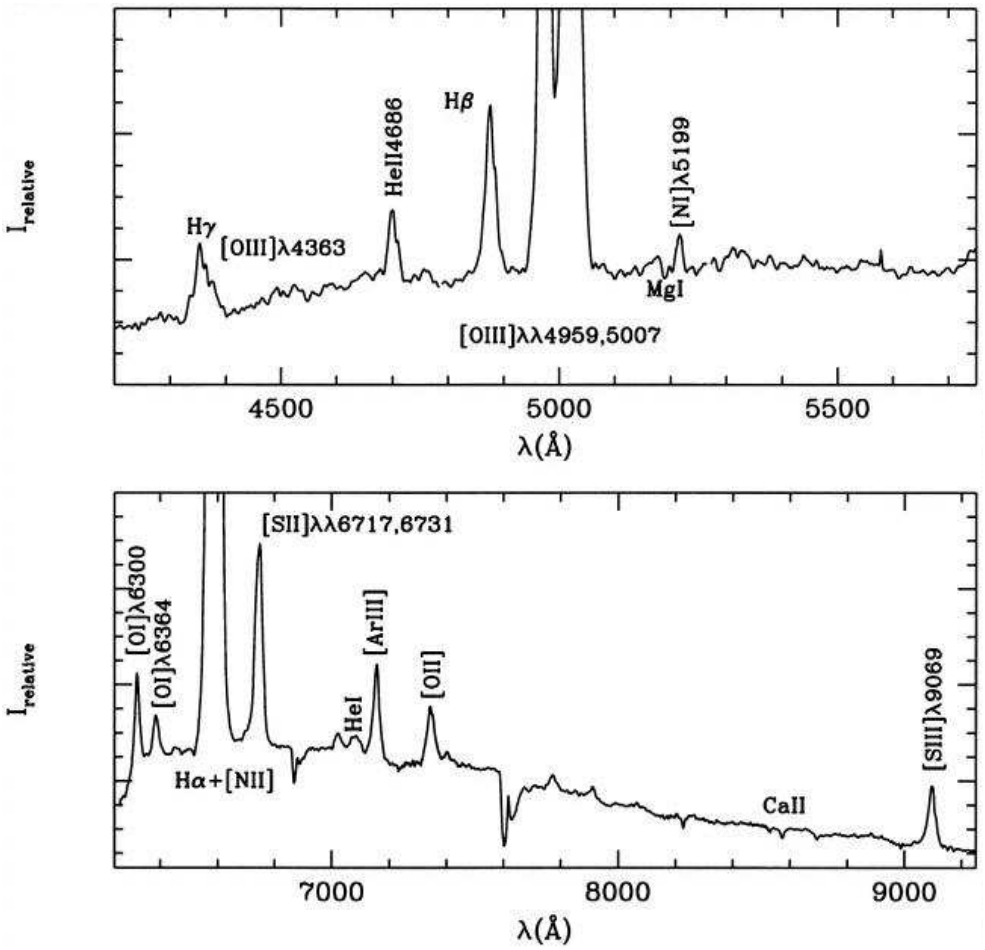

Optical spectrum of NGC 1068

(García-Lorenzo et al., 1999, Fig. 4)

1908: Edward A. Fath: There are emission lines in NGC 1068, similar to planetary nebulae.

This was part of Fath's PhD!

Note: High ionization levels, large width of lines

1918: H. Curtis

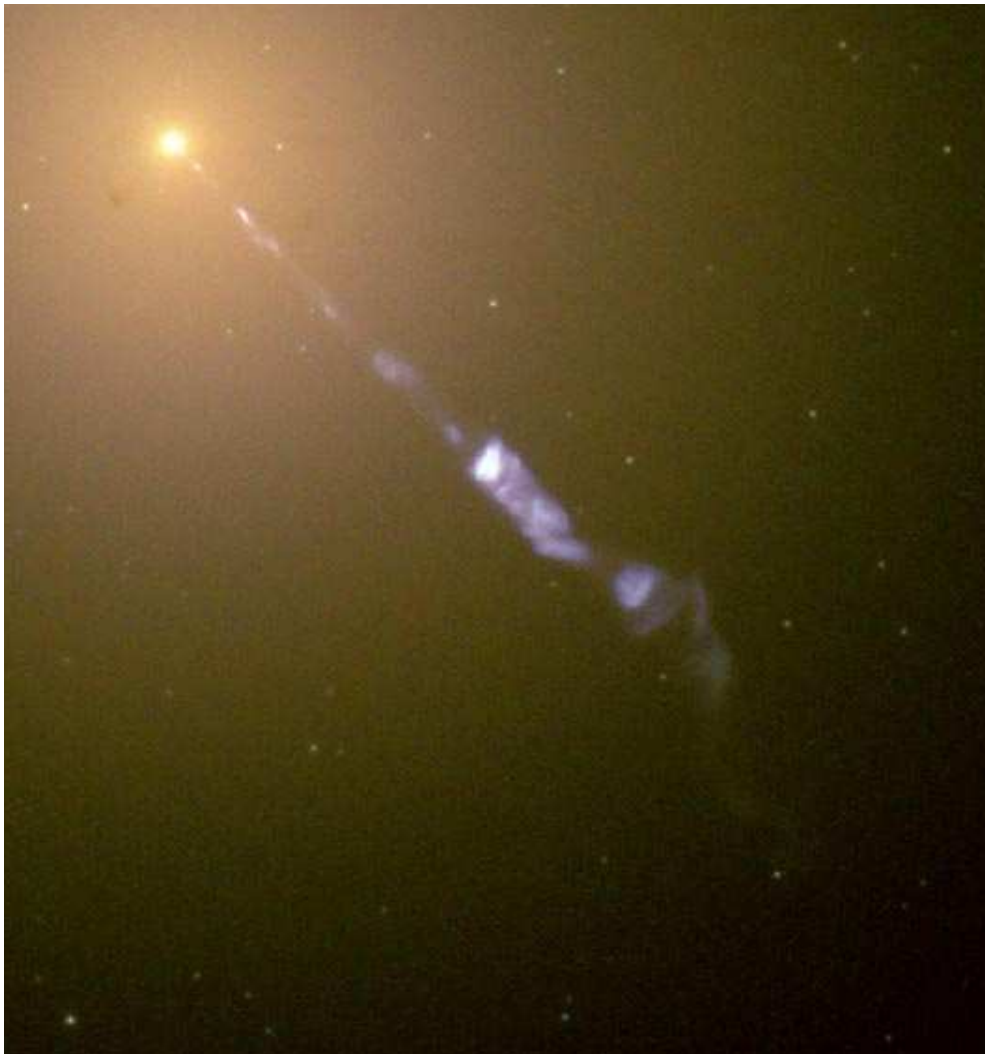

HST

1918: Heber D. Curtis: “[M87 exhibits] a curious straight ray. . . apparently connected with the nucleus by a thin line of matter”.

$\Longrightarrow$ M87 contains an optical jet

1926: E. Hubble

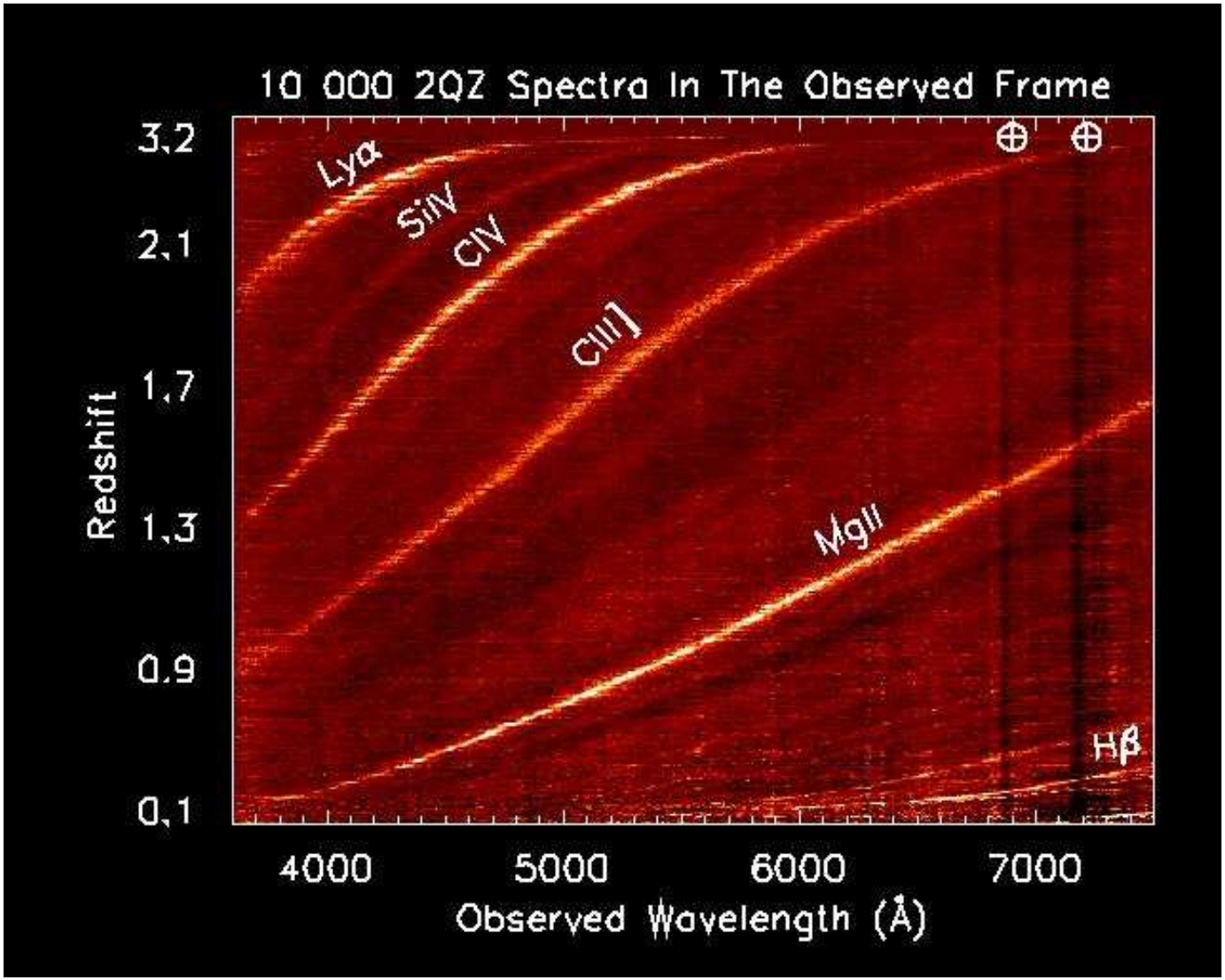

courtesy 2DF survey

1926: Edwin Hubble:

- Emission lines in NGC 1068, NGC 4051, NGC 4151
- Spectral features in nebulae are redshifted $\Longrightarrow$ nebulae are extragalactic!

Reminder: $z = \Delta\lambda/\lambda = v/c$, $v = Hd$ where $H \sim 75\,\mathrm{km\,s^{-1}\,Mpc^{-1}}$.

1943: C. Seyfert

NUCLEAR EMISSION IN SPIRAL NEBULAE*

CARL K. SEYFERT†

ABSTRACT

Spectrograms of dispersion 37–200 A/mm have been obtained of six extragalactic nebulae with high-excitation nuclear emission lines superposed on a normal G-type spectrum. All the stronger emission lines from λ 3727 to λ 6731 found in planetaries like NGC 7027 appear in the spectra of the two brightest spirals observed, NGC 1068 and NGC 4151.

Apparent relative intensities of the emission lines in the six spirals were reduced to true relative intensities. Color temperatures of the continua of each spiral were determined for this purpose.

The observed relative intensities of the emission lines exhibit large variations from nebula to nebula. Profiles of the emission lines show that all the lines are broadened, presumably by Doppler motion, by amounts varying up to 8500 km/sec for the total width of the hydrogen lines in NGC 3516 and NGC 7469. The hydrogen lines in NGC 4151 have relatively narrow cores with wide wings, 7500 km/sec in total breadth. Similar wings are found for the Balmer lines in NGC 7469. The lines of the other ions show no evidence of wide wings. Some of the lines exhibit strong asymmetries, usually in the sense that the violet side of the line is stronger than the red.

In NGC 7469 the absorption K line of *Ca* II is shallow and 50 A wide, at least twice as wide as in normal spirals.

Absorption minima are found in six of the stronger emission lines in NGC 1068, in one line in NGC 4151, and one in NGC 7469. Evidence from measures of wave length and equivalent widths suggests that these absorption minima arise from the G-type spectra on which the emissions are superposed.

The maximum width of the Balmer emission lines seems to increase with the absolute magnitude of the nucleus and with the ratio of the light in the nucleus to the total light of the nebula. The emission lines in the brightest diffuse nebulae in other extragalactic objects do not appear to have wide emission lines similar to those found in the nuclei of emission spirals.

(Seyfert, 1943)

1943: Carl Seyfert: Recognization of spiral galaxies with optical emission lines as a class $\Longrightarrow$ Seyfert galaxies

1954: W. Baade and R. Minkowski

W. Baade (Mt. Wilson Obs.)

IDENTIFICATION OF THE RADIO SOURCES IN CASSIOPEIA, CYGNUS A, AND PUPPIS A

W. BAADE AND R. MINKOWSKI
MOUNT WILSON AND PALOMAR OBSERVATORIES
CARNEGIE INSTITUTION OF WASHINGTON
CALIFORNIA INSTITUTE OF TECHNOLOGY
Received June 19, 1953

ABSTRACT

The radio sources in Cassiopeia and Puppis A are identified with a new type of galactic emission nebulosity. The outstanding features of these nebulosities are very large internal random velocities. The radio source Cygnus A is an extragalactic object, two galaxies in actual collision.

Only very few individual sources of cosmic radio emission have been identified with conspicuous astronomical objects.[1] Although the sources in Cassiopeia[2] and Cygnus A[3]

(Baade & Minkowski, 1954)

1954: Walter Baade and Rudolph Minkowski: optical counterparts to radio sources Cyg A (NGC 5128), Vir A (M87), Per A (NGC 1275).

Cyg A: First ultra-luminous AGN (2nd brightest radio source in the sky; $L \sim 10^{45}\,\mathrm{erg\,s^{-1}}$).

1959: L. Woltjer

EMISSION NUCLEI IN GALAXIES

L. WOLTJER*
Yerkes Observatory, University of Chicago
Received February 16, 1959

ABSTRACT

Some galaxies which show wide emission lines in the spectra of their nuclei are discussed. It is shown that, on statistical grounds, the nuclear emission must last for several times 10^8 years at least. The nuclei are extremely narrow, of the order of 100 parsecs, and, if a normal mass-to-light ratio applies, extremely massive. The width of the emission lines, which indicates velocities of a few thousand kilometers per second, is probably due to fast motions, circular or random, in the gravitational fields of the nuclei. The high star density in the nuclei may provide a source of excitation. In the nucleus of our own Galaxy the radio source Sagittarius gives evidence of strong magnetic fields and large amounts of relativistic particles. A mass of a few times 10^8 solar masses is needed to prevent disintegration of the source. The Andromeda Nebula has a nucleus with a somewhat smaller mass. The occurrence of dense nuclei may be a common characteristic of many galaxies.

(Woltjer, 1959)

1959: Lodewijk Woltjer: AGN have huge masses.

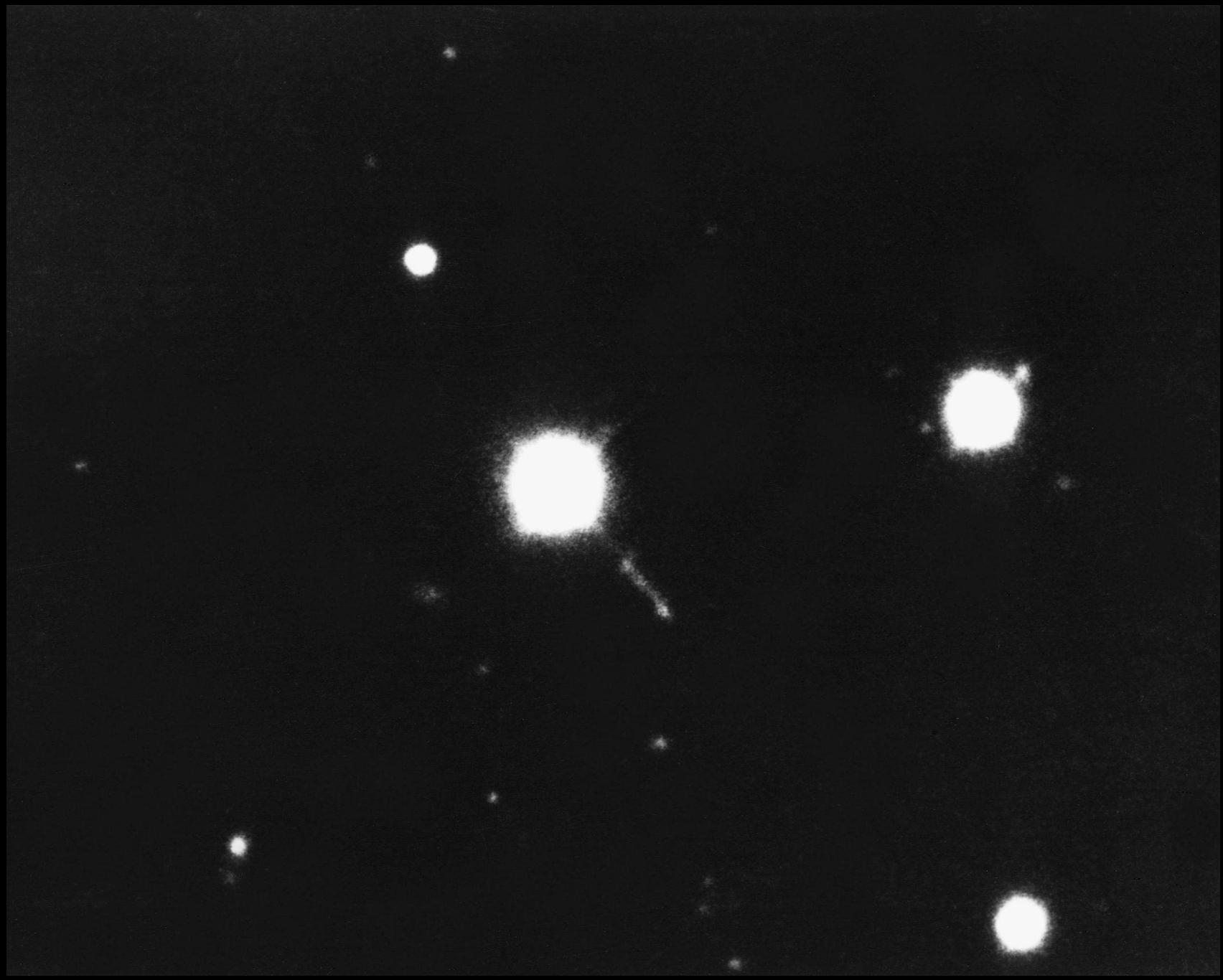

3C273 (4 m Myall telescope, NOAO/AURA/NSF)

1963: M. Schmidt

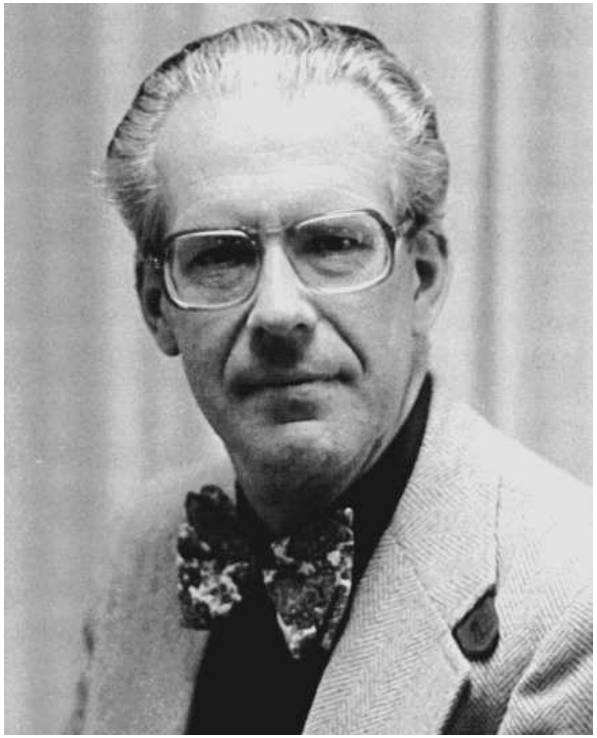

M. Schmidt (Caltech)

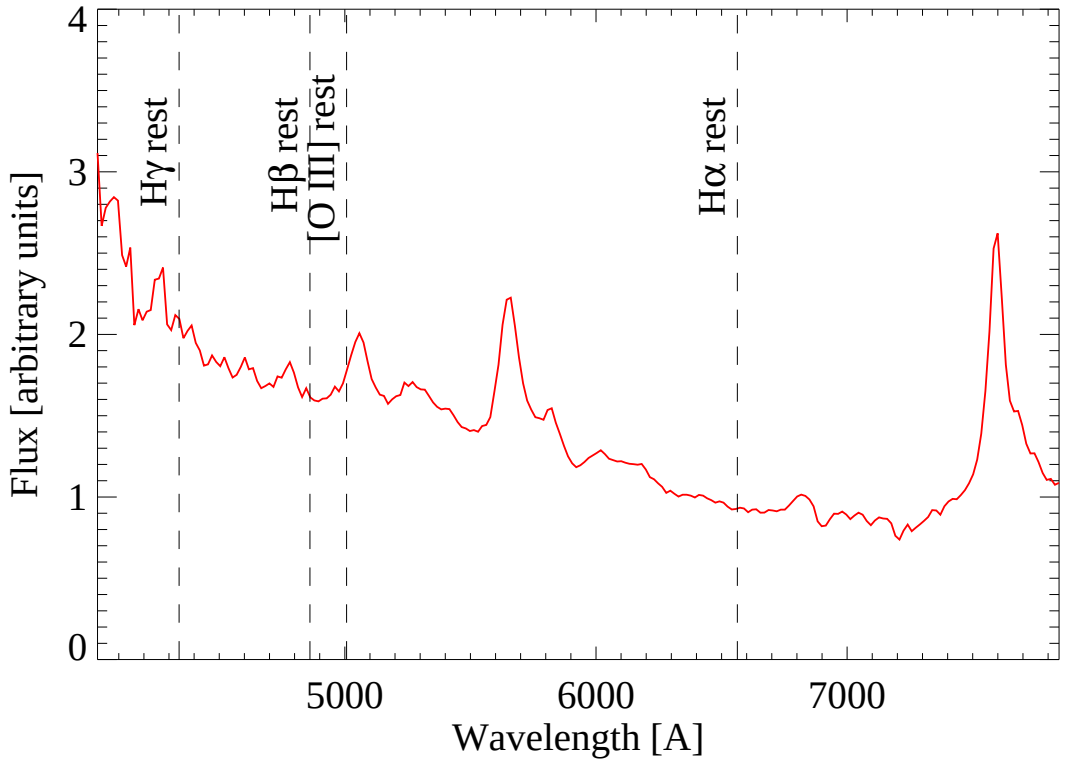

3C273 (Rondi et al., Pic du Midi)

1963: M. Schmidt

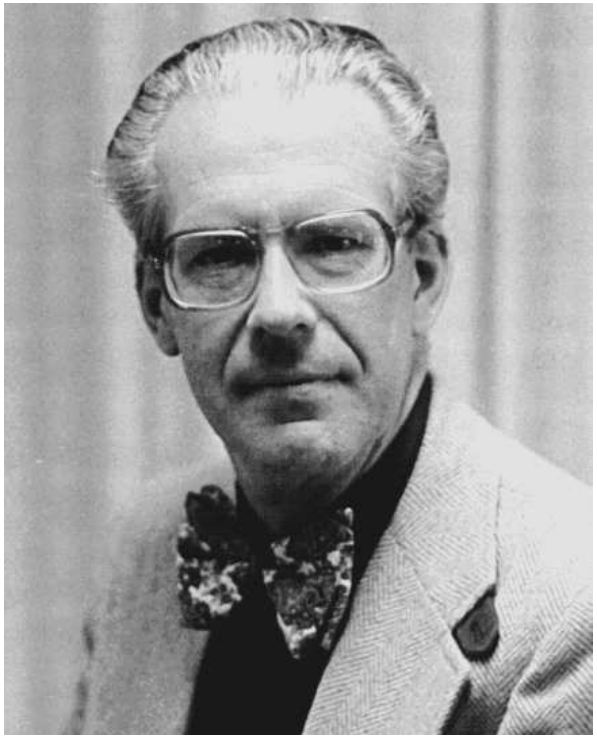

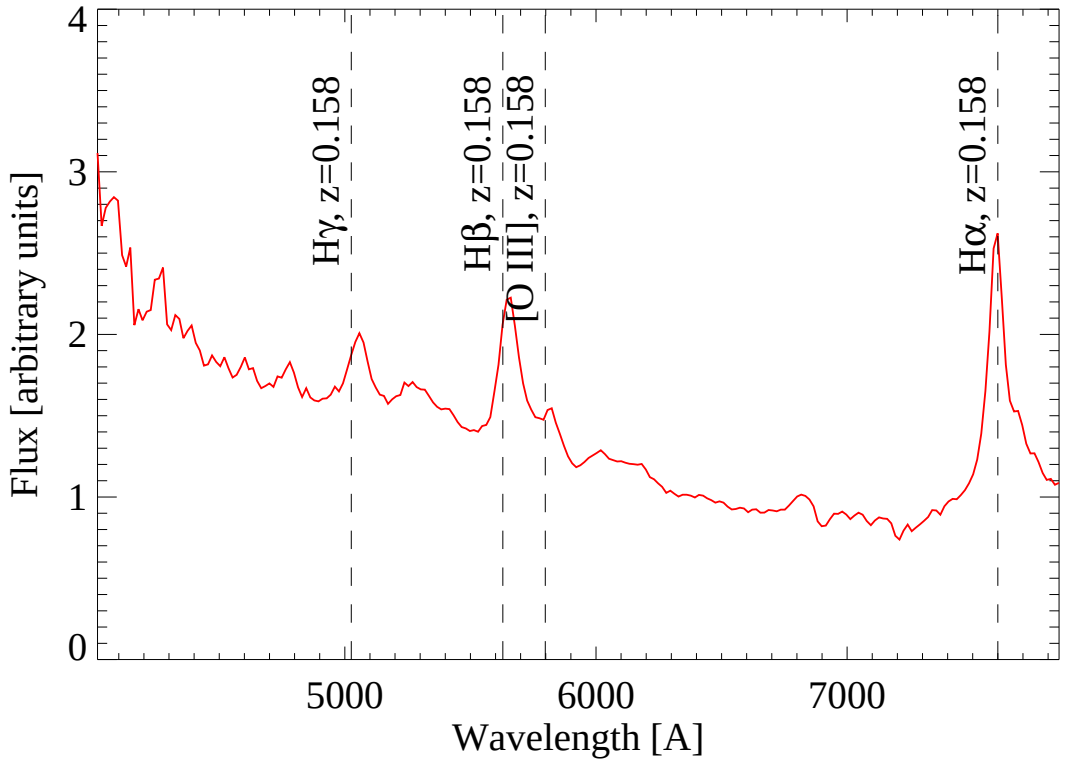

M. Schmidt (Caltech)

3C273 (Rondi et al., Pic du Midi)

1963: Maarten Schmidt: 3C273 has $z = 0.158 \Longrightarrow$ AGN are far away!

shortly later: 1963: J. Greenstein and Th. Matthews: 3C48 has $z = 0.368$

Nomenclature: Quasar/QSO (from “quasi stellar radio source”: radio emitting AGN)

Galaxy M87

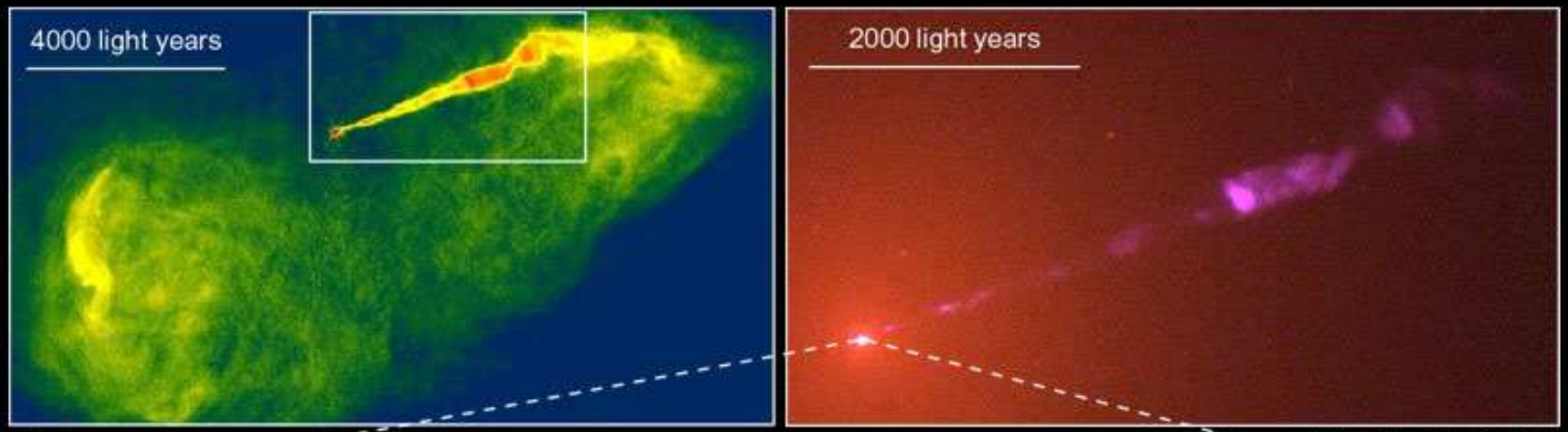

VLA
Radio

HST • WFPC2
Visible

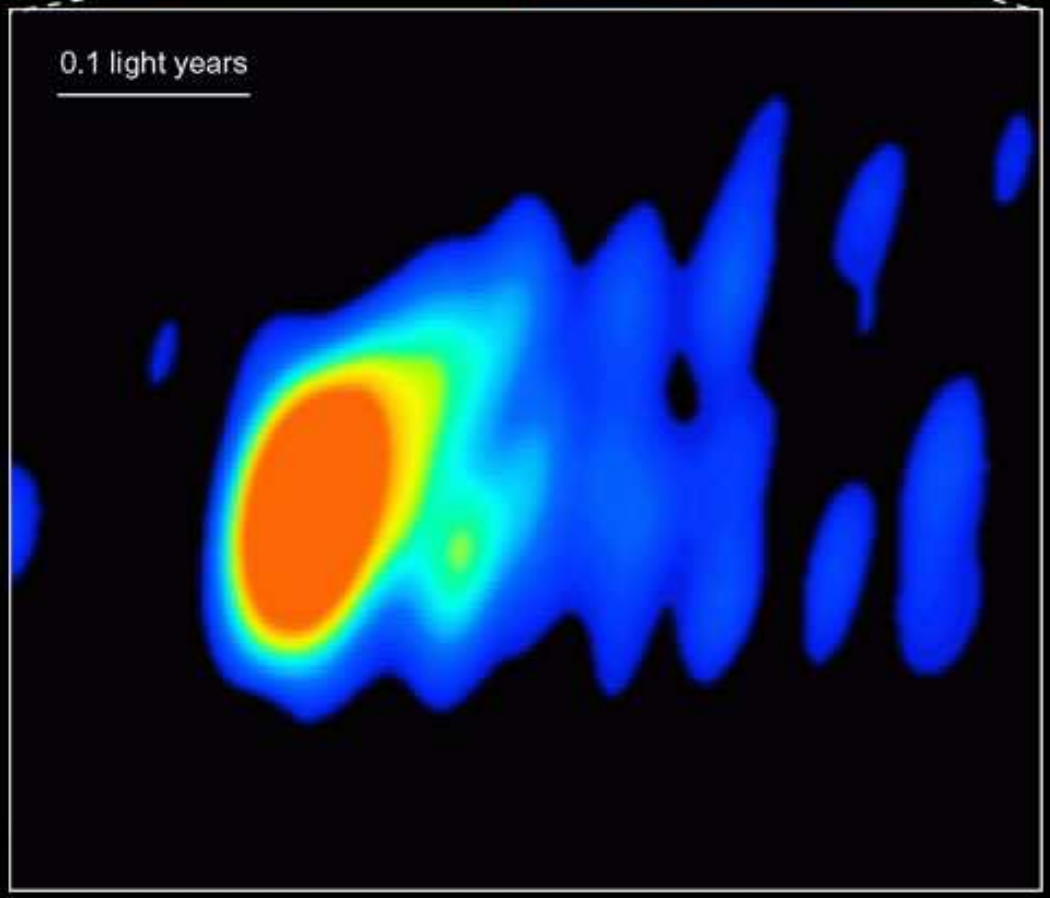

VLBA
Radio

NASA, NRAO and J. Biretta (STScI) • STScI-PRC99-43

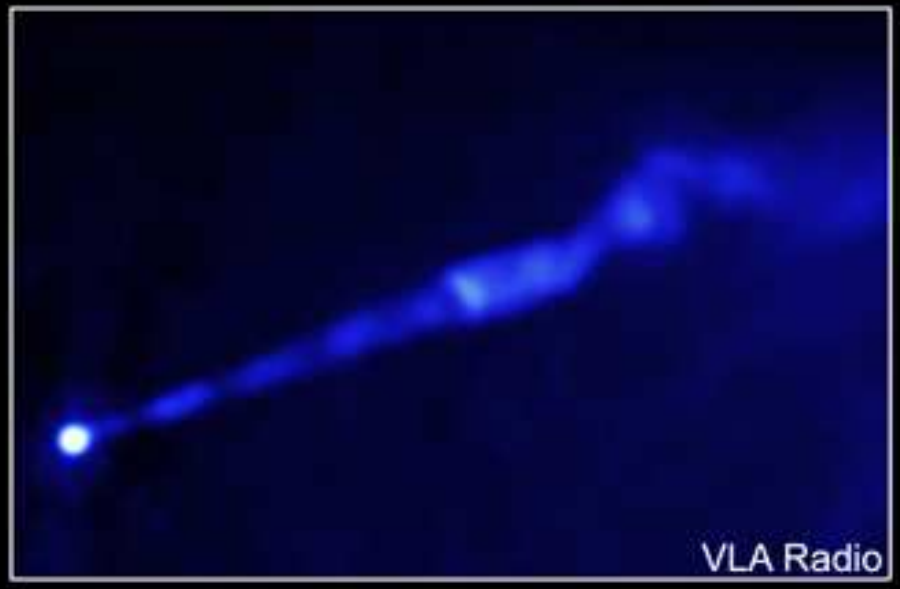

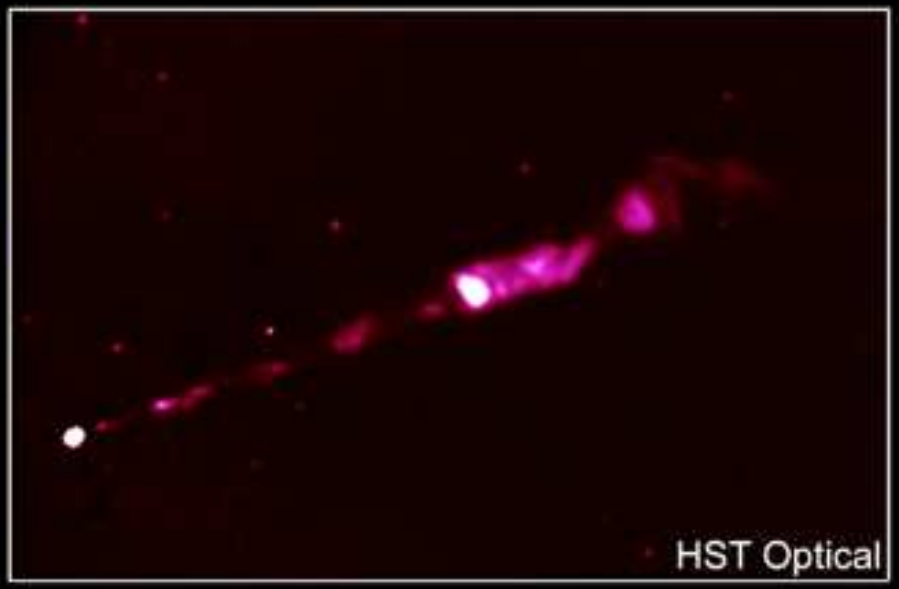

X-ray: NASA/CXC/MIT/H.Marshall et al. Radio: F.Zhou, F.Owen (NRAO), J.Biretta (STScI)
Optical: NASA/STScI/UMBC/E.Perlman et al.

Jets are visible in all wavebands

AGN Continua

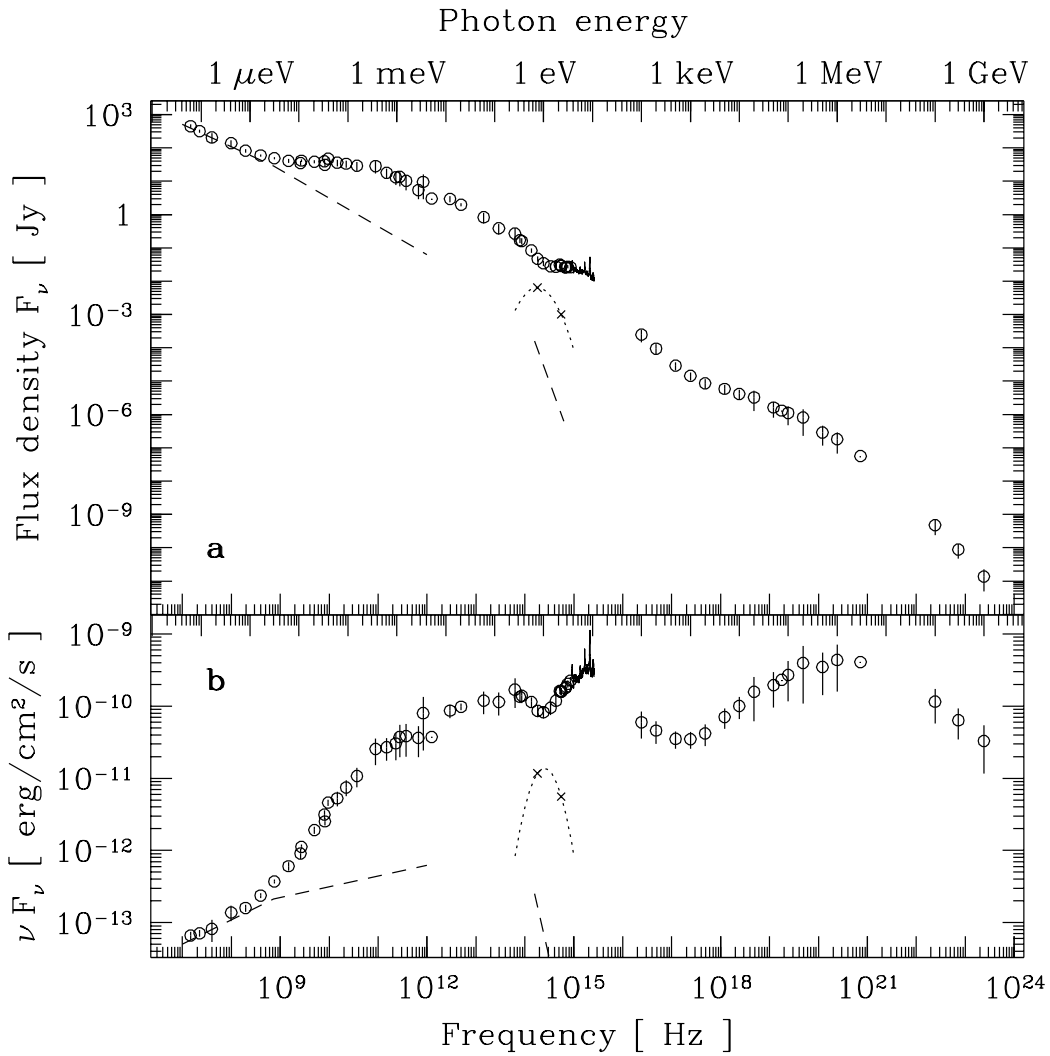

Türler et al. (1999): Spectral Energy Distribution (SED) of 3C 273

AGN Broad Band Spectra are Powerlaws

The observed flux density, F_ν, is roughly

$$F_\nu \propto \nu^{-\alpha} \tag{2.1}$$

where $\alpha \sim 1$

$\Longrightarrow$ νF_ν-spectrum is flat.

Total luminosities are $10^{42}\,\mathrm{erg\,s^{-1}}$ ($= 10^9\,L_\odot$) and more, i.e., comparable to that of galaxies

Accretion Power

AGN have high luminosities: What is the energy source?

1. Nuclear Fusion

Typical reactions à la

$$4\mathrm{p} \longrightarrow {}^4\mathrm{He} + \Delta mc^2$$

Liberated energy:

Fusion produces $\sim 6 \times 10^{18}\,\mathrm{erg\,g^{-1}} = 6 \times 10^{11}\,\mathrm{J\,g^{-1}}$

($\Delta E_{\mathrm{nuc}} \sim 0.007 m_{\mathrm{p}} c^2$)

Accretion Power

AGN have high luminosities: What is the energy source?

1. Nuclear Fusion

Typical reactions à la

$$4\mathrm{p} \longrightarrow {}^4\mathrm{He} + \Delta mc^2$$

Liberated energy:

Fusion produces $\sim 6 \times 10^{18}\,\mathrm{erg\,g^{-1}} = 6 \times 10^{11}\,\mathrm{J\,g^{-1}}$

($\Delta E_{\mathrm{nuc}} \sim 0.007 m_{\mathrm{p}} c^2$)

2. Gravitation

Accretion of mass m from ∞ onto a black hole with radius R_{S} gives

$$\Delta E_{\mathrm{acc}} = \frac{GMm}{R_{\mathrm{S}}} \text{ where } R_{\mathrm{S}} = \frac{2GM}{c^2}$$

Accretion yields $\sim 10^{20}\,\mathrm{erg\,g^{-1}} = 10^{13}\,\mathrm{J\,g^{-1}}$

($\Delta E_{\mathrm{acc}} \sim 0.1\, m_{\mathrm{p}} c^2$)

Accretion Power

AGN have high luminosities: What is the energy source?

1. Nuclear Fusion

Typical reactions à la

$$4\mathrm{p} \longrightarrow {}^4\mathrm{He} + \Delta mc^2$$

Liberated energy:

Fusion produces $\sim 6 \times 10^{18}\,\mathrm{erg\,g^{-1}} = 6 \times 10^{11}\,\mathrm{J\,g^{-1}}$

($\Delta E_{\mathrm{nuc}} \sim 0.007 m_{\mathrm{p}} c^2$)

2. Gravitation

Accretion of mass m from ∞ onto a black hole with radius R_{S} gives

$$\Delta E_{\mathrm{acc}} = \frac{GMm}{R_{\mathrm{S}}} \text{ where } R_{\mathrm{S}} = \frac{2GM}{c^2}$$

Accretion yields $\sim 10^{20}\,\mathrm{erg\,g^{-1}} = 10^{13}\,\mathrm{J\,g^{-1}}$

($\Delta E_{\mathrm{acc}} \sim 0.1\, m_{\mathrm{p}} c^2$)

$\Longrightarrow$ Accretion of material onto a black hole is the most likely energy source ("Black Hole paradigm")

. . . to power a luminous AGN, $1 \ldots 2\,\mathrm{M_\odot\,yr^{-1}}$ are sufficient.

Baade, W., & Minkowski, R. 1954, ApJ, 119, 206
García-Lorenzo, B., Mediavilla, E., & Arribas, S. 1999, ApJ, 518, 190
Seyfert, C. K., 1943, ApJ, 97, 28
Türler, M., Paltani, S., Courvoisier, T. J.-L., et al. 1999, A&AS, 134, 89
Woltjer, L., 1959, ApJ, 130, 38

AGN Taxonomy

Introduction

Purpose of this chapter: Phenomenology of AGN

Structure:

1. The AGN Zoo
   (a) Seyfert galaxies
   (b) Quasars, QSOs
   (c) Radio Galaxies: Fanaroff-Riley classification
   (d) BL Lacs, OVVs, Blazars
2. The Unification Paradigm

See Urry & Padovani (1995) and Lawrence (1987) for the gory details.

Seyfert Galaxies: Optical Images

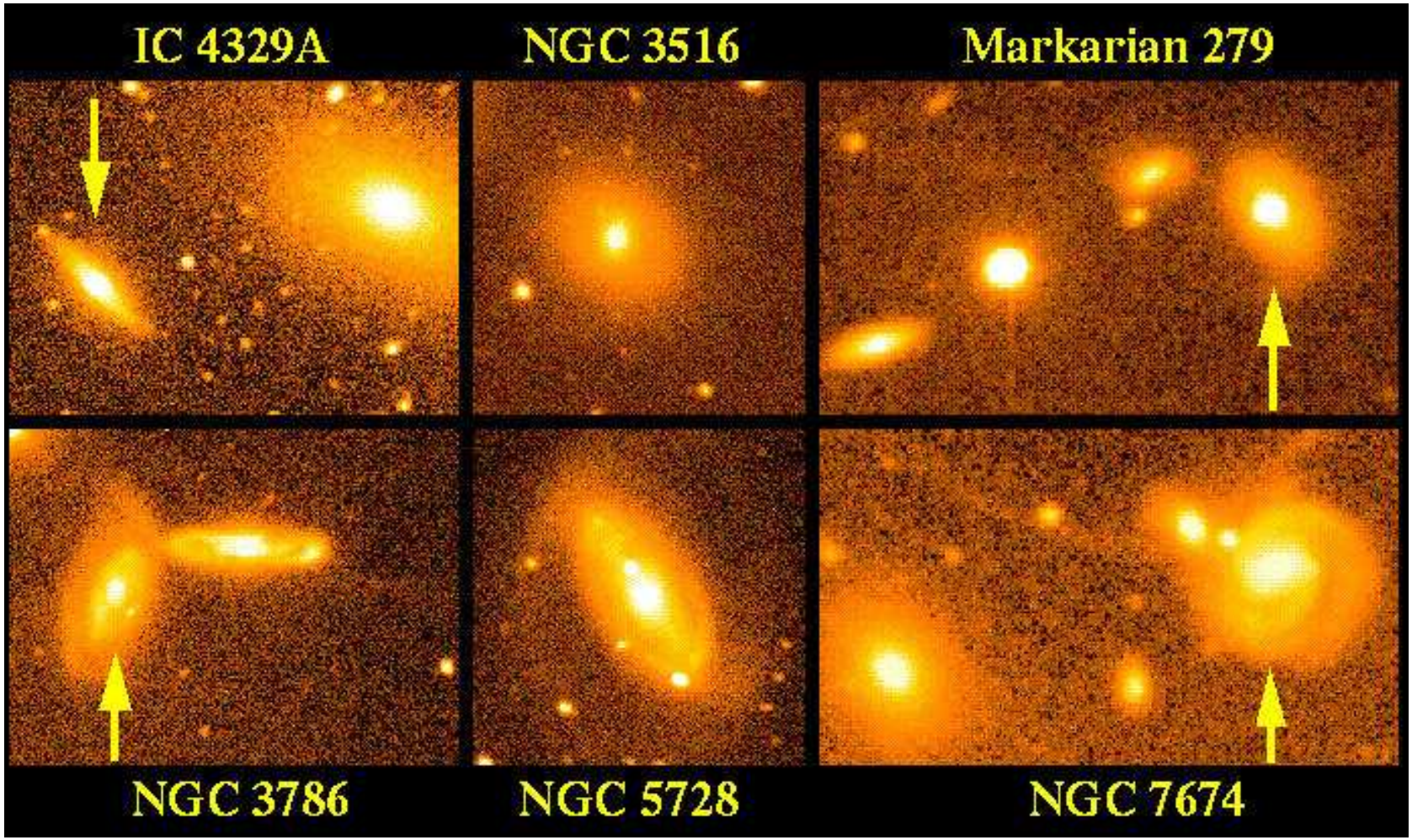

W. Keel

Seyfert galaxies: point-like centers of galaxies, generally host galaxy detectable.

Seyfert 1: Optical Spectrum

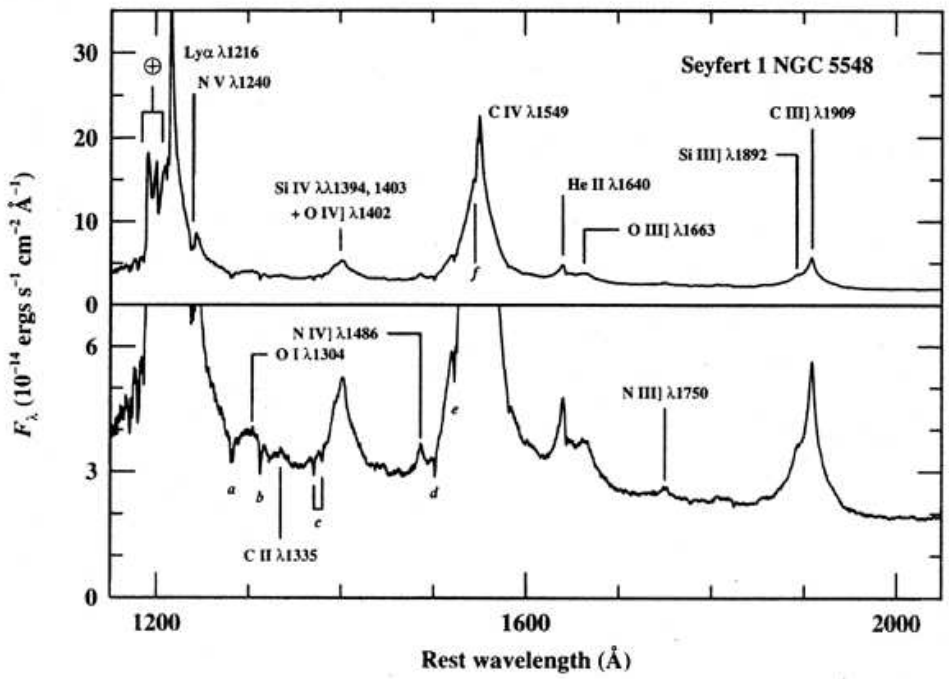

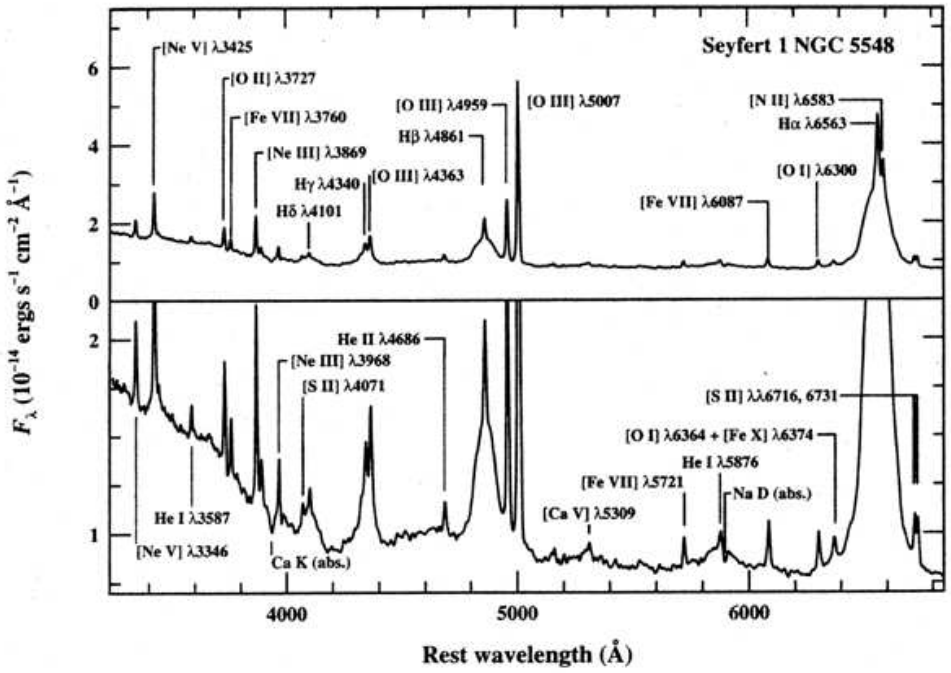

(Peterson, 1997)

UV/optical spectrum of NGC 5548: a typical Seyfert 1 Galaxy.

Before interpreting Seyfert spectrum: need to take quick refresher in atomic physics

Reminder: Atomic Physics

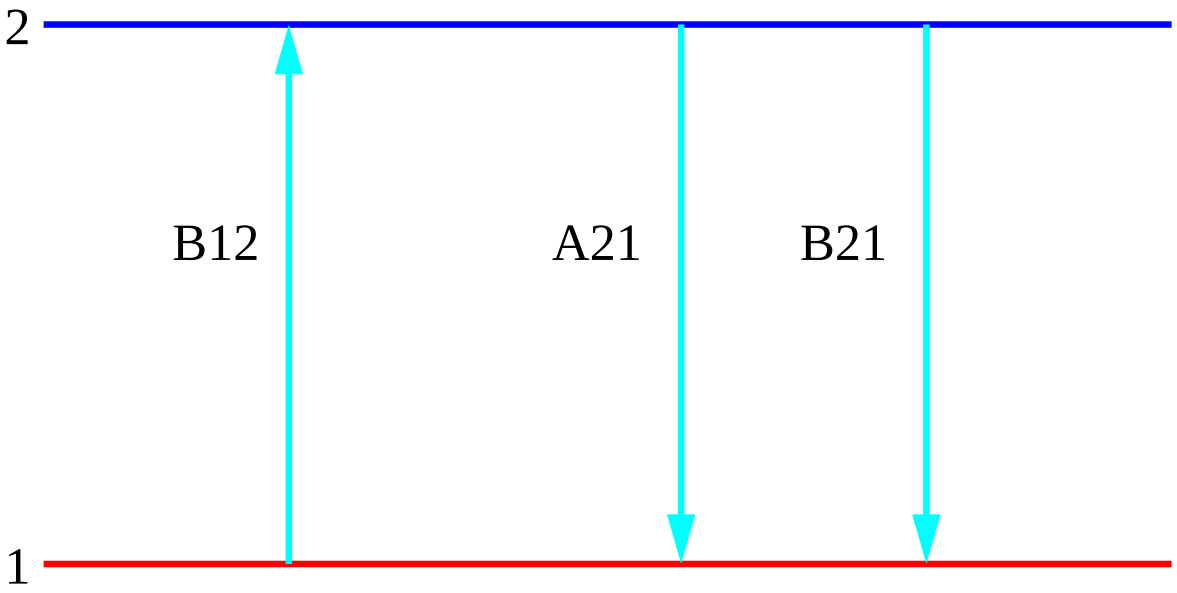

Line emission for transition $m \longrightarrow n$ described by Einstein A coefficient:

Power emitted per unit volume:

$$\frac{\mathrm{d}P}{\mathrm{d}V} = N_2 h\nu_{21} A_{21} \qquad (3.1)$$

where N_2: number density of atoms in level 2, $h\nu_{21}$: energy of transition.

Relationship to QM:

$$A_{12} = \left(\frac{8\pi^2 e^2}{m_\mathrm{e} c^3}\right) \nu_{12}^2 f_{12} \qquad (3.2)$$

f_{12}: "oscillator strength" (from QM, $\propto |\langle 1|\psi|2\rangle|^2$).

B-coefficients: stimulated absorption and emission, i.e., for B_{21}: $\mathrm{d}P/\mathrm{d}V = N_2 h\nu_{21} B_{21} I_{\nu_{21}}$, note $g_1 B_{12} = g_2 B_{21}$, $A_{21} = \frac{2h\nu_{21}^3}{c^2} B_{21}$.

Reminder: Atomic Physics

Allowed lines : electric dipole transition ($\Delta S = 0$, $\Delta L = 0, \pm 1$, $\Delta l = \pm 1$, $\Delta J = 0, \pm 1$, $\Delta M_J = 0, \pm 1$).

Typical Einstein Coefficient: $A_{21} \gtrsim 10^8\,\mathrm{s}^{-1}$

Example: Lyman-Series of Hydrogen.

Semi-forbidden lines: typically due to magnetic dipole (M1) transitions with selection rule $\Delta S = 1$.

Typical Einstein coefficient: $A_{21} \sim 10^4\,\mathrm{s}^{-1}$.

Example: C III]λ1909Å.

Forbidden lines: electric quadrupole (E2) transitions, selection rules $\Delta L = 0, \pm 1, \pm 2$, $\Delta J = 0, \pm 1, \pm 2$ (but still $0 \not\to 0$!).

Typical Einstein coefficient: $A_{21} \sim 10\,\mathrm{s}^{-1}$.

Example: O III]λ5007Å.

Generally, forbidden lines are observed in emission (after collisional excitation) $\Longrightarrow$ require low density medium!

Seyfert 1: Optical Spectrum, cont'd.

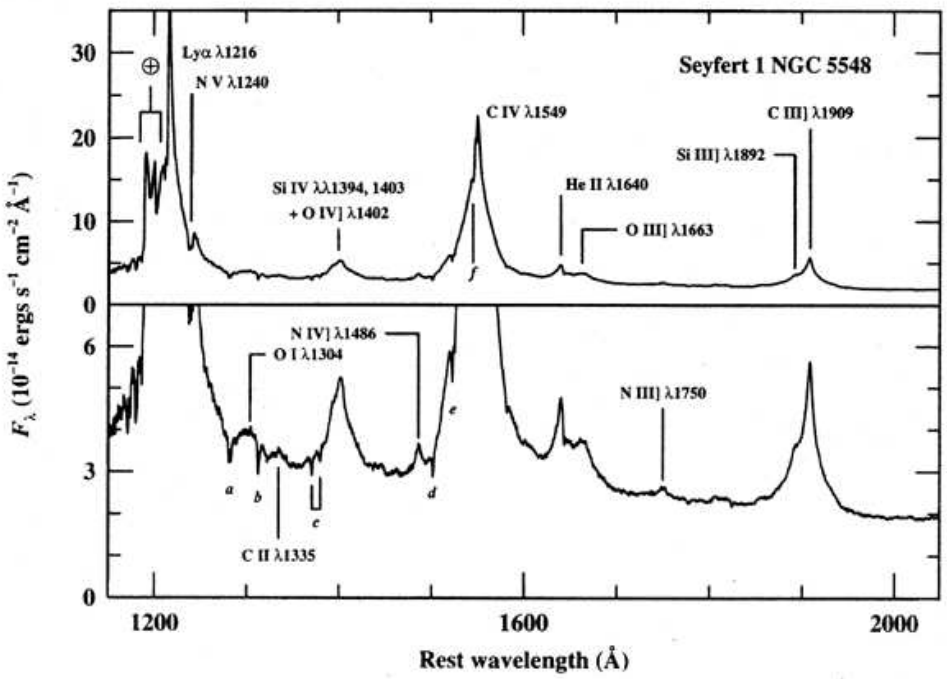

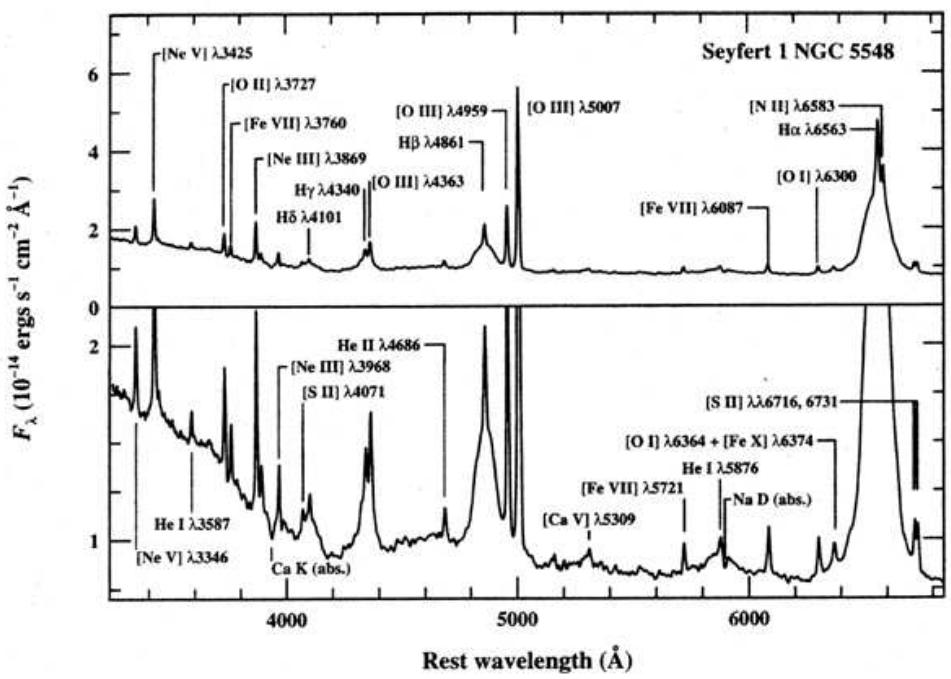

Let's look at the Seyfert 1 NGC 5548 again:

- broad allowed lines (e.g., Balmer series), Full width at half maximum (FWHM) up to $10^4\,\mathrm{km\,s^{-1}}$ from high density medium ($n_\mathrm{e} \gtrsim 10^9\,\mathrm{cm^{-3}}$).
- narrow forbidden lines (e.g., $[\mathrm{O\,III}5007]$), FWHM $\sim$ few$\cdot 10^2\,\mathrm{km\,s^{-1}}$ from a low density medium ($n_\mathrm{e} \sim 10^3\,\mathrm{cm^{-3}} \ldots 10^6\,\mathrm{cm^{-3}}$).

Reminder: From the Doppler effect: $\Delta\lambda/\lambda = v/c$.

Seyfert 2

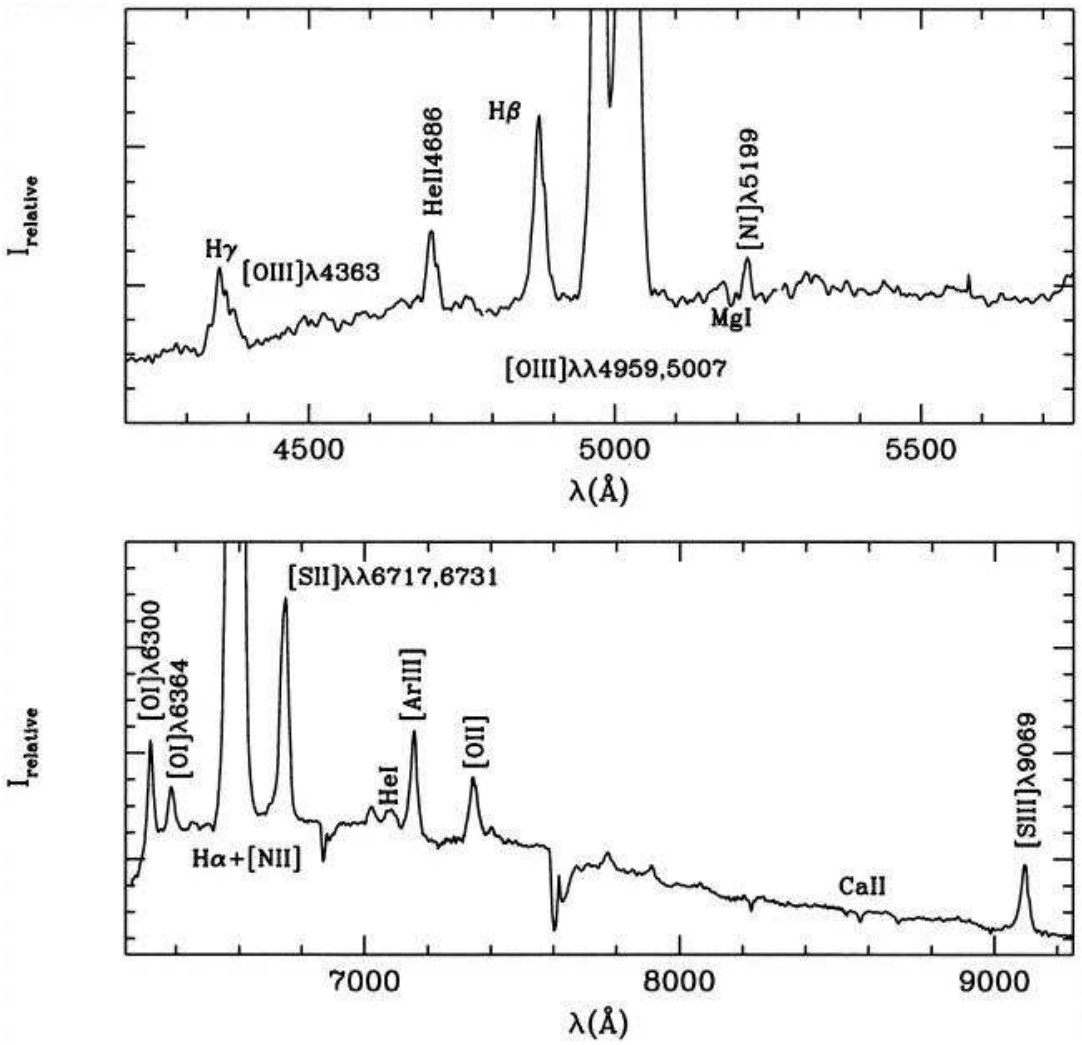

(García-Lorenzo et al., 1999, Fig. 4)

Optical spectrum of the Seyfert 2 Galaxy NGC 1068:

- Weak continuum (compared to Seyfert 1s).
- Narrow forbidden lines, FWHM $\sim$ few $\cdot\, 10^2\,\mathrm{km\,s^{-1}}$.
- No broad lines
- Absorption lines from underlying galaxy (mainly late-type giants).

Summary: Narrow Line Systems

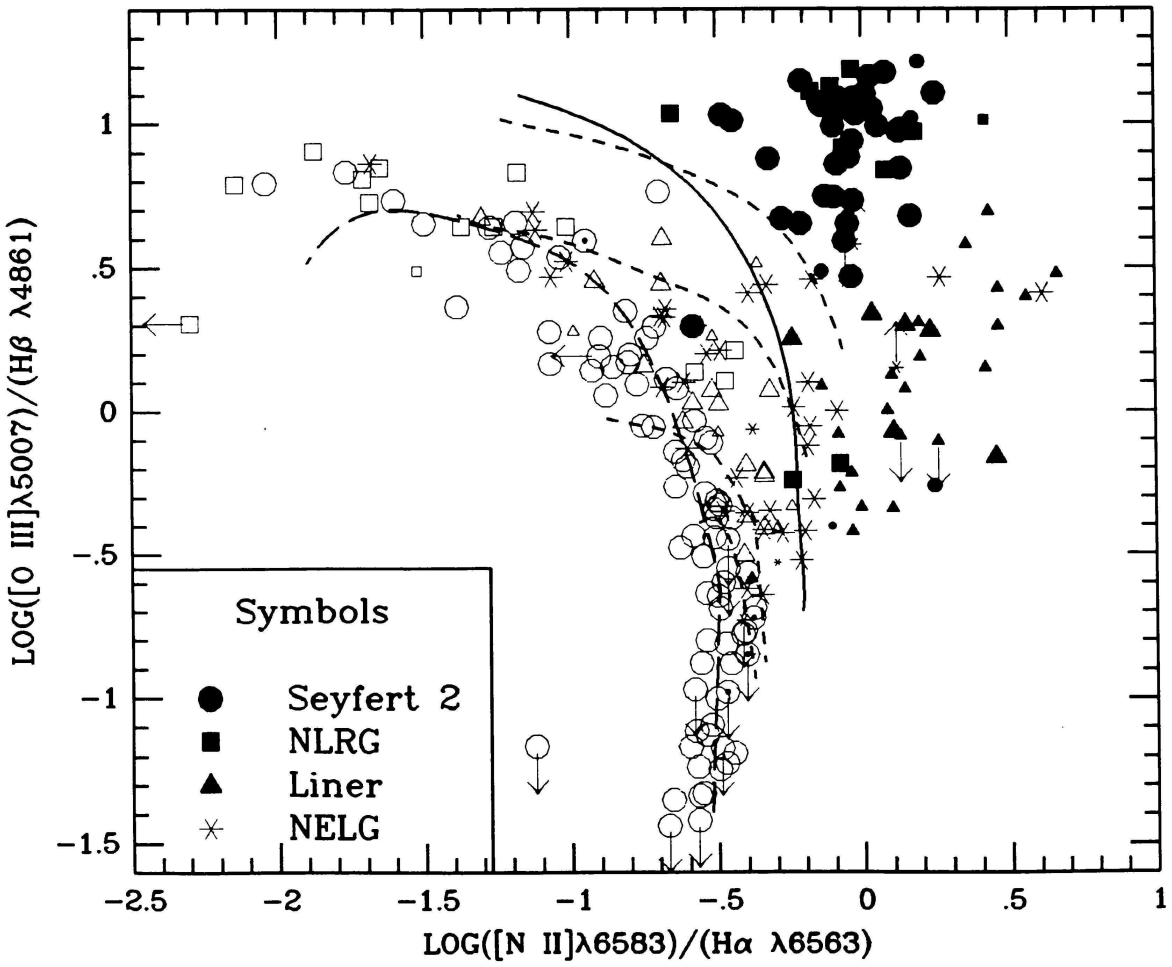

Veilleux & Osterbrock (1987, Fig. 1)

Final classification of Narrow Line Systems: ratios of prominent lines

$\Longrightarrow$ see Baldwin et al. (1981) and Veilleux & Osterbrock (1987) for details (“BPT diagram”).

For Seyferts, there are also intermediate classes, e.g., Sy 1.5, Sy 1.7, Sy 1.9, sorted by decreasing width of Balmer lines.

Generally: Seyferts: $[\mathrm{O\ III}]/\mathrm{H}\beta > 3$ and not a H II region.

QSOs and Quasars

The brightest AGN:

Quasars: Quasi-stellar Radio Sources

QSOs: Quasi-Stellar Objects

Typical absolute luminosities: $M_\mathrm{B} < -21.5 + 5 \log h_0$ where $h_0 = H_0/100\,\mathrm{km\,s^{-1}\,Mpc^{-1}}$.

All quasars show at least some radio emission.

To distinguish, use radio to optical flux ratio (Kellermann et al., 1989), $R_\mathrm{r\text{-}o} = F(6\,\mathrm{GHz})/F(4400\,\text{Å})$:

radio-loud: $R_\mathrm{r\text{-}o} = 10$–$1000$

radio-quiet: $0.1 < R_\mathrm{r\text{-}o} < 1$

There are $\sim$10$\times$ more radio-quiet QSOs than radio-loud ones.

QSOs and Quasars

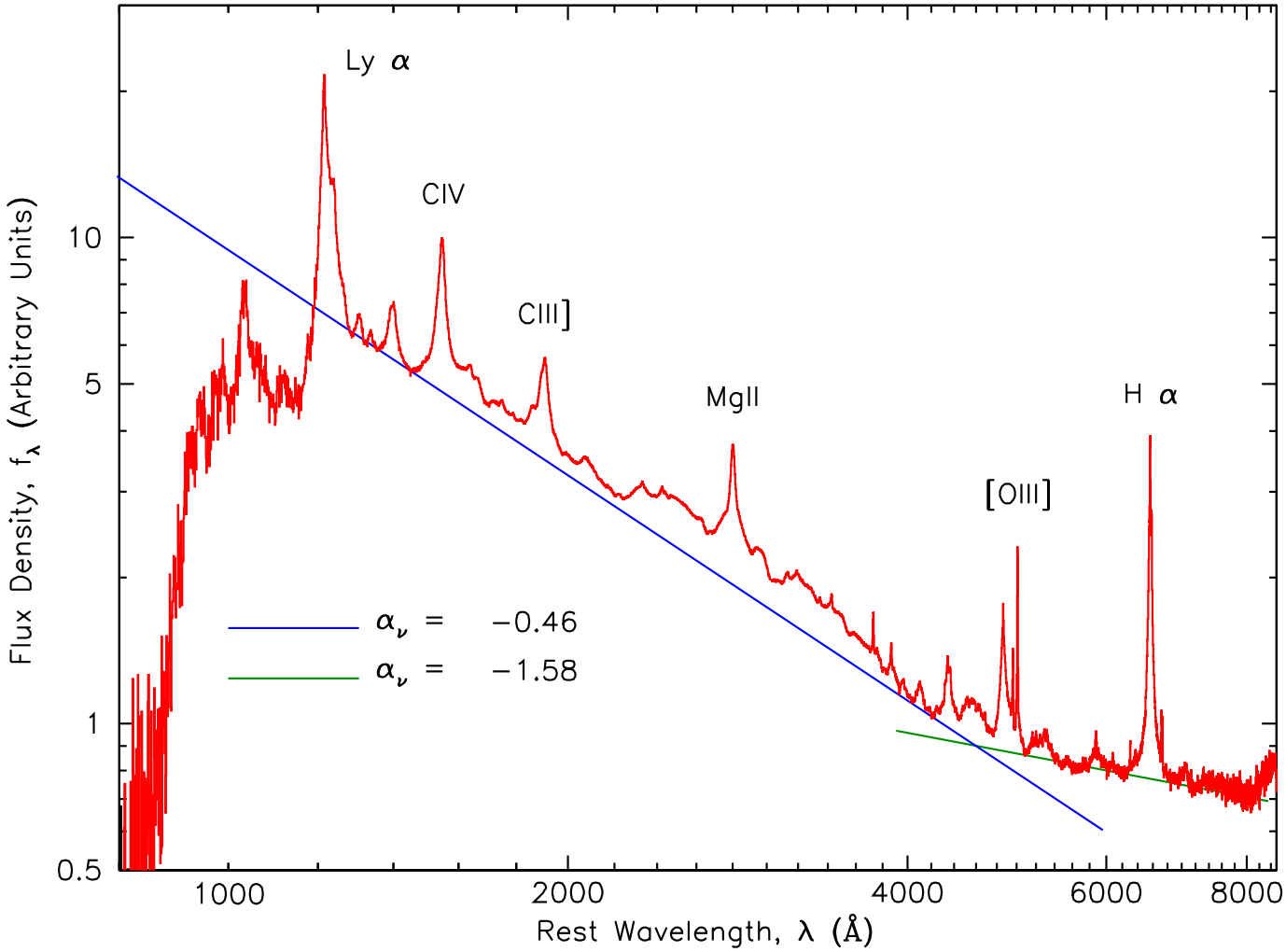

Average SDSS QSO spectrum, based on ∼2200 spectra (after Vanden Berk et al., 2001)

Optical spectra of QSOs are very similar to those of Seyfert galaxies

The powerful radio galaxy Cygnus A at $z = 0.057$ ($d = 230$ Mpc).

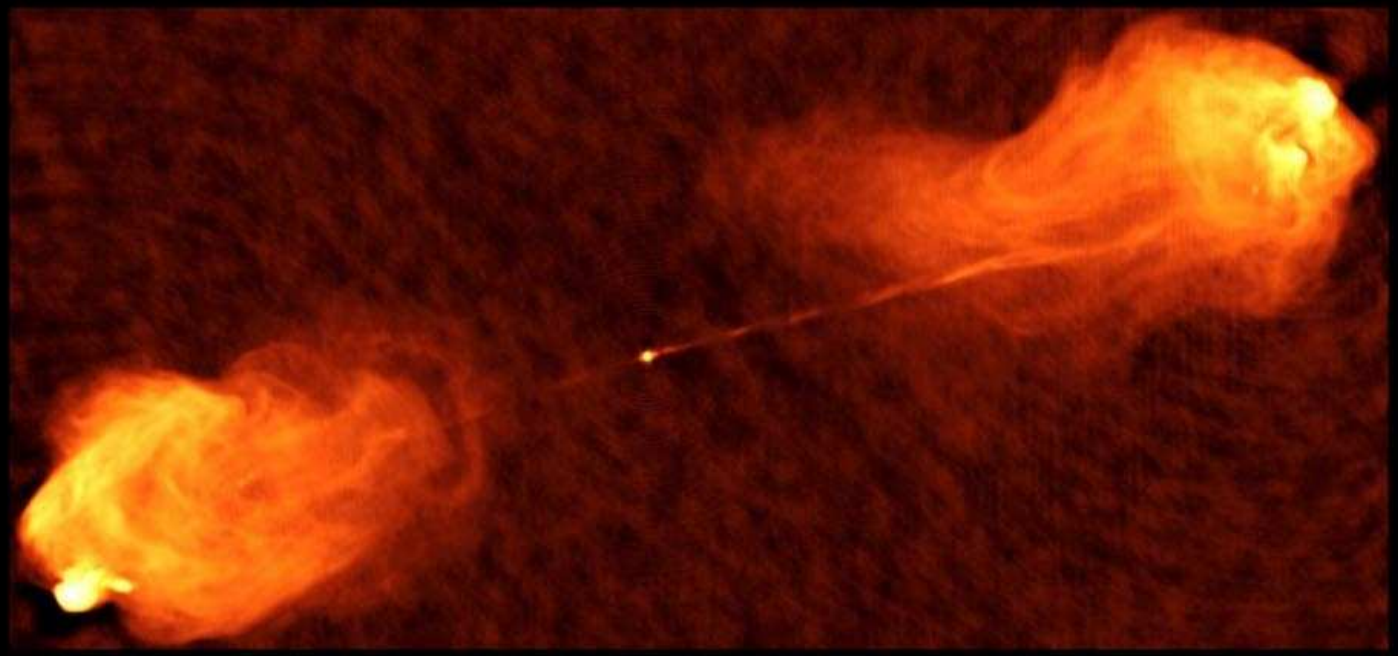

Radio (VLA: 6 cm); Credit: NRAO/AUI

Size: ~ 2.2 arcmin ~ 600000 ly, about eight times the size of the Galaxy!

Radio morphology: Core – Jets – Hotspots – Lobes

The powerful radio galaxy Cygnus A at $z = 0.057$ ($d = 230$ Mpc).

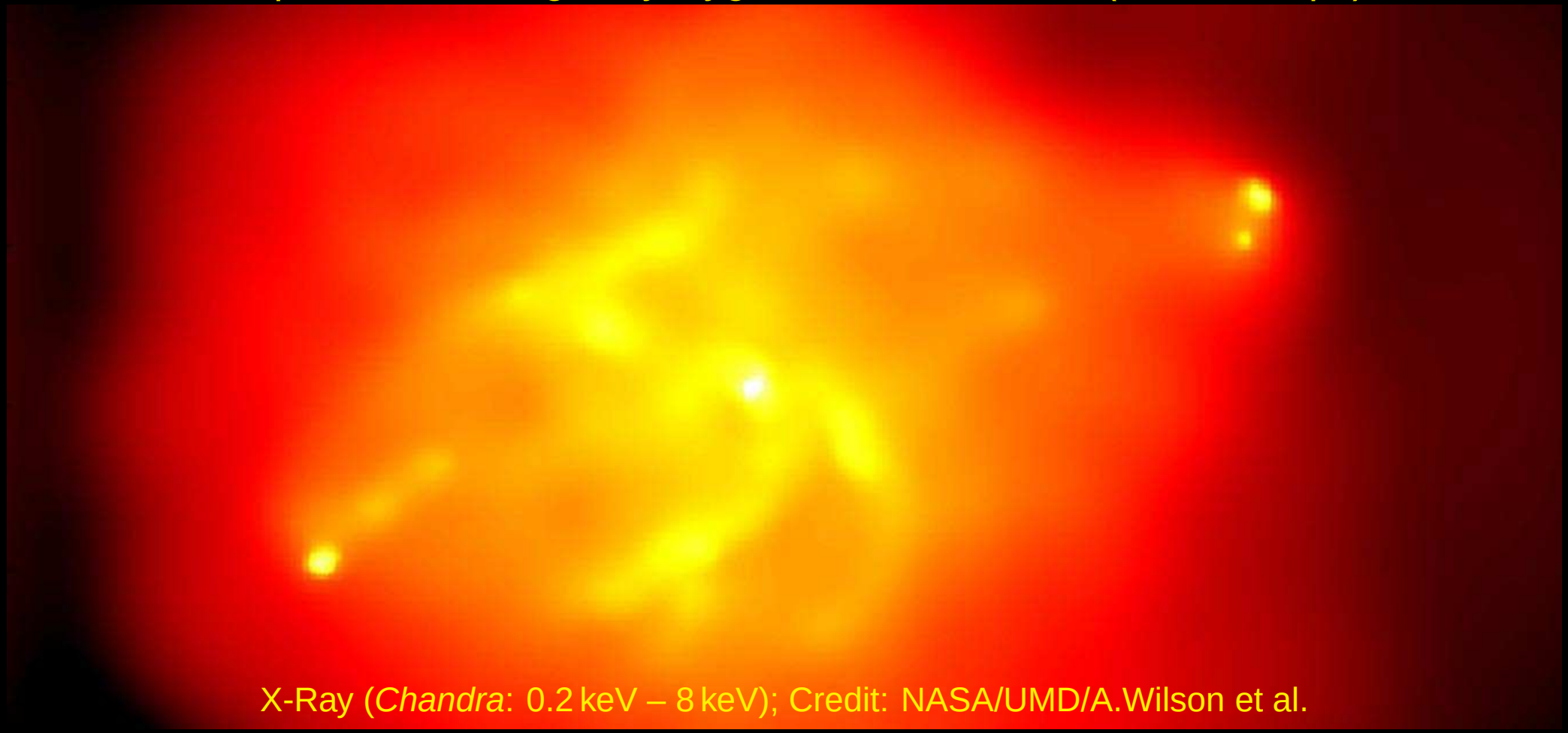

X-Ray (*Chandra*: 0.2 keV – 8 keV); Credit: NASA/UMD/A.Wilson et al.

Size: $\sim$ 2.2 arcmin $\sim$ 600000 ly, about eight times the size of the Galaxy!

Radio morphology: Core – Jets – Hotspots – Lobes

X-Ray morphology: Nucleus – Cavity – Hotspots

Fornax A: Radio (VLA) overlaid on optical (STScI/POSS-II); Credit: NRAO/AUI and J. M. Uson

Fanaroff-Riley Classes

Many radio loud objects show jets.

Classification: Fanaroff-Riley Classes (after Fanaroff & Riley 1974):

FR 1: “Fanaroff-Riley type 1”

- nucleus dominates
- less luminous
- bright
- broad jets ending in plumes
- two asymmetric jets

FR 2: “Fanaroff-Riley type 2”

- luminous radio sources
- lobes dominate
- often only one-sided weak jets ending in radio lobes

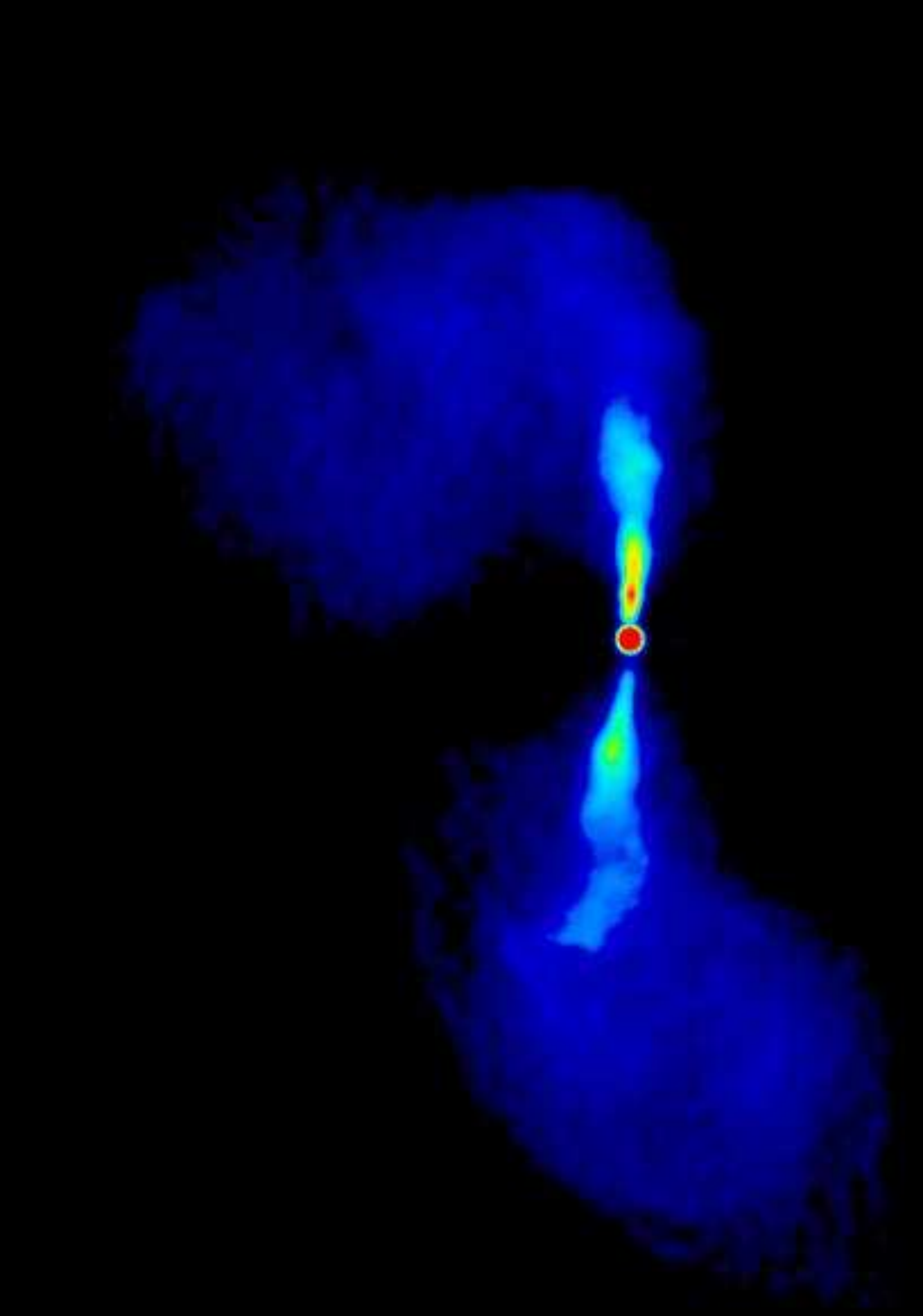

Radio image of M84 (3C272.1):
A typical FR 1 galaxy

Laing & Bridle (1987); VLA 4885 MHz,
$134'' \times 170''$; see also
http://www.jb.man.ac.uk/atlas/other/3

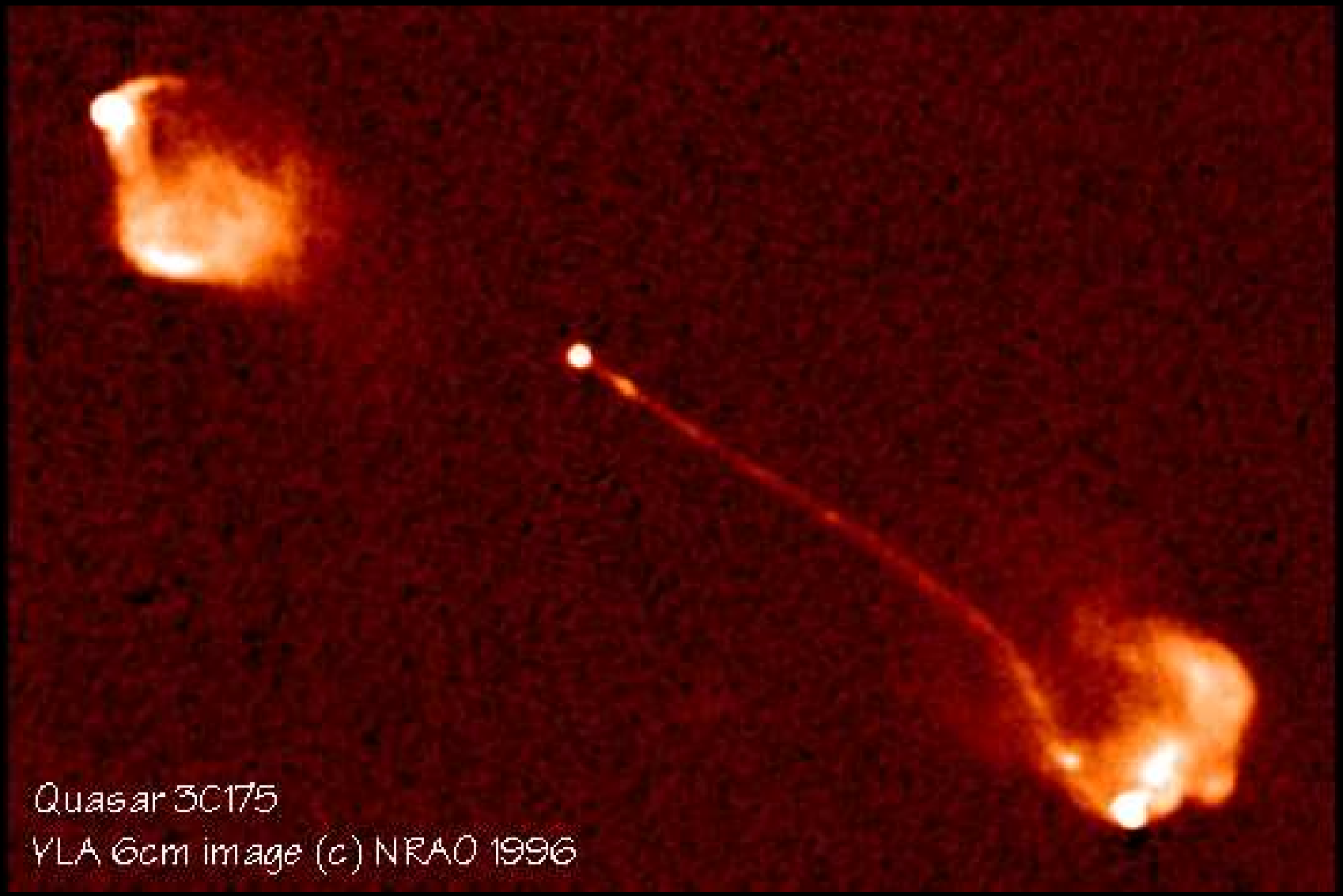

A. Bridle (priv. comm.)

Radio image of 3C175 ($z = 0.768$):

A typical FR 2 galaxy with a one sided jet

Edge brightening $\Longrightarrow$ Shock heating due to interaction with ambient intergalactic medium (IGM)

BL Lac and OVVs

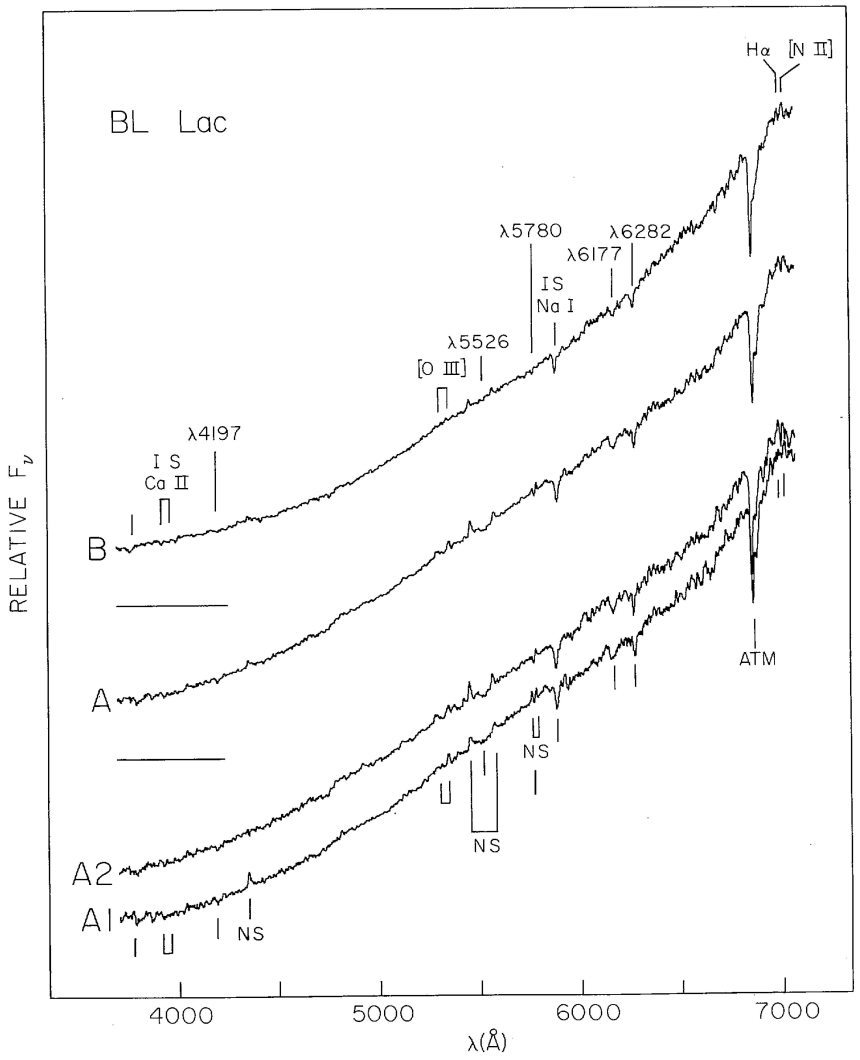

(Miller & Hawley, 1977, Fig. 1)

Most AGN show continuum variability (see later), but some show fast, large amplitude variability: blazars.

Blazars do not fit the FR 1/2 classification scheme. Typically, they show unresolved (on arcsec scales) nuclear emission.

Subclasses:

- Optically Violent Variables: OVVs: $\Delta m \gtrsim 0.1$ mag.
- BL Lac Objects: after prototype BL Lacertae (originally classified as a star, $m_B = 14$–16 mag): virtual absence of emission lines above continuum
- Flat-spectrum radio quasars (FSRQs): more luminous versions of BL Lacs

BL Lac and OVVs

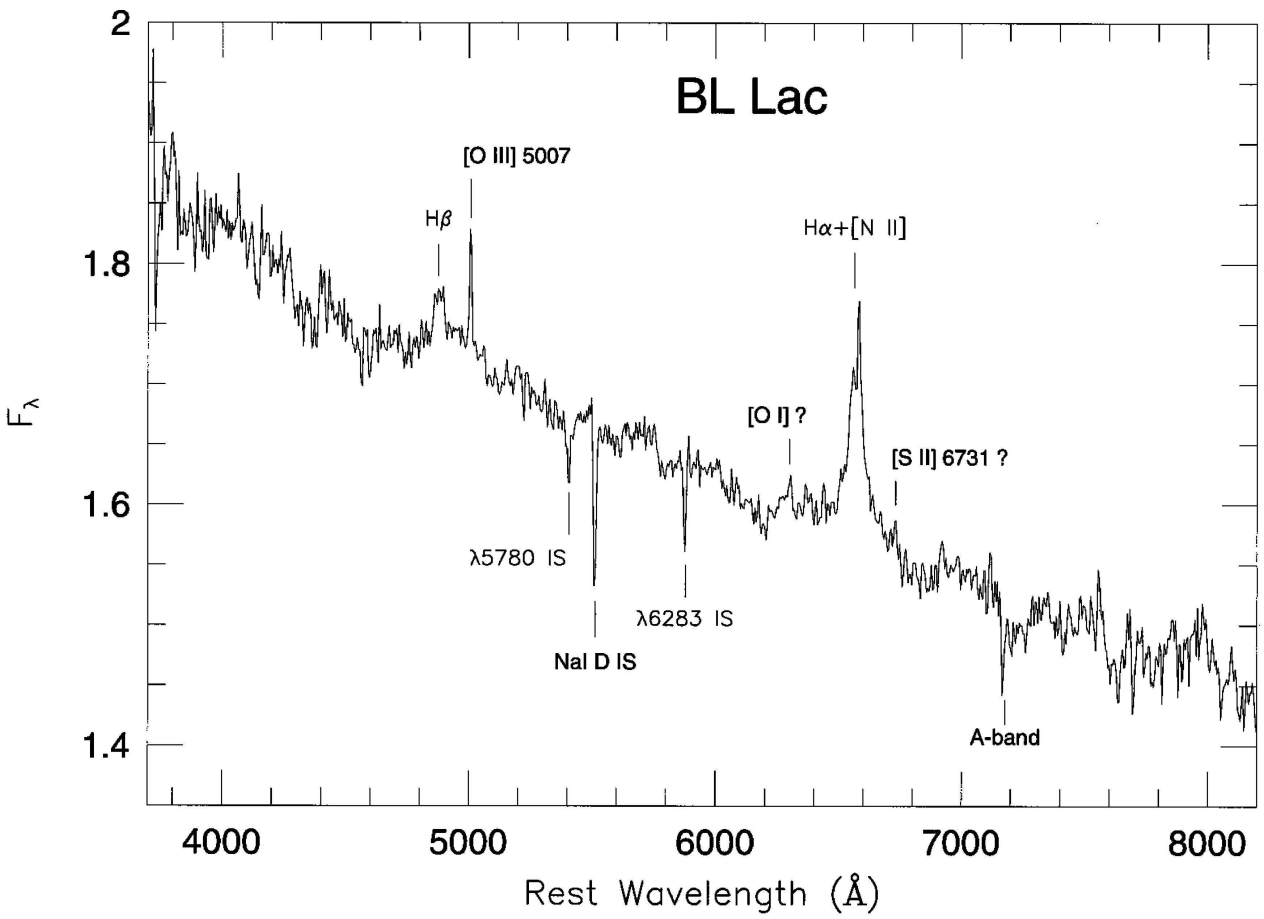

(Vermeulen et al., 1995, “When is BL Lac not a BL Lac?”, Fig. 3)

In weak phases, BL Lac shows a spectrum $F_\nu \propto \nu^{-1.7}$ (strongly polarized, synchrotron radiation) and broad emission lines $\Longrightarrow$ typical AGN continuum!

$\Longrightarrow$ There seems to be a continuum between Seyferts, QSOs, and Blazars $\Longrightarrow$

Same physics? $\Longrightarrow$ Unification.

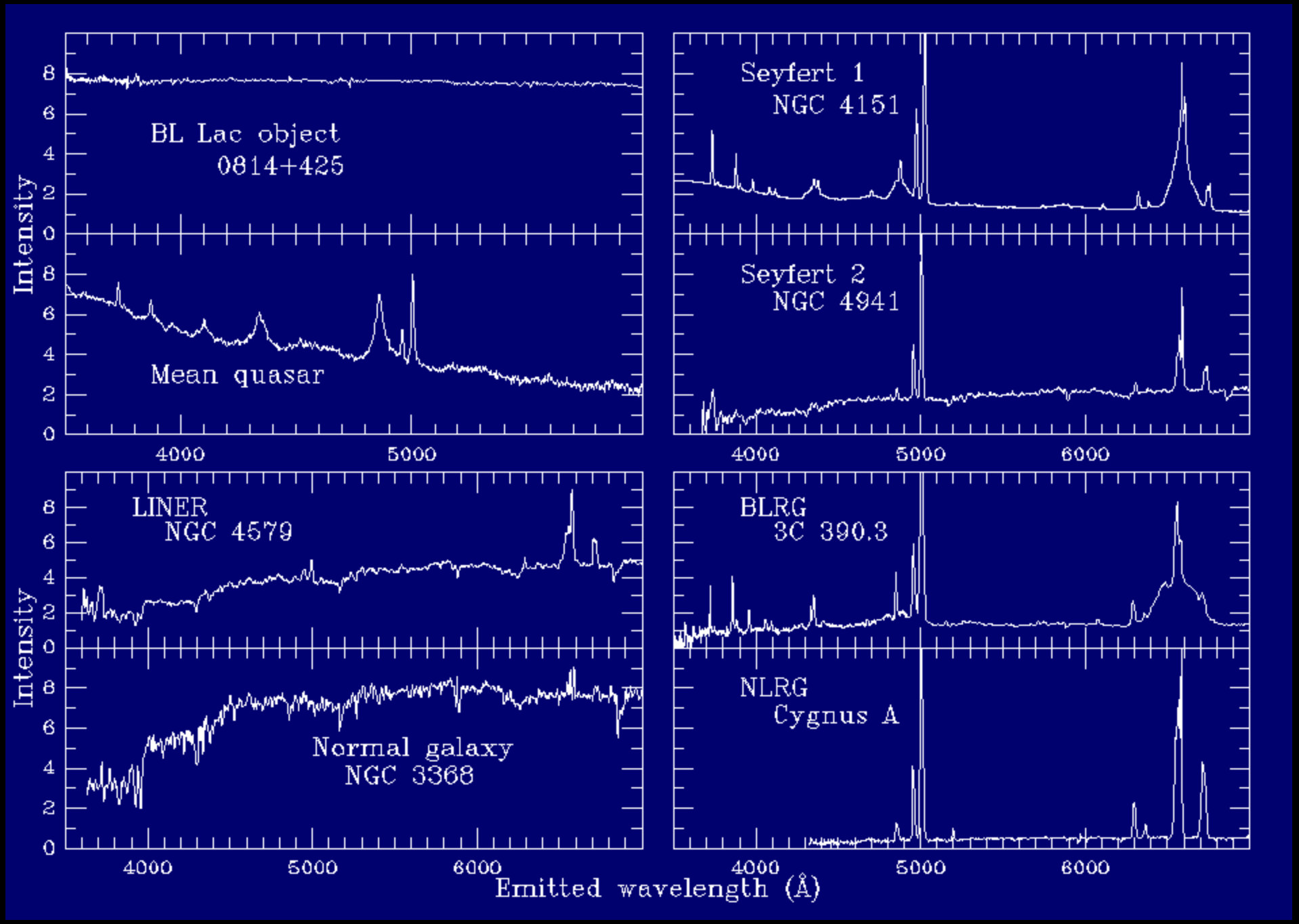

(W. Keel, priv. comm.)

Summary of optical spectra of different AGN types

Space Densities

Current space densities of various AGN (Peterson, 1997; Marzke et al., 1994):

Type	Density (Gpc^{-3})
Total Galaxy Density	
Spirals	$1.5 \times 10^7\, h_0^3$
Ellipticals	$1.0 \times 10^7\, h_0^3$
Radio Quiet AGN	
Sy 2	$8 \times 10^5\, h_0^3$
Sy 1	$3 \times 10^5\, h_0^3$
QSO	$800\, h_0^3$
Radio Loud AGN	
FR 1	$2 \times 10^4\, h_0^3$
BL Lac	$600\, h_0^3$
FR 2	$80\, h_0^3$
Radio loud QSOs	$20\, h_0^3$

$\Longrightarrow$ $\sim$10% of all galaxies are AGN.

$\Longrightarrow$ $\sim$2% of all AGN are radio loud.

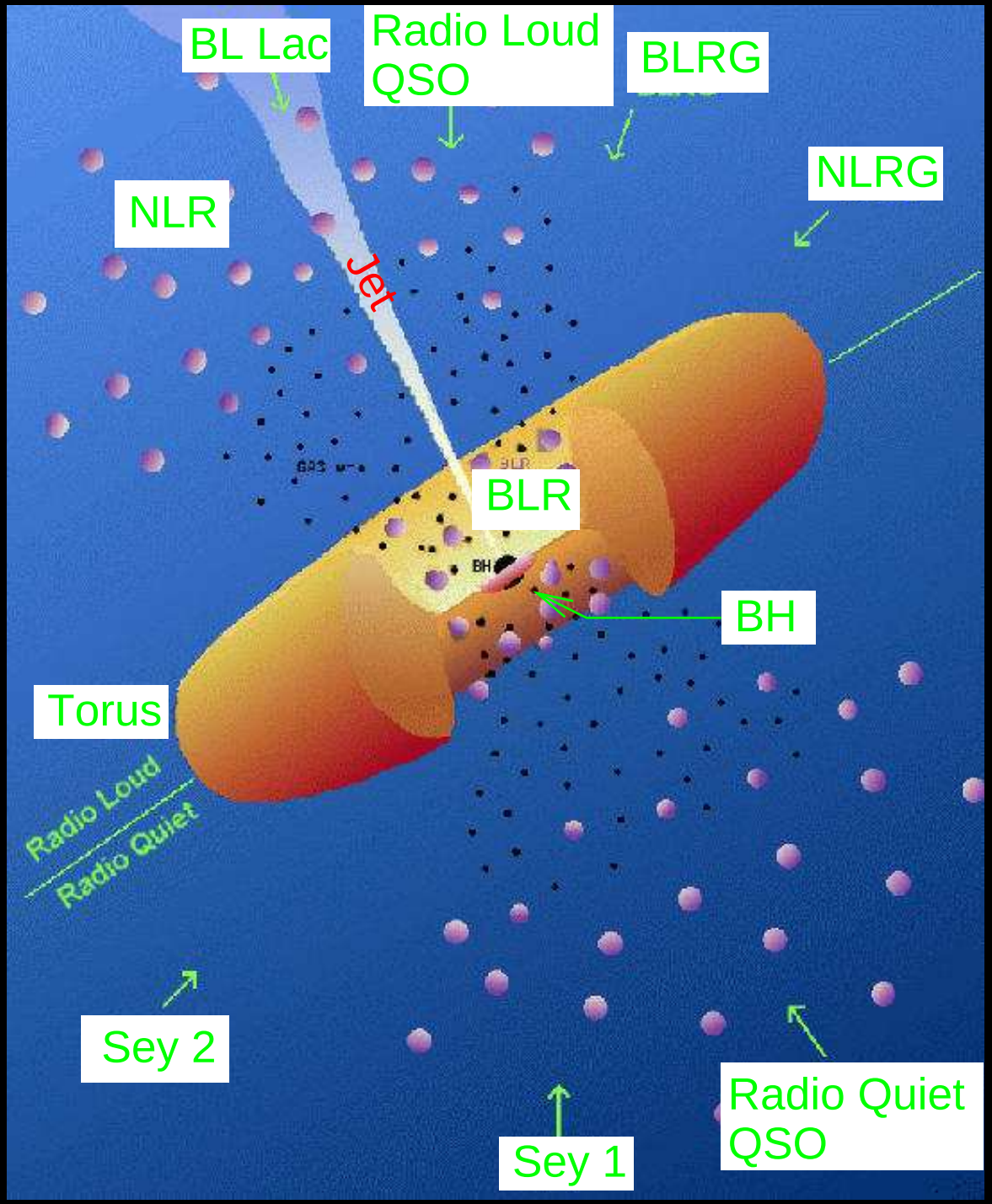

Unified Model: All AGN types are due to the same physics, different phenomenology just due to different viewing angle (and luminosity).

(Urry & Padovani, 1995, NOTE: logarithmic length scale!)

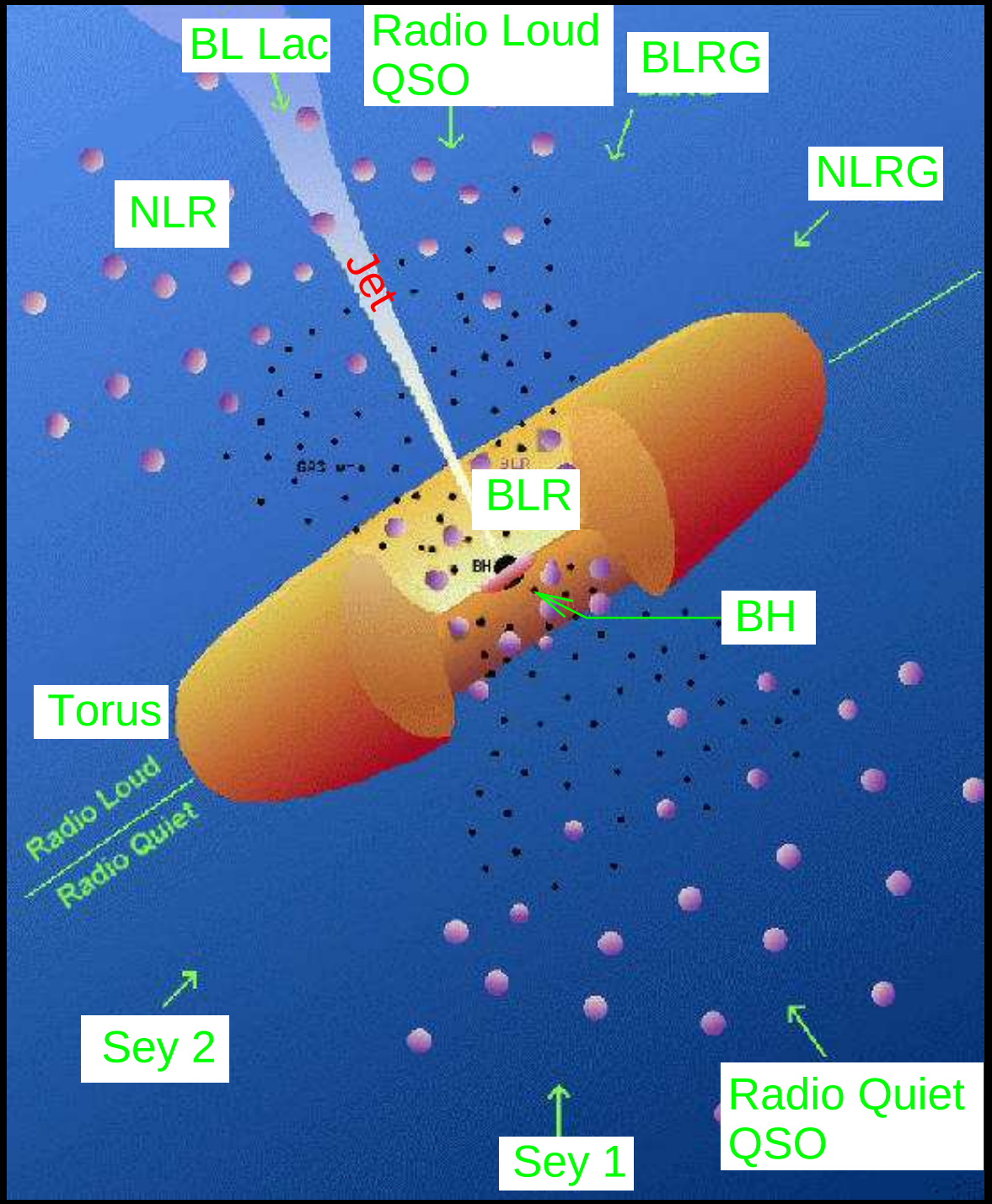

Physical properties of components:

Accretion disk: $r \sim 10^{-3}$ pc,

$n \sim 10^{15}$ cm^{-3},

$kT \sim 50$ eV $\cdot\, r^{-3/4}$,

$v \sim 0.3c$ at inner edge.

Broad Line Region (BLR):

$r \sim 0.01$–0.1 pc (=light days),

$n \sim 10^{10}$ cm^{-3},

$v \sim 1000$–5000 km s^{-1},

$T \sim 10^4$ K

Torus: $r \sim 1$– few 10 pc,

$n \sim 10^3$–10^6 cm^{-3},

T: cold

Narrow Line Region (NLR):

$r \sim 100$–1000 pc,

$n \sim 10^3$–10^6 cm^{-3},

$v \sim$ few $\cdot\, 100$ km s^{-1},

$T \sim 10^4$ K

See, e.g., Antonucci (1993) for a review.

Unification

Simplified Unification (Peterson, 1997)

Radio	*Orientation*	
Properties	Face-on	Edge-on
Radio Quiet	Seyfert 1	Seyfert 2
	QSO	Far IR Galaxy?
Radio Loud	BL Lac	FR I
	BLRG	NLRG
	Quasar/OVV	FR II

Observational Evidence: NGC 1068

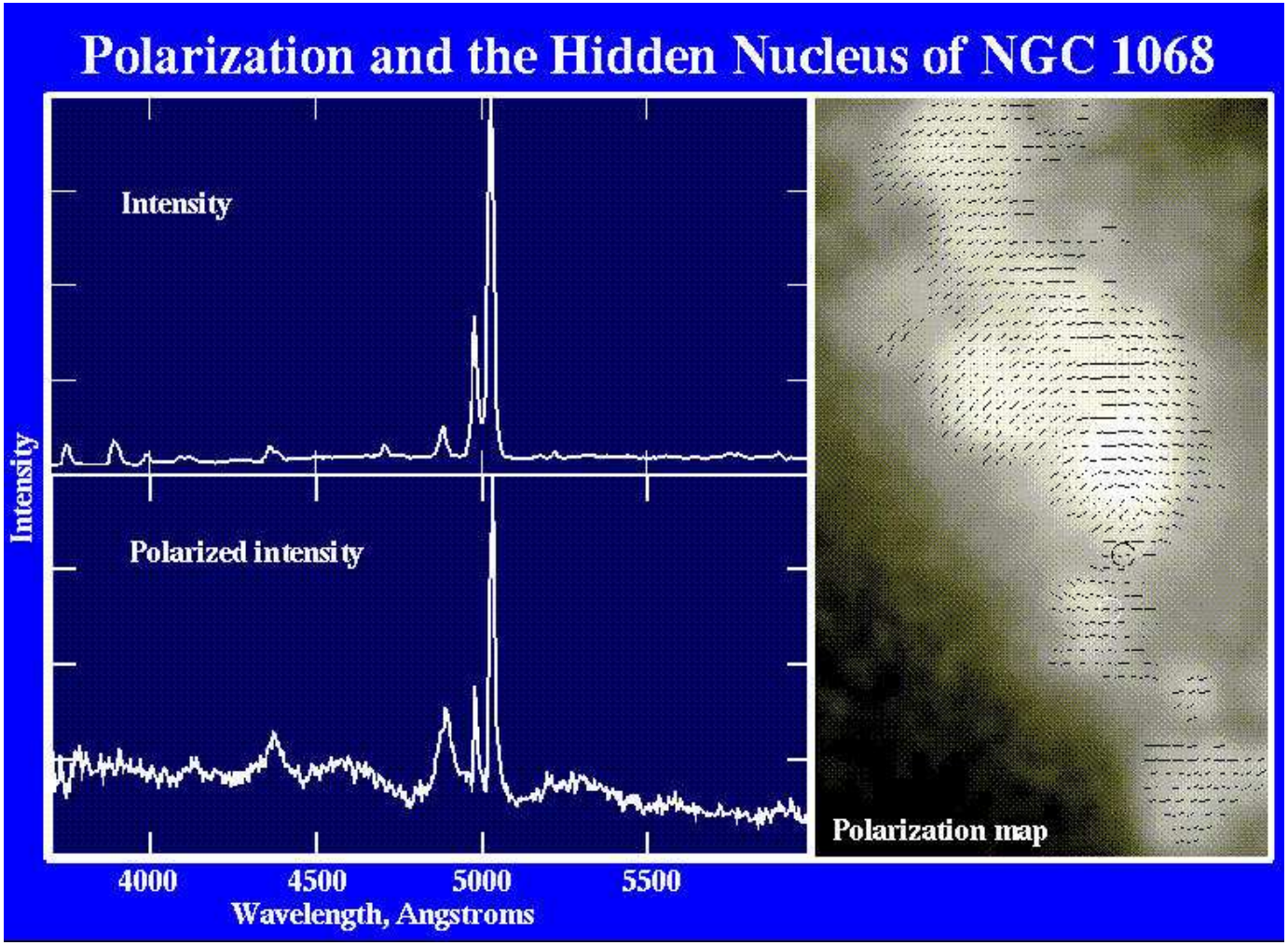

W. Keel

Antonucci & Miller (1985): In polarized light, the Seyfert 2 NGC 1068 shows broad lines and a spectrum similar to Seyfert 1 galaxies.

$\Longrightarrow$ Scattered radiation from the BLR!

16% polarization $\Longrightarrow$ single scattering (multiple scatterings would depolarize!); note that lines from NLR are *not* polarized $\Longrightarrow$ no scattering!

Observational Evidence: Spectral Variations

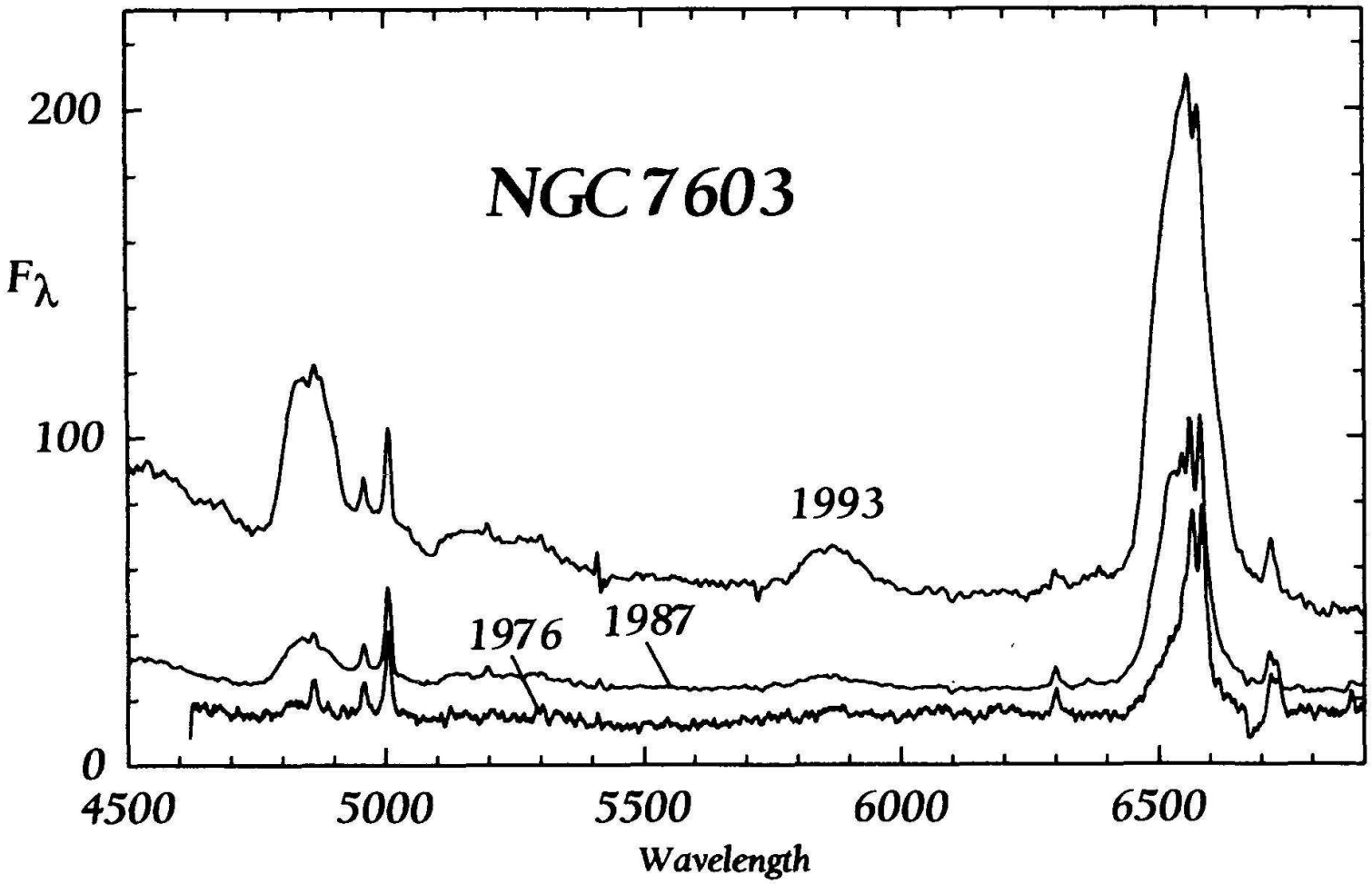

(Goodrich, 1995, Fig. 7)

Some Seyferts change type, e.g., from Sy 2 to Sy 1 within a few years.

Observational Evidence: Imaging of the Torus?

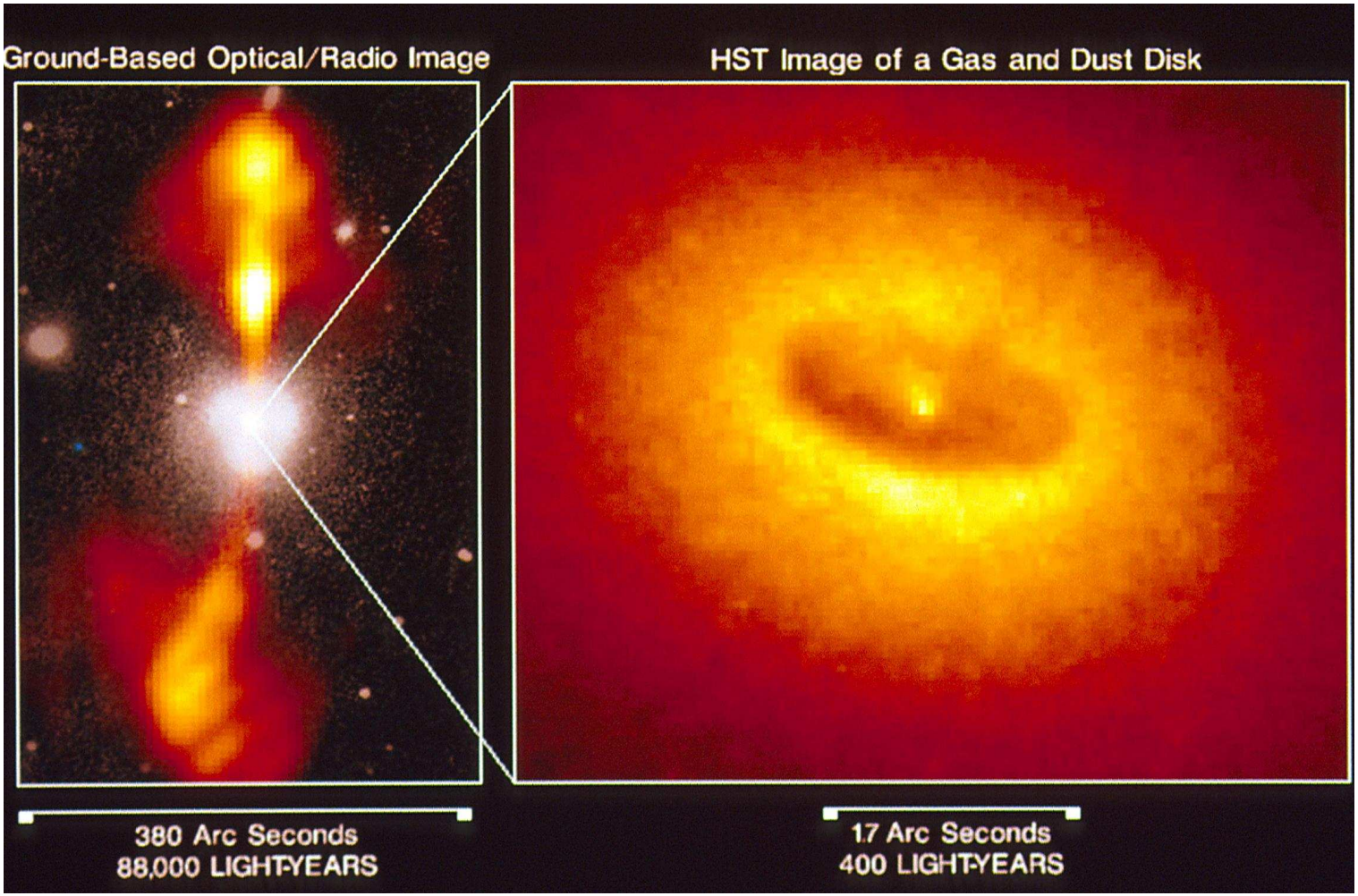

NGC 4261 (HST/WFPC)

Some nearby Seyferts show torus-like structures in their centers.

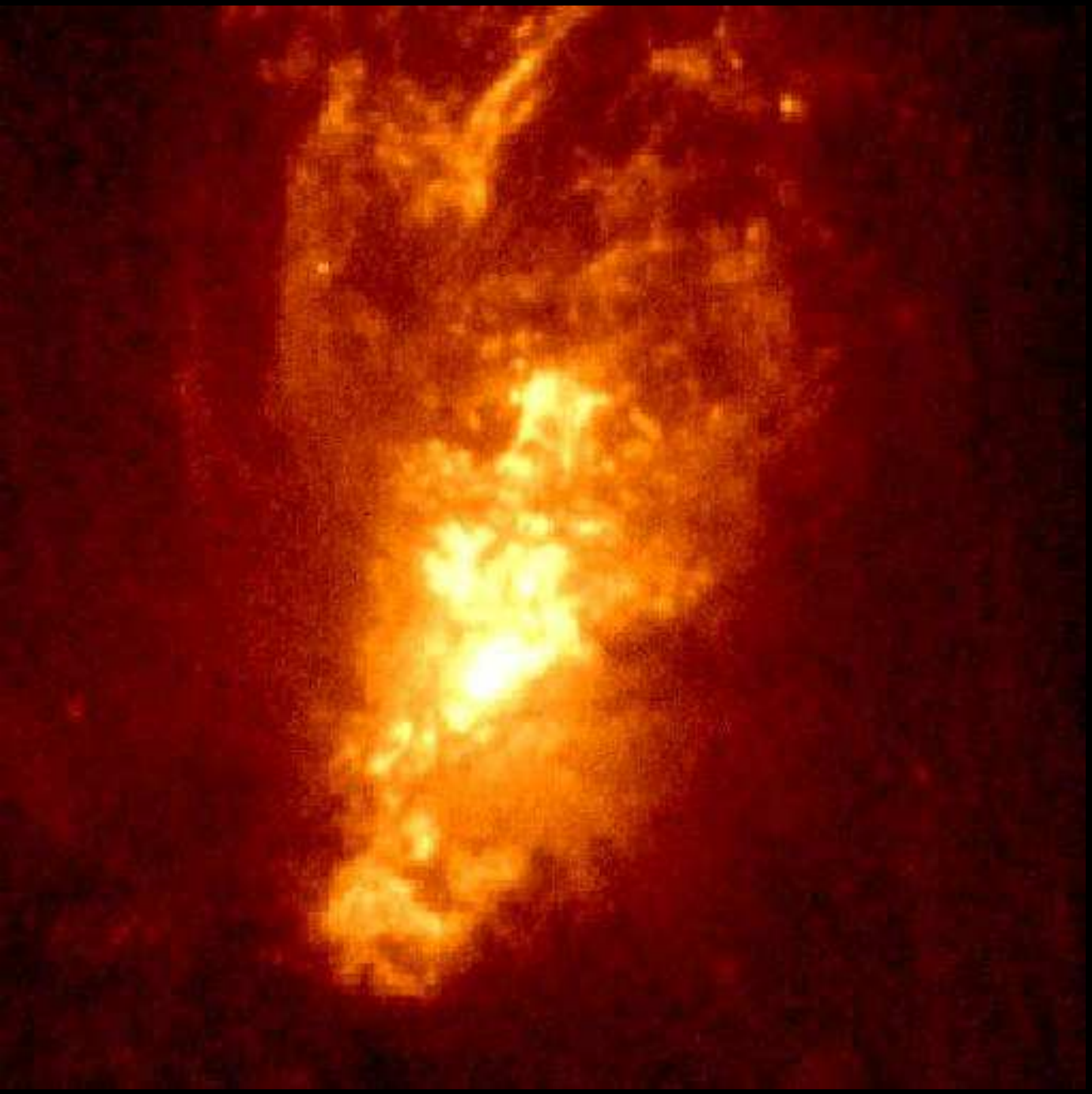

Ionization in the center of NGC 1068 (Sy 2; HST)

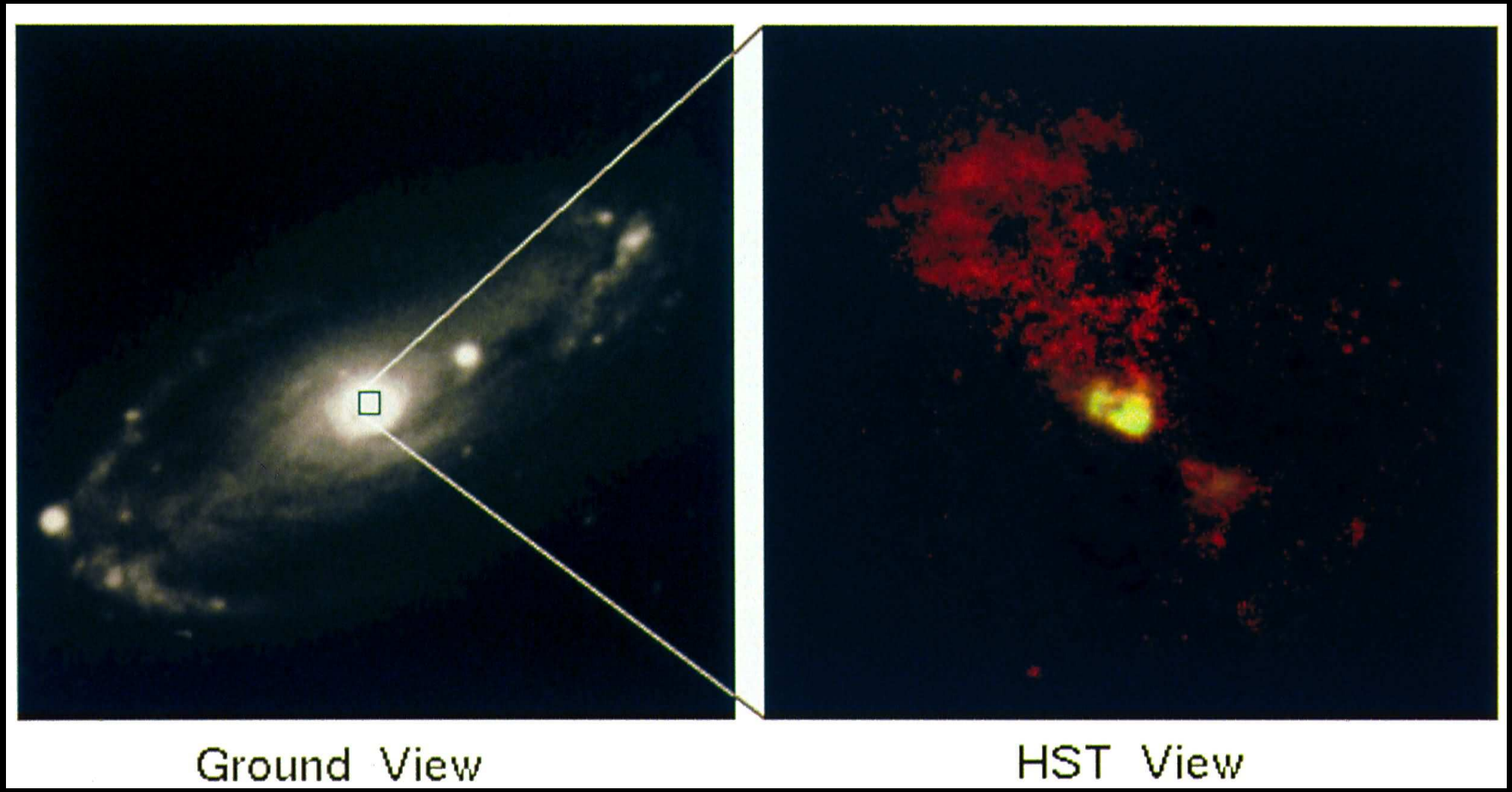

NGC 5728 (Sy 2, HST; green: [O III] $\lambda\lambda$ 4959, 5007 Å, red: Hα and [N II], $\lambda\lambda$ 6548, 6583 Å, plus continua)

Wilson et al. 1993

Ionization cone of NGC 5728: line emission of ionized species aligned with radio structure (to within 2°), *not* aligned with galaxy. Extent of structure: $\sim$1.8 kpc

Observational Evidence: Absorption

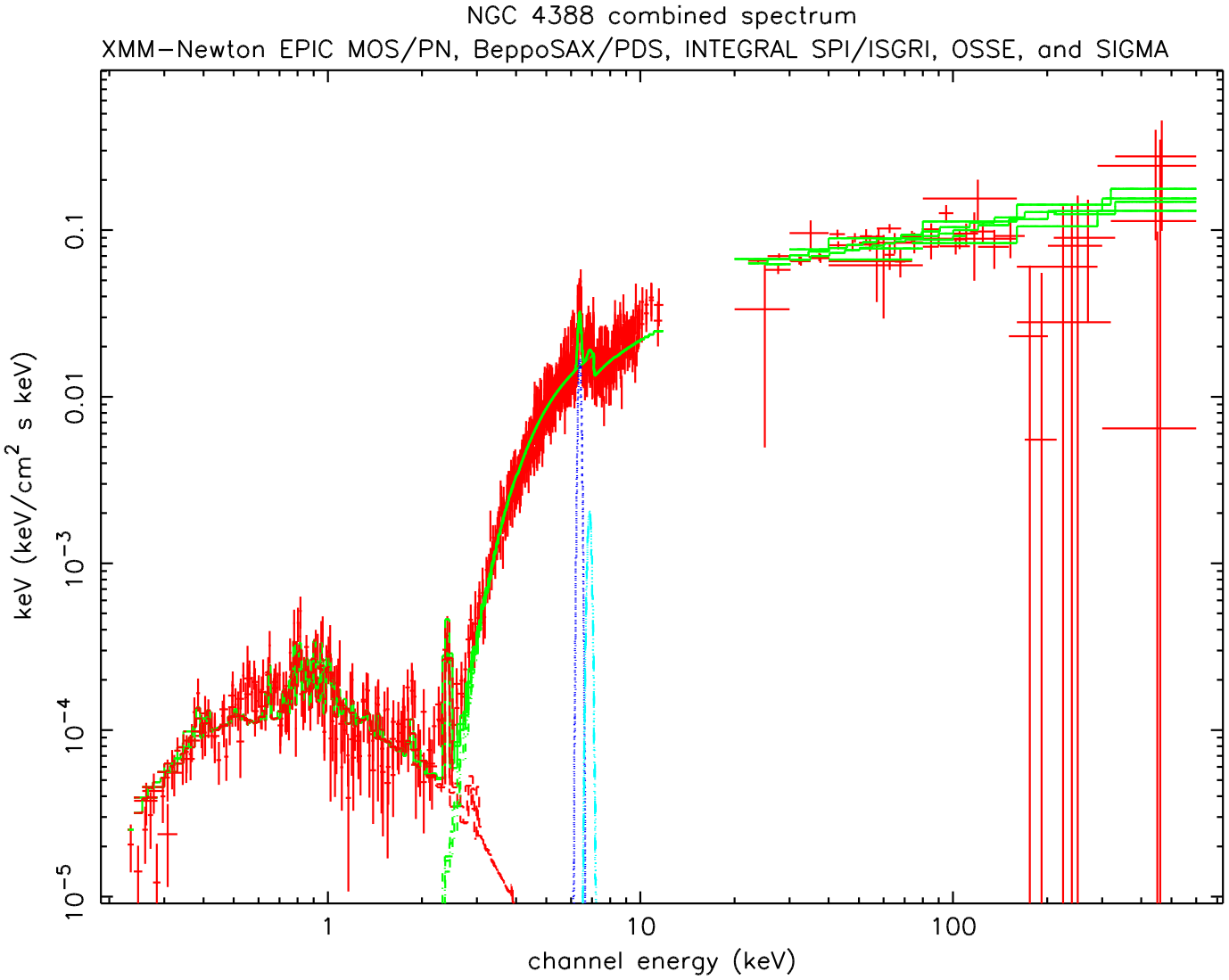

X-ray spectroscopy allows to penetrate even high columns of absorbing gas.

(Beckmann et al., 2004)

Reason: photo-absorption cross section is $\propto E^{-3}$, crosses Thomson cross section at $\sim$10 keV.

Observational Evidence: Absorption

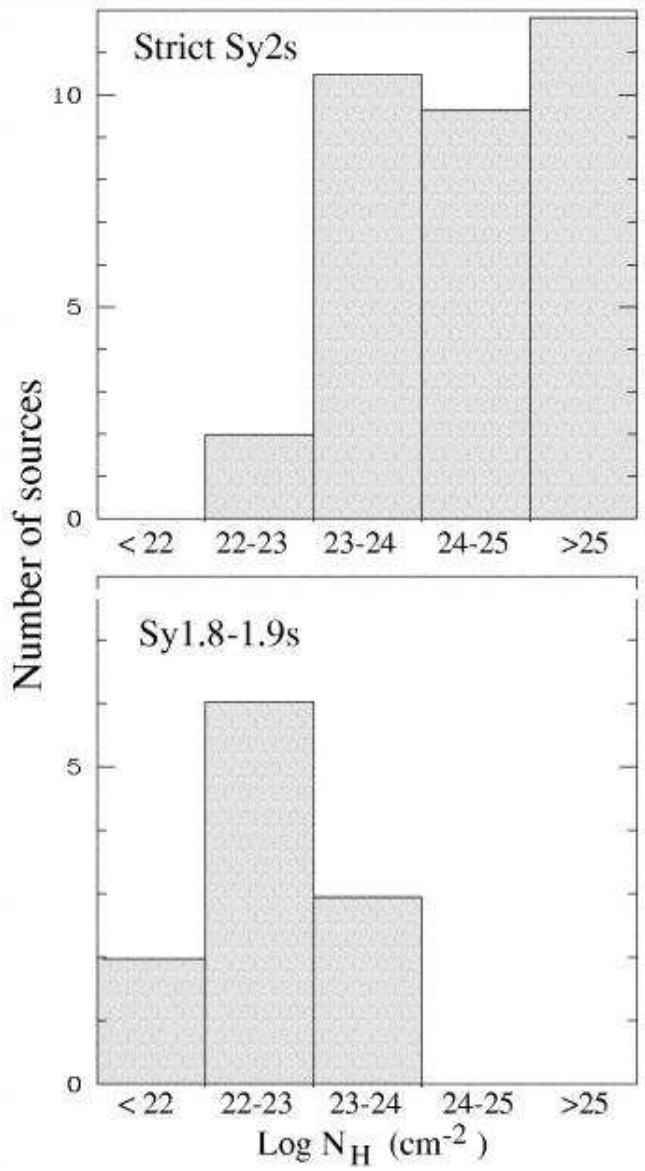

Risaliti et al. (1999): From X-ray studies:

- 75% of Seyfert 2's are heavily obscured, i.e., have $N_{\mathrm{H}} \geq 10^{23}\,\mathrm{cm}^{-2}$.
- 50% of Seyfert 2's are Compton thick, i.e., have $N_{\mathrm{H}} \geq 10^{24}\,\mathrm{cm}^{-2}$.
- N_{H} for Sy 2 is higher than that for Sy 1.8, 1.9.

where N_{H} is the column density of Hydrogen,

$$N_{\mathrm{H}} = \int_0^r n_{\mathrm{H}} dr \tag{3.3}$$

determined from X-ray absorption.

(Risaliti et al., 1999, Fig. 5)

Summary

- Puzzling zoo of AGN can be described by simple geometric model: black hole surrounded by obscuring torus
- Radio loud vs. radio quiet: presence of jet
- Observations mainly support unified model

Antonucci, R., 1993, Ann. Rev. Astron. Astrophys., 31, 473
Antonucci, R. R. J., & Miller, J. S. 1985, ApJ, 297, 621
Baldwin, J. A., Phillips, M. M., & Terlevich, R. 1981, PASP, 93, 5
Bartel, N., Shapiro, I. I., Huchra, J. P., & Kuhr, H. 1984, ApJ, 279, 112
Beckmann, V., Gehrels, N., Favre, P., et al. 2004, ApJ, 614, 641
Fanaroff, B. L., & Riley, J. M. 1974, MNRAS, 167, 31P
García-Lorenzo, B., Mediavilla, E., & Arribas, S. 1999, ApJ, 518, 190
Goodrich, R. W., 1995, ApJ, 440, 141
Ho, L. C., 1996, in The Physics of Liners in View of Recent Observations, ed. M. Eracleous, A. Koratkar, C. Leitherer, L. Ho, Astron. Soc. Pacific, Conf. Ser. 103, 103
Irwin, M. J., Ibata, R. A., Lewis, G. F., & Totten, E. J. 1998, ApJ, 505, 529
Kellermann, K. I., Sramek, R., Schmidt, M., Shaffer, D. B., & Green, R. 1989, AJ, 98, 1195
Laing, R. A., & Bridle, A. H. 1987, MNRAS, 228, 557
Lawrence, A., 1987, PASP, 99, 309
Marzke, R. O., Geller, M. J., Huchra, J. P., & Corwin, Jr., H. G. 1994, AJ, 108, 437
Miller, J. S., & Hawley, S. A. 1977, ApJ, 212, L47
Peterson, B. M., 1997, An Introduction to Active Galactic Nuclei, (Cambridge: Cambridge Univ. Press)
Risaliti, G., Maiolino, R., & Salvati, M. 1999, ApJ, 522, 157
Türler, M., Paltani, S., Courvoisier, T. J.-L., et al. 1999, A&AS, 134, 89
Urry, C. M., & Padovani, P. 1995, PASP, 107, 803
Vanden Berk, D. E., Richards, G. T., Bauer, A., et al. 2001, AJ, 122, 549
Veilleux, S., & Osterbrock, D. E. 1987, ApJS, 63, 295
Vermeulen, R. C., Ogle, P. M., Tran, H. D., et al. 1995, ApJ, 452, L5
Wilson, A. S., Braatz, J. A., Heckman, T. M., Krolik, J. H., & Miley, G. K. 1993, ApJ, 419, L61

Accretion and Accretion Disks

Introduction

AGN are powered by accretion

$\Longrightarrow$ need to look at accretion as a physical mechanism.

Unfortunately, this will have to be somewhat theoretical, but this cannot be avoided...

Structure of this chapter:

1. Accretion Luminosity: Eddington luminosity
2. Accretion Disks: Theory
3. Accretion Disks: Confrontation with observations

Literature

- J. Frank, A. King, D. Raine, 2002, Accretion Power in Astrophysics, 3rd edition, Cambridge Univ. Press

  The standard textbook on accretion, covering all relevant areas of the field.

- T. Padmanabhan, 2001, Theoretical Astrophysics, II. Stars and Stellar Systems, Cambridge Univ. Press

  See introduction to this lecture.

- N.I. Shakura & R. Sunyaev, 1973, Black Holes in Binary Systems. Observational Appearance. Astron. Astrophys. **24**, 337

  The fundamental paper, which *really* started the field.

- J.E. Pringle, 1981, Accretion Disks in Astrophysics, Ann. Rev. Astron. Astrophys. **19**, 137

  Concise review of classical accretion disk theory.

Eddington luminosity

Assume mass M

Eddington luminosity

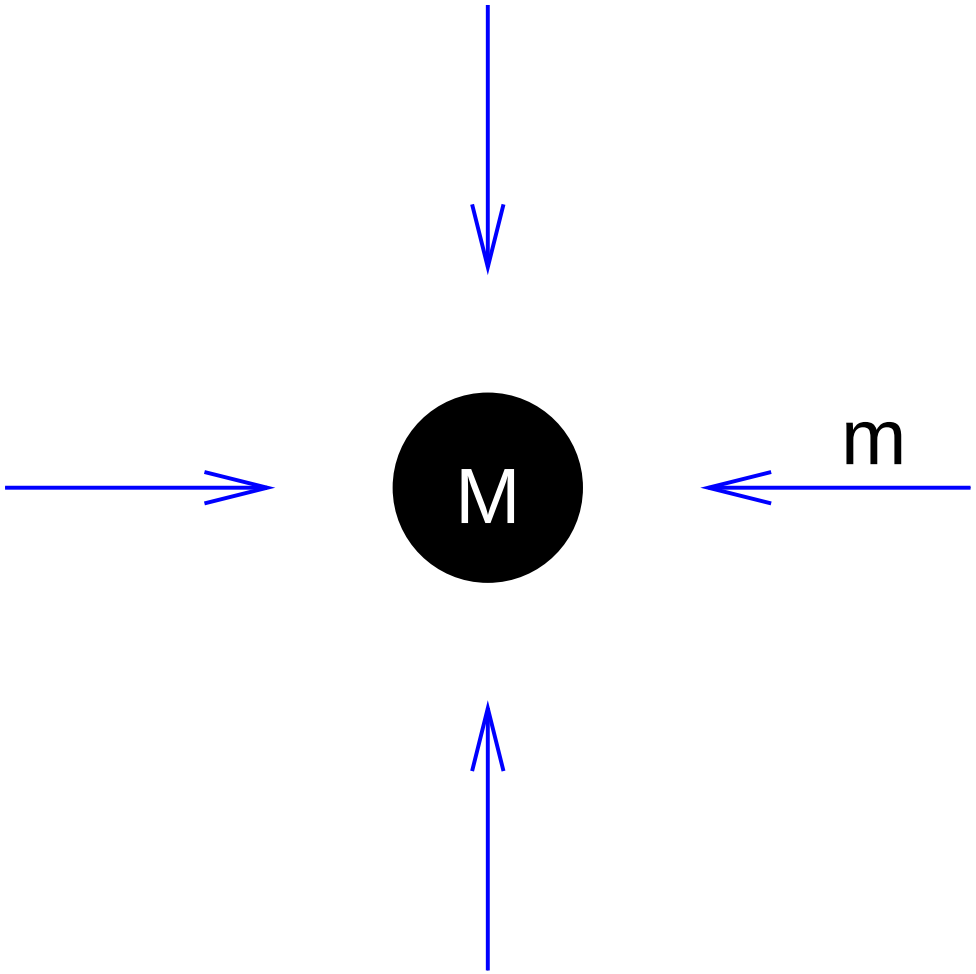

Assume mass M spherically symmetrically accreting ionized hydrogen gas.

Eddington luminosity

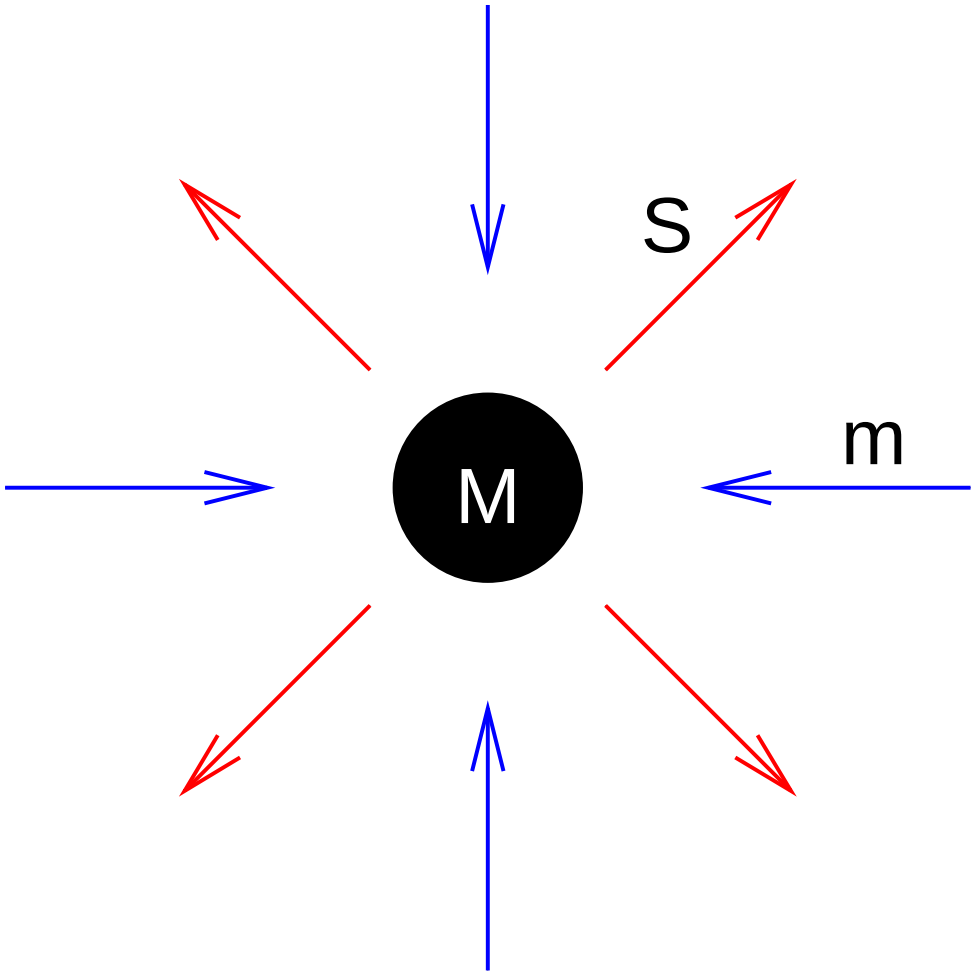

Assume mass M spherically symmetrically accreting ionized hydrogen gas.

At radius r, accretion produces energy flux S.

Eddington luminosity

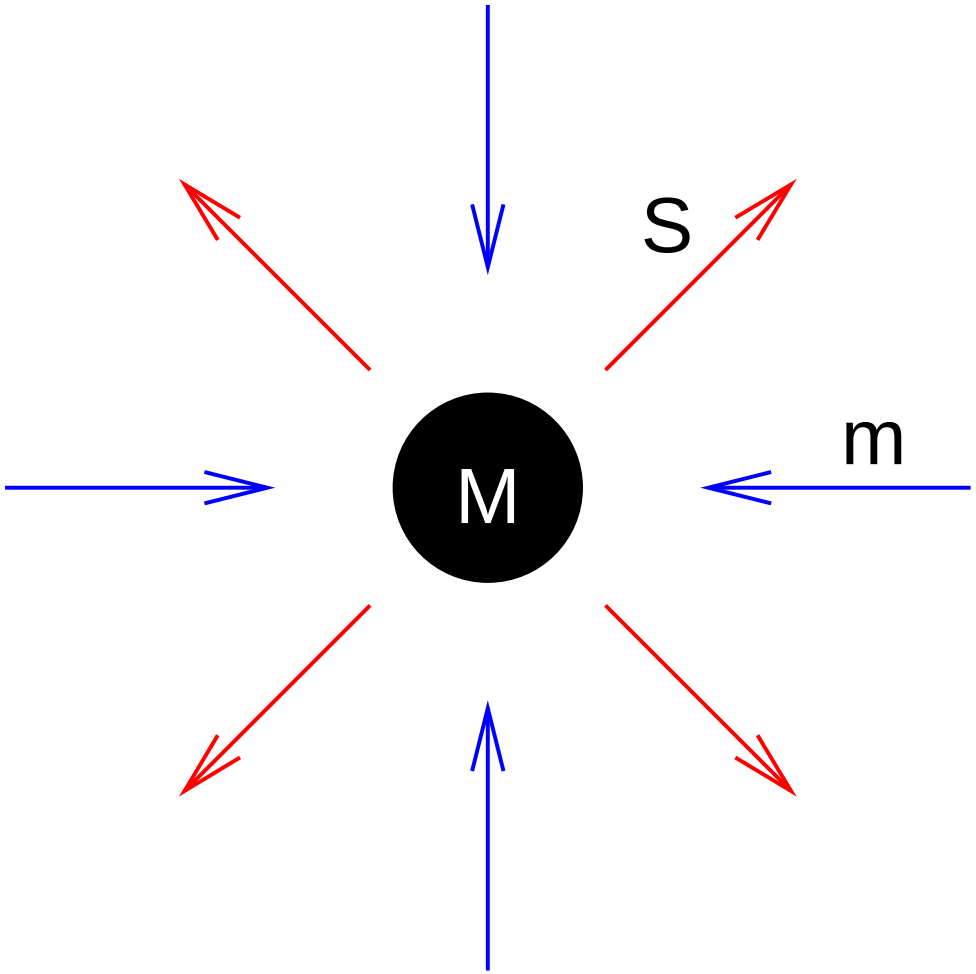

Assume mass M spherically symmetrically accreting ionized hydrogen gas.

At radius r, accretion produces energy flux S.

Important: Interaction between accreted material and radiation!

Eddington luminosity

Force balance on accreted electrons and protons:

Eddington luminosity

Force balance on accreted electrons and protons:

Inward force: gravitation:

$$F_{\mathrm{g}} = \frac{GMm_{\mathrm{p}}}{r^2} \tag{4.1}$$

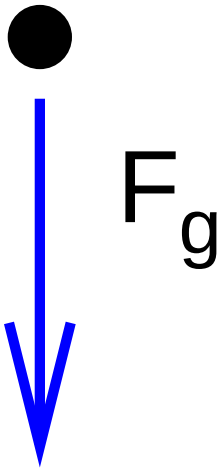

Eddington luminosity

Force balance on accreted electrons and protons:

Inward force: gravitation:

$$F_{\mathrm{g}} = \frac{GMm_{\mathrm{p}}}{r^2} \tag{4.2}$$

Outward force: radiation force:

$$F_{\mathrm{rad}} = \frac{\sigma_{\mathrm{T}} S}{c} \tag{4.3}$$

where energy flux S is given by

$$S = \frac{L}{4\pi r^2} \tag{4.4}$$

where L: luminosity.

Eddington luminosity

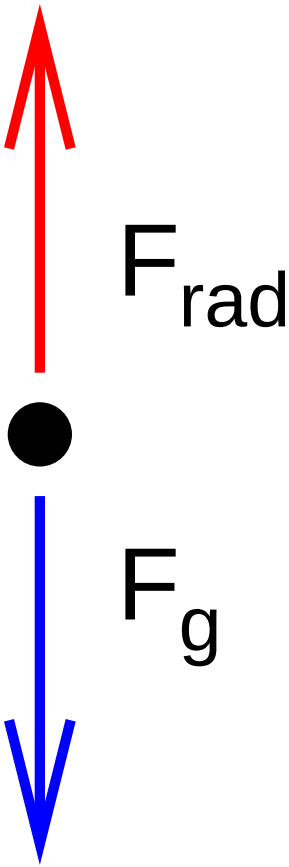

Force balance on accreted electrons and protons:

Inward force: gravitation:

$$F_{\mathrm{g}} = \frac{GMm_{\mathrm{p}}}{r^2} \tag{4.5}$$

Outward force: radiation force:

$$F_{\mathrm{rad}} = \frac{\sigma_{\mathrm{T}} S}{c} \tag{4.6}$$

where energy flux S is given by

$$S = \frac{L}{4\pi r^2} \tag{4.7}$$

where L: luminosity.

Note: $\sigma_{\mathrm{T}} \propto (m_{\mathrm{e}}/m_{\mathrm{p}})^2$, so negligable for protons.

But: strong Coulomb coupling between electrons and protons $\Longrightarrow$ F_{rad} also has effect on protons!

Eddington luminosity

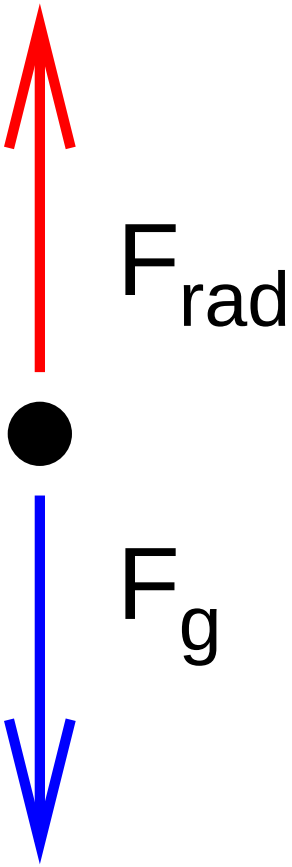

Accretion is only possible if gravitation dominates:

$$\frac{GMm_\mathrm{p}}{r^2} > \frac{\sigma_\mathrm{T} S}{c} = \frac{\sigma_\mathrm{T}}{c} \cdot \frac{L}{4\pi r^2} \tag{4.8}$$

and therefore

$$L < L_\mathrm{Edd} = \frac{4\pi G M m_\mathrm{p} c}{\sigma_\mathrm{T}} \tag{4.9}$$

or, in astronomically meaningful units

$$L < 1.3 \times 10^{38}\,\mathrm{erg\,s^{-1}} \cdot \frac{M}{M_\odot} \tag{4.10}$$

where L_Edd is called the Eddington luminosity.

But remember the assumptions entering the derivation: spherically symmetric accretion of fully ionized pure hydrogen gas.

Eddington luminosity

Characterize accretion process through the accretion efficiency, η:

$$L = \eta \cdot \dot{M} c^2 \tag{4.11}$$

where $\dot{M}$: mass accretion rate (e.g., g s^{-1} or $M_\odot$ yr^{-1}).

Therefore maximum accretion rate ("Eddington rate"):

$$\dot{m} = \frac{L_{\mathrm{Edd}}}{\eta c^2} \sim 2 \cdot \left(\frac{M}{10^8\, M_\odot} \right)\ M_\odot\,\mathrm{yr}^{-1} \tag{4.12}$$

(for $\eta = 0.1$)

Emitted spectrum

Characterize photon by its radiation temperature, T_{rad}:

$$h\nu \sim kT_{\text{rad}} \quad \Longrightarrow \quad T_{\text{rad}} = h\nu/k \tag{4.13}$$

Emitted spectrum

Characterize photon by its radiation temperature, $T_{\rm rad}$:

$$h\nu \sim kT_{\rm rad} \quad \Longrightarrow \quad T_{\rm rad} = h\nu/k \tag{4.14}$$

Optically thick medium: blackbody radiation

$$T_{\rm b} = \left(\frac{L}{4\pi R^2 \sigma_{\rm SB}} \right)^{1/4} \tag{4.15}$$

Emitted spectrum

Characterize photon by its radiation temperature, T_{rad}:

$$h\nu \sim kT_{\mathrm{rad}} \quad \Longrightarrow \quad T_{\mathrm{rad}} = h\nu/k \tag{4.16}$$

Optically thick medium: blackbody radiation

$$T_{\mathrm{b}} = \left(\frac{L}{4\pi R^2 \sigma_{\mathrm{SB}}} \right)^{1/4} \tag{4.17}$$

Optically thin medium: L directly converted into radiation without further interactions $\Longrightarrow$ mean particle energy

$$T_{\mathrm{th}} = \frac{GMm_{\mathrm{p}}}{3kR} \tag{4.18}$$

Emitted spectrum

Characterize photon by its radiation temperature, T_{rad}:

$$h\nu \sim kT_{\text{rad}} \quad \Longrightarrow \quad T_{\text{rad}} = h\nu/k \tag{4.19}$$

Optically thick medium: blackbody radiation

$$T_{\text{b}} = \left(\frac{L}{4\pi R^2 \sigma_{\text{SB}}} \right)^{1/4} \tag{4.20}$$

Optically thin medium: L directly converted into radiation without further interactions $\Longrightarrow$ mean particle energy

$$T_{\text{th}} = \frac{GMm_{\text{p}}}{3kR} \tag{4.21}$$

Plugging in numbers for a typical solar mass compact object (NS/BH):

$$T_{\text{rad}} \sim 1\,\text{keV} \quad \text{and} \quad T_{\text{bb}} \sim 50\,\text{MeV} \tag{4.22}$$

Accreting objects are broadband emitters in the X-rays and gamma-rays.

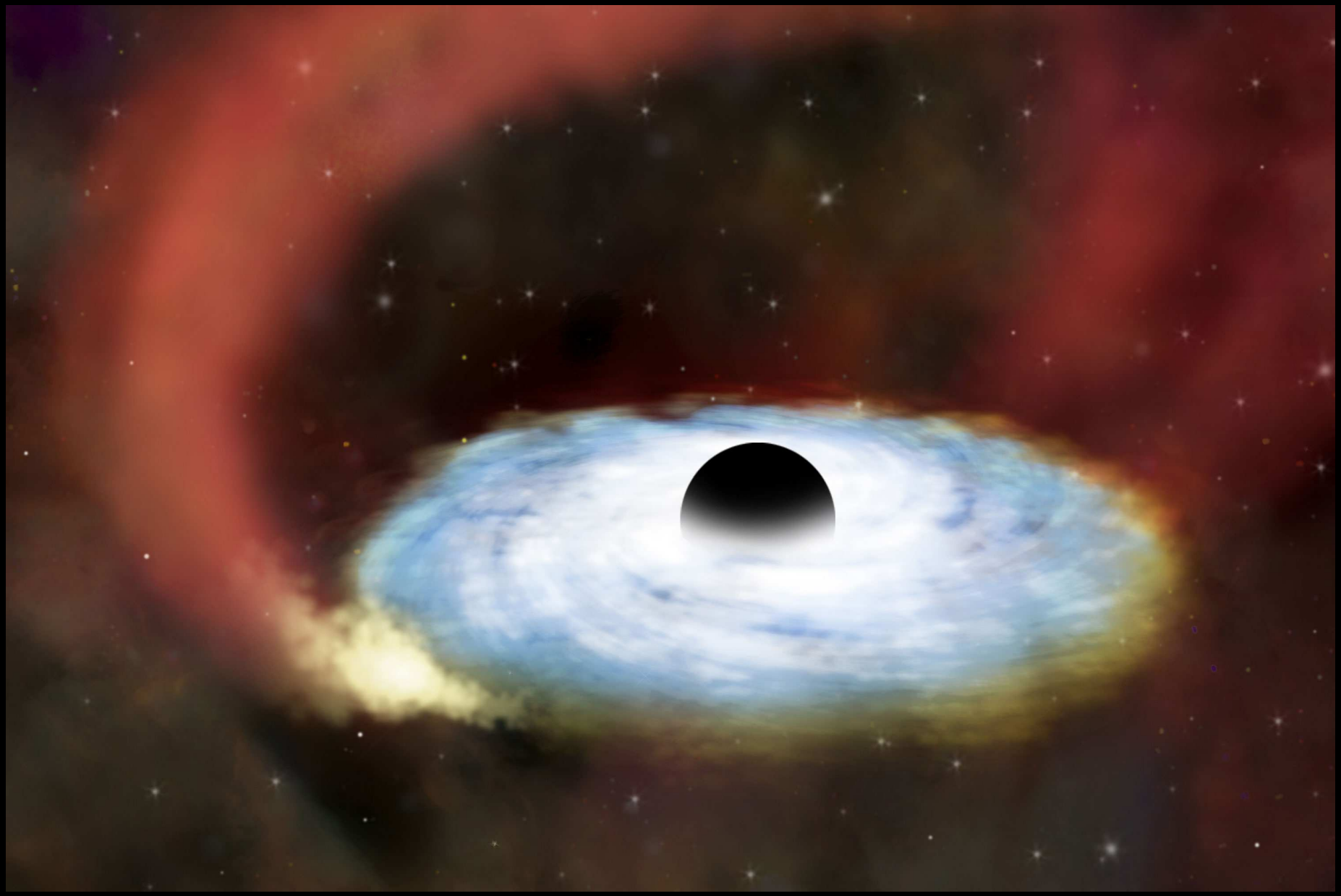

NASA/CXC/SAO

Source of matter: probably disrupted stars

$\Longrightarrow$ accreted matter has angular momentum

$\Longrightarrow$ accretion disk forms.

Thin Disks

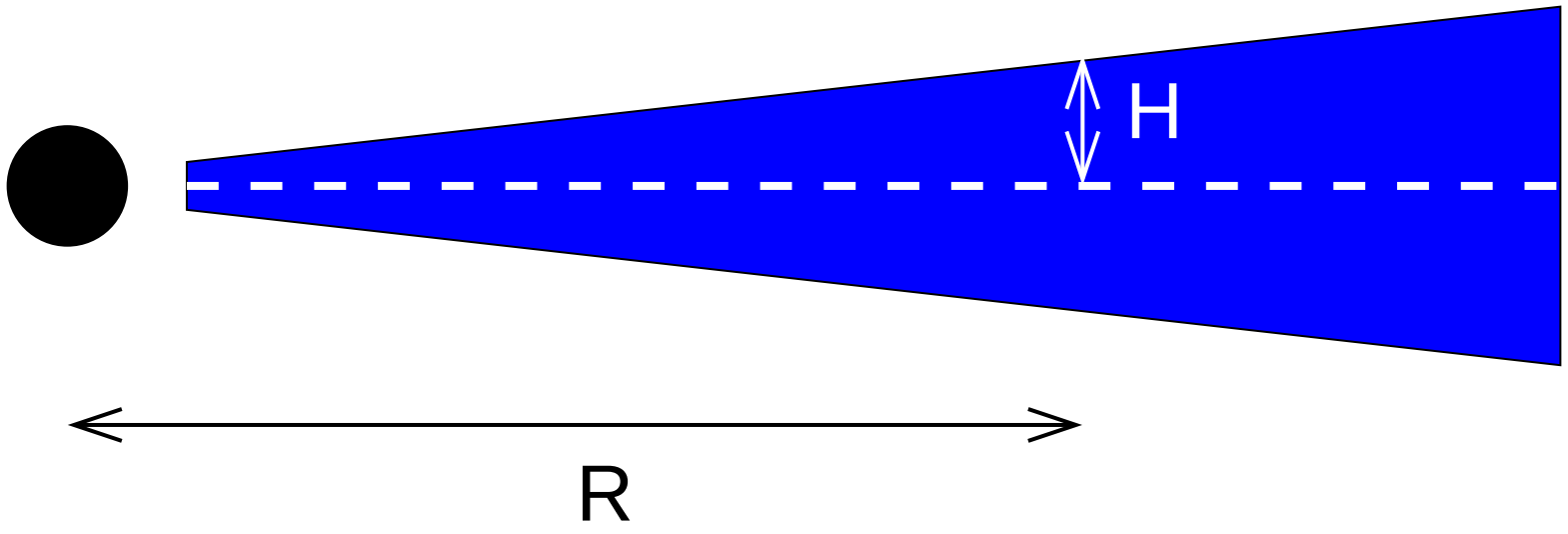

Most important case: thin accretion disks, i.e., vertical thickness, H, much smaller than radius R:

$$H \ll R \tag{4.23}$$

$\Longrightarrow$ Requires that radiation pressure is negligable

$\Longrightarrow$ $L \ll L_{\text{Edd}}$

Thin Disks

Most important result of disk theory: temperature profile

Exact calculations show:

$$T(r) = \left\{ \frac{3GM\dot{M}}{4\pi r^3 \sigma_{\rm SB}} \left[1 - \left(\frac{R_*}{r} \right)^{1/2} \right] \right\}^{1/4}$$

$$= 6.8 \times 10^5\,{\rm K} \cdot \eta^{-1/4} \left(\frac{L}{L_{\rm Edd}} \right)^{1/2} L_{46}^{-1/4} \mathcal{R}^{1/4} x^{-3/4} \quad (4.24)$$

where $\eta = L_{\rm Edd}/\dot{M}_{\rm Edd}c^2$, $x = c^2 r/2GM$, $\mathcal{R} = (1 - (R_*/r)^{1/2})$.

Radial dependence of T:

$$T(r) \propto r^{-3/4}$$

Dependence on mass (note: for BH inner radius $R_* \propto M$!):

$$T_{\rm in} \propto (\dot{M}/M^2)^{1/4}$$

AGN disks are colder than disks around galactic BH

Thin Disks: Emitted Spectrum

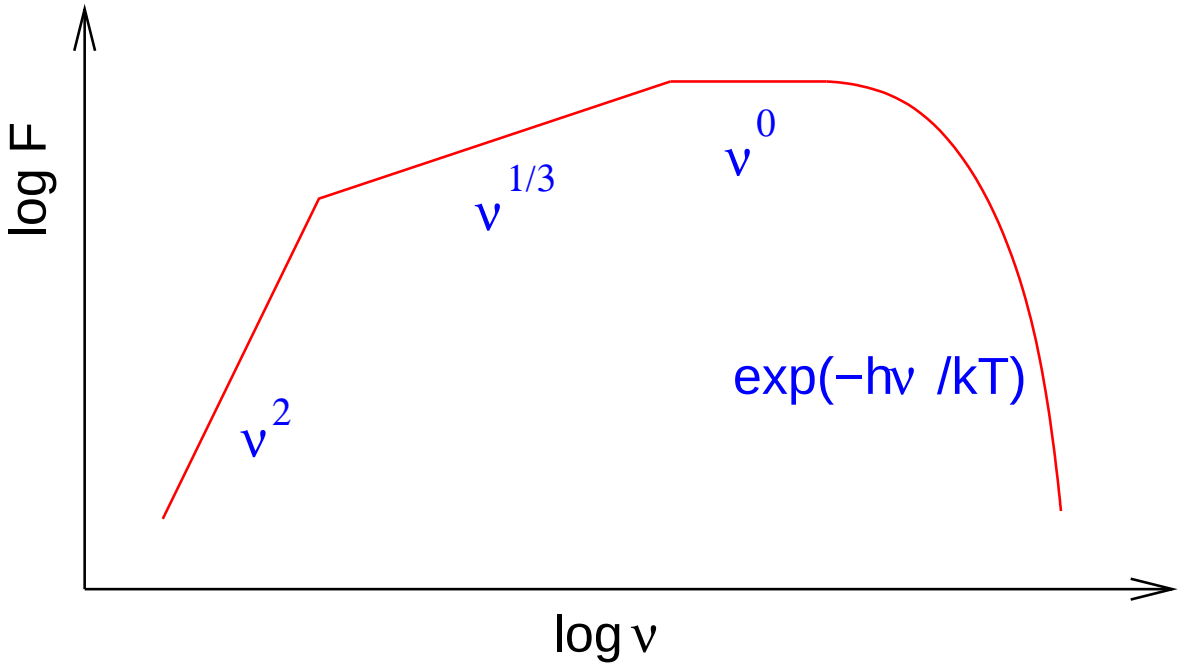

If disk is optically thick, then locally emitted spectrum is a black body, $B_\nu(T(r))$.

Total emitted spectrum obtained by integrating over disk

$$F_\nu = \int_{R_*}^{R_{\text{out}}} B_\nu(T(r))\, 2\pi r\, dr \tag{4.25}$$

The resulting spectrum looks essentially like a stretched black body.

Thin Disks: Emitted Spectrum

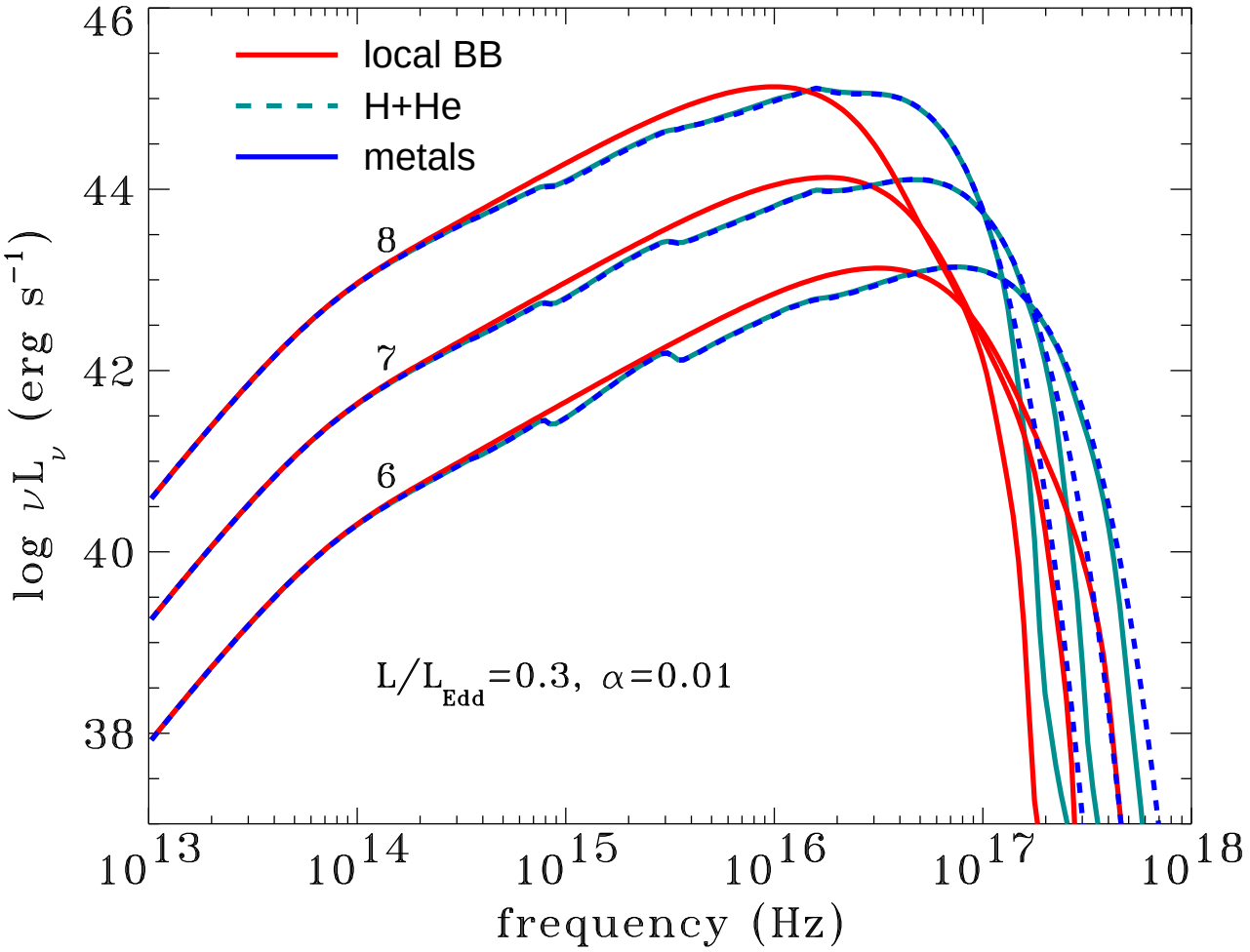

Hubeny et al., 2001, Fig. 13

In reality: accretion disk spectrum depends on

- elemental composition (“metallicity”)
- viscosity (“α-parameter”)
- ionization state and luminosity of disk ($\dot{M}$)
- properties of compact object

and many further parameters

Until today: no really satisfactory disk model available.

Thin Disks: Emitted Spectrum

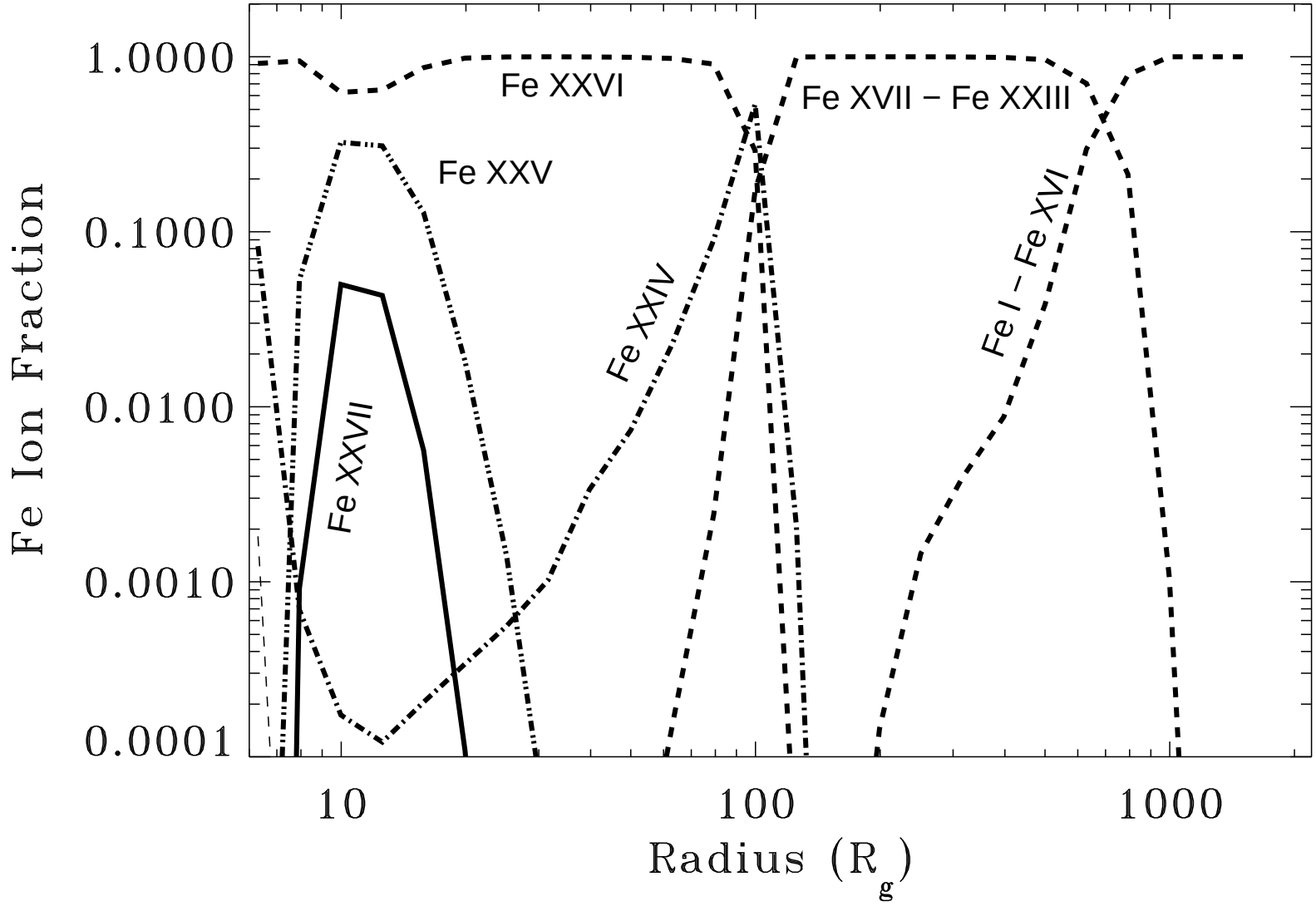

Fe species in a disk around a Galactic BH (Davis et al., 2005, Fig. 6)

Viscosity

Most important unknown in accretion disk theory: viscosity

even though it dropped out of $T(r)$!

Earth: viscosity of fluids typically due to molecular interactions (molecular viscosity).

Kinematic viscosity:

$$\nu_{\mathrm{mol}} \sim \lambda_{\mathrm{mfp}} c_{\mathrm{s}} \tag{4.26}$$

where the mean free path

$$\lambda_{\mathrm{mfp}} \sim \frac{1}{n\sigma} \sim 6.4 \times 10^4 \left(\frac{T^2}{n}\right) \,\mathrm{cm} \tag{4.27}$$

and the speed of sound

$$c_{\mathrm{s}} \sim 10^4 T^{1/2} \,\mathrm{cm\,s^{-1}} \tag{4.28}$$

such that

$$\nu_{\mathrm{mol}} \sim 6.4 \times 10^8 \, T^{5/2} n^{-1} \,\mathrm{cm^2\,s^{-1}} \tag{4.29}$$

Viscosity

Viscosity is important for small Reynolds numbers ("laminar flow"), where

$$\mathrm{Re} = \frac{\text{inertial force}}{\text{viscous force}} \sim \frac{\rho R v}{\rho \nu} = \frac{R v}{\nu} \tag{4.30}$$

Follows from Navier-Stokes Equations

Using typical accretion disk parameters:

$$\mathrm{Re}_{\mathrm{mol}} \sim 2 \times 10^{14} \left(\frac{M}{M_\odot}\right)^{1/2} \left(\frac{R}{10^{10}\,\mathrm{cm}}\right)^{1/2} \left(\frac{n}{10^{15}\,\mathrm{cm}^{-3}}\right) \left(\frac{T}{10^{4}\,\mathrm{K}}\right)^{-5/2} \tag{4.31}$$

$\Longrightarrow$ Molecular viscosity is irrelevant for astrophysical disks!

since $\mathrm{Re} \gtrsim 10^3$: turbulence $\Longrightarrow$ Shakura & Sunyaev posit turbulent viscosity

$$\nu_{\mathrm{turb}} \sim v_{\mathrm{turb}} \ell_{\mathrm{turb}} \sim \alpha\, c_{\mathrm{s}} \cdot H \tag{4.32}$$

where $\alpha \lesssim 1$ and $\ell_{\mathrm{turb}} \lesssim H$ typical size for turbulent eddies.

Viscosity

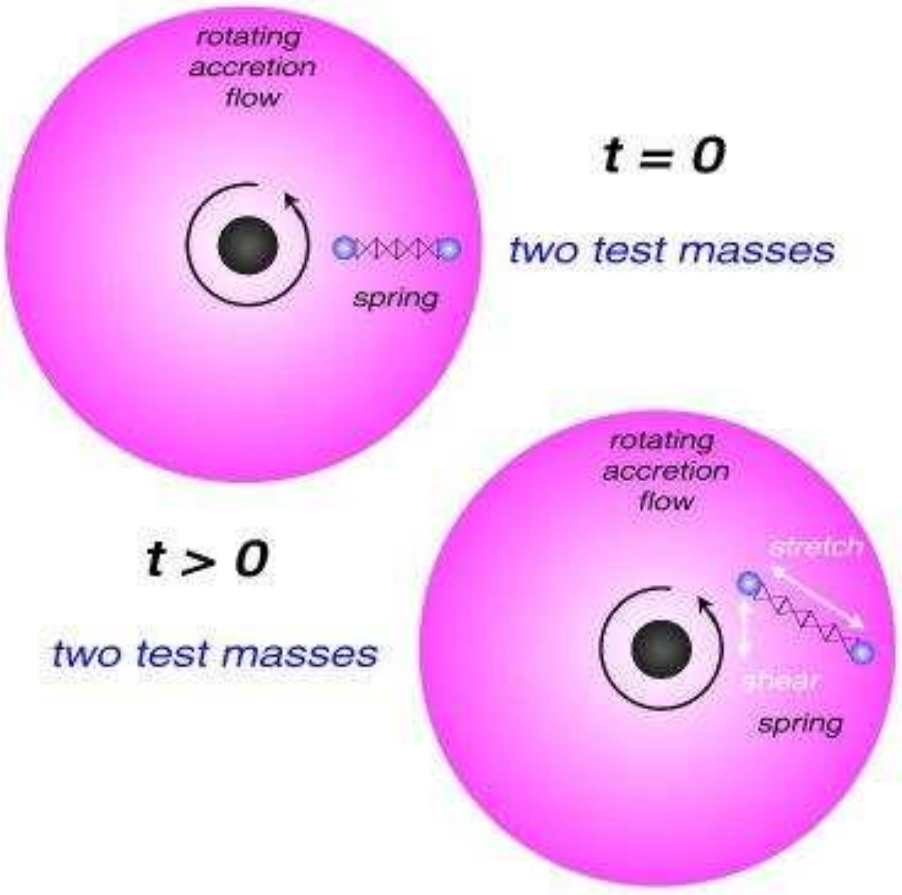

R. Müller

Mechanical analogy of MRI: spring in differentially rotating medium.

Physics of turbulent viscosity is unknown, however, α prescription yields good agreement between theory and observations.

Possible origin: Magnetorotational instability (MRI): MHD instability amplifying B-field inhomogeneities caused by small initial radial displacements in accretion disk

$\Longrightarrow$ angular momentum transport

(Balbus & Hawley 1991, going back to Velikhov 1959 and Chandrasekhar (1961).

Accretion Disks in AGN

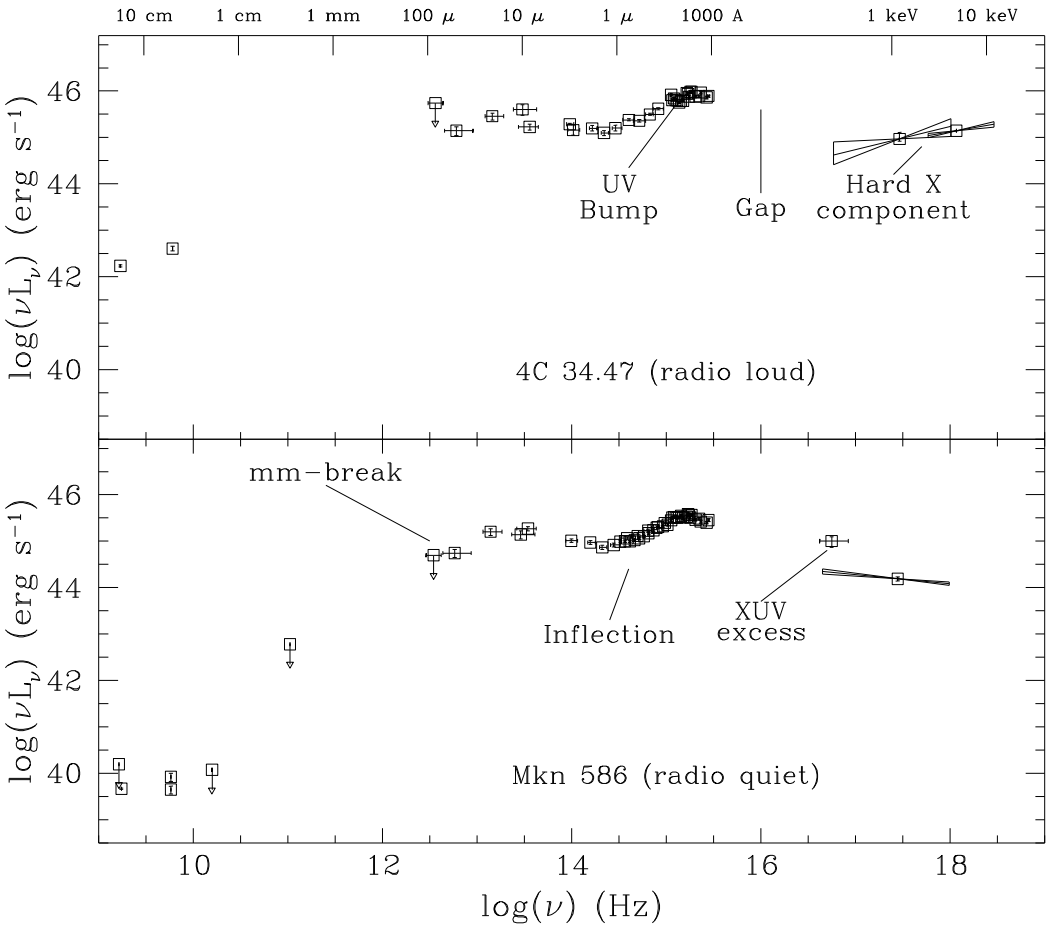

Spectral Energy Distribution of radio-loud and radio-quiet AGN (Elvis et al., 1994)

Big Blue Bump: Excess radiation in ∼UV range $\Longrightarrow$ disk?

IR Bump: Excess radiation in ∼IR range $\Longrightarrow$ dust? (peak T: 2000 K; dust sublimation?)

IR Bump

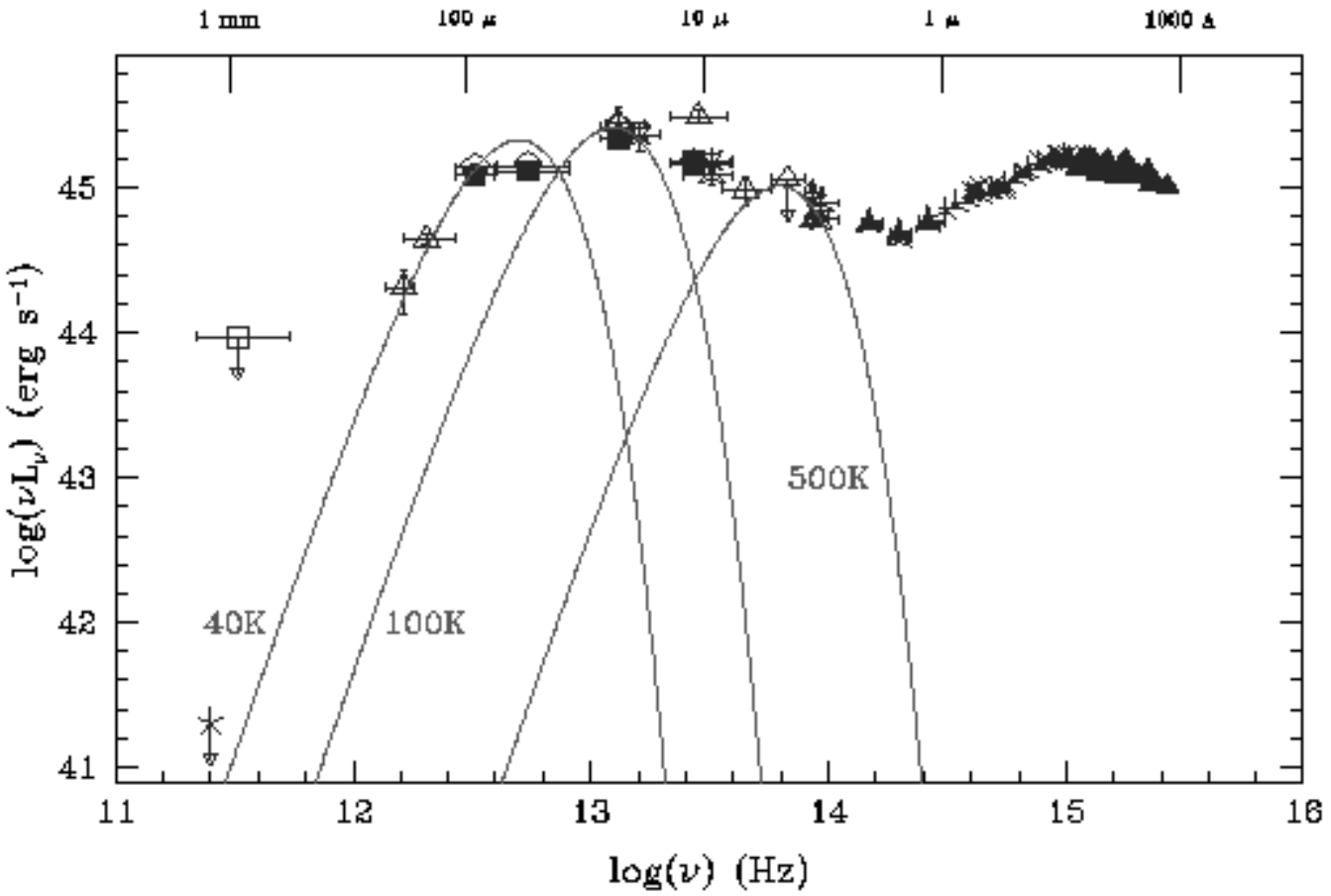

mm–optical SED of PG1351+640: dust has wide range of temperatures (Wilkes, 2004).

IR-Bump: too cold for disk, has substructure $\Longrightarrow$ different emission regions.

UV Bump

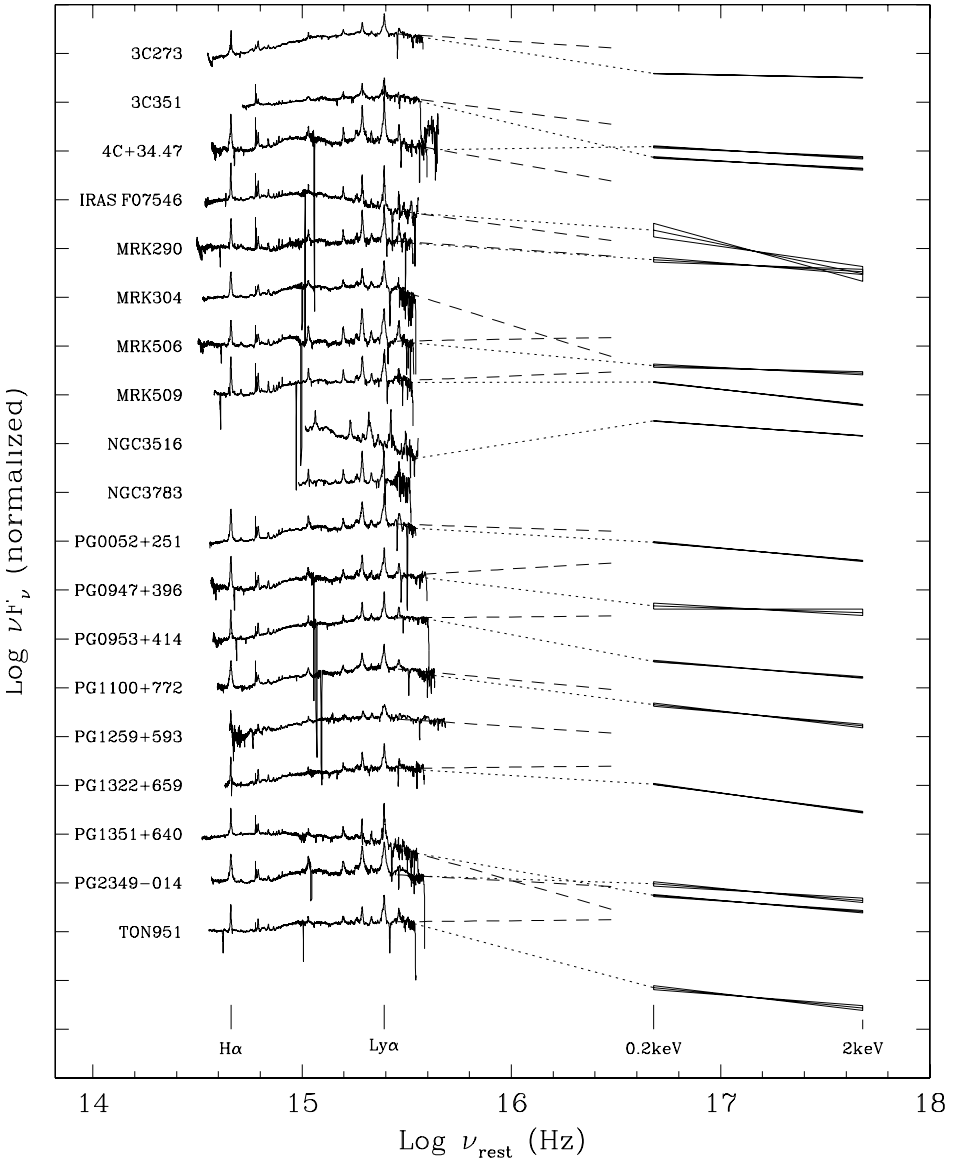

In *some* AGN: extrapolated UV power law smoothly matches the X-ray continuum.

Remember: $f_\nu \propto \nu^{-\alpha}$

Break wavelengh between 800 and 1600 Å, in rough agreement with accretion disk models.

Theory of the break: H-Lyman edge, possibly smeared by Comptonization or relativistic effects.

However: no correlation between UV slope and BH mass as expected from accretion disk models?!?

(Shang et al., 2005)

Galactic Black Holes

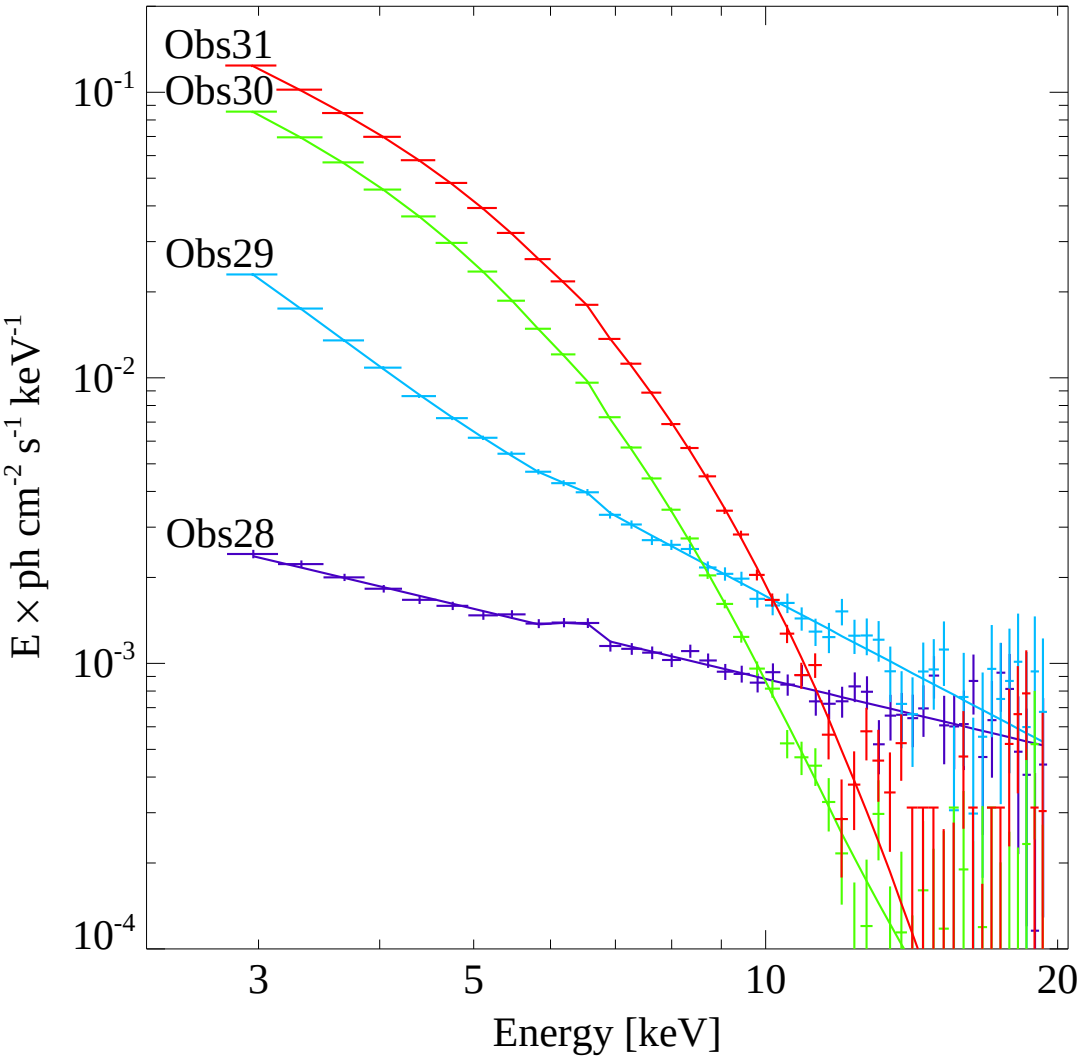

LMC X-3, (Wilms et al., 2001)

Problem with AGN: peak of disk in UV

$\Longrightarrow$ Galactic Black Holes: T is higher

Find ok agreement between accretion disk models and theory.

In general: models with just $T \propto r^{-3/4}$ and no additional (atomic) physics seem to work best?!?

Galactic Black Holes

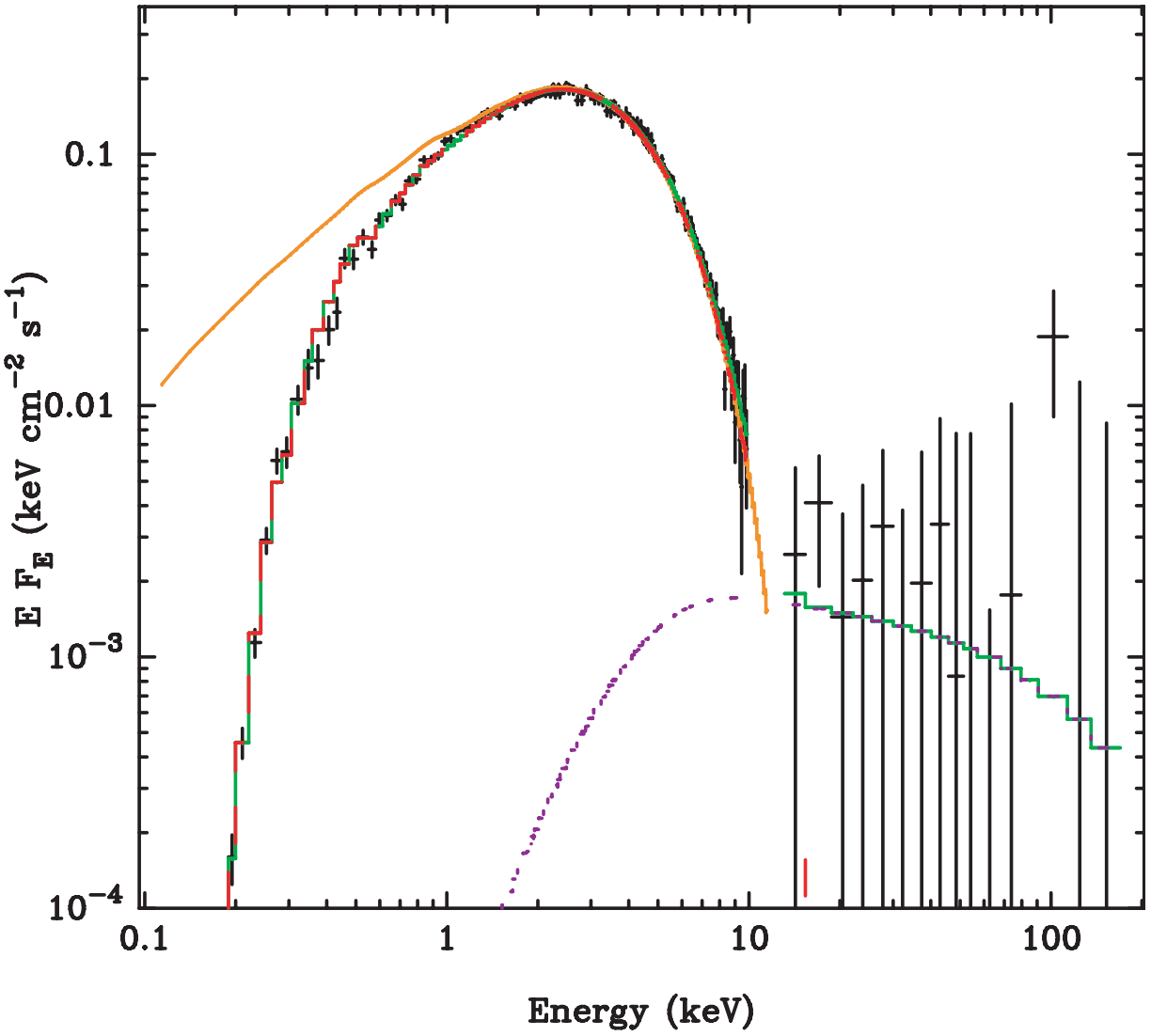

(Davis et al., 2006)

Comparison of self-consistent accretion disk model with LMC X-3 data $\Longrightarrow$ good agreement, although values of α smaller than expected (fits find $0.01 < \alpha < 0.1$ instead of 0.1–0.8).

Top red line: inferred accretion disk spectrum without interstellar absorption.

Balbus, S. A., & Hawley, J. F. 1991, ApJ, 376, 214
Chandrasekhar, S., 1961, Hydrodynamic and Hydromagnetic Stability, (Oxford: Oxford Univ. Press), (reprinted 1981 by Dover, New York)
Davis, S. W., Blaes, O. M., Hubeny, I., & Turner, N. J. 2005, ApJ, 621, 372
Davis, S. W., Done, C., & Blaes, O. M. 2006, ApJ, 647, 525
Elvis, M., Wilkes, B. J., McDowell, J. C., et al. 1994, ApJS, 95, 1
Hawley, J. F., & Krolik, J. H. 2002, ApJ, 566, 164
Shang, Z., Brotherton, M. S., Green, R. F., et al. 2005, ApJ, 619, 41
Türler, M., Paltani, S., Courvoisier, T. J.-L., et al. 1999, A&AS, 134, 89
Velikhov, E. P., 1959, Sov. Phys. – JETP, 9, 995
Wilkes, B., 2004, in AGN Physics with the Sloan Digital Sky Survey, ed. G. T. Richards, P. B. Hall, Astron. Soc. Pacific, Conf. Ser. 311, 37
Wilms, J., Nowak, M. A., Pottschmidt, K., et al. 2001, MNRAS, 320, 327

Black Hole Paradigm

Structure

AGN have power law continua.

Purpose of this lecture: investigate physical origin of the continuum emission.

Structure:

1. Continuum formation
2. Compton Scattering and Comptonization
3. Source of hot electrons
4. X-ray Reflection
5. Measuring Black Hole Properties: Relativistic Broadened Fe Kα Lines

Continuum Emission

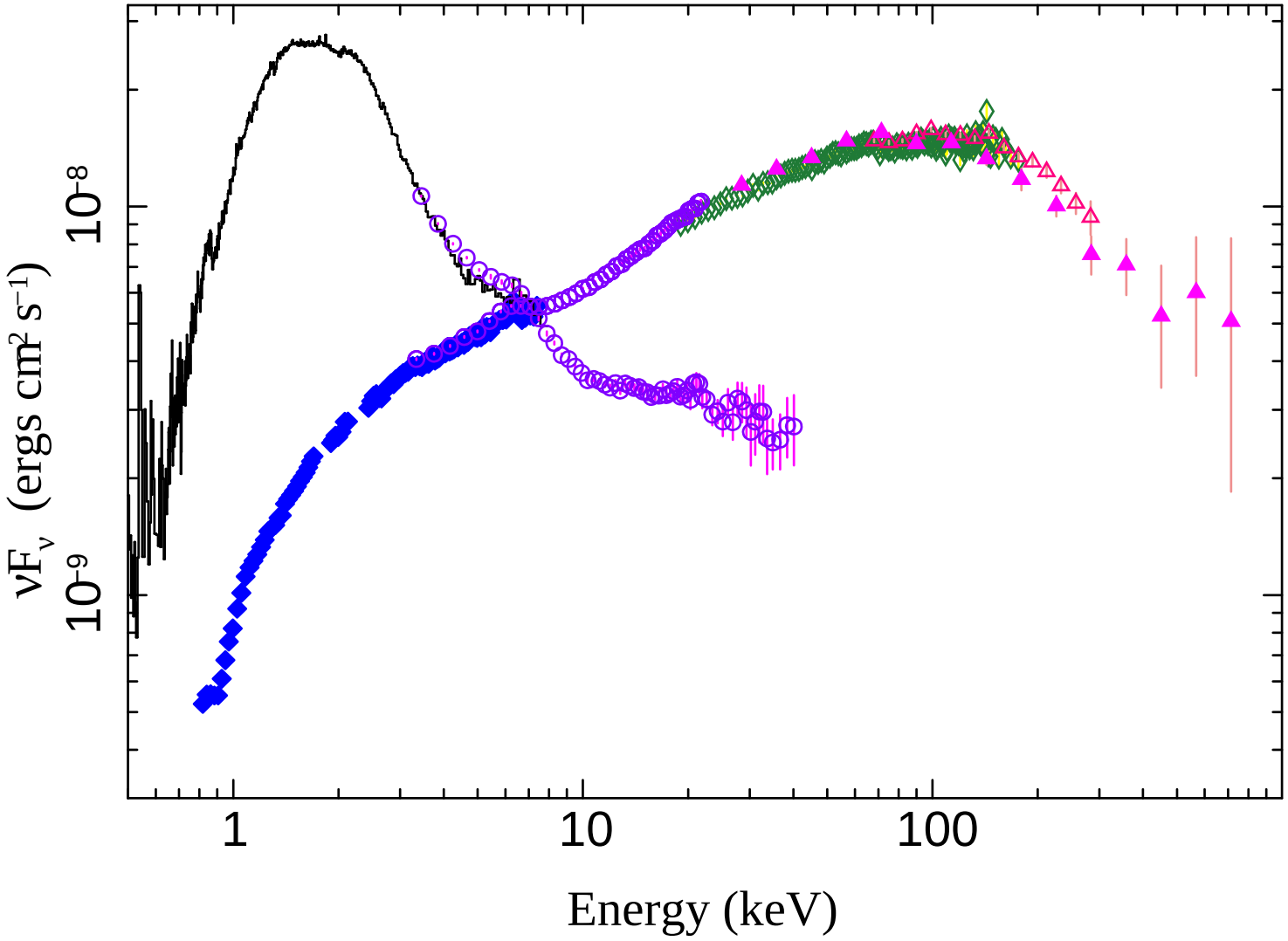

Typical X-ray spectra of galactic black holes

AGN are similar

($L \sim 3\% L_{\rm Edd}$; $L_{\rm Edd} = 10^{38}\,{\rm erg\,s^{-1}} = 10^5\,L_\odot$)

Cyg X-1 (Nowak, et al., 2011)

Continuum Emission

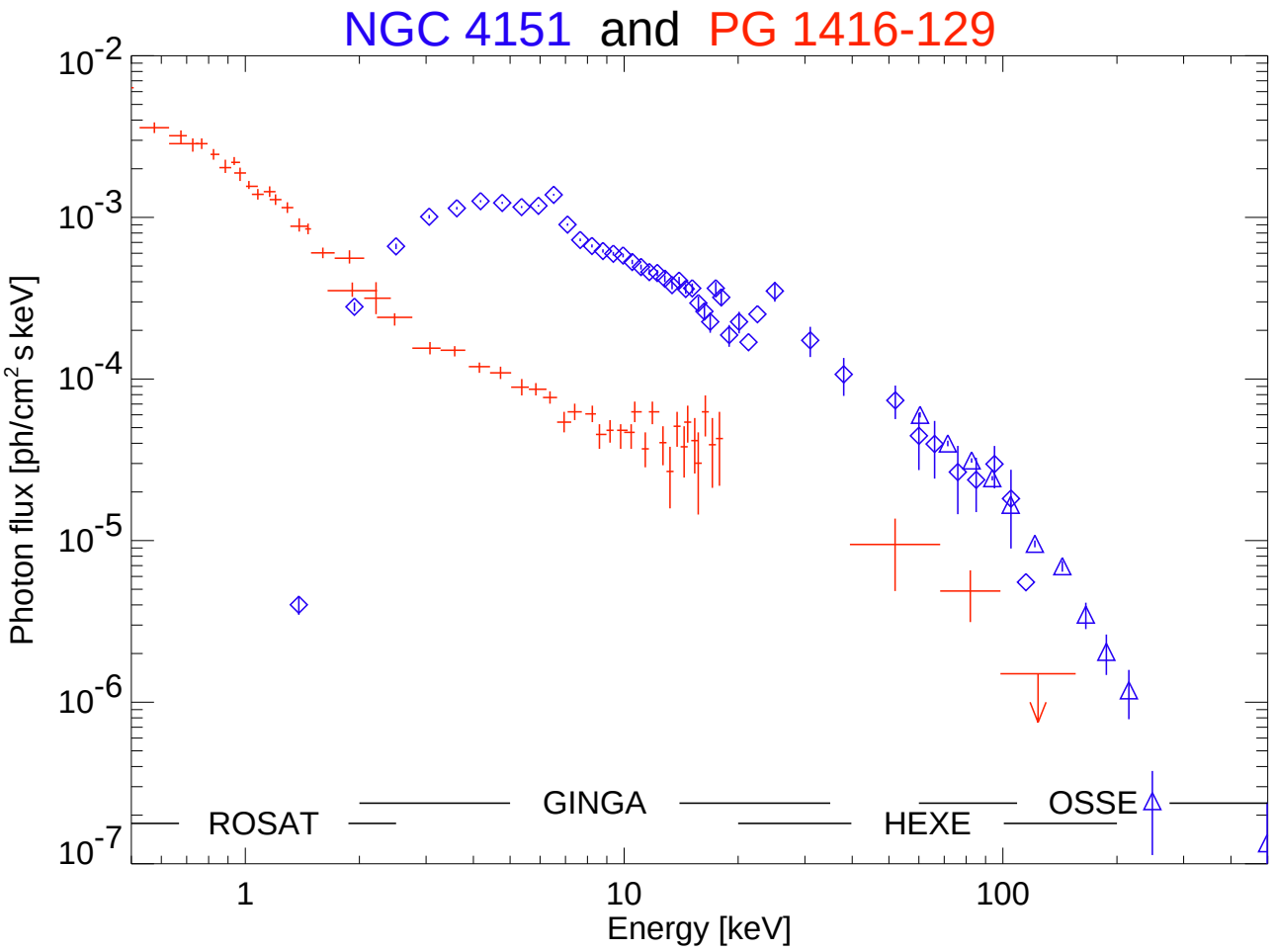

(PG 1416−129: de Kool et al., 1994, Williams et al., 1992, Staubert & Maisack, 1996; NGC 4151: Maisack 1991, 1993)

Note: NGC 4151 not corrected for interstellar absorption.

Spectral shape of AGN very similar to galactic Black Holes $\Longrightarrow$ Same physical mechanism (=Comptonization) responsible!

Compton Scattering

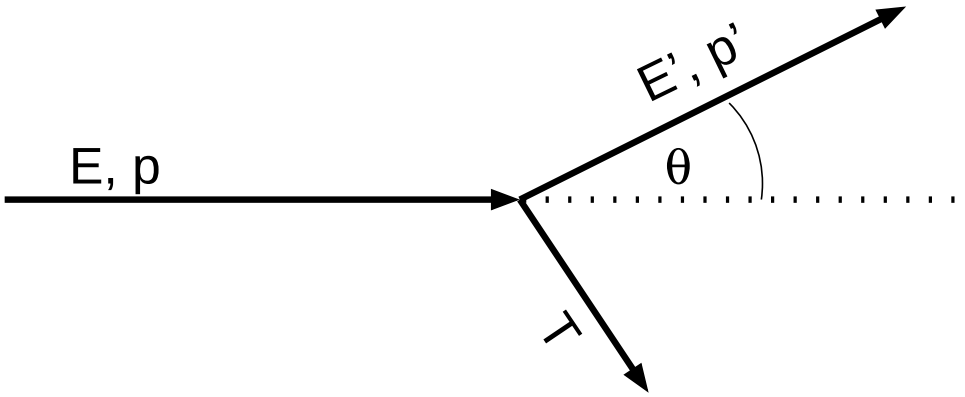

Thomson scattering: initial and final photon energy are identical.

But: in QM: light consists of photons

$\Longrightarrow$ Scattering: photon changes direction

$\Longrightarrow$ Momentum change

$\Longrightarrow$ Energy change!

This process is called Compton scattering.

Energy/wavelength change in scattering (see handout):

$$E' = \frac{E}{1 + \frac{E}{m_e c^2}(1 - \cos\theta)} \sim E\left(1 - \frac{E}{m_e c^2}(1 - \cos\theta)\right) \tag{5.1}$$

$$\lambda' - \lambda = \frac{h}{m_e c}(1 - \cos\theta) \tag{5.2}$$

where $h/m_e c = 2.426 \times 10^{-12}$ m (Compton wavelength).

Averaging over θ, for $E \ll m_e c$:

$$\frac{\Delta E}{E} \approx -\frac{E}{m_e c^2} \tag{5.3}$$

E.g., at 6.4 keV, $\Delta E \approx 0.2$ keV.

Compton Scattering

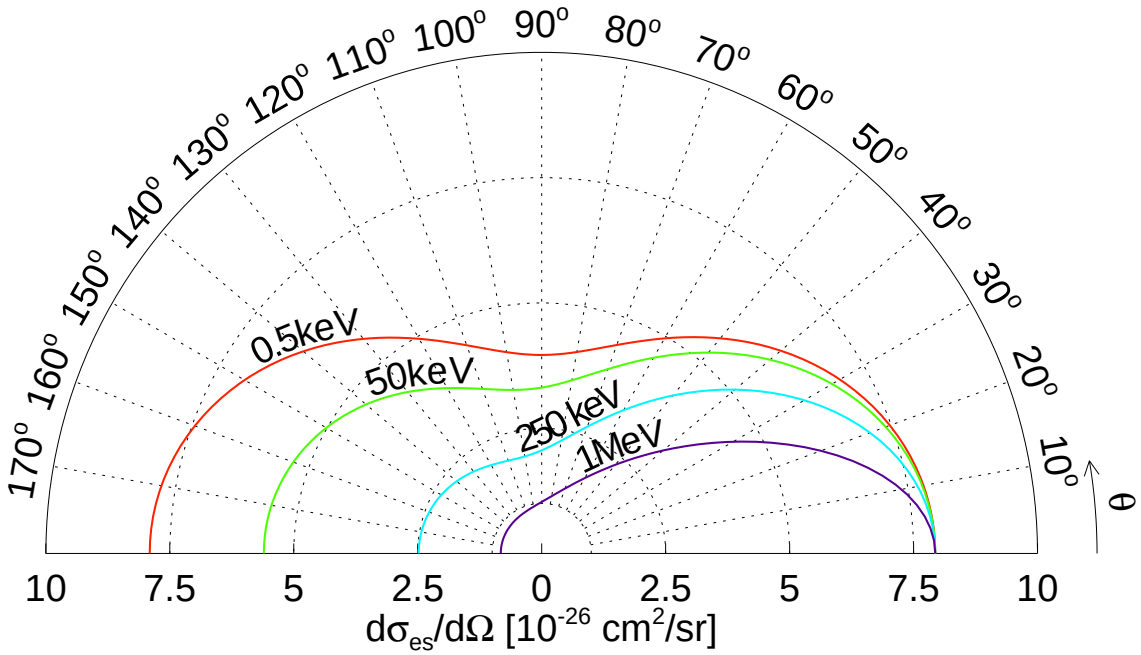

The proper derivation of cross section is done in quantum electrodynamics.
In the limit of low energies: will find Thomson result, for higher energies: relativistic effects become important.

For unpolarized radiation,

$$\frac{d\sigma_{\rm es}}{d\Omega} = \frac{3}{16\pi}\sigma_{\rm T}\left(\frac{E'}{E}\right)^2\left(\frac{E}{E'}+\frac{E'}{E}-\sin^2\theta\right) \qquad (5.4)$$

(Klein-Nishina formula).

Compton Scattering

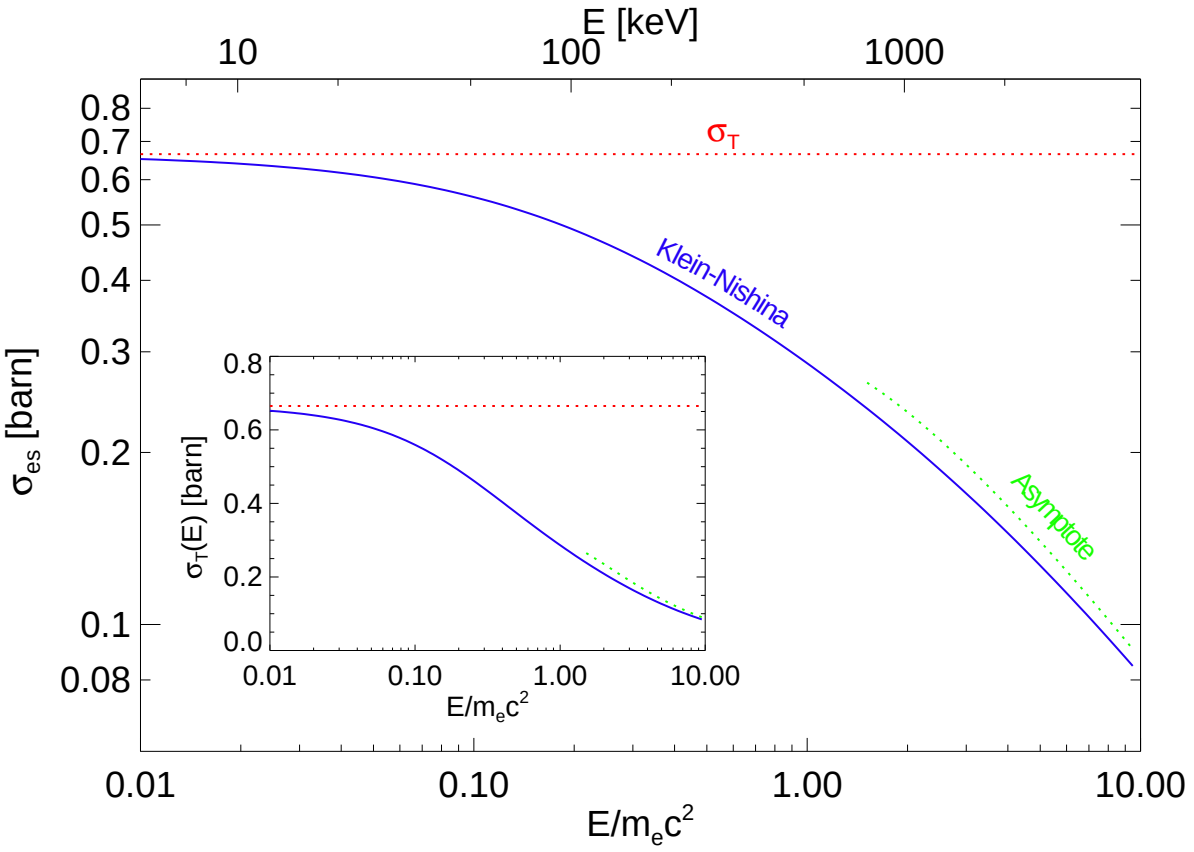

1 barn $= 10^{-28}$ m^2

Integrating over $d\sigma_{es}/d\Omega$ gives total cross-section:

$$\sigma_{es} = \frac{3}{4}\sigma_T \left[\frac{1+x}{x^3}\left\{\frac{2x(1+x)}{1+2x} - \ln(1+2x)\right\} + \frac{1}{2x}\ln(1+2x) - \frac{1+3x}{(1+2x)^2}\right] \qquad (5.5)$$

where $x = E/m_e c^2$.

Energy Exchange

For non-stationary electrons, use previous formulae and Lorentz transform photon into electron's frame of rest (FoR):

1. Lab system $\Rightarrow$ electron's frame of rest:

$$E_{\text{FoR}} = E_{\text{Lab}}\gamma(1 - \beta\cos\theta) \tag{5.6}$$

2. Scattering occurs, gives E'_{FoR}.
3. Electron's frame of rest $\Rightarrow$ Lab system:

$$E'_{\text{Lab}} = E'_{\text{FoR}}\gamma(1 + \beta\cos\theta') \tag{5.7}$$

Therefore, if electron is relativistic:

$$E'_{\text{Lab}} \sim \gamma^2 E_{\text{Lab}} \tag{5.8}$$

since (on average) θ, θ' are $\mathcal{O}(\pi/2)$ (beaming!).

Thus: Energy transfer is *very* efficient.

As shown in the following, in Compton scattering the radiation field is amplified by a factor γ^2.

We first look at the energy budget of one single scattering.

The total power *emitted* in the frame of rest of the electron is given by

$$\left.\frac{dE'_{\text{FoR}}}{dt_{\text{FoR}}}\right|_{\text{em}} = \int c\sigma_{\text{T}} E'_{\text{FoR}} V'(E'_{\text{FoR}}) dE'_{\text{FoR}} \tag{5.9}$$

where $V'(E')$ is the photon energy density distribution (number of photons per cubic metre with an energy between E' and $E' + dE'$).

This power is Lorentz invariant:

$$\frac{V_{\text{Lab}}(E_{\text{Lab}})dE_{\text{Lab}}}{E_{\text{Lab}}} = \frac{V_{\text{FoR}}(E_{\text{FoR}})dE_{\text{FoR}}}{E_{\text{FoR}}} \tag{5.10}$$

In the "Thomson limit" one assumes that the energy change of the photon in the rest frame of the electron is small,

$$E'_{\text{FoR}} = E_{\text{FoR}} \tag{5.11}$$

(this limit was also used in the derivation of Eq. (5.8)). Furthermore one can show that the power is Lorentz invariant:

$$\frac{dE_{\text{FoR}}}{dt_{\text{FoR}}} = \frac{dE_{\text{Lab}}}{dt_{\text{Lab}}} \tag{5.12}$$

(this follows from the fact that energy and time are both "time-like quantities", i.e., the formulae for the Lorentz transform of energy and time are the same).

Therefore

$$\left.\frac{dE_{\text{Lab}}}{dt_{\text{Lab}}}\right|_{\text{em}} = c\sigma_{\text{T}} \int E_{\text{FoR}}^2 \frac{V_{\text{FoR}} dE_{\text{FoR}}}{E_{\text{FoR}}} \tag{5.13}$$

$$= c\sigma_{\text{T}} \int E_{\text{FoR}}^2 \frac{V_{\text{Lab}} dE_{\text{Lab}}}{E_{\text{Lab}}} \tag{5.14}$$

... Lorentz transforming E_{FoR}

$$= c\sigma_{\text{T}}\gamma^2 \int (1 - \beta\cos\theta)^2 E_{\text{Lab}} V_{\text{Lab}} dE_{\text{Lab}} \tag{5.15}$$

... averaging over angles ($\langle\cos\theta\rangle = 0$, $\langle\cos^2\theta\rangle = \frac{1}{3}$)

$$= c\sigma_{\text{T}}\gamma^2 \left(1 + \frac{\beta^2}{3}\right) U_{\text{rad}} \tag{5.16}$$

where

$$U_{\text{rad}} = \int EV(E)dE \tag{5.17}$$

(initial photon energy density).

To determine the power gain of the photons, we need to subtract the power irradiated onto the electron,

$$\left.\frac{dE_{\text{Lab}}}{dt_{\text{Lab}}}\right|_{\text{inc}} = c\sigma_{\text{T}} \int EV(E)dE = \sigma_{\text{T}} c U_{\text{rad}} \tag{5.18}$$

Therefore, since

$$\gamma^2 - 1 = \gamma^2\beta^2 \tag{5.19}$$

the net power gain of the photon field is

$$P_{\text{compt}} = \left.\frac{dE_{\text{Lab}}}{dt}\right|_{\text{em}} - \left.\frac{dE_{\text{Lab}}}{dt}\right|_{\text{inc}} \tag{5.20}$$

$$= \frac{4}{3}\sigma_{\text{T}} c\gamma^2\beta^2 U_{\text{rad}} \tag{5.21}$$

Amplification factor

As shown before, in the electron frame of rest,

$$\frac{\Delta E}{E} = -\frac{E}{m_{\mathrm{e}}c^2} \tag{5.3}$$

Assuming a thermal (Maxwell) distribution of electrons (i.e., they're not at rest), using the equations from the previous slides one can show that the relative energy change is given by

$$\frac{\Delta E}{E} = \frac{4kT - E}{m_{\mathrm{e}}c^2} = A \tag{5.22}$$

where A is the Compton amplification factor.

Thus:

$E \lesssim 4kT_{\mathrm{e}} \Longrightarrow$ Photons gain energy, gas cools down.

$E \gtrsim 4kT_{\mathrm{e}} \Longrightarrow$ Photons loose energy, gas heats up.

Amplification factor

In reality, photons will scatter more than once before leaving the hot electron medium.

The *total* relative energy change of photons by traversal of a hot ($E \ll kT_\mathrm{e}$) medium with electron density n_e and size ℓ is then approximately

$$\left(\text{rel. energy change } y\right) = \frac{\text{rel. energy change}}{\text{scattering}} \times \left(\text{\# scatterings}\right) \tag{5.23}$$

The number of scatterings is $\max(\tau_\mathrm{e}, \tau_\mathrm{e}^2)$, where $\tau_\mathrm{e} = n_\mathrm{e}\sigma_\mathrm{T}\ell$ (“optical depth”), such that

$$y = \frac{4kT_\mathrm{e}}{m_\mathrm{e}c^2}\max(\tau_\mathrm{e}, \tau_\mathrm{e}^2) \tag{5.24}$$

“Compton y-Parameter”

Amplification factor

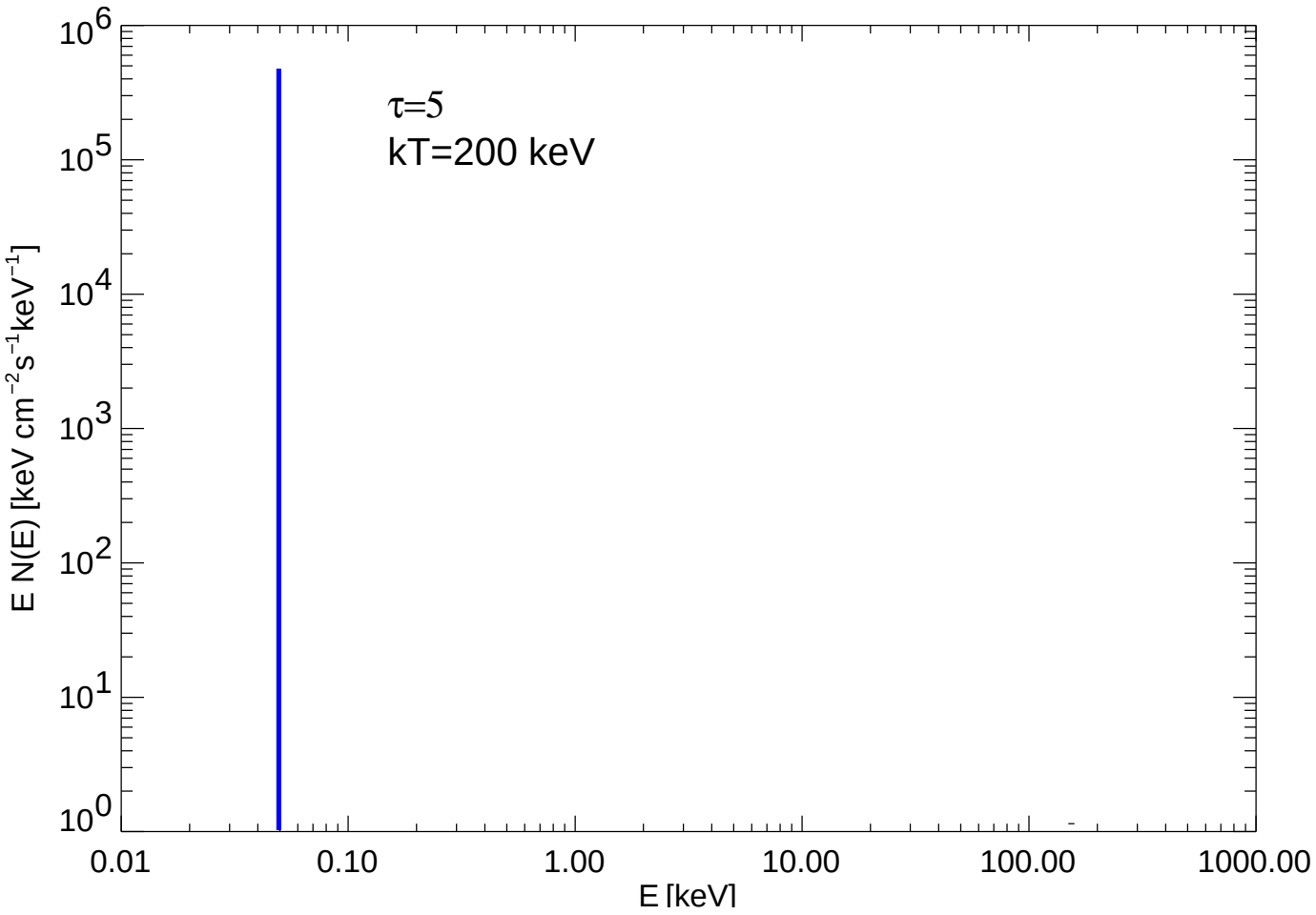

Amplification factor

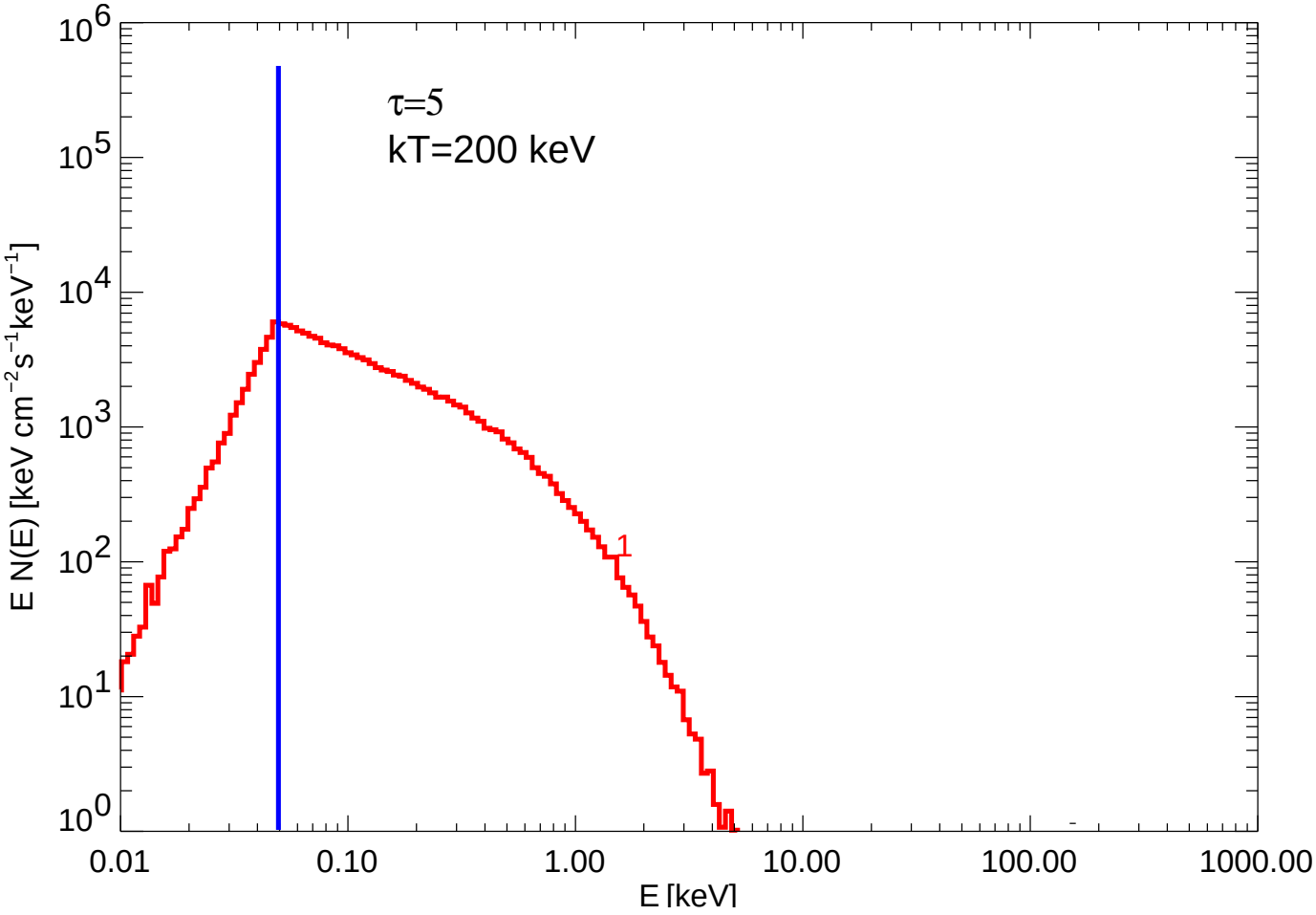

Amplification factor

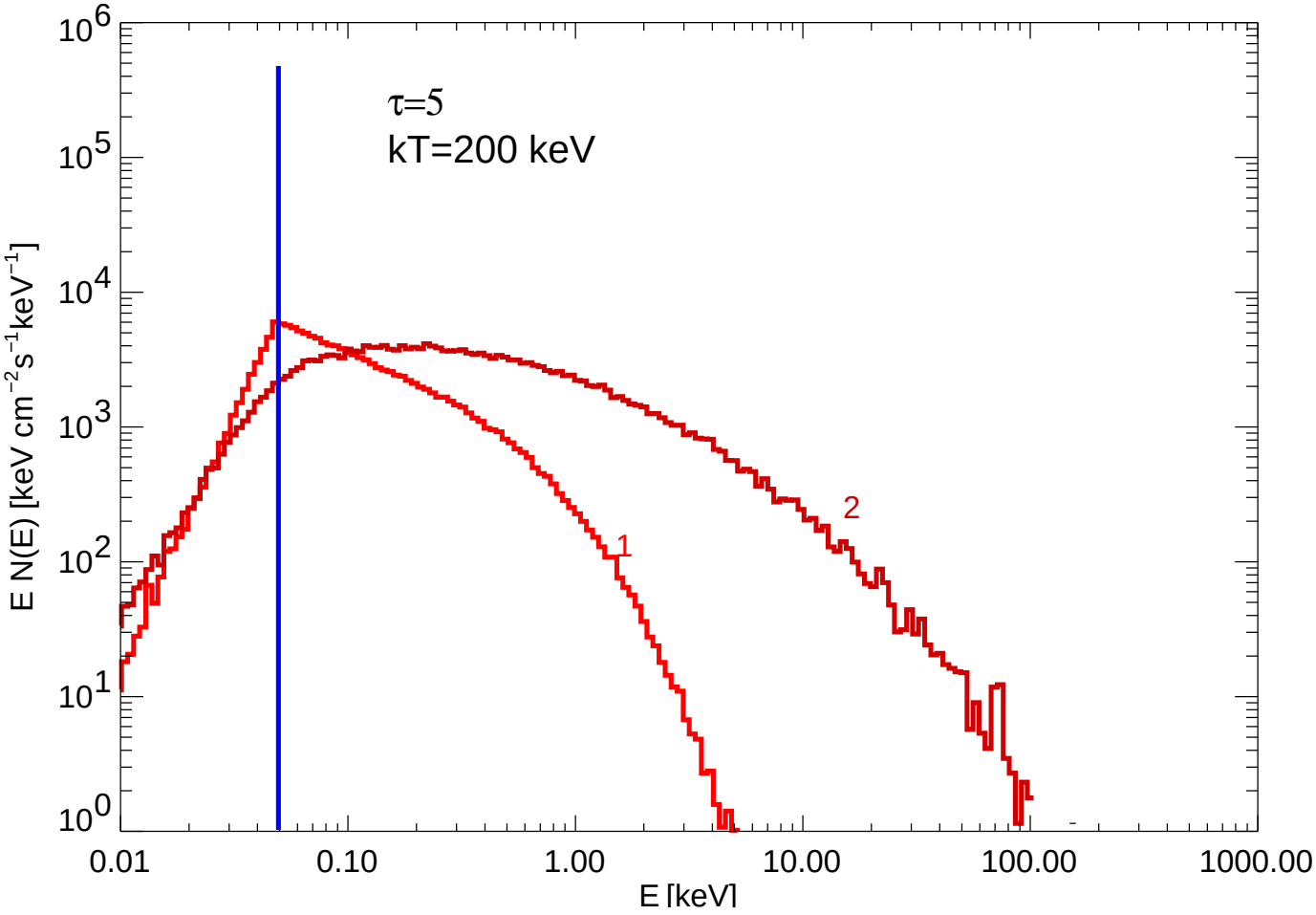

Amplification factor

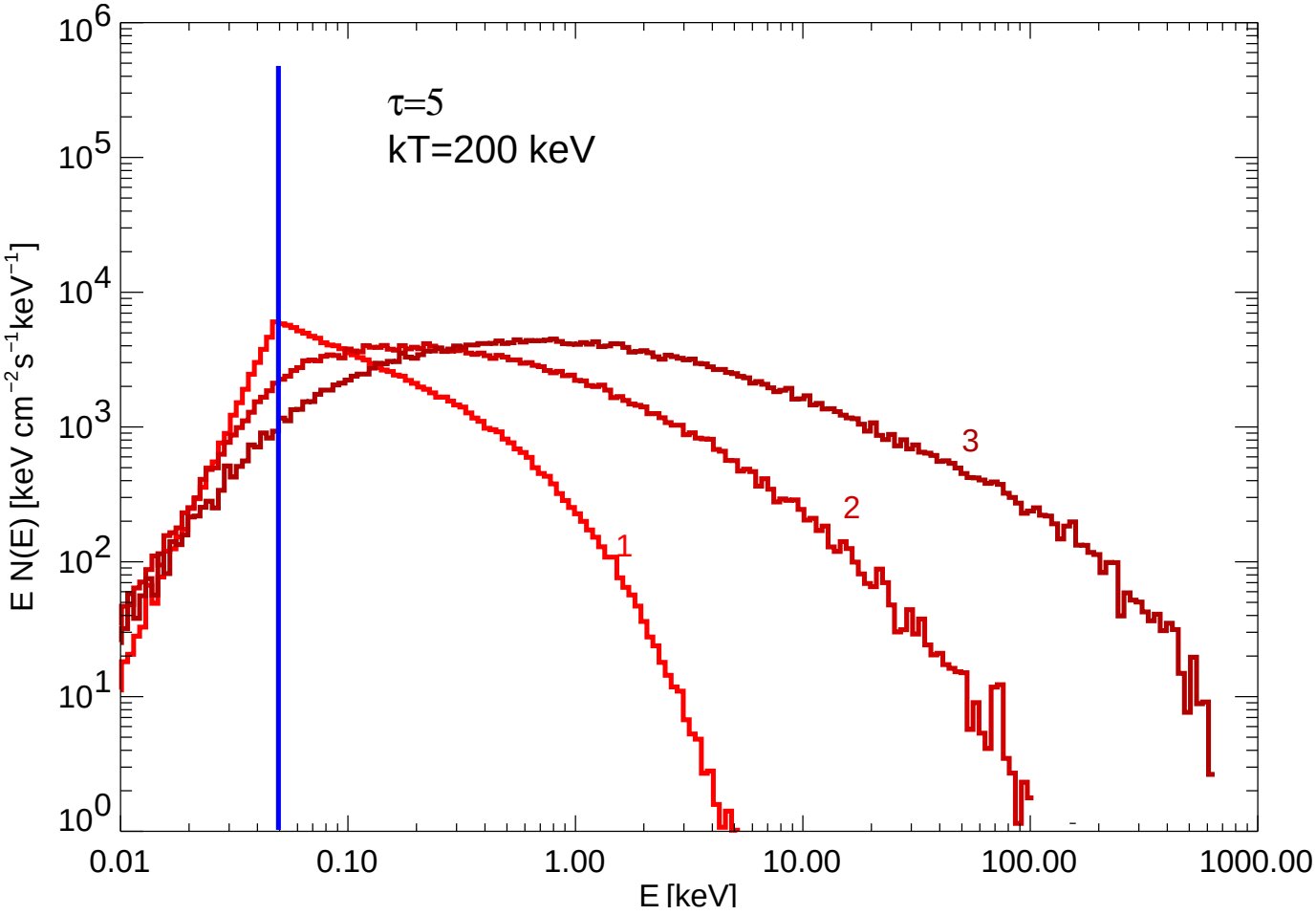

Amplification factor

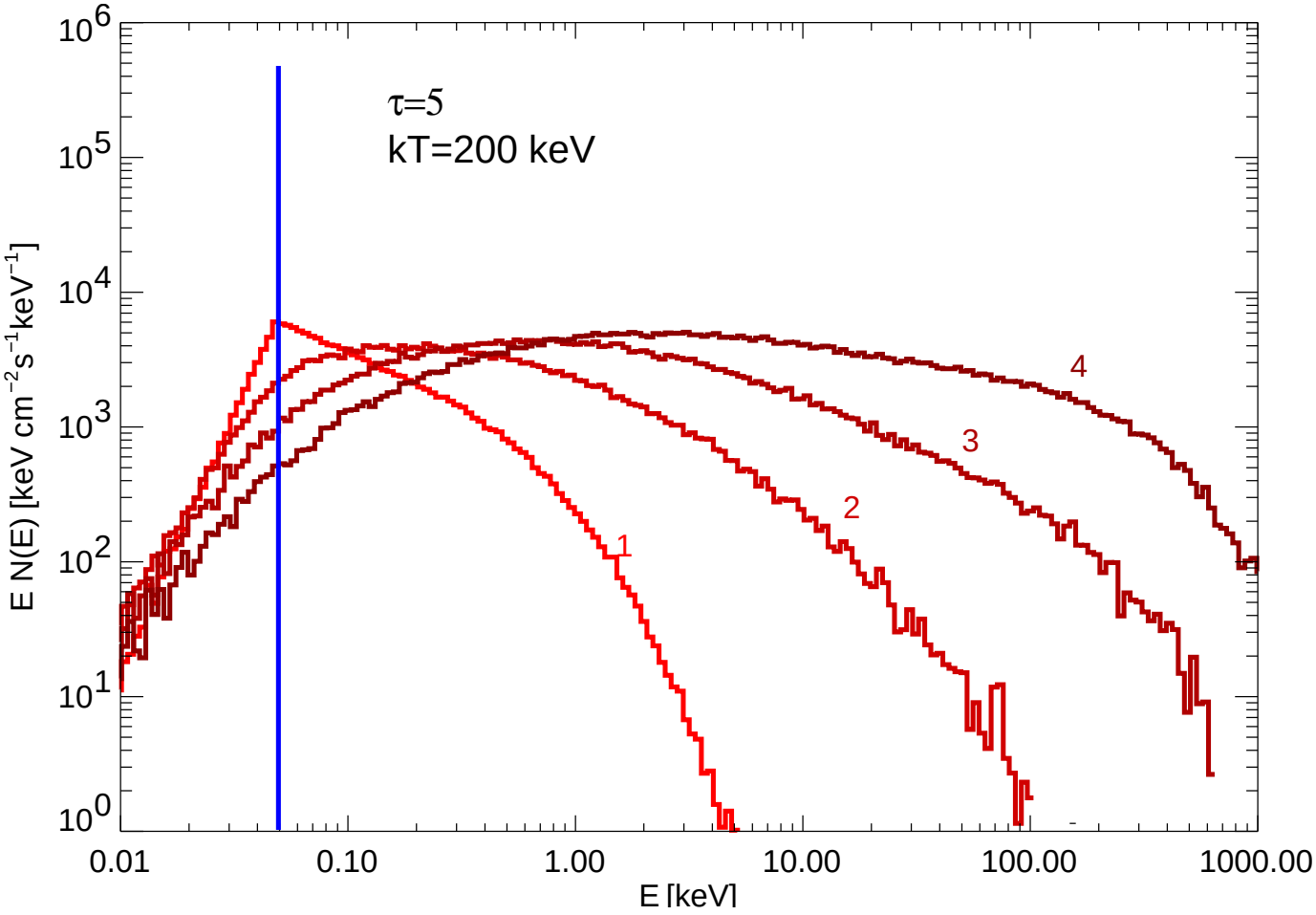

Amplification factor

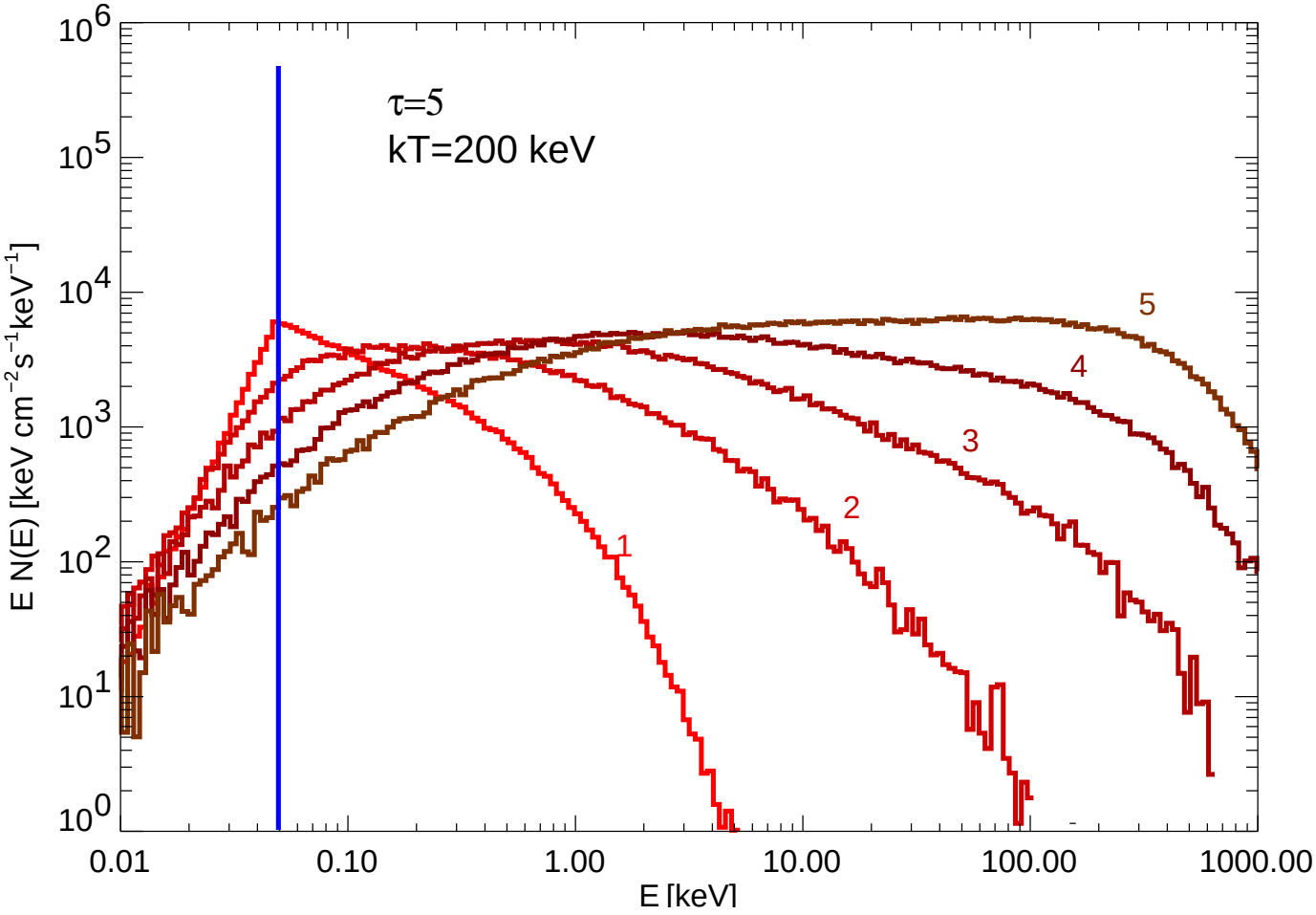

Amplification factor

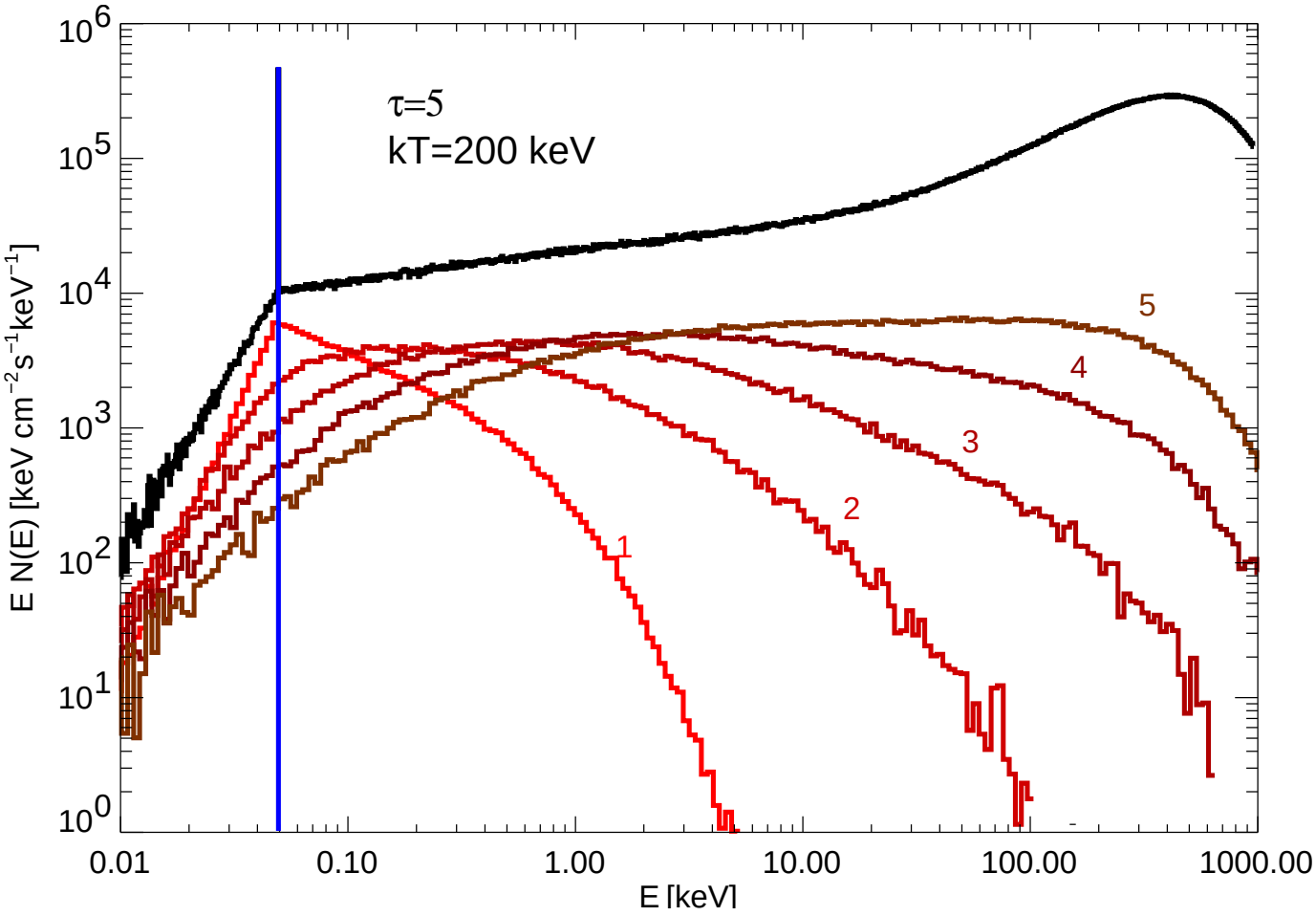

Monte Carlo simulation shows: Spectrum is $\Longrightarrow$ Power law with exponential cut-off (here: with additional “Wien hump”, see next slide)

Amplification factor

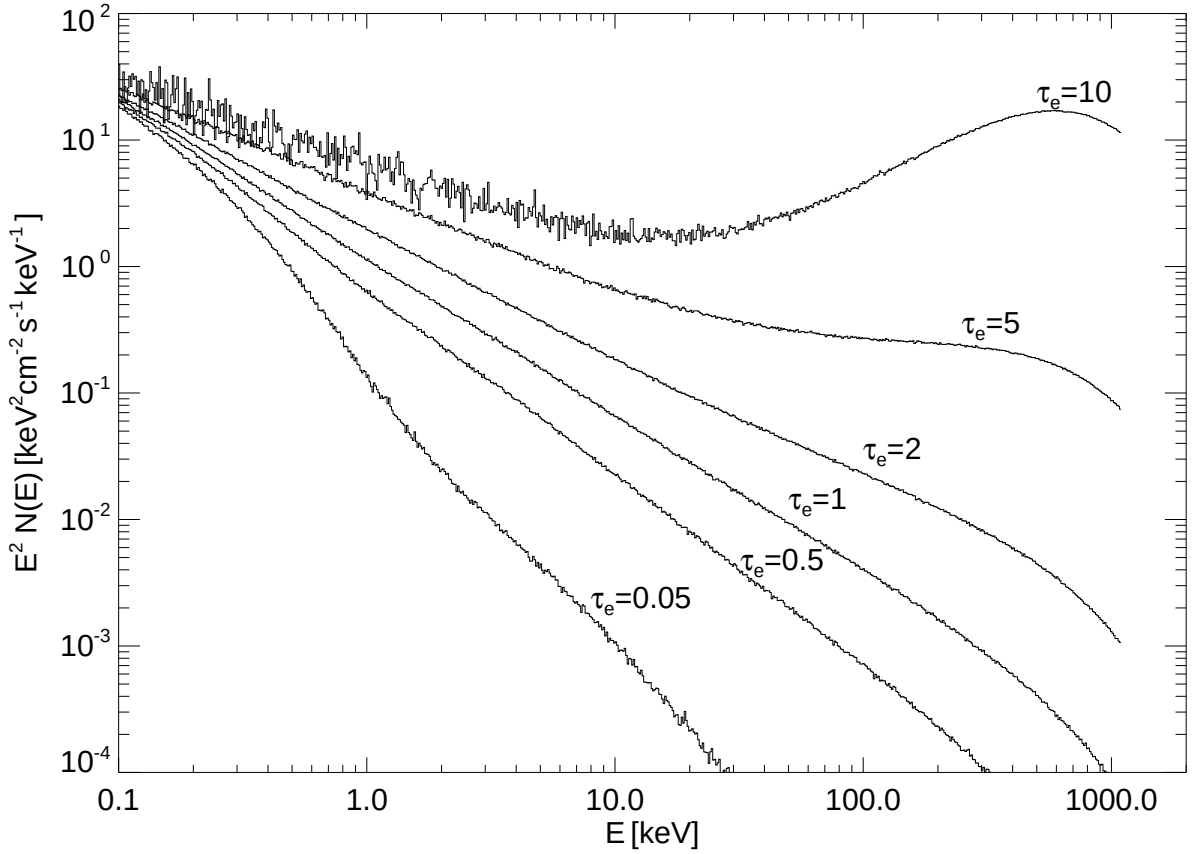

Sphere with $kT_e = 0.7 m_e c^2$ ($\sim$ 360 keV), seed photons come from center of sphere.

$y \ll 1$: pure power-law.
$y < 1$: power-law with exponential cut-off
$y \gg 1$: "Saturated Comptonization".

Saturated Comptonization has never been observed.

Amplification factor

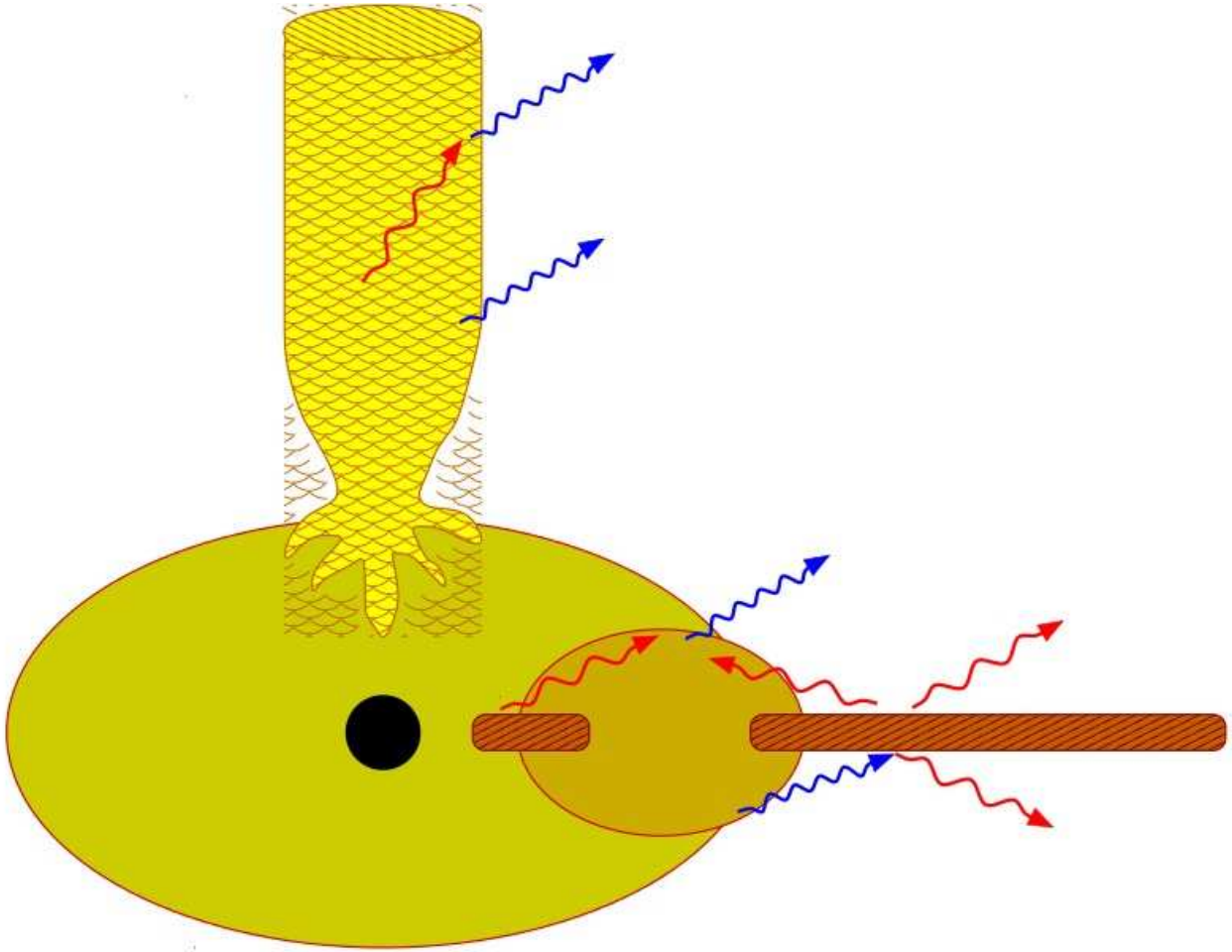

The origin of the Comptonized spectrum is still debated:

- sandwich corona models/sphere+disk: Haardt & Maraschi (1991),Dove et al. (1998),. . .
  $\Longrightarrow$ Comptonization from a hot electron plasma surrounding the disk
- lamppost models: Matt et al. (1992), Markoff et al. (2005), Miniutti et al. (2007),. . .
  $\Longrightarrow$ Comptonization from the base of a jet

(Nowak et al., 2011)

Simple Reflection

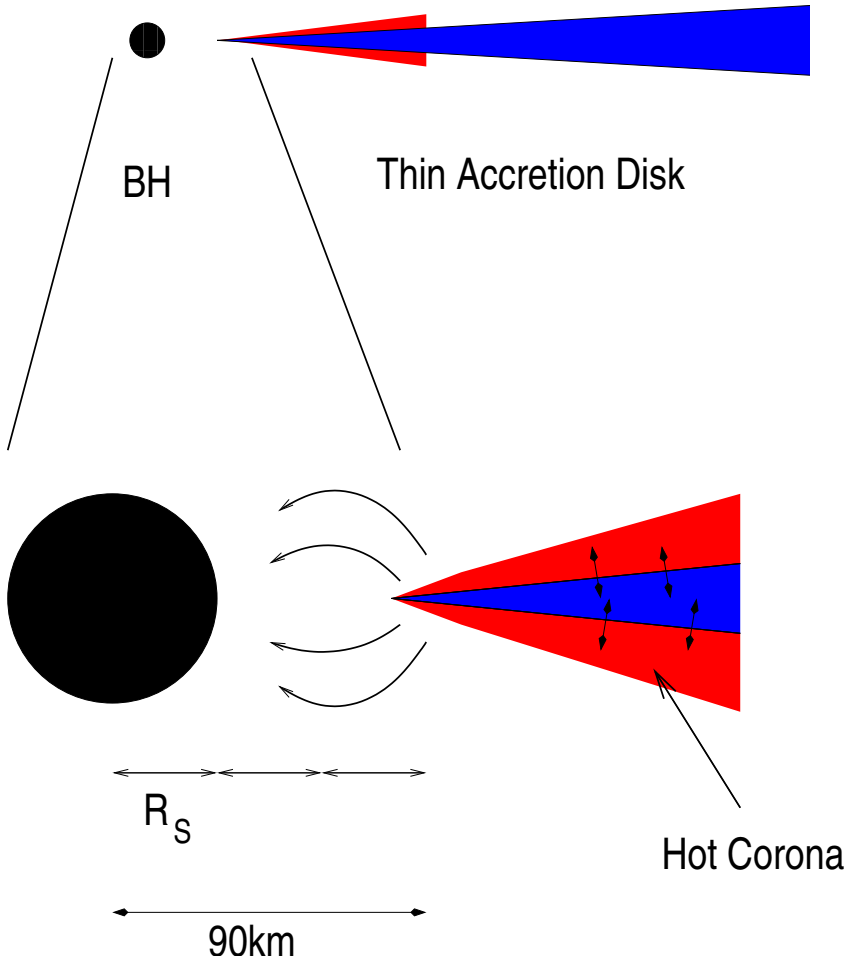

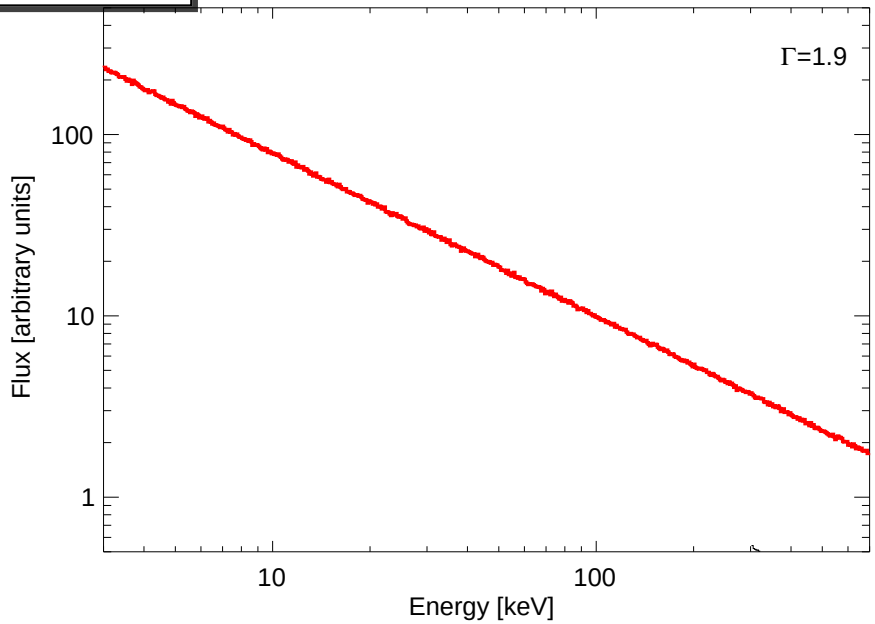

XRB/AGN X-Ray Spectrum:

- Comptonization of soft X-rays from accretion disk in hot corona ($T \sim 10^8$ K): power law continuum.

Simple Reflection

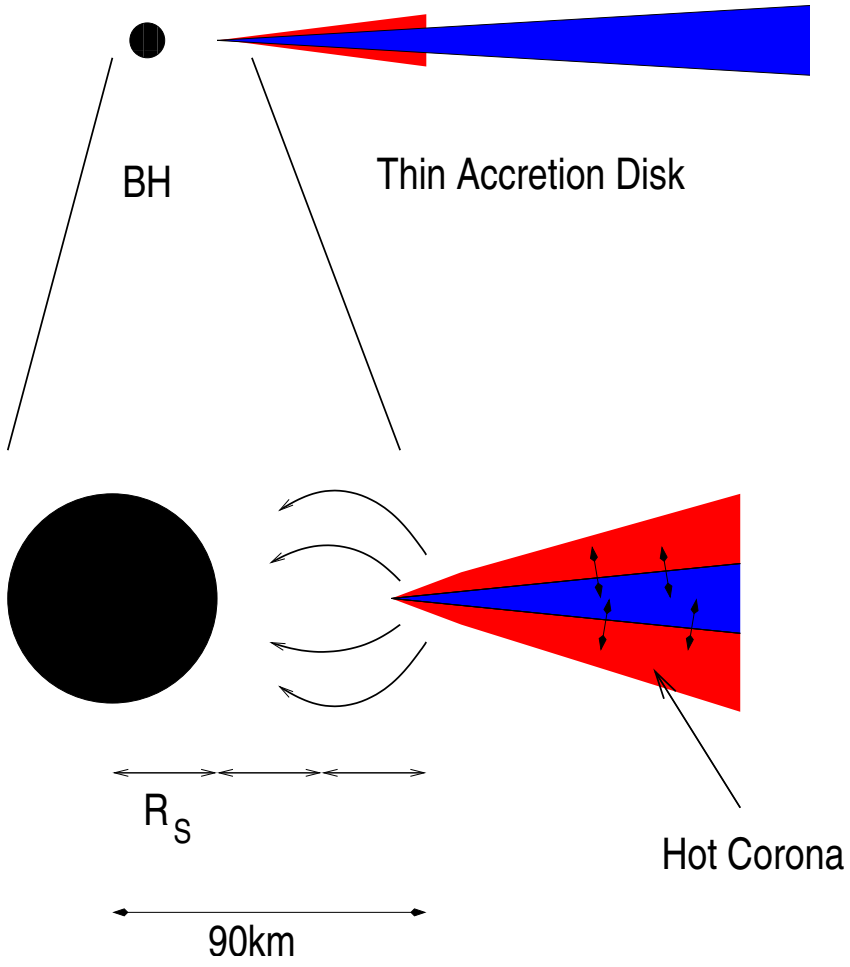

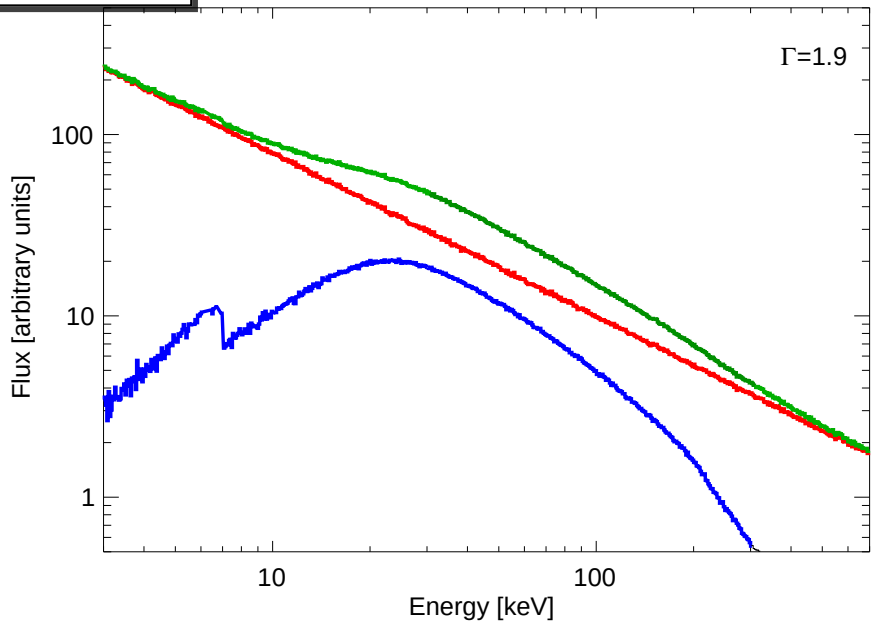

XRB/AGN X-Ray Spectrum:

- Comptonization of soft X-rays from accretion disk in hot corona ($T \sim 10^8$ K): power law continuum.
- Thomson scattering of power law photons in disk: Compton Reflection Hump

Simple Reflection

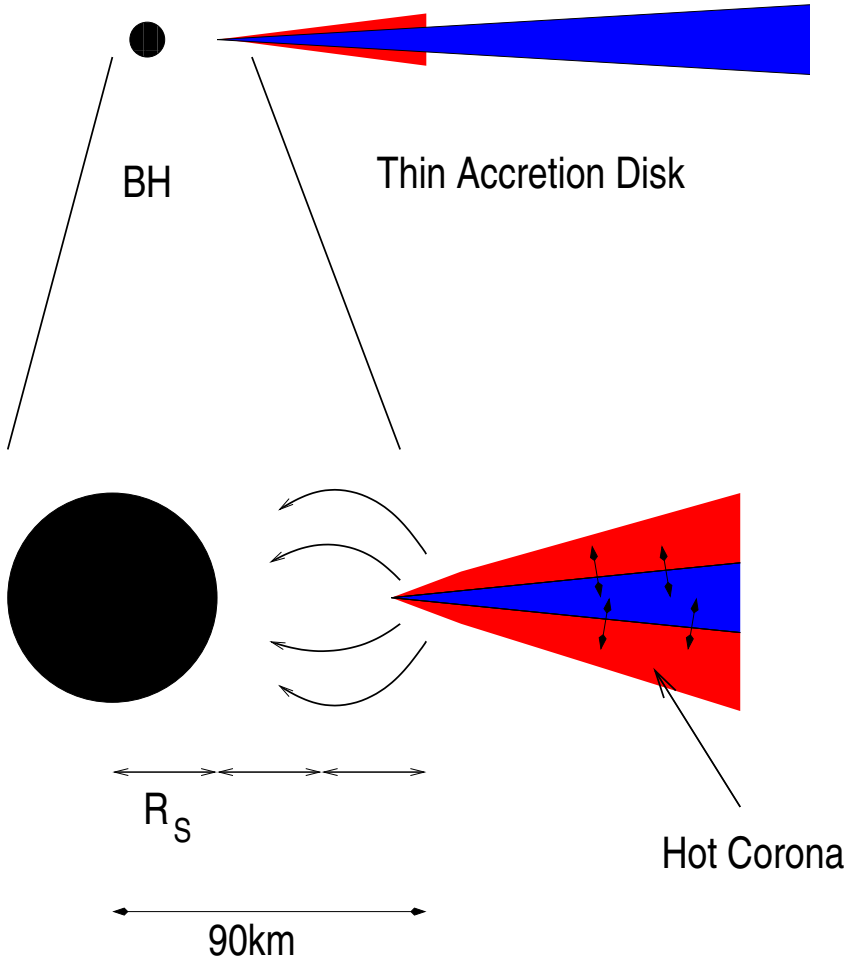

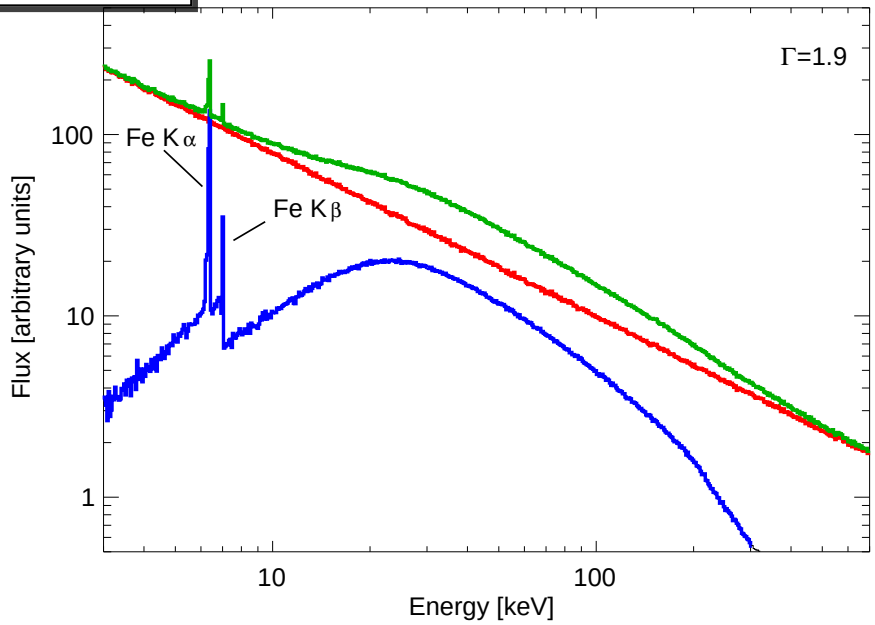

XRB/AGN X-Ray Spectrum:

- Comptonization of soft X-rays from accretion disk in hot corona ($T \sim 10^8$ K): power law continuum.
- Thomson scattering of power law photons in disk: Compton Reflection Hump
- Photoabsorption of power law photons in disk: fluorescent Fe Kα Line at $\sim$6.4 keV

Models: Guilbert & Rees (1988), Lightman & White (1988), Magdziarz & Zdziarski (1995), Ross & Fabian (2007). Reviews: Turner & Miller (2009), Fabian & Ross (2010)

Simple Reflection

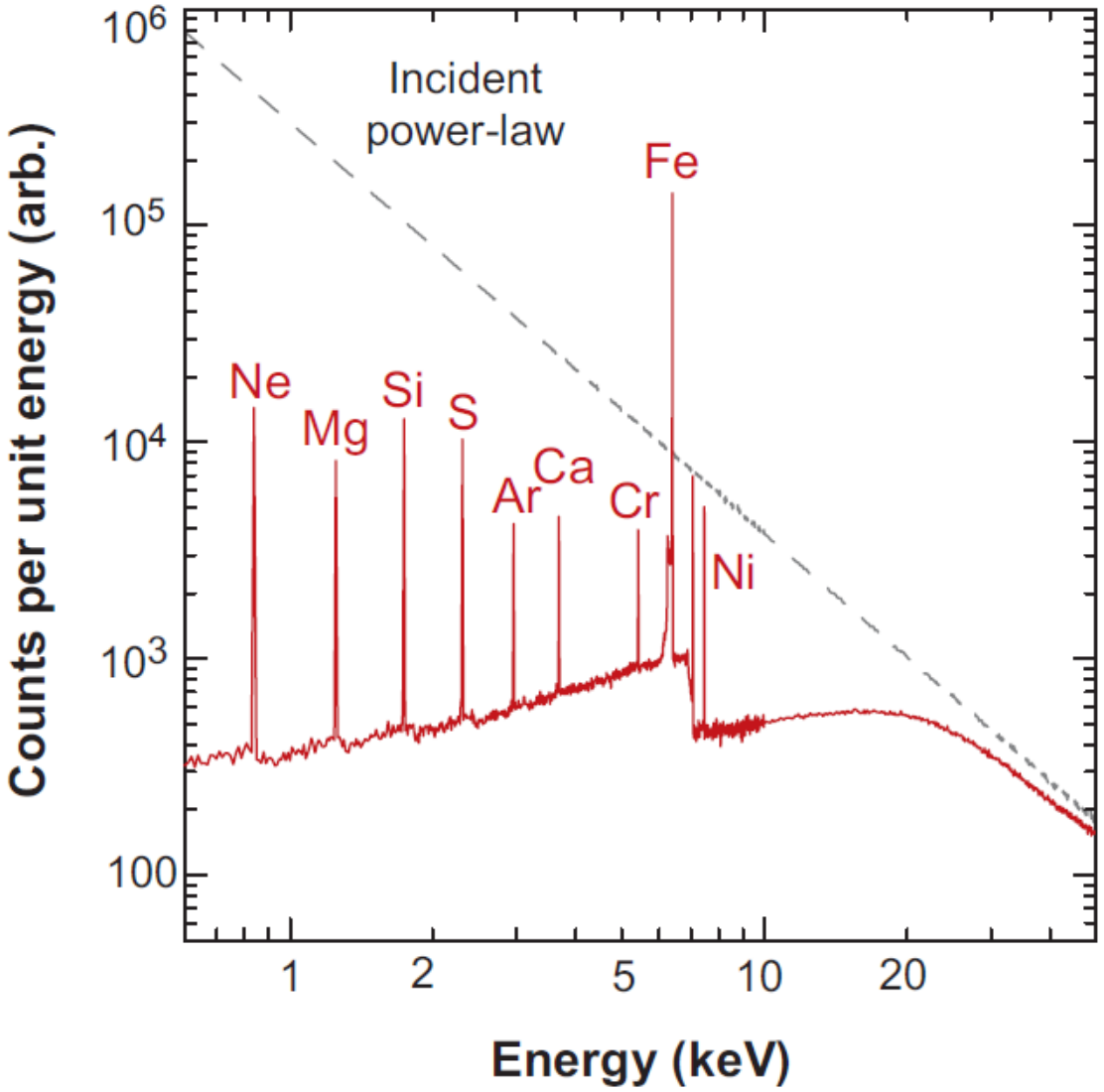

Prediction of neutral reflection models: fluorescent emission lines at low energies

(Reynolds, 1996)

Ionized Reflection

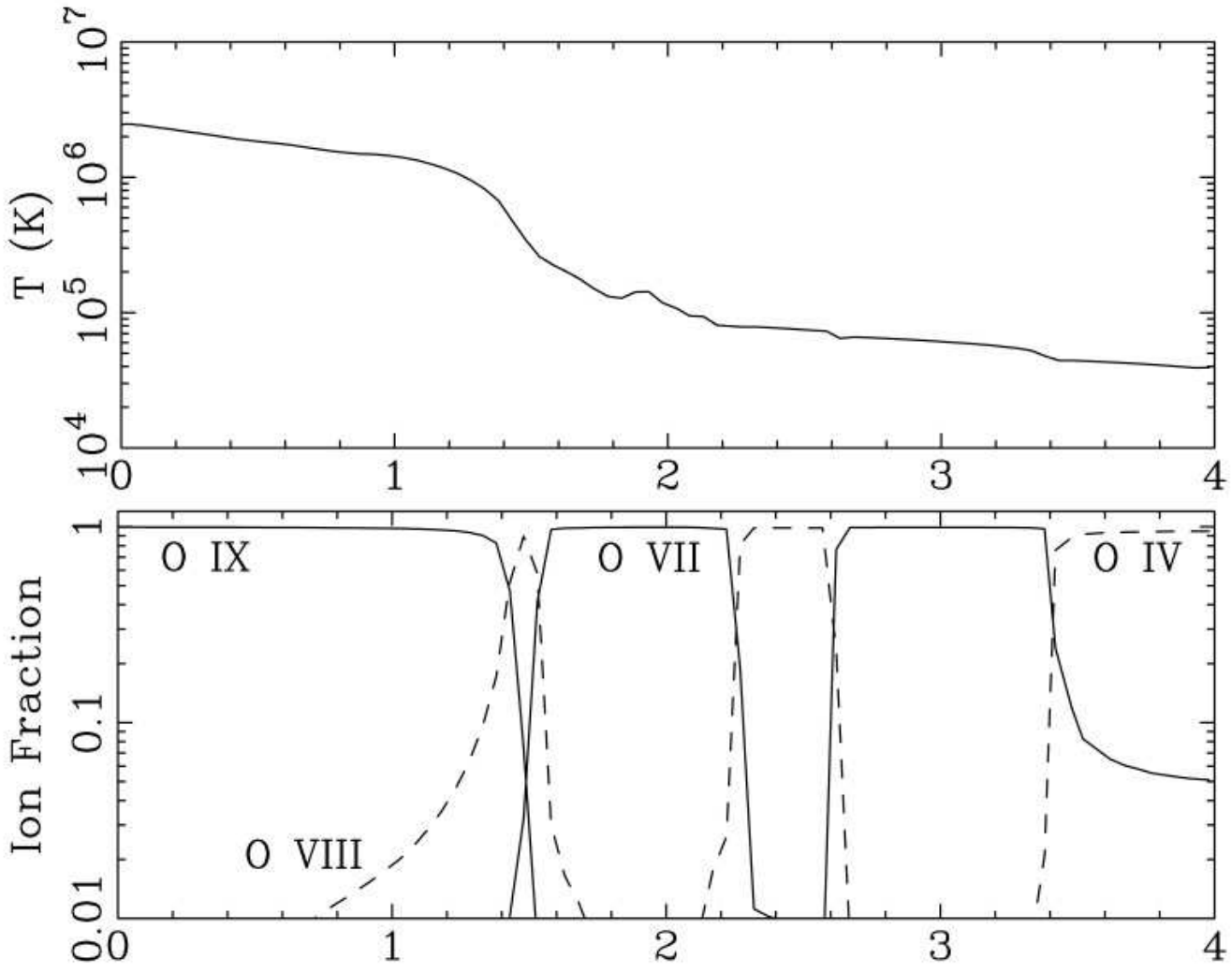

So far: neutral medium.

More realistic (Ross et al., 1999; Ross & Fabian, 2007; García & Kallman, 2010): ionized transition layer on disk surface.

(García & Kallman, 2010)

Ionized Reflection

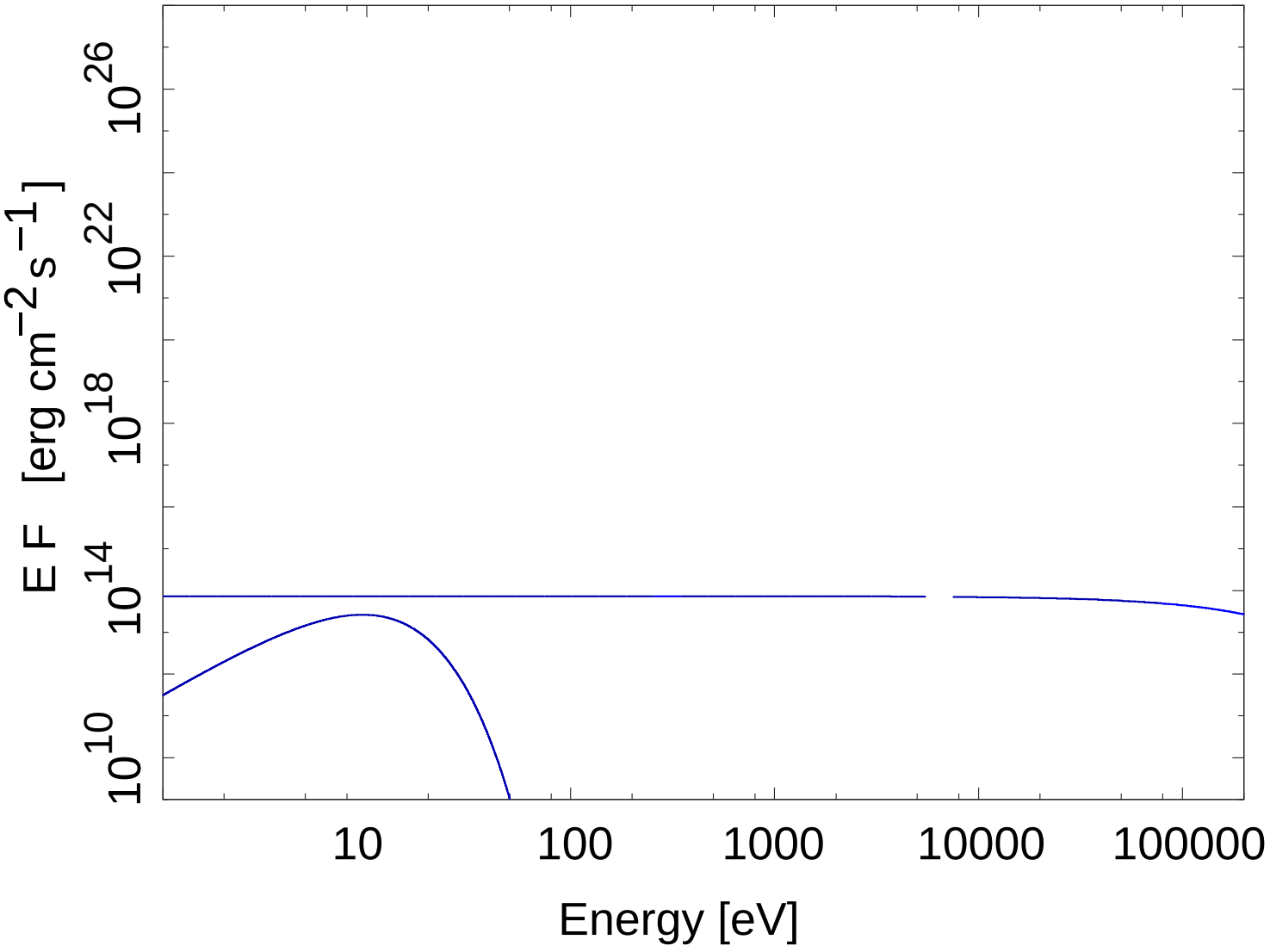

Ross & Fabian (2007, "`reflionx`"): Ionization: less absorption of lower Z elements $\Longrightarrow$ recovery of low energy emission, forest of emission lines

ionization parameter: $\xi = 4\pi F_{\mathrm{X}}/n_{\mathrm{e}}$

Update with improved atomic physics: García & Kallman (2010), García et al. (2011)

(Fig. after García & Kallman, 2010)

Ionized Reflection

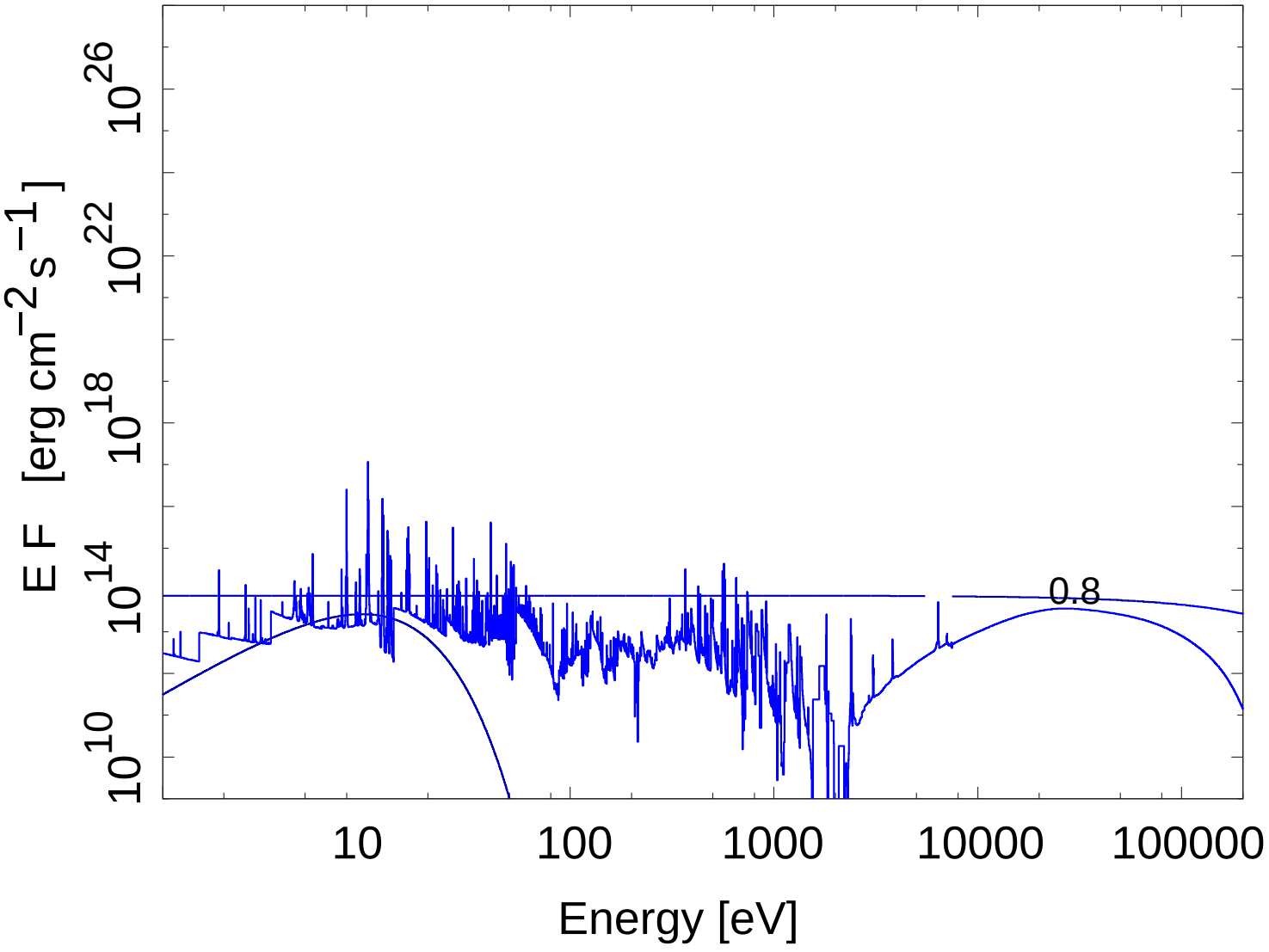

Ross & Fabian (2007, "`reflionx`"): Ionization: less absorption of lower Z elements $\Longrightarrow$ recovery of low energy emission, forest of emission lines

ionization parameter: $\xi = 4\pi F_{\mathrm{X}}/n_{\mathrm{e}}$

Update with improved atomic physics: García & Kallman (2010), García et al. (2011)

(Fig. after García & Kallman, 2010)

Ionized Reflection

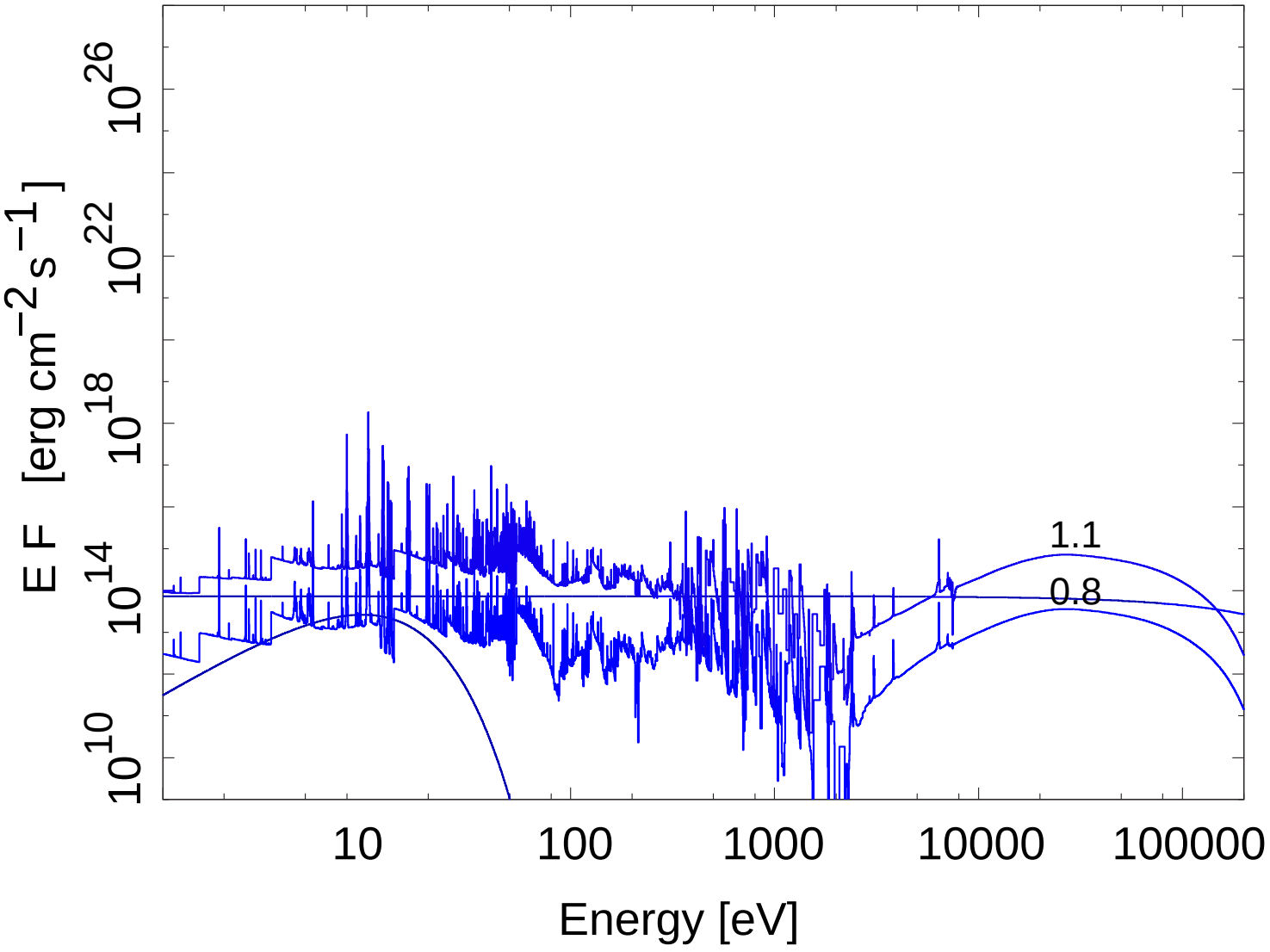

Ross & Fabian (2007, "`reflionx`"): Ionization: less absorption of lower Z elements $\Longrightarrow$ recovery of low energy emission, forest of emission lines

ionization parameter: $\xi = 4\pi F_{\mathrm{X}}/n_{\mathrm{e}}$

Update with improved atomic physics: García & Kallman (2010), García et al. (2011)

(Fig. after García & Kallman, 2010)

Ionized Reflection

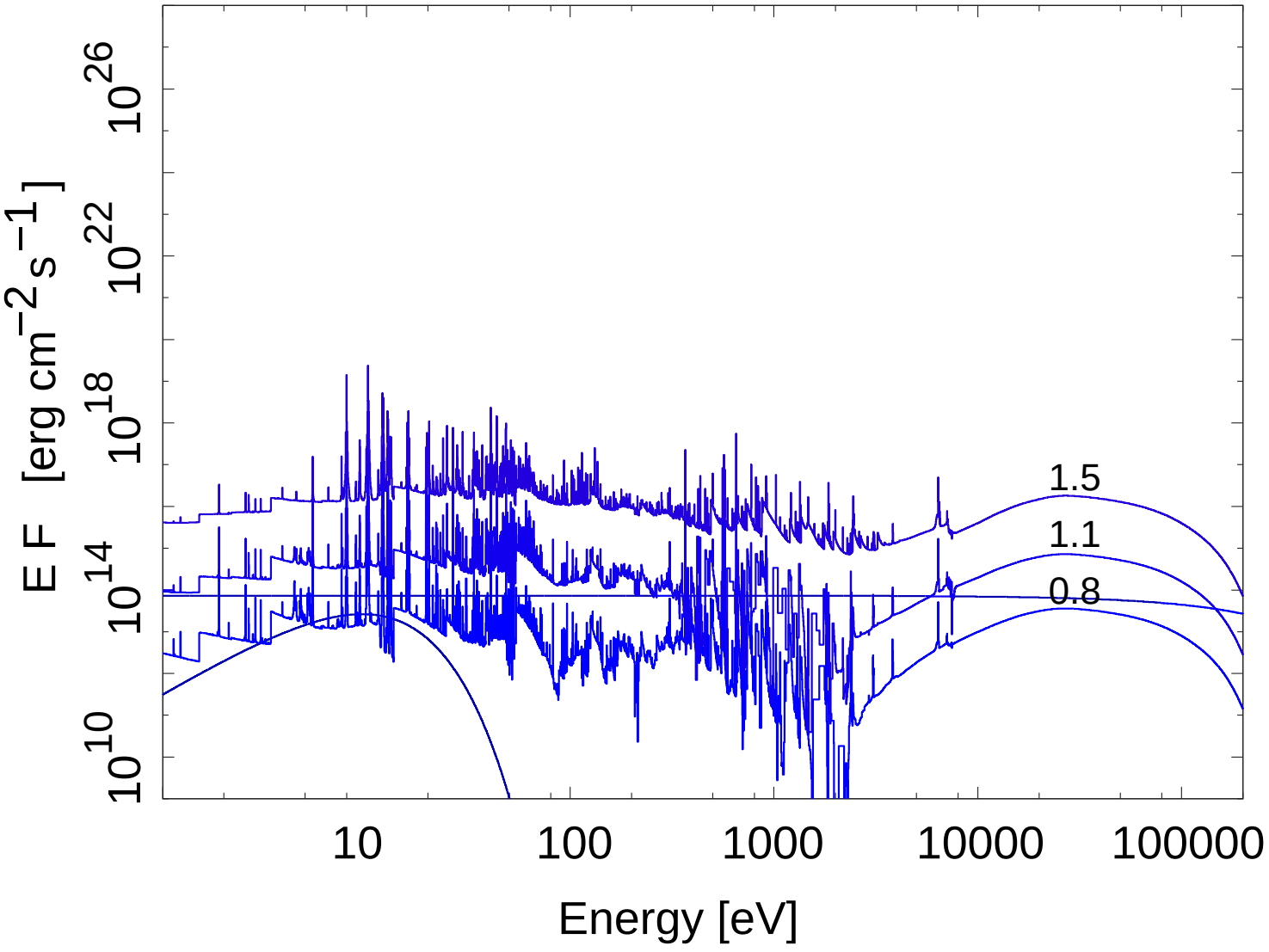

Ross & Fabian (2007, "`reflionx`"): Ionization: less absorption of lower Z elements $\Longrightarrow$ recovery of low energy emission, forest of emission lines

ionization parameter: $\xi = 4\pi F_{\mathrm{X}}/n_{\mathrm{e}}$

Update with improved atomic physics: García & Kallman (2010), García et al. (2011)

(Fig. after García & Kallman, 2010)

Ionized Reflection

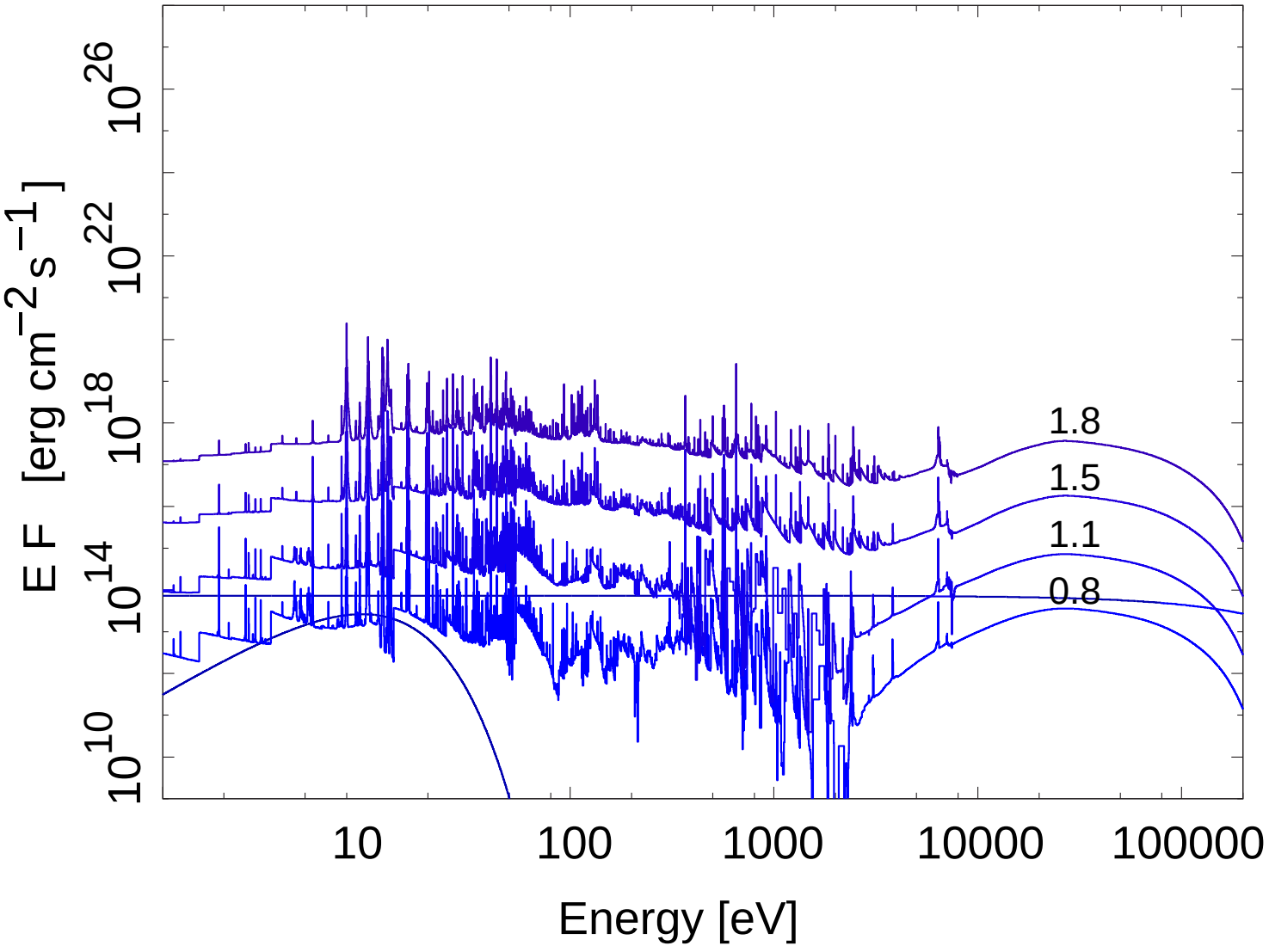

Ross & Fabian (2007, "`reflionx`"): Ionization: less absorption of lower Z elements $\Longrightarrow$ recovery of low energy emission, forest of emission lines

ionization parameter: $\xi = 4\pi F_{\mathrm{X}}/n_{\mathrm{e}}$

Update with improved atomic physics: García & Kallman (2010), García et al. (2011)

(Fig. after García & Kallman, 2010)

Ionized Reflection

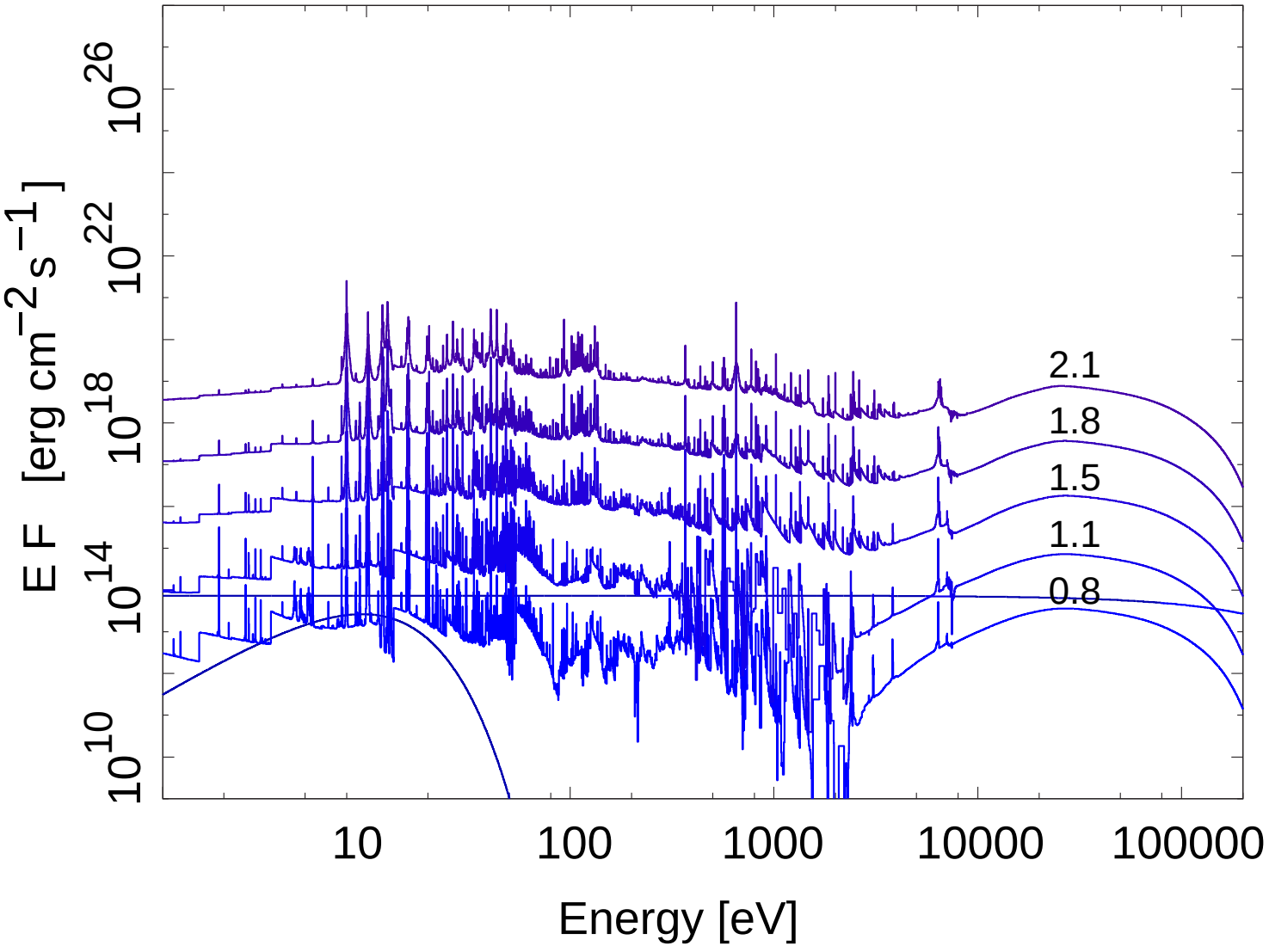

Ross & Fabian (2007, "`reflionx`"): Ionization: less absorption of lower Z elements $\Longrightarrow$ recovery of low energy emission, forest of emission lines

ionization parameter: $\xi = 4\pi F_{\mathrm{X}}/n_{\mathrm{e}}$

Update with improved atomic physics: García & Kallman (2010), García et al. (2011)

(Fig. after García & Kallman, 2010)

Ionized Reflection

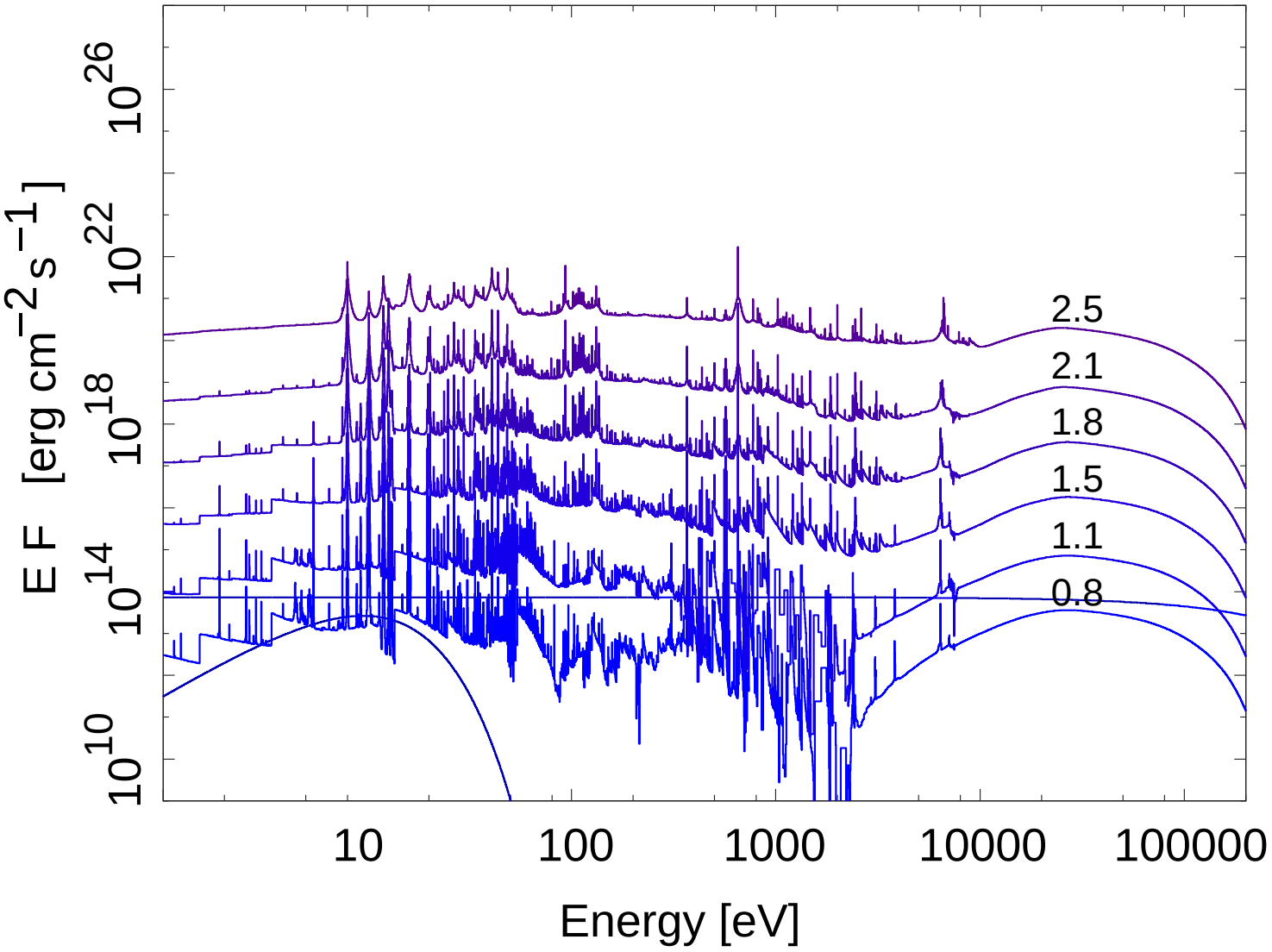

Ross & Fabian (2007, "`reflionx`"): Ionization: less absorption of lower Z elements $\Longrightarrow$ recovery of low energy emission, forest of emission lines

ionization parameter: $\xi = 4\pi F_{\mathrm{X}}/n_{\mathrm{e}}$

Update with improved atomic physics: García & Kallman (2010), García et al. (2011)

(Fig. after García & Kallman, 2010)

Ionized Reflection

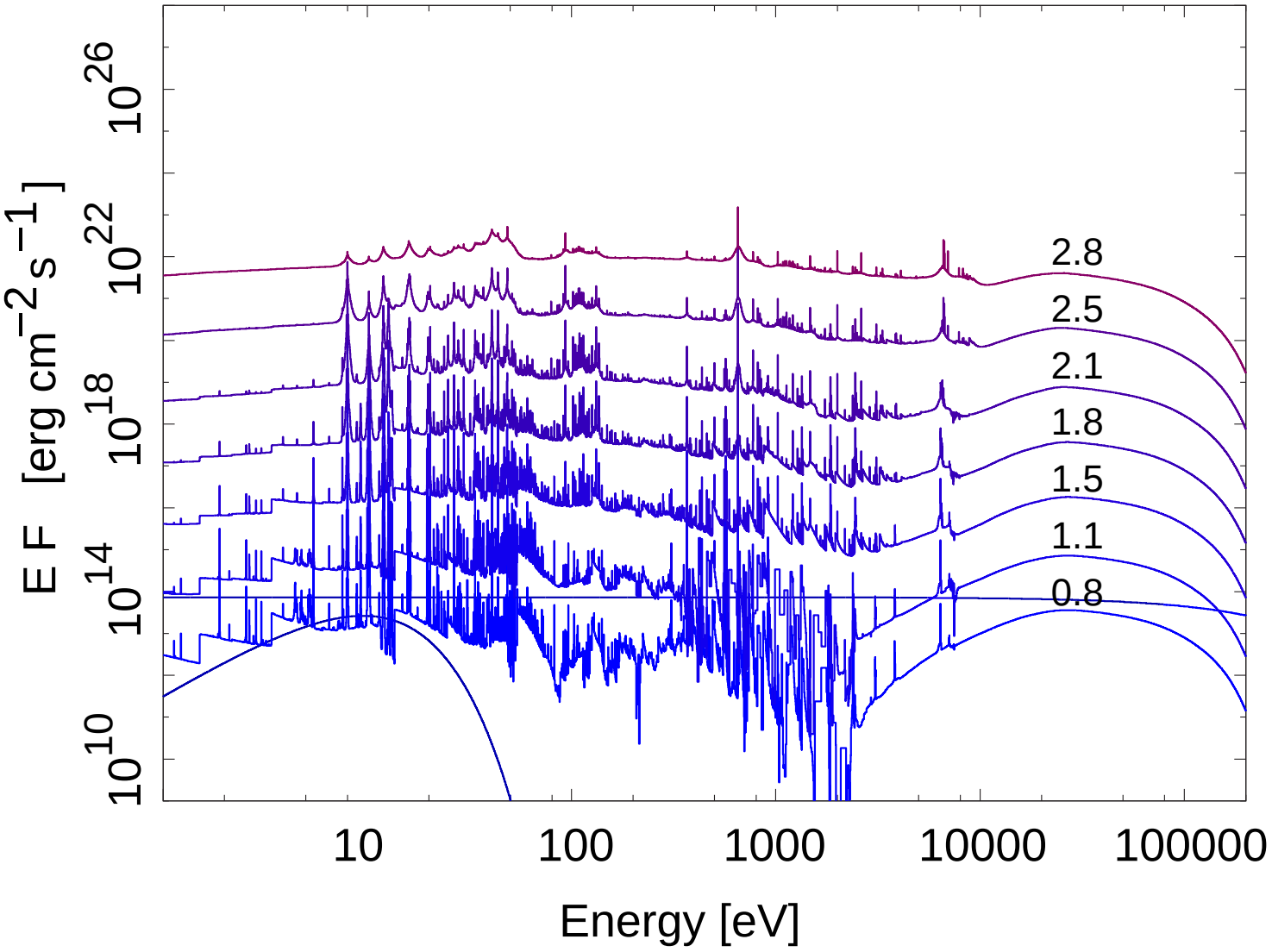

Ross & Fabian (2007, "`reflionx`"): Ionization: less absorption of lower Z elements $\Longrightarrow$ recovery of low energy emission, forest of emission lines

ionization parameter: $\xi = 4\pi F_{\mathrm{X}}/n_{\mathrm{e}}$

Update with improved atomic physics: García & Kallman (2010), García et al. (2011)

(Fig. after García & Kallman, 2010)

Ionized Reflection

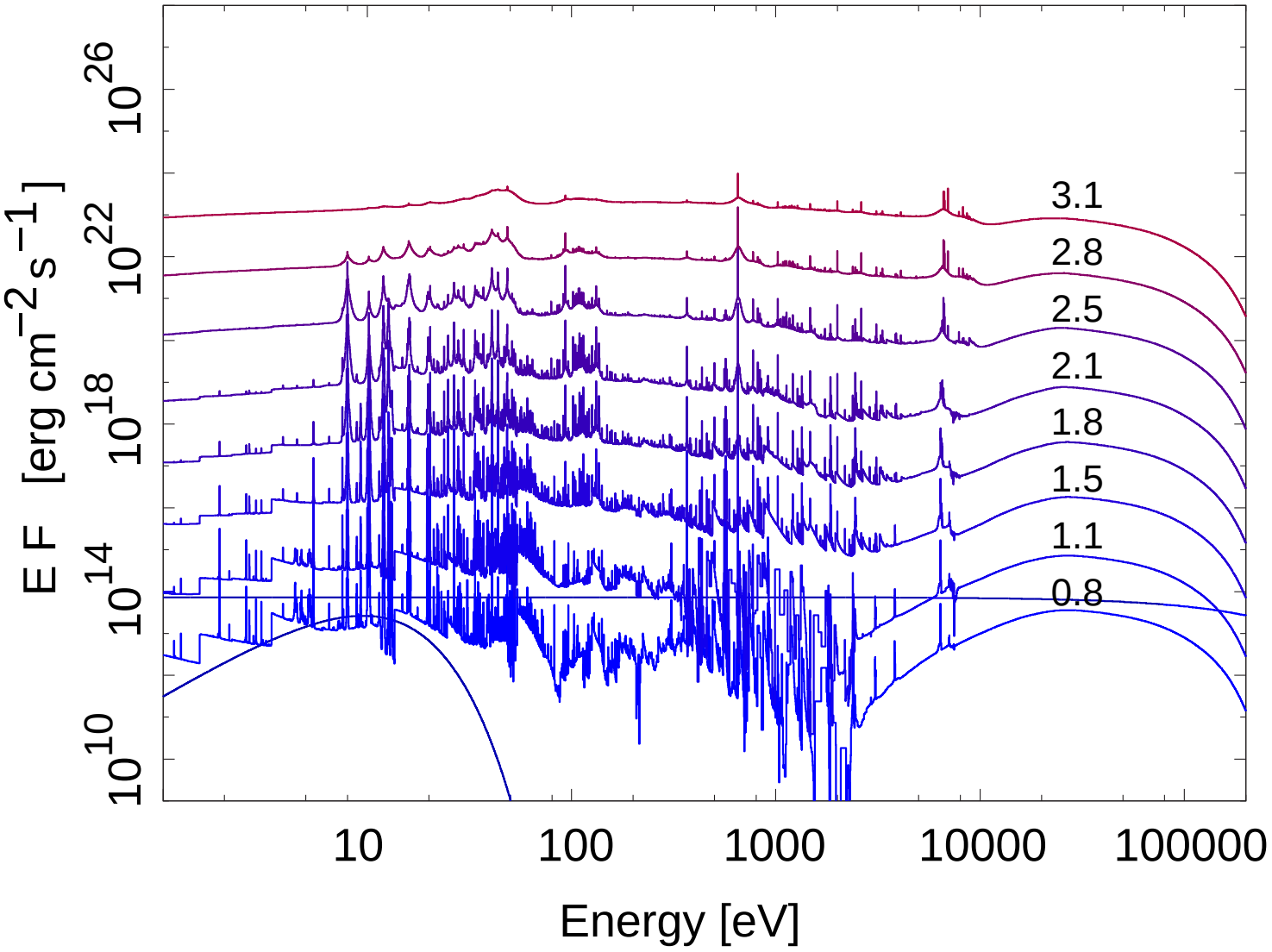

Ross & Fabian (2007, "`reflionx`"): Ionization: less absorption of lower Z elements $\Longrightarrow$ recovery of low energy emission, forest of emission lines

ionization parameter: $\xi = 4\pi F_{\mathrm{X}}/n_{\mathrm{e}}$

Update with improved atomic physics: García & Kallman (2010), García et al. (2011)

(Fig. after García & Kallman, 2010)

Ionized Reflection

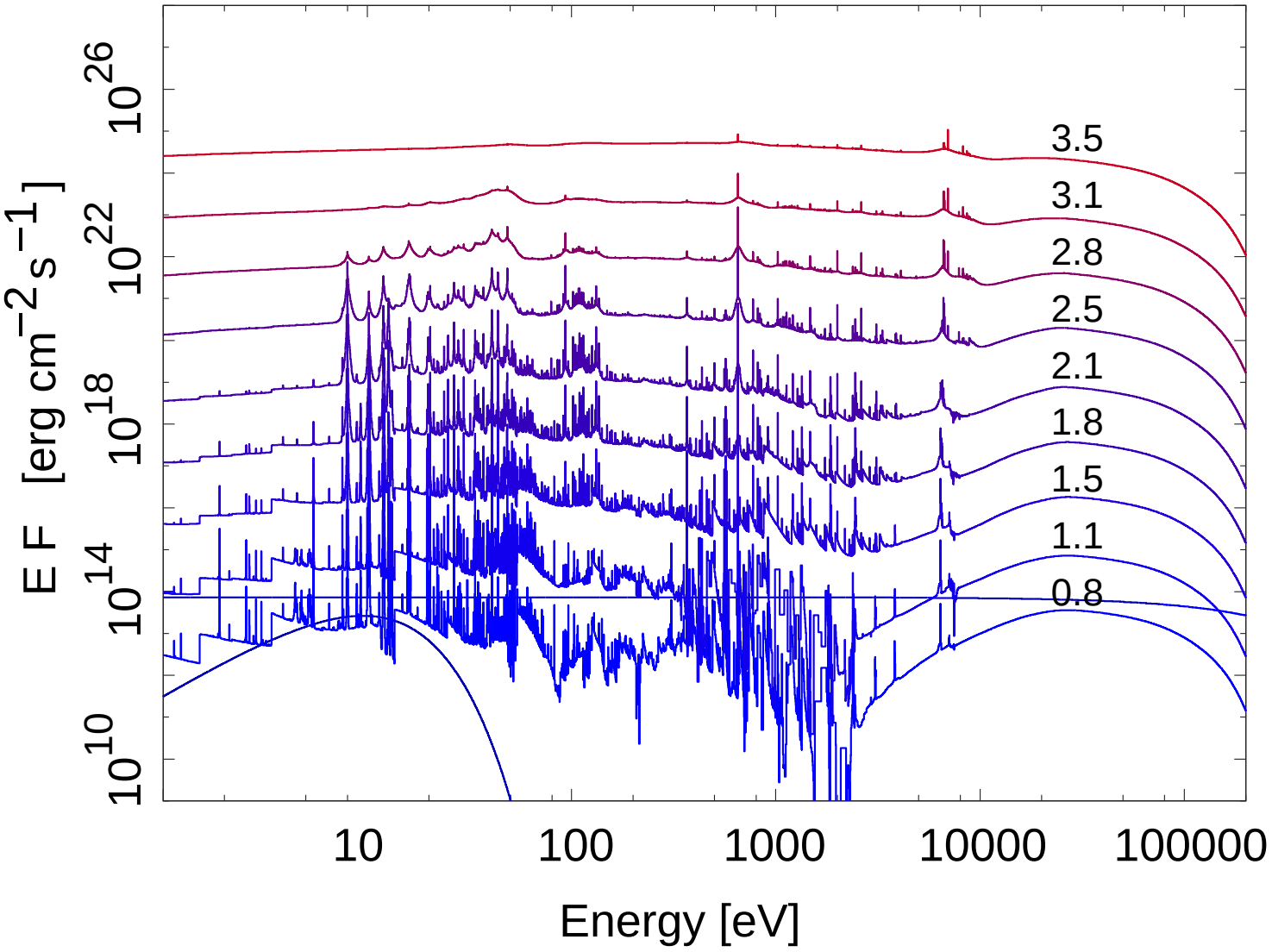

Ross & Fabian (2007, "`reflionx`"): Ionization: less absorption of lower Z elements $\Longrightarrow$ recovery of low energy emission, forest of emission lines

ionization parameter: $\xi = 4\pi F_{\mathrm{X}}/n_{\mathrm{e}}$

Update with improved atomic physics: García & Kallman (2010), García et al. (2011)

(Fig. after García & Kallman, 2010)

Ionized Reflection

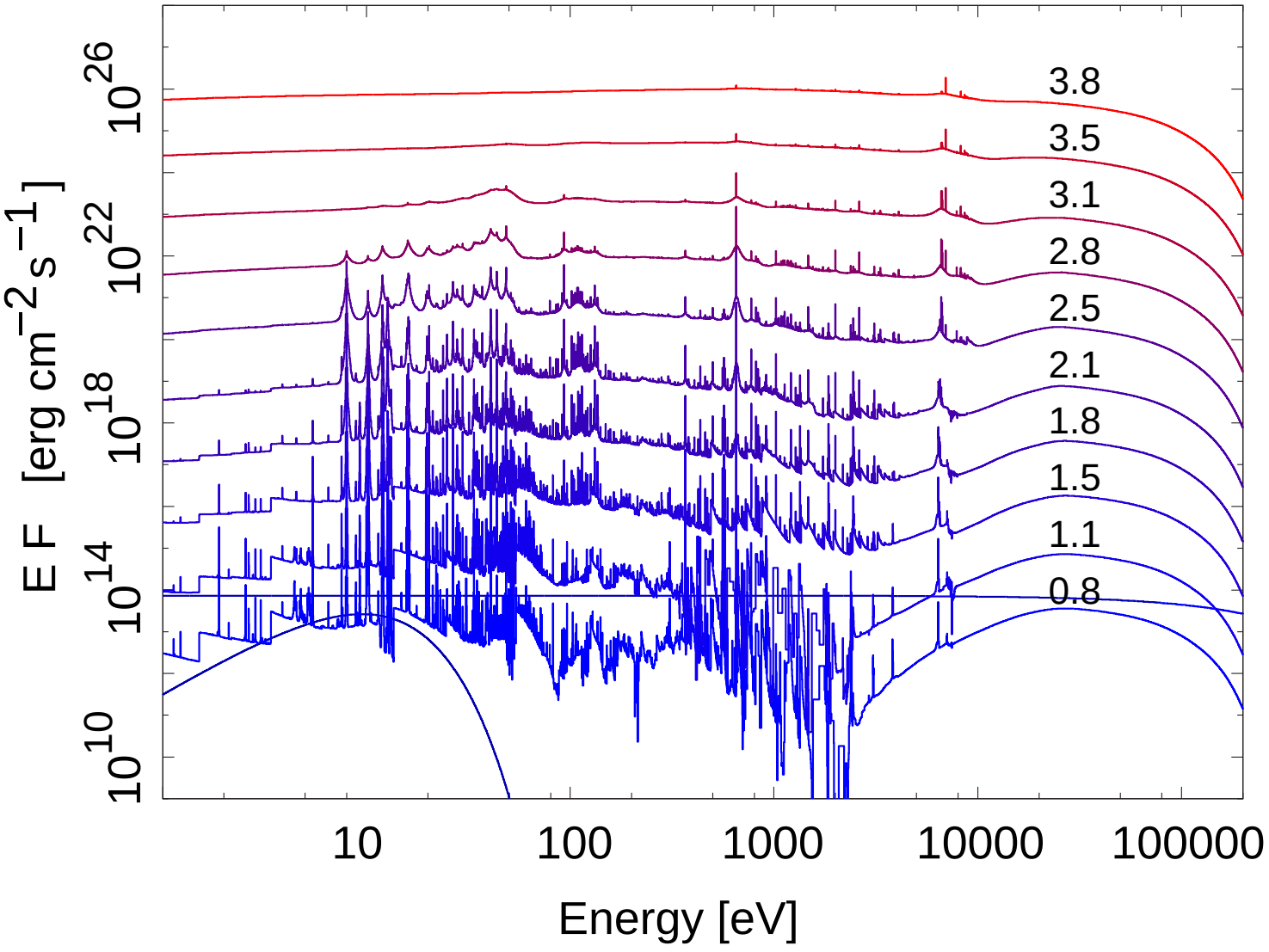

Ross & Fabian (2007, "`reflionx`"): Ionization: less absorption of lower Z elements $\Longrightarrow$ recovery of low energy emission, forest of emission lines

ionization parameter: $\xi = 4\pi F_{\mathrm{X}}/n_{\mathrm{e}}$

Update with improved atomic physics: García & Kallman (2010), García et al. (2011)

(Fig. after García & Kallman, 2010)

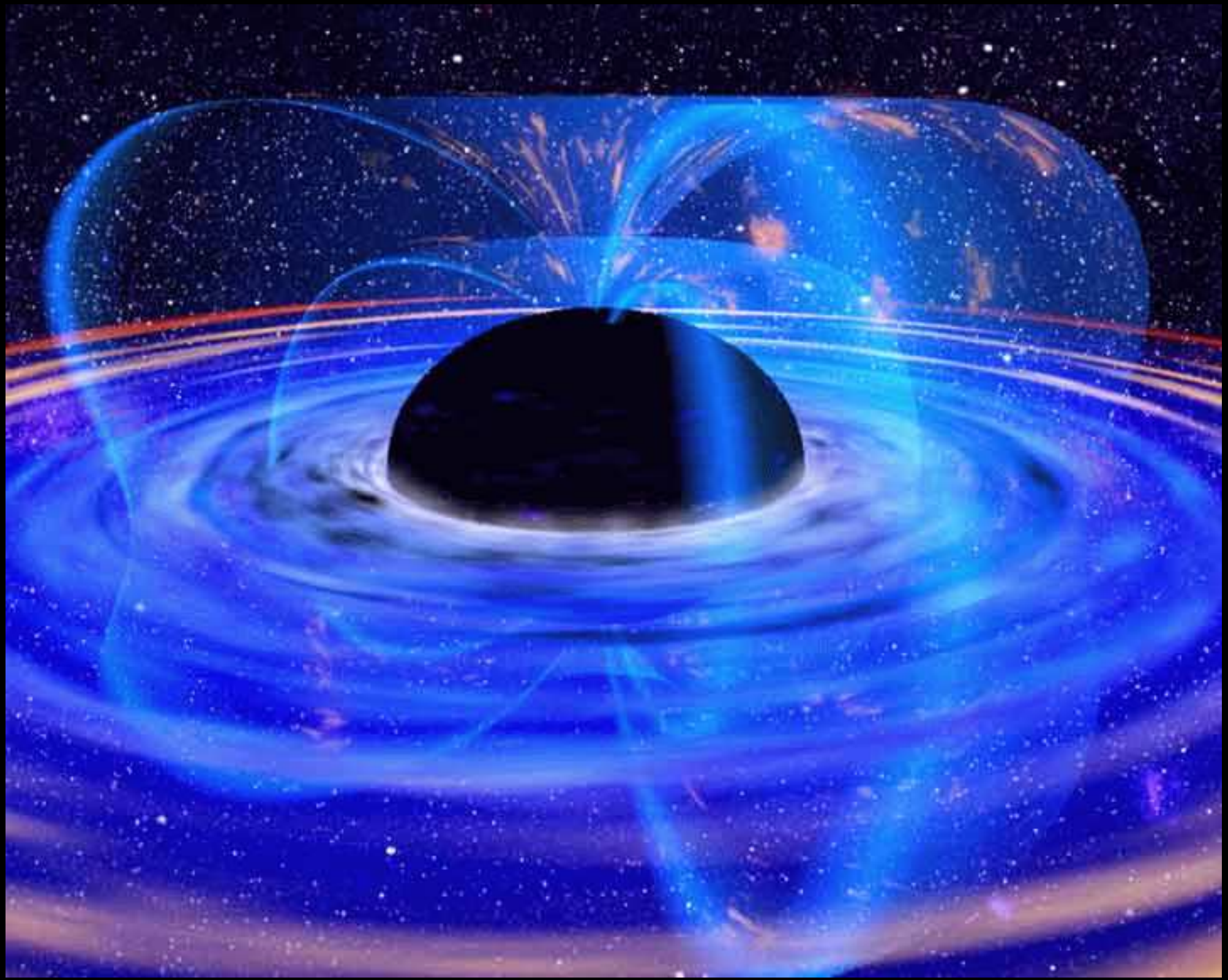

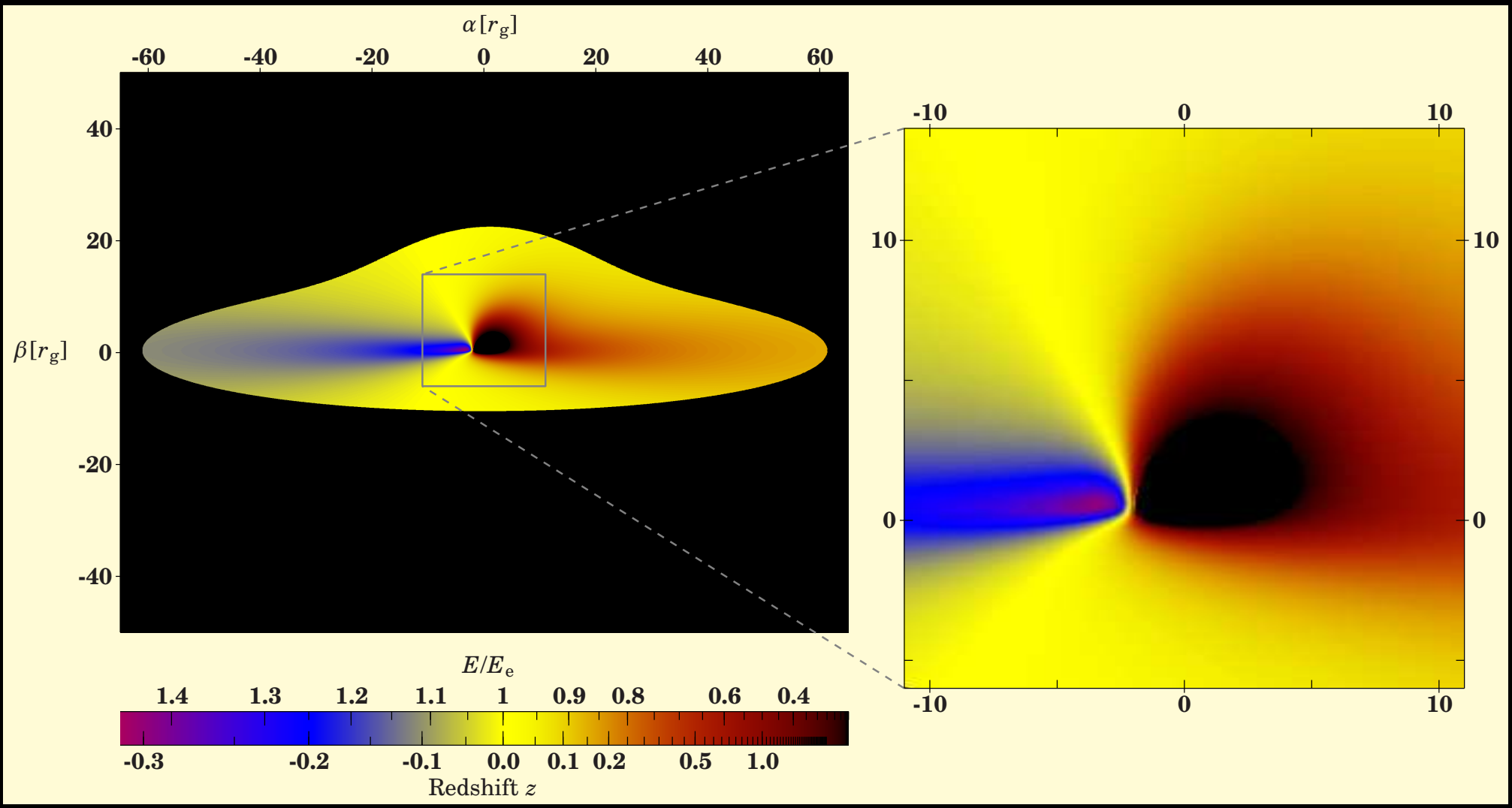

(Dauser, 2010)

Close to the black hole, we need to include relativistic effects: special relativistic beaming, light bending, and gravitational redshifts.

(Cunningham, 1975; Fabian et al., 1989; Laor, 1991; Dovčiak et al., 2004; Dauser et al., 2010)

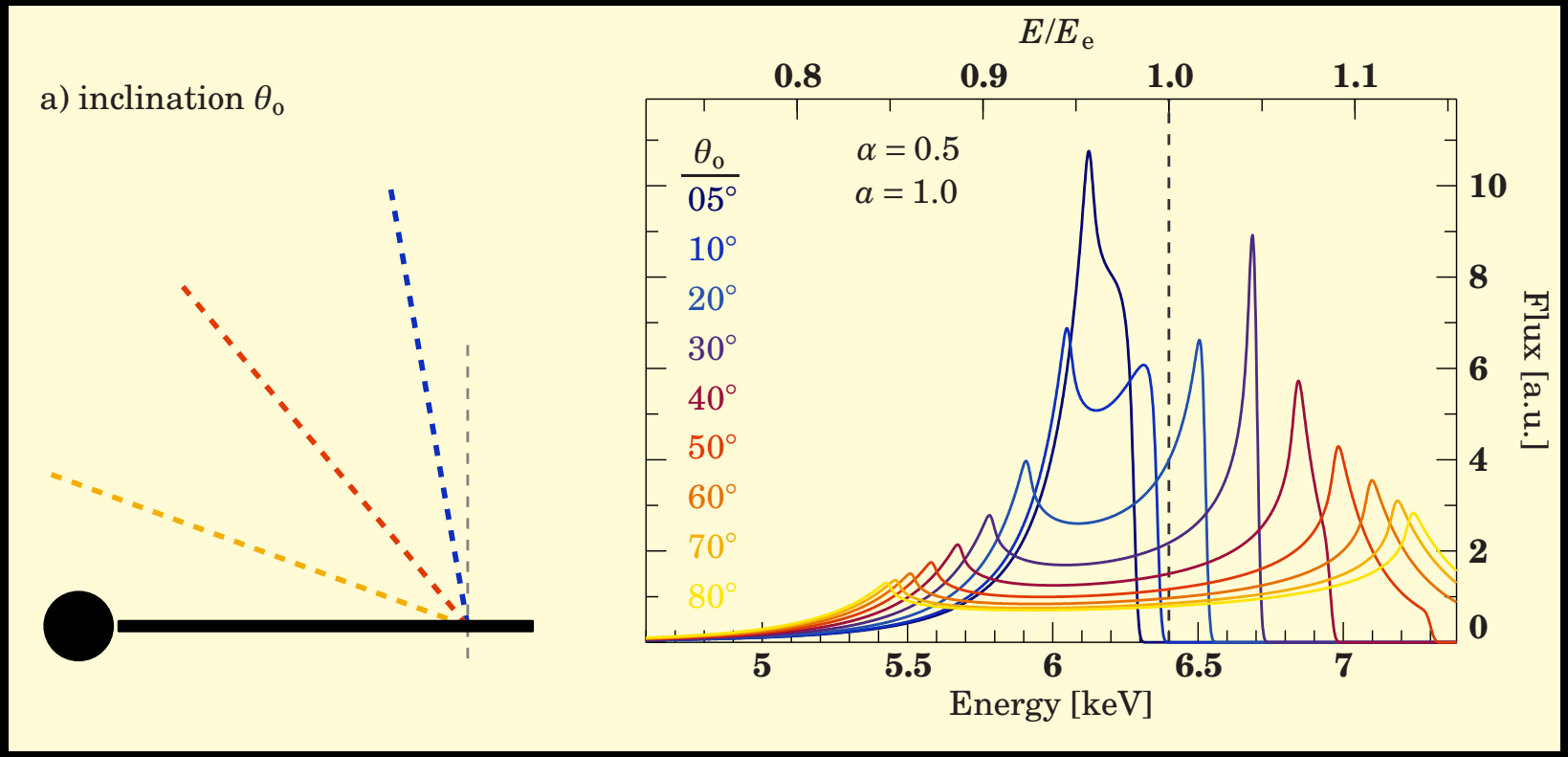

(Dauser, 2010)

Line profile has strong diagnostic potential: inclination

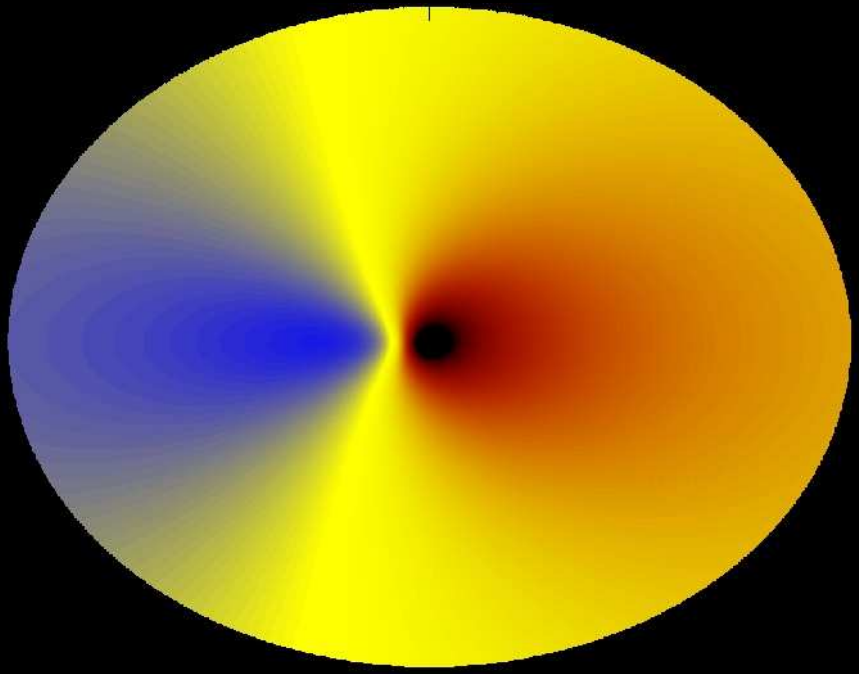

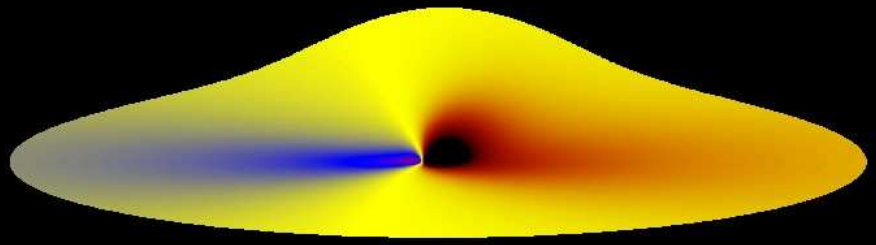

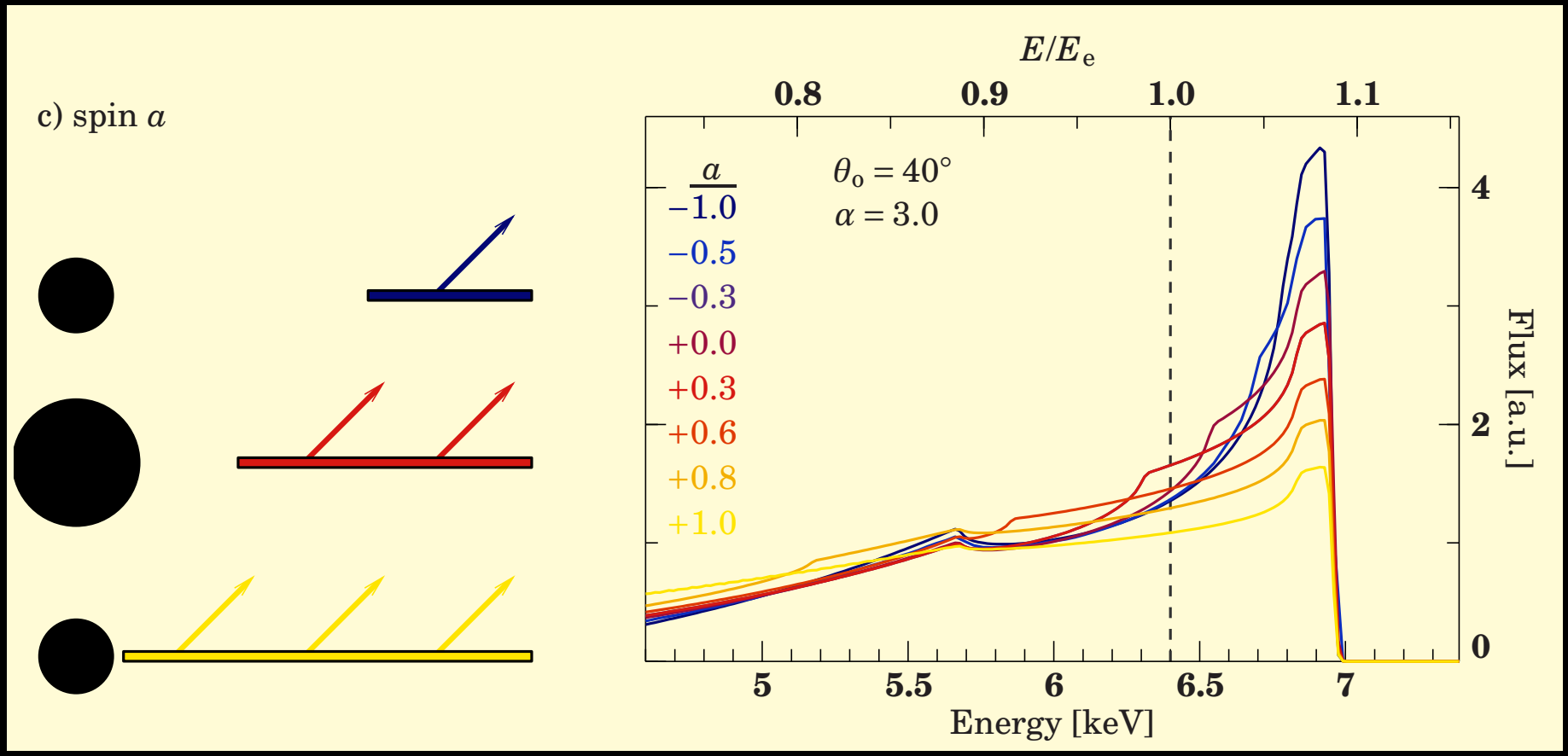

(Dauser, 2010)

Line profile has diagnostic potential:
black hole spin (“holy grail”)

“negative spin”: angular momenta of disk and BH are antiparallel, also a stable configuration (King et al., 2008)

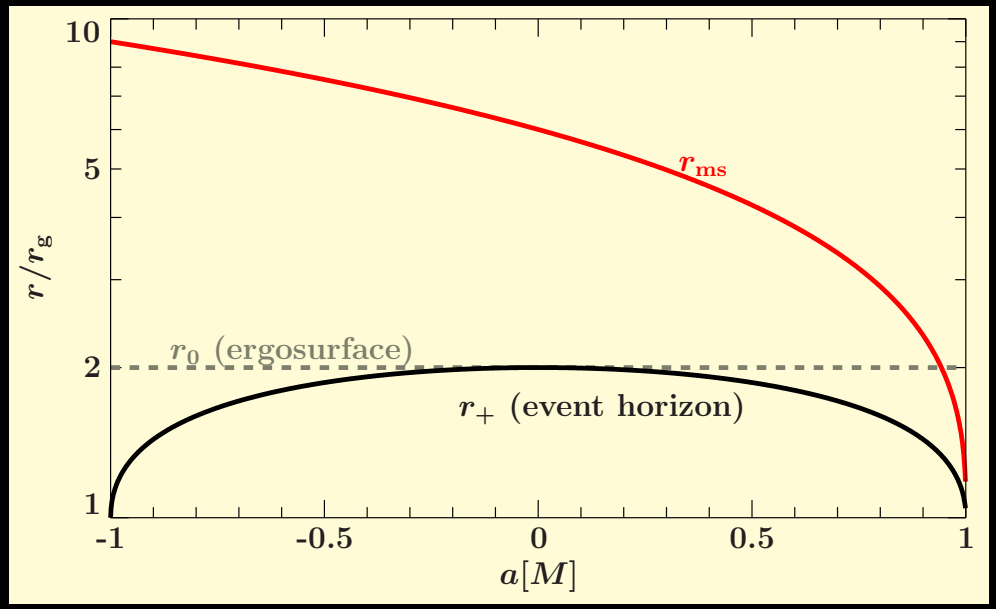

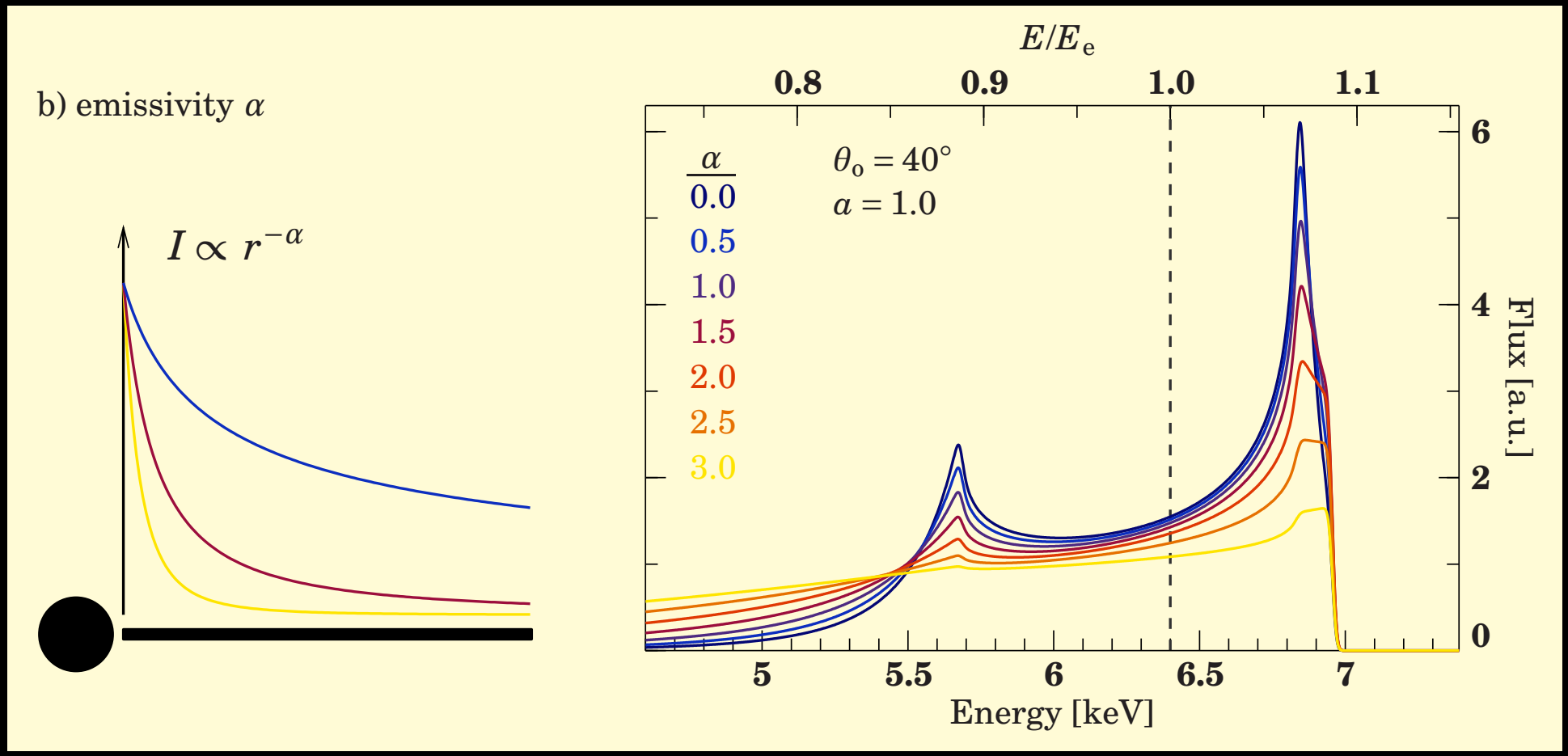

(Dauser, 2010)

Line profile has diagnostic potential: disk emissivity (=energy release per unit area)

for an α-disk: $\alpha \sim 3$

Relativistic Kα Lines

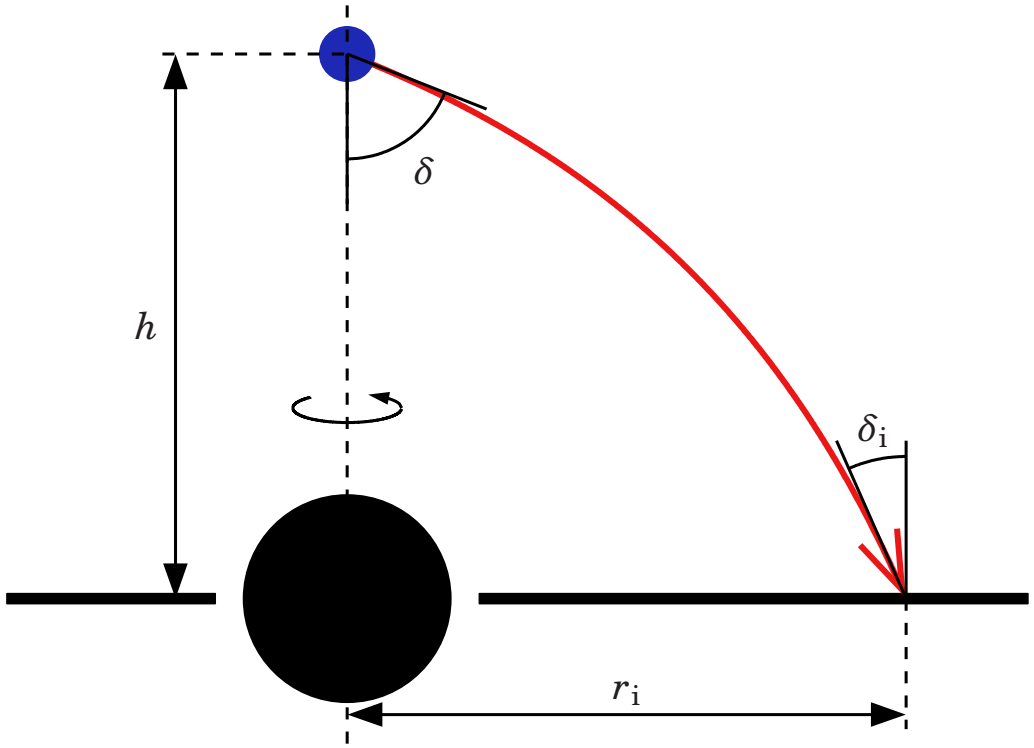

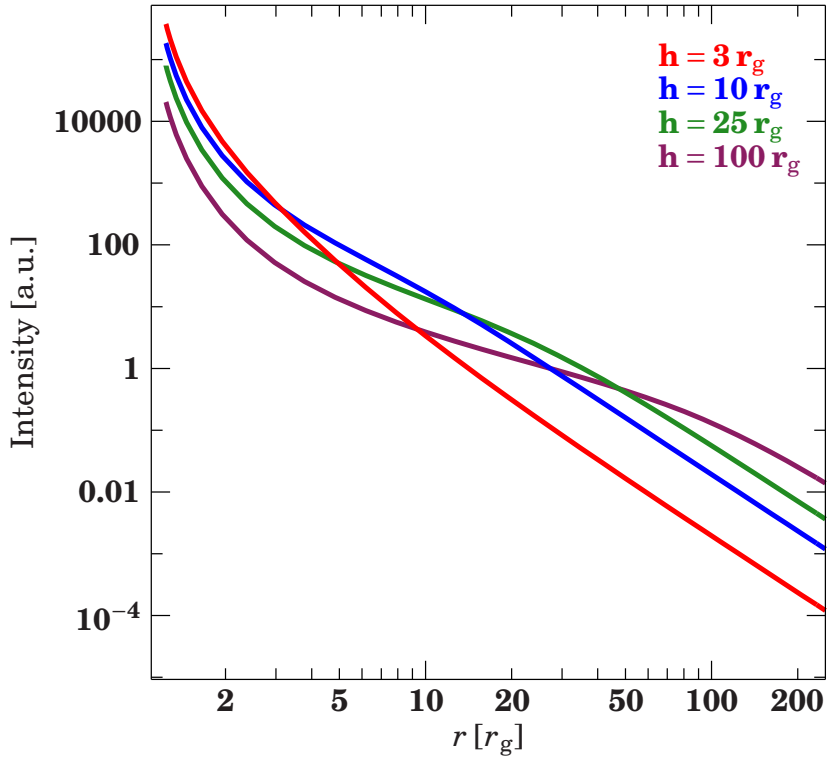

- Disks: emissivity α not well constrained
- Lamppost geometry: emissivity only depends on height above BH

Relativistic Smearing

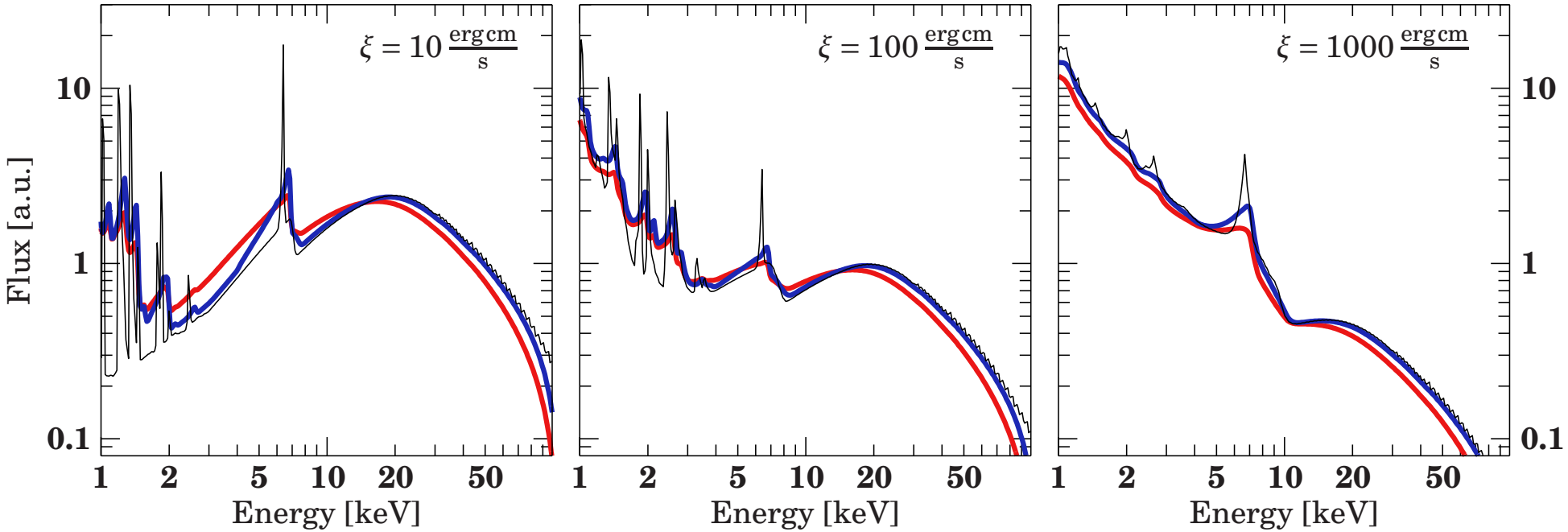

(Dauser, 2010)

Relativistic smearing affects the whole reflection spectrum

Only modeling a strong emission line with relativistic effects and ignoring the reflection continuum is wrong.

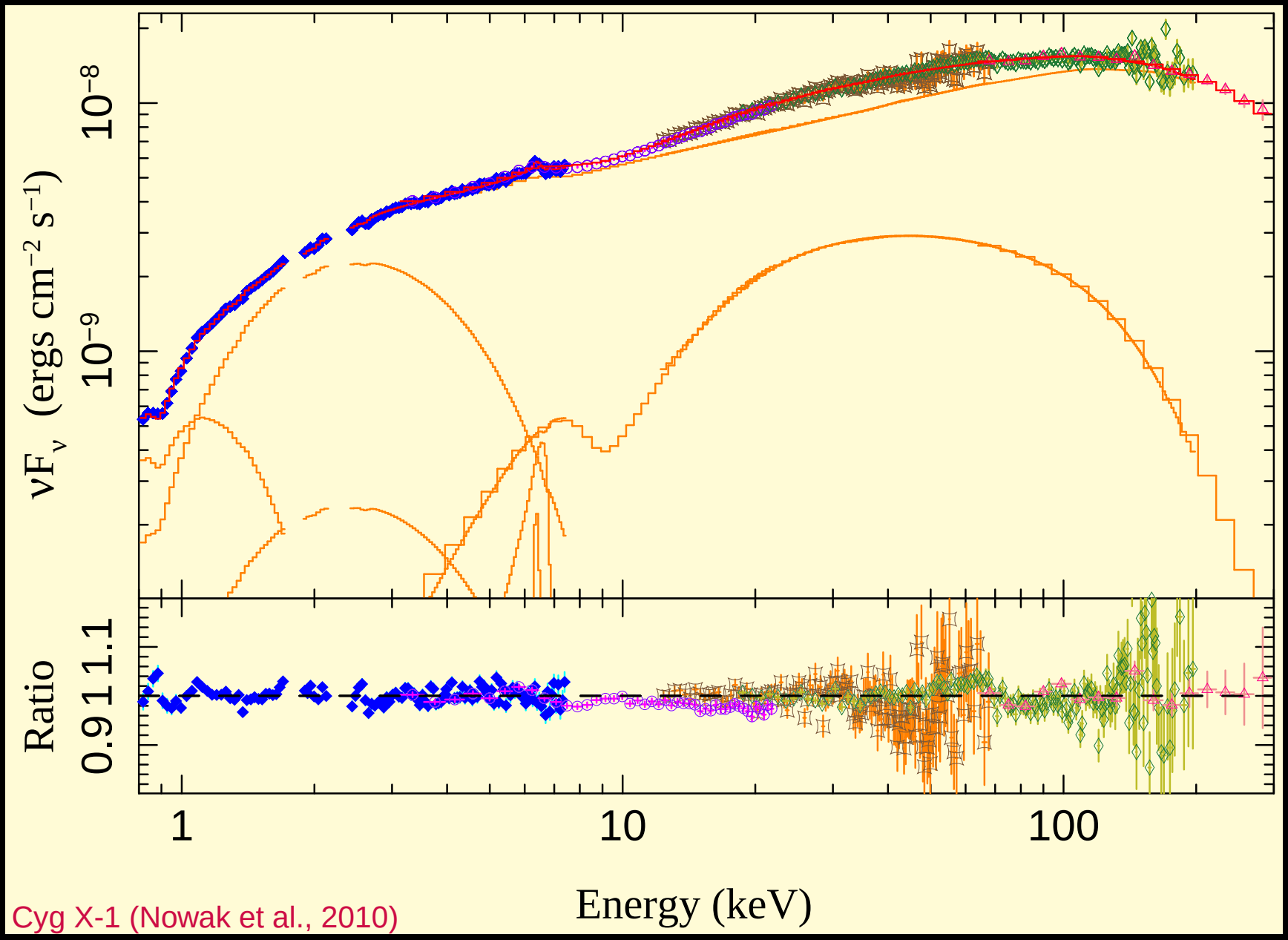

Cyg X-1 (Nowak et al., 2010)

Thermal Comptonization plus reflection explain the broad-band spectrum very well.

Tests better done in Galactic sources, since S/N much better

Broad Lines in AGN

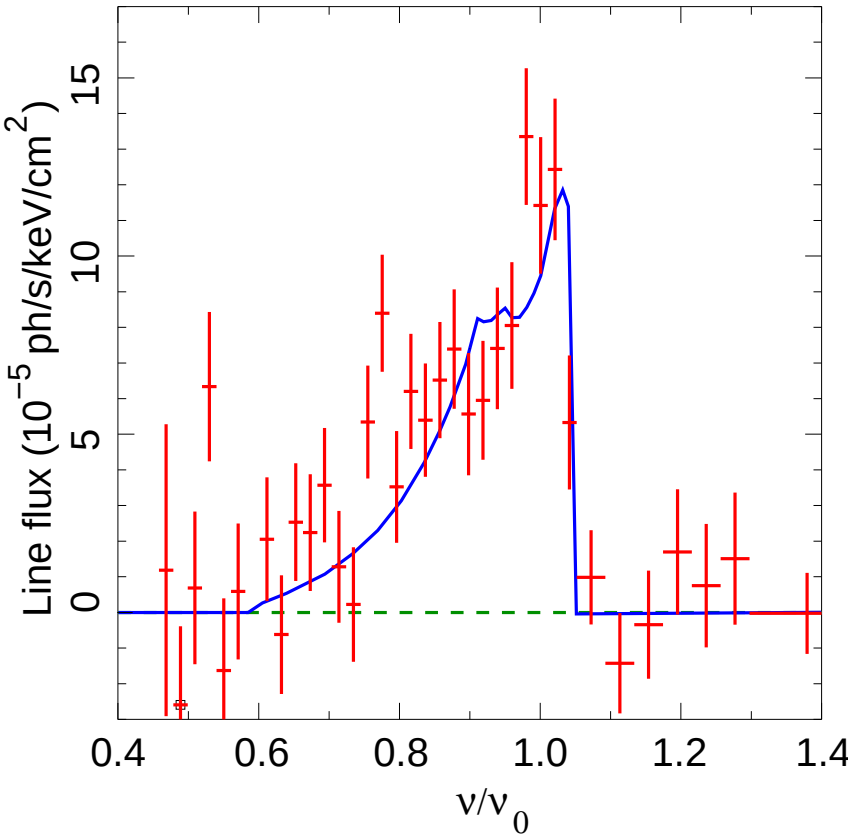

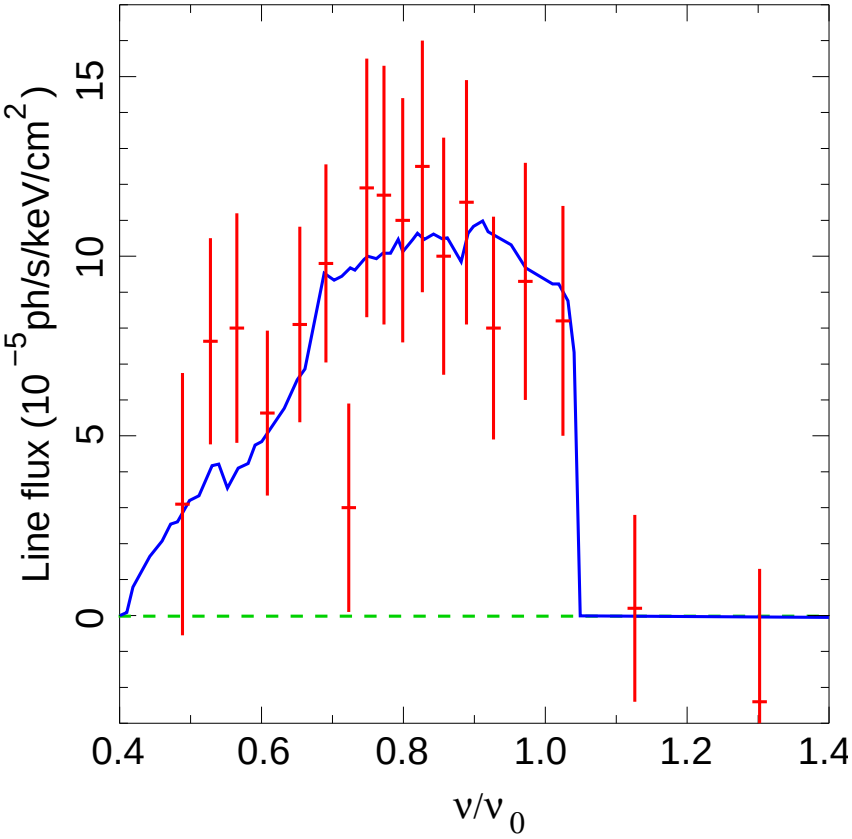

MCG−6-30-15 ($z = 0.008$): first AGN with relativistic disk line

Tanaka et al. (1995): time averaged *ASCA* spectrum: line skew symmetric
$\Longrightarrow$ Schwarzschild black hole.

Iwasawa et al. (1996): “deep minimum state”: extremely broad line
$\Longrightarrow$ Kerr Black Hole.

Broad Lines in AGN

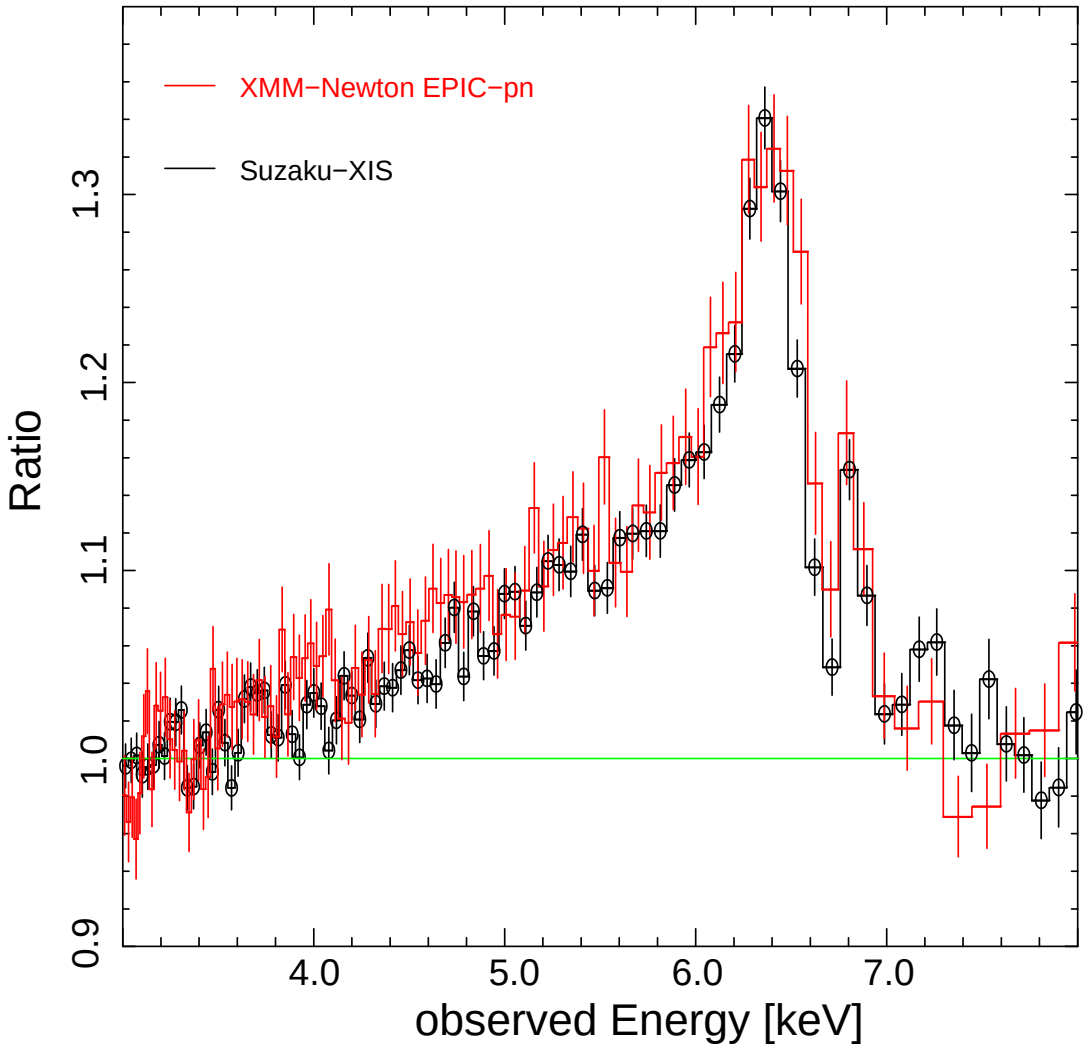

Suzaku (2006 Jan; ∼350 ksec; Miniutti et al. 2007)

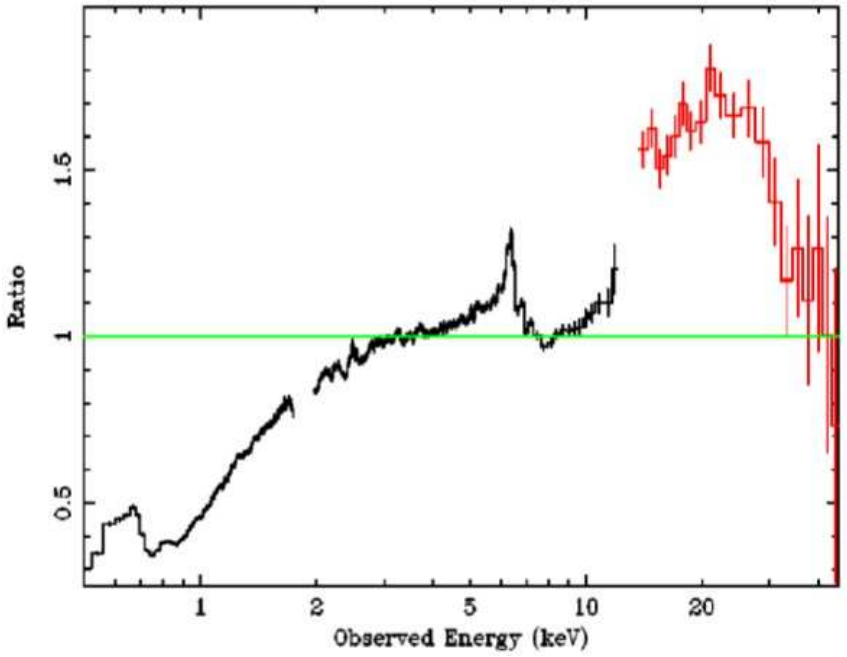

Brenneman & Reynolds (2006): Angular momentum of BH in MGC−6-30-15: $a = 0.989^{+0.009}_{-0.002}$.

Assuming no emission from within innermost stable circular orbit, (too) tightly constrained geometry.

Broad Lines in AGN

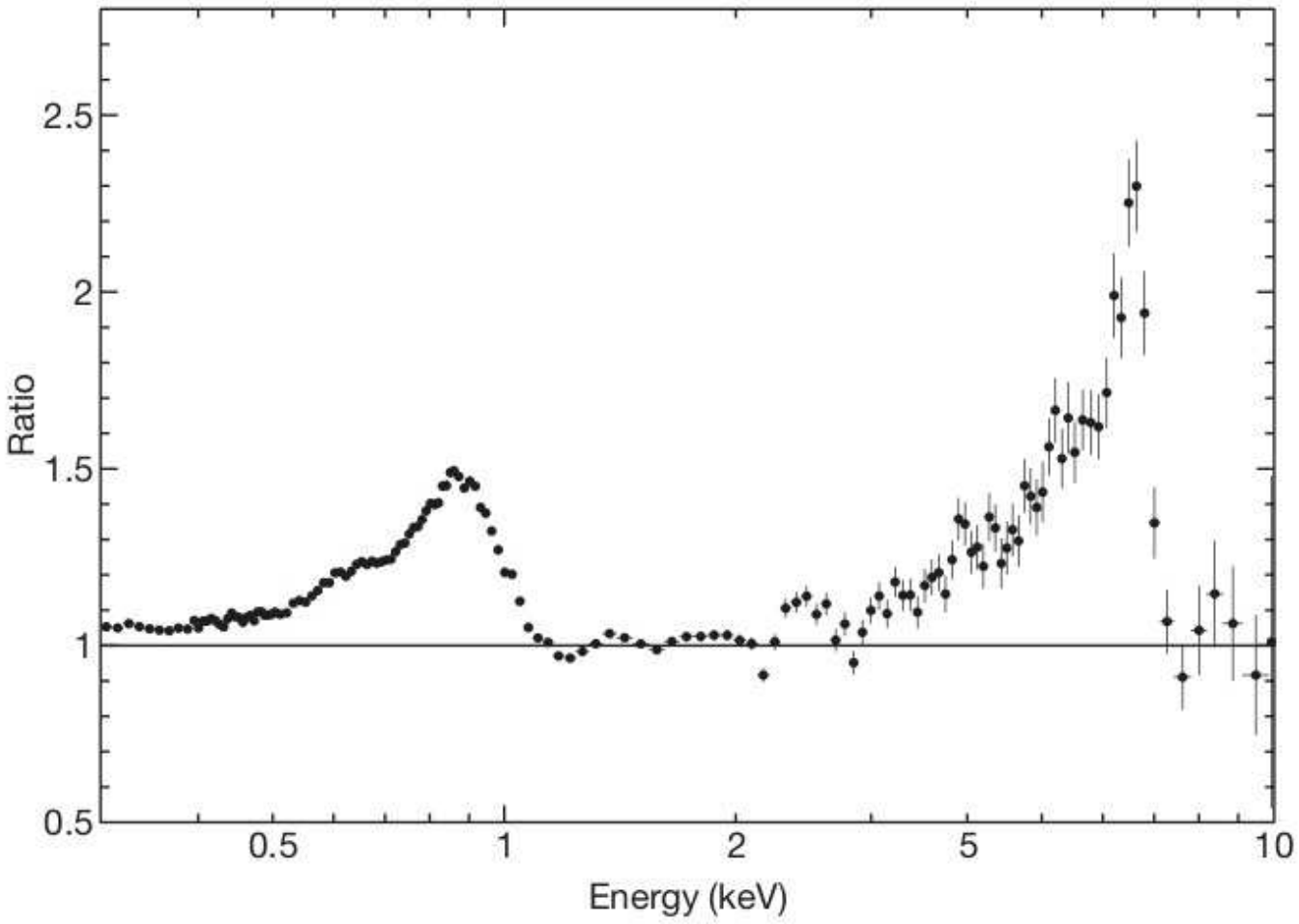

(Fabian et al., 2009)

1H0707−495 (NL Sy1): relativistically broadened Fe Kα *and* Lα lines; $a > 0.98$

Similar results also for IRAS13224−3809 (Ponti et al., 2010)

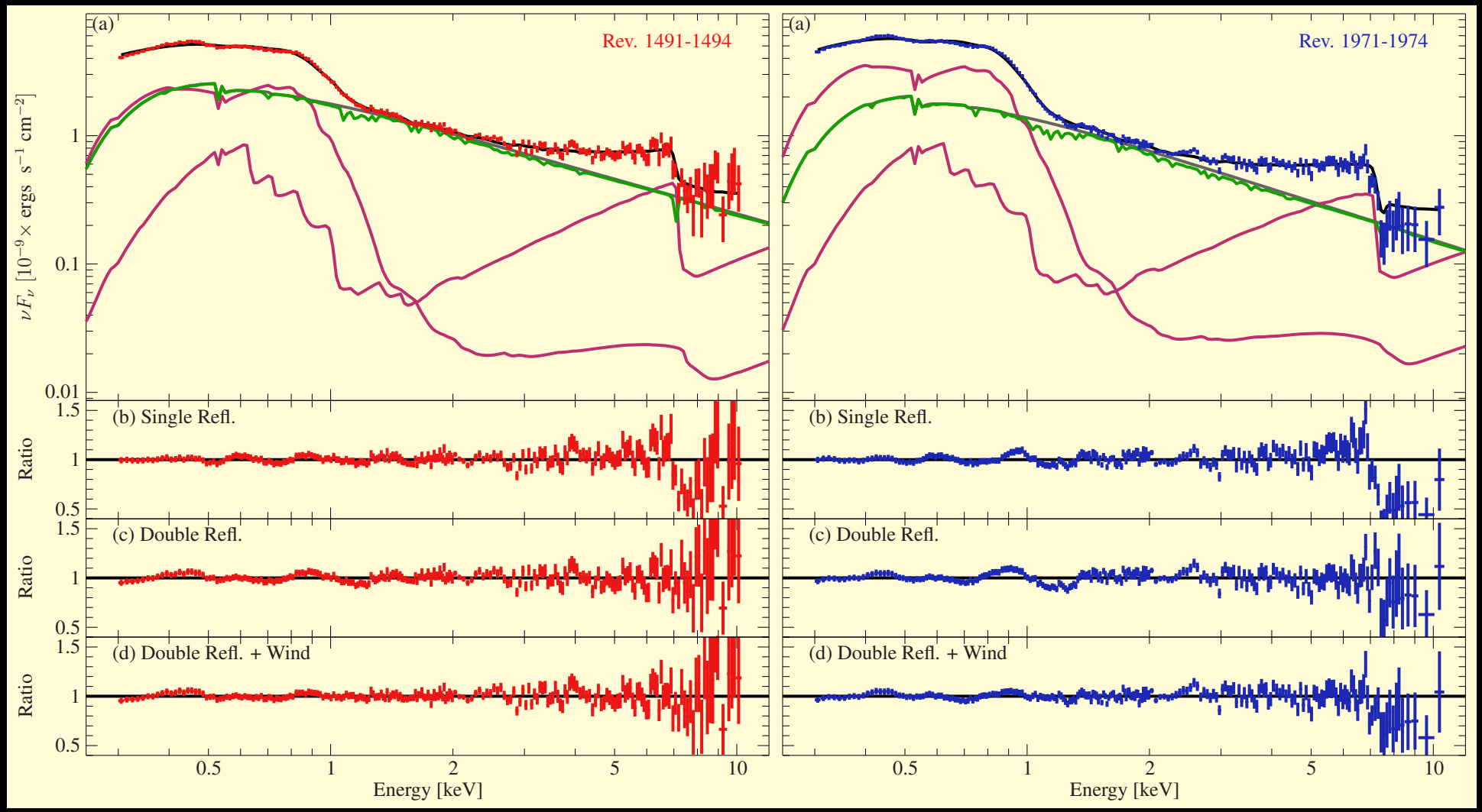

Dauser et al. (2011, submitted)

full decomposition of the spectrum of 1H0707−495

Broad Lines in AGN

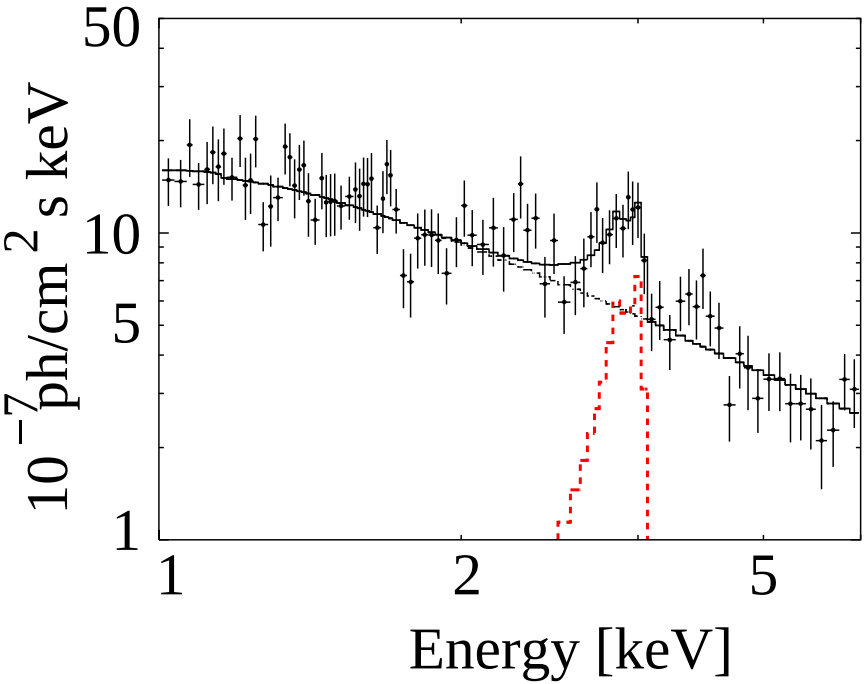

(Comastri et al. 2004; *Chandra*)

CXO J123716.7+621733 (CDF-N; $z = 1.146$)

Broad Fe Kα lines already present in high-z universe!

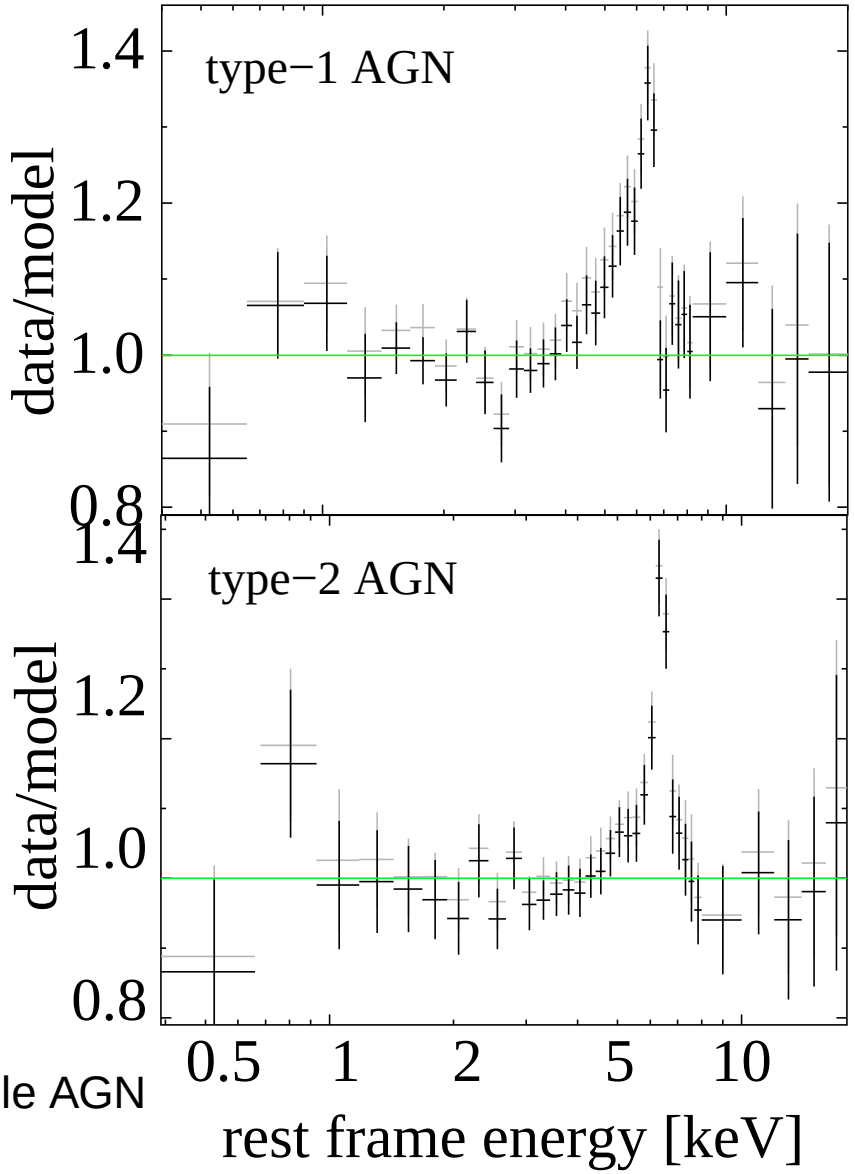

Average Fe line for the Lockman hole AGN

(Streblyanska et al., 2005)

non detections

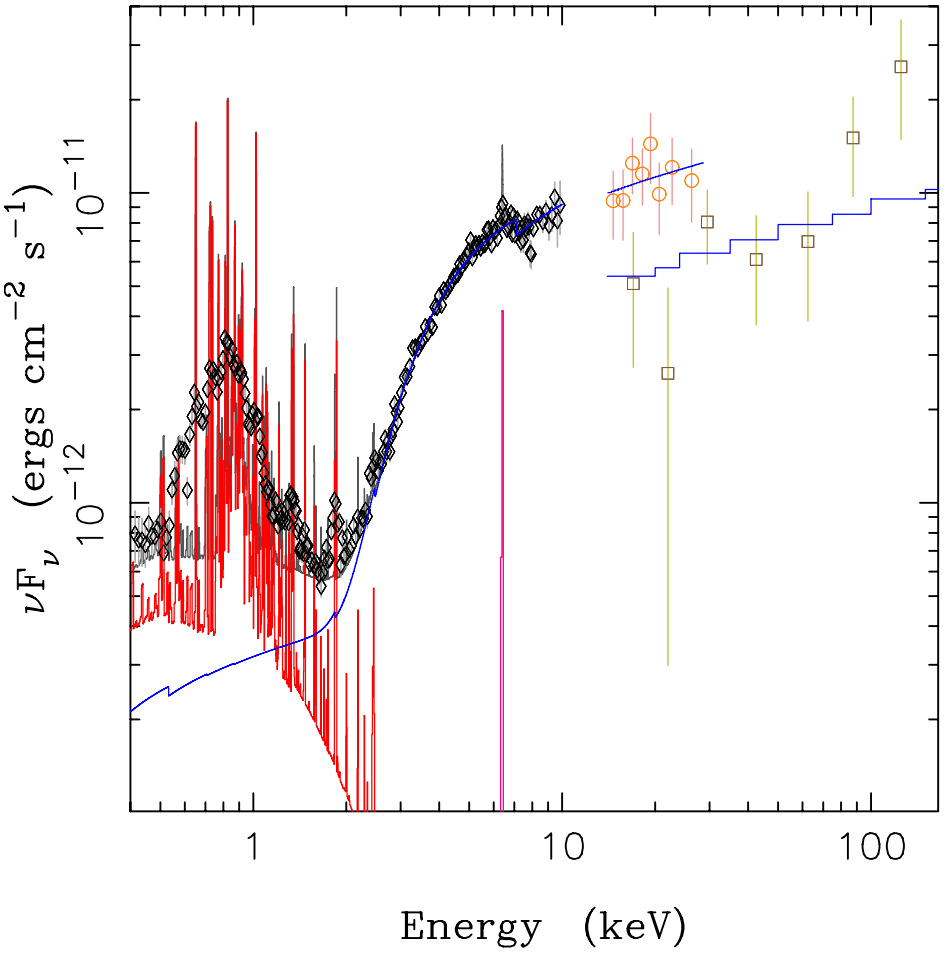

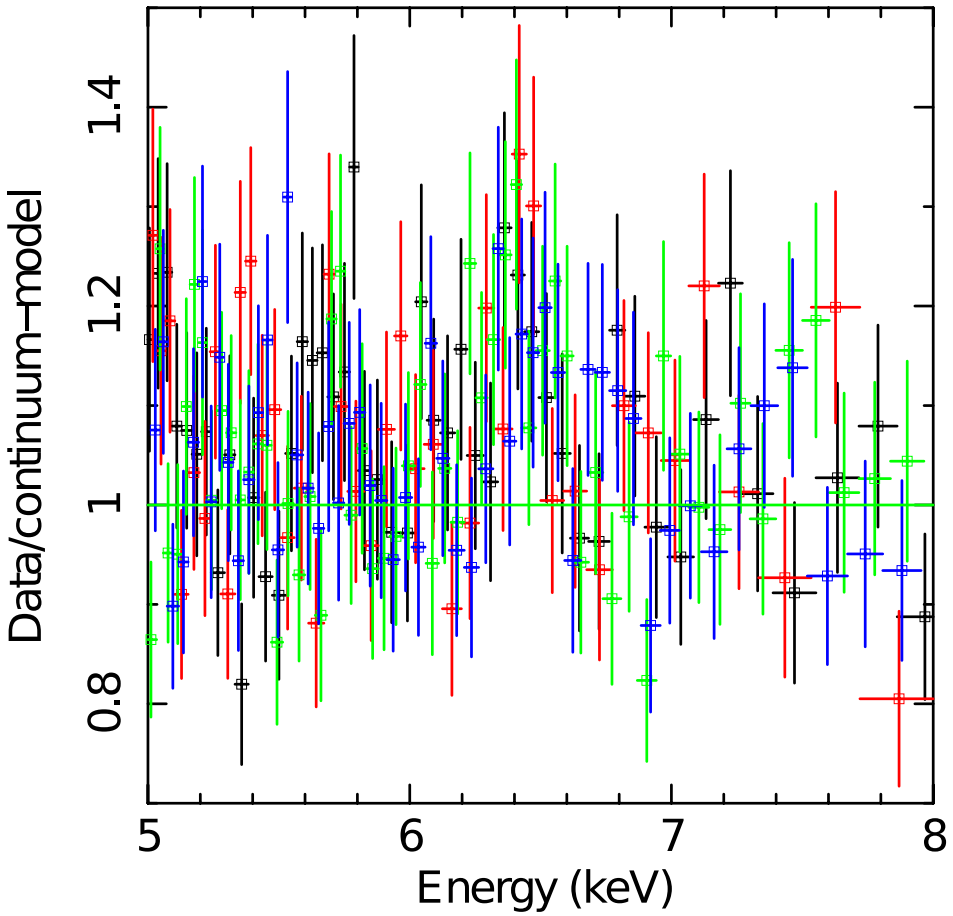

NGC 4258 (Reynolds, et al., 2008; Suzaku, Swift)

But: Some AGN do *not* show relativistic lines!

non detections

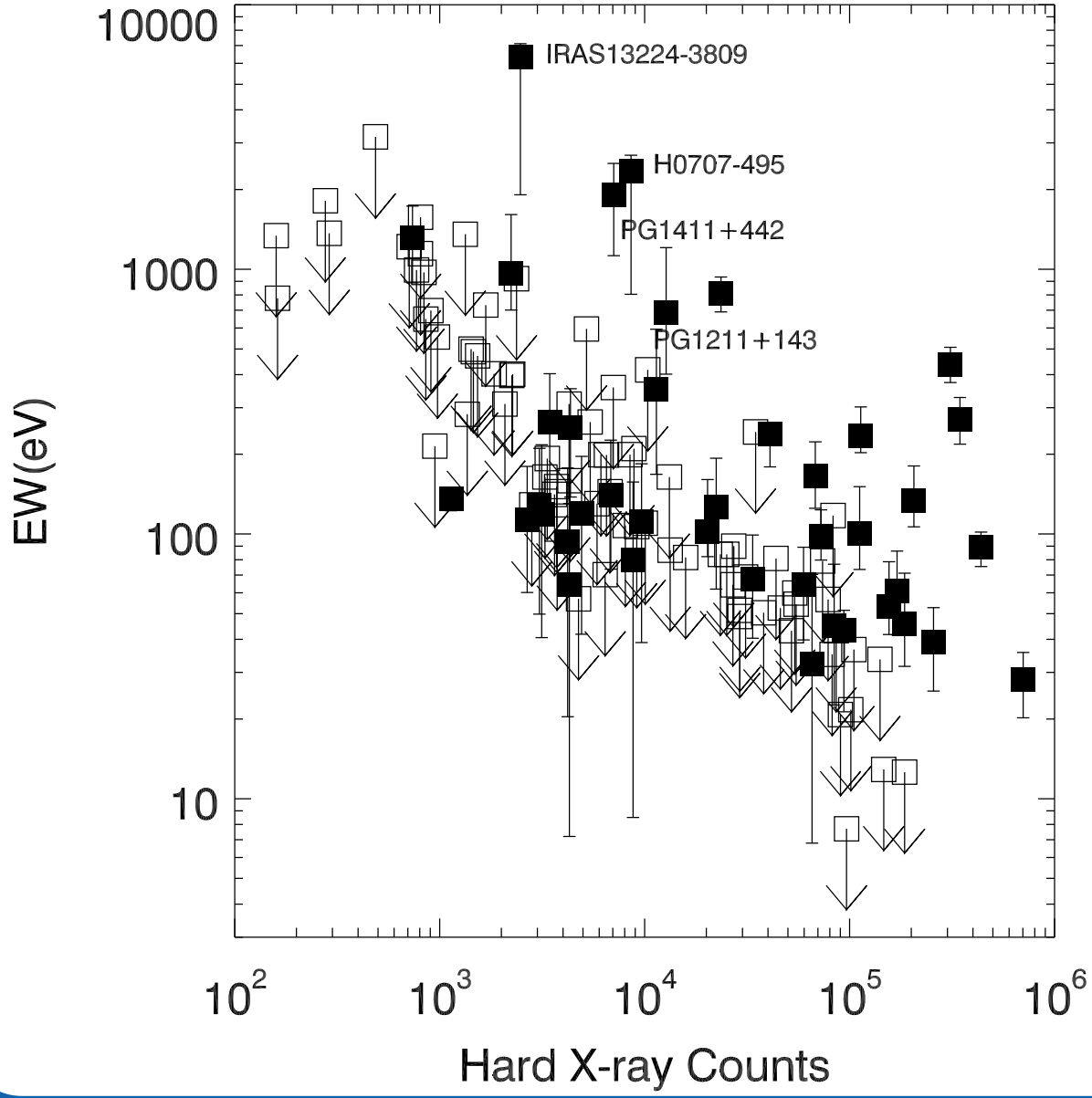

Guainazzi et al. (2006): non-detections due to ionization and detection significance

200000 photons are needed to unequivocally detect broad line in an AGN.

Bałucińska-Church M., Church M.J., 2000, Mon. Not. R. Astron. Soc. 312, L55
Brenneman L.W., Reynolds C.S., 2006, Astrophys. J. 652, 1028
Caballero-García M.D., Miller J.M., Díaz Trigo M., et al., 2009, Astrophys. J. 692, 1339
Comastri A., Brusa M., Civano F., 2004, Mon. Not. R. Astron. Soc. 351, L9
Cunningham C.T., 1975, Astrophys. J. 202, 788
Dauser T., 2010, Diplomarbeit, Universität Erlangen-Nürnberg
Dauser T., Wilms J., Reynolds C.S., Brenneman L.W., 2010, Mon. Not. R. Astron. Soc. 409, 1534
Dove J.B., Wilms J., Nowak M.A., et al., 1998, Mon. Not. R. Astron. Soc. 289, 729
Dovčiak M., Karas V., Yaqoob T., 2004, Astrophys. J., Suppl. Ser. 153, 205
Fabian A.C., Rees M.J., Stella L., White N., 1989, Mon. Not. R. Astron. Soc. 238, 729
Fabian A.C., Ross R.R., 2010, Space Sci. Rev. 157, 167
Fabian A.C., Zoghbi A., Ross R.R., et al., 2009, Nature 459, 540
Fritz S., Wilms J., Pottschmidt K., et al., 2006, In: Sunyaev R., Grebenev S., Winkler C. (eds.) The 6th Integral Workshop: The Obscured Universe. ESA SP-622, ESA Publications Division, Noordwijk, p.341
García J., Kallman T.R., 2010, Astrophys. J. 718, 695
García J., Kallman T.R., Mushotzky R.F., 2011, Astrophys. J. 731, 131
Guainazzi M., Bianchi S., Dovčiak M., 2006, Astron. Nachr. 327, 1032
Guilbert P.W., Rees M.J., 1988, Mon. Not. R. Astron. Soc. 233, 475
Haardt F., Maraschi L., 1991, Astrophys. J. 380, L51
Iwasawa K., Fabian A.C., Reynolds C.S., et al., 1996, Mon. Not. R. Astron. Soc. 282, 1038
King A.R., Pringle J.E., Hofmann J.A., 2008, Mon. Not. R. Astron. Soc. 385, 1621
Laor A., 1991, Astrophys. J. 376, 90
Lightman A.P., White T.R., 1988, Astrophys. J. 335, 57
Magdziarz P., Zdziarski A.A., 1995, Mon. Not. R. Astron. Soc. 273, 837
Malzac J., Belmont R., Fabian A.C., 2009, Mon. Not. R. Astron. Soc. 400, 1512
Markoff S., Nowak M.A., Wilms J., 2005, Astrophys. J. 635, 1203
Matt G., Perola G.C., Piro L., Stella L., 1992, Astron. Astrophys. 257, 63
Miller J., 2007, Ann. Rev. Astron. Astrophys. 45, 441
Miller J.M., Fabian A.C., Reynolds C.S., et al., 2004, Astrophys. J. 606, L131
Miller J.M., Fabian A.C., Wijnands R., et al., 2002, Astrophys. J. 578, 348
Miller J.M., Fabian A.C., Wijnands R., et al., 2002, Astrophys. J. 570, L69
Miller J.M., Reynolds C.S., Fabian A.C., et al., 2008, Astrophys. J. 679, L113
Miller J.M., Reynolds C.S., Fabian A.C., et al., 2009, Astrophys. J. 697, 900

Miniutti G., Fabian A.C., Anabuki N., et al., 2007, Publ. Astron. Soc. Jpn. 59, 315
Nowak M.A., Hanke M., Trowbridge S.N., et al., 2010, Astrophys. J. 728, 13
Nowak M.A., Hanke M., Trowbridge S.N., et al., 2011, Astrophys. J. 728, 13
Nowak M.A., Wilms J., Dove J.B., 2002, Mon. Not. R. Astron. Soc. 332, 856
Ponti G., Gallo L.C., Fabian A.C., et al., 2010, Mon. Not. R. Astron. Soc. 406, 2591
Reynolds C.S., 1996, Ph.D. thesis, University of Cambridge
Ross R.R., Fabian A.C., 2007, Mon. Not. R. Astron. Soc. 381, 1697
Ross R.R., Fabian A.C., Young A.J., 1999, Mon. Not. R. Astron. Soc. 306, 461
Streblyanska A., Hasinger G., Finoguenov A., et al., 2005, Astron. Astrophys. 432, 395
Tanaka Y., Nandra K., Fabian A.C., et al., 1995, Nature 375, 659
Turner T.J., Miller L., 2009, Astron. Astrophys. Rev. 17, 47
Wilms J., Reynolds C.S., Begelman M.C., et al., 2001, Mon. Not. R. Astron. Soc. 328, L27

Jets and Radio Loud AGN

M87: Image Credit & Copyright: Adam Block, Mt. Lemmon SkyCenter, U. Arizona

The M87 Jet

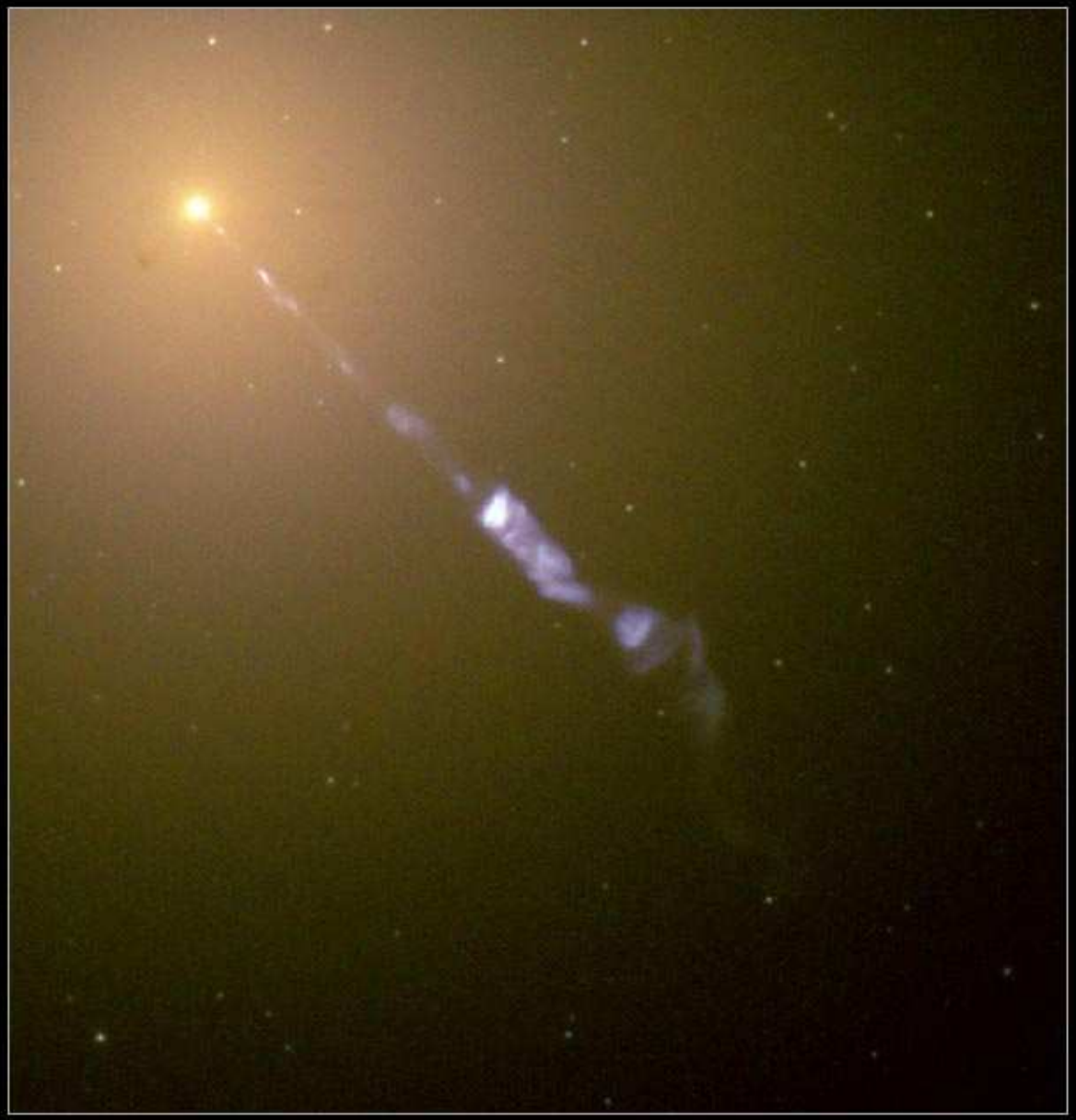

Hubble Heritage

PRC00-20 • Space Telescope Science Institute • NASA and The Hubble Heritage Team (STScI/AURA)

The M87 Jet

Hubble Heritage

PRC00-20 • Space Telescope Science Institute • NASA and The Hubble Heritage Team (STScI/AURA)

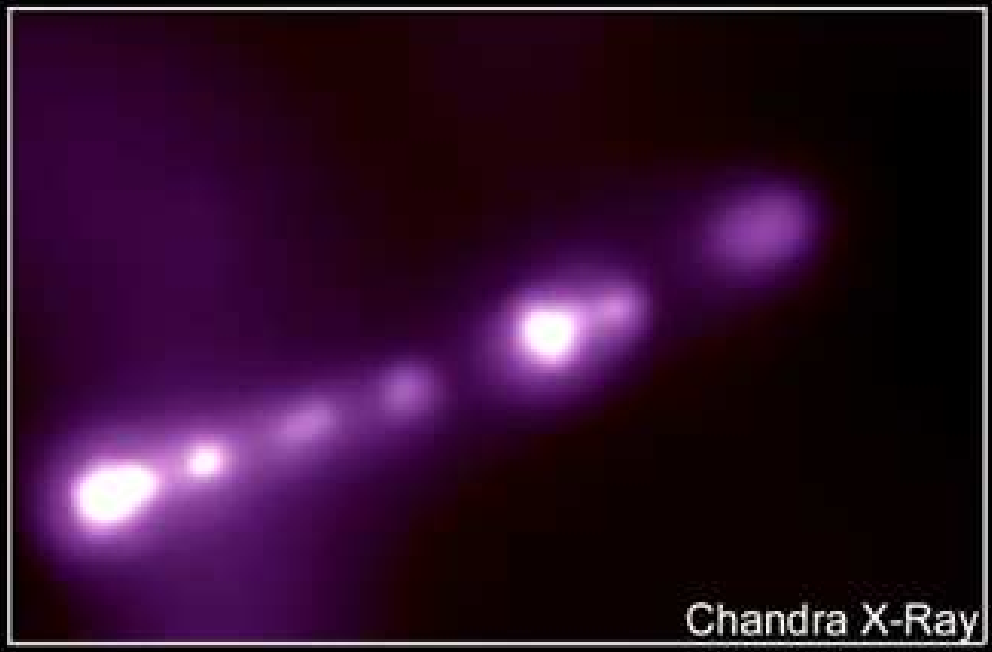

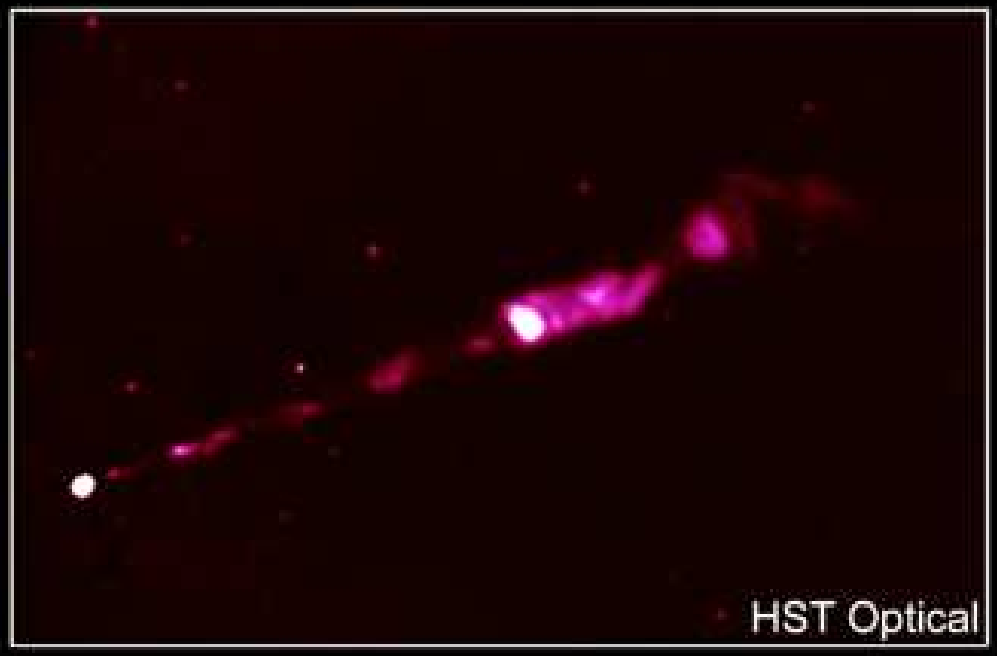

Credit: X-ray: NASA/CXC/MIT/H.Marshall et al. Radio: F. Zhou, F.Owen (NRAO), J.Biretta (STScI)

Optical: NASA/STScI/UMBC/E.Perlman et al.

AGN Jets

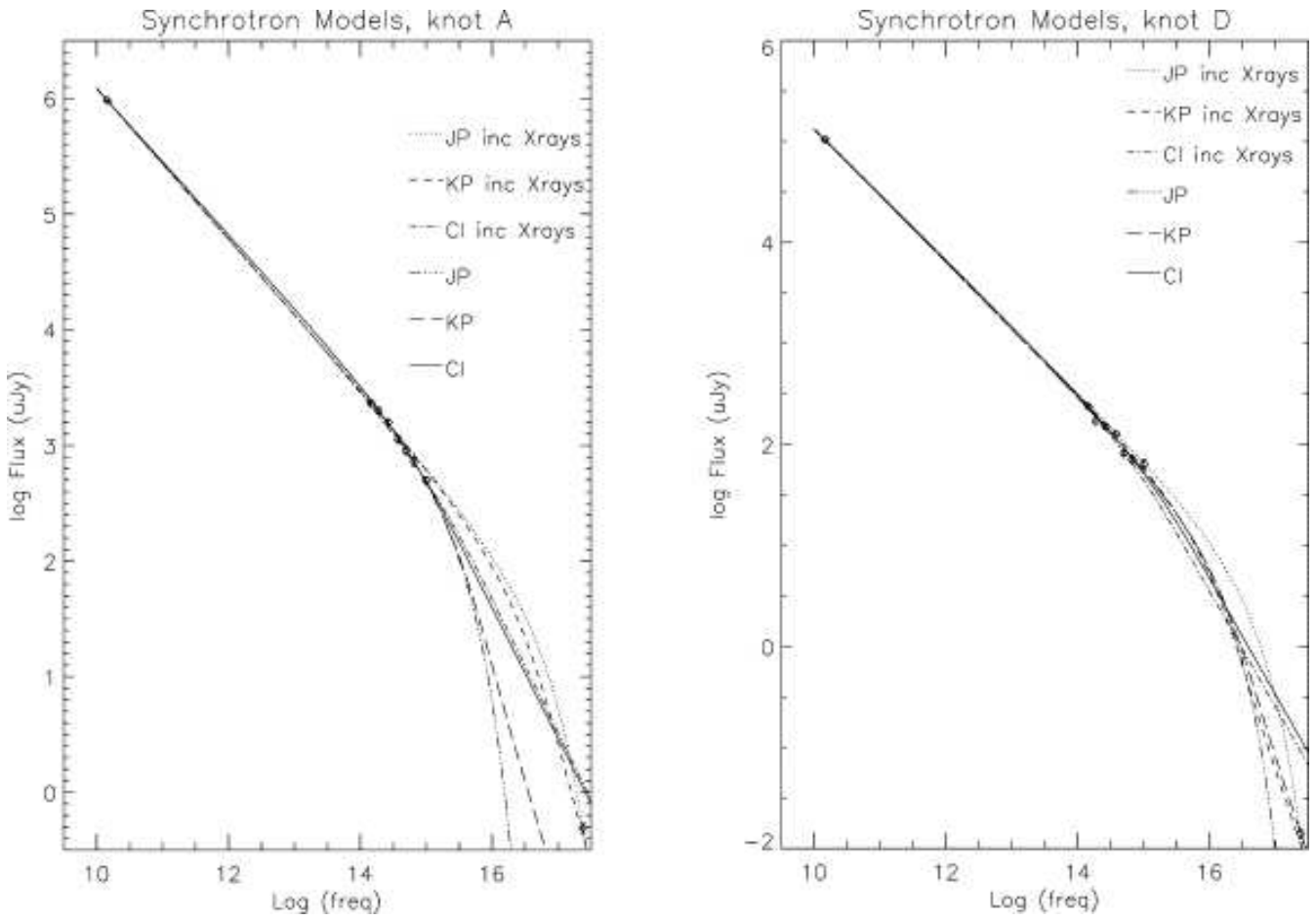

(M87; Perlman et al., 2002)

Spectral shape of jet emission is a power law $\Longrightarrow$ synchrotron radiation

Typical power law index: $\alpha \sim 0.65$ between radio and optical.

Synchrotron Radiation

Most important jet emission process in the radio band: synchrotron radiation.

Moving electron in magnetic field ($\mathbf{E} = 0$): In Gaussian units, the Lorentz-Force is

$$\frac{d\mathbf{p}}{dt} = \frac{e}{c}\mathbf{v} \times \mathbf{B} \quad \text{where} \quad \mathbf{p} = \frac{m_\mathrm{e}\mathbf{v}}{\sqrt{1-\beta^2}} = \gamma m_\mathrm{e}\mathbf{v} \tag{6.1}$$

where

$$\gamma = \frac{1}{\sqrt{1-\beta^2}} \quad \text{and where} \quad \beta = \frac{v}{c} \tag{6.2}$$

Results in helical motion around the B-field line with the frequency

$$\omega_B = \frac{eB}{\gamma m_\mathrm{e} c} = \frac{\omega_\mathrm{L}}{\gamma} \tag{6.3}$$

where the Larmor frequency (also Cyclotron frequency, gyrofrequency)

$$\omega_\mathrm{L} = 2\pi\nu_\mathrm{L} = \frac{eB}{m_\mathrm{e} c} \tag{6.4}$$

Numerical values

Numerically, the Larmor frequency is

$$\nu_{\mathrm{L}} = 2.8 B_{1\,\mathrm{G}}\,\mathrm{MHz} \tag{6.5}$$

The radius of the orbit (Larmor radius) is

$$R_{\mathrm{L}} = \frac{\gamma v_{\perp}}{\omega_{\mathrm{L}}} \sim 2\,\mathrm{AU} \cdot \frac{E}{1\,\mathrm{GeV}} \cdot \left(\frac{B}{10^{-6}\,\mathrm{G}}\right)^{-1} \tag{6.6}$$

$$\sim 300\,\mathrm{km} \cdot \frac{E}{1\,\mathrm{GeV}} \cdot \left(\frac{B}{1\,\mathrm{G}}\right)^{-1} \tag{6.7}$$

i.e., small on cosmical scales

Units and orders of magnitude:

- $1\,\mathrm{G} = 10^{-4}\,\mathrm{T}$,
- the typical B-field in the interstellar medium is $\sim 10^{-6}\,\mathrm{G}$,
- close to the centers of AGN $B \sim 1\,\mathrm{G}$.

Radiated Energy

Motion around B-field lines: acceleration.

But accelerated charges emit radiation (Larmor's formula):

$$P = \frac{dW}{dt} = \frac{q^2\dot{v}^2}{4\pi c^3}\int \sin^2\theta \mathrm{d}\Omega = \frac{2q^2\dot{v}^2}{3c^3} \tag{6.8}$$

Assumption of isotropic velocity distribution, relativistic electrons ($\beta \longrightarrow 1$), and a messy derivation (see Rybicki & Lightman) yields for the average emitted power of an electron in a B-field

$$\langle P_{\mathrm{em}} \rangle = \frac{4}{3}\beta^2\gamma^2 c\sigma_{\mathrm{T}} U_B \tag{6.9}$$

with $U_B = B^2/8\pi$, the magnetic field energy density, and $\sigma_{\mathrm{T}} = 8\pi e^2/(3m_{\mathrm{e}}^2c^4)$, the Thomson cross section.

Note: Since $E = \gamma m_{\mathrm{e}} c^2 \Longrightarrow P \propto E^2 U_{\mathrm{B}}$.

Note: $P_{\mathrm{em}} \propto \sigma_{\mathrm{T}} \propto m_{\mathrm{e}}^{-2} \Longrightarrow$ Synchrotron radiation from charged particles with larger mass (protons,...) is negligible.

Note: Life-time of particles of energy E is

$$t_{1/2} \sim \frac{E}{P} \propto \frac{1}{B^2 E} = 5\,\mathrm{s}\left(\frac{B}{1\,\mathrm{T}}\right)^{-2}\gamma^{-1} = 1.6\times 10^7\,\mathrm{years}\left(\frac{B}{10^{-7}\,\mathrm{T}}\right)^{-2}\gamma^{-1} \tag{6.10}$$

Radiated Energy

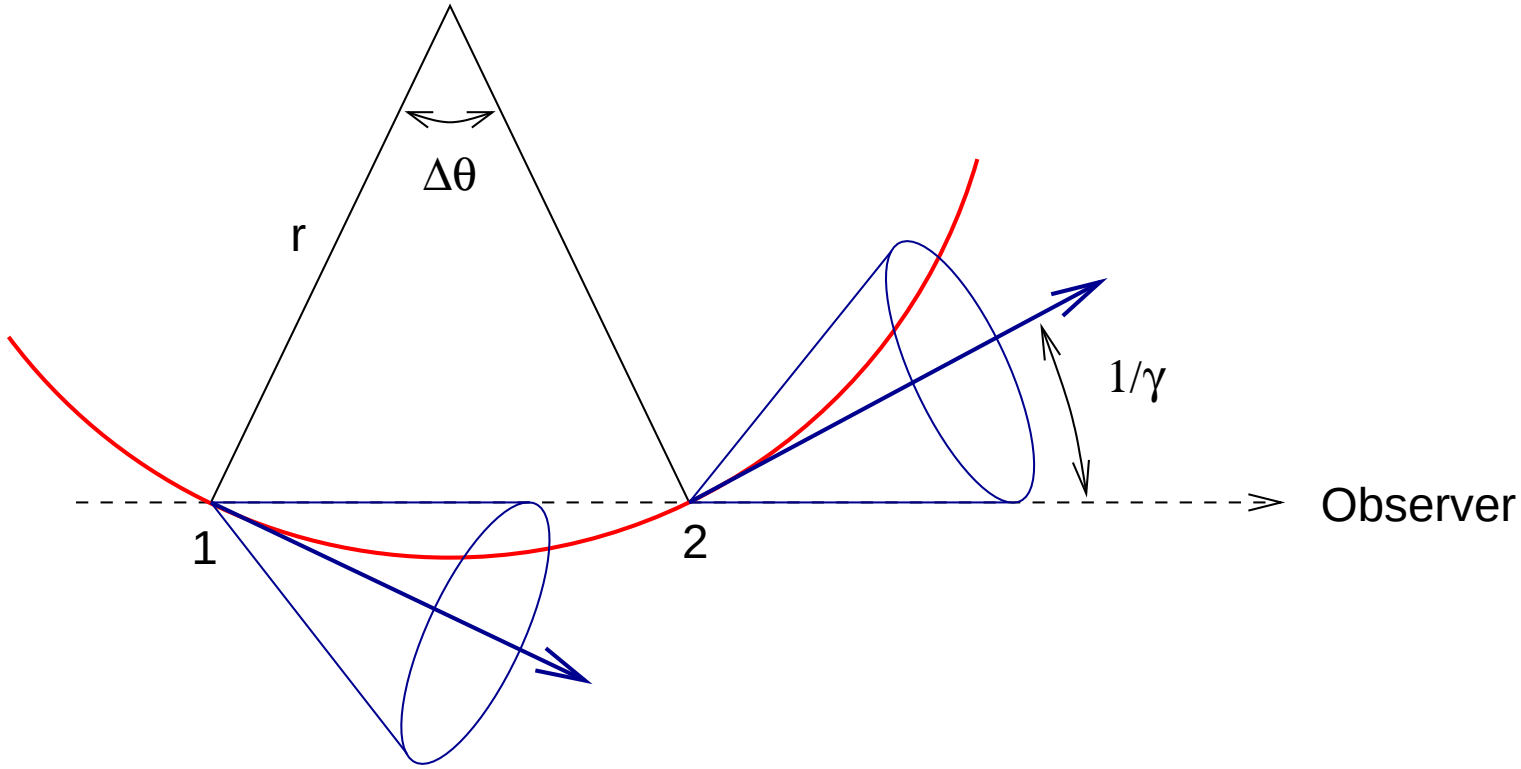

(after Fig. 6.2 of Rybicki & Lightman, 1979)

Relativistic electrons: radiation is forward beamed into cone with opening angle $\Delta\theta \sim 1/\gamma$. In the Electron frame of rest: beam passes observer during time

$$\Delta t = \frac{\Delta\theta}{\omega_B} = \frac{m_e c\gamma}{eB}\frac{2}{\gamma} = \frac{2}{\omega_L} \qquad (6.11)$$

Radiated Energy

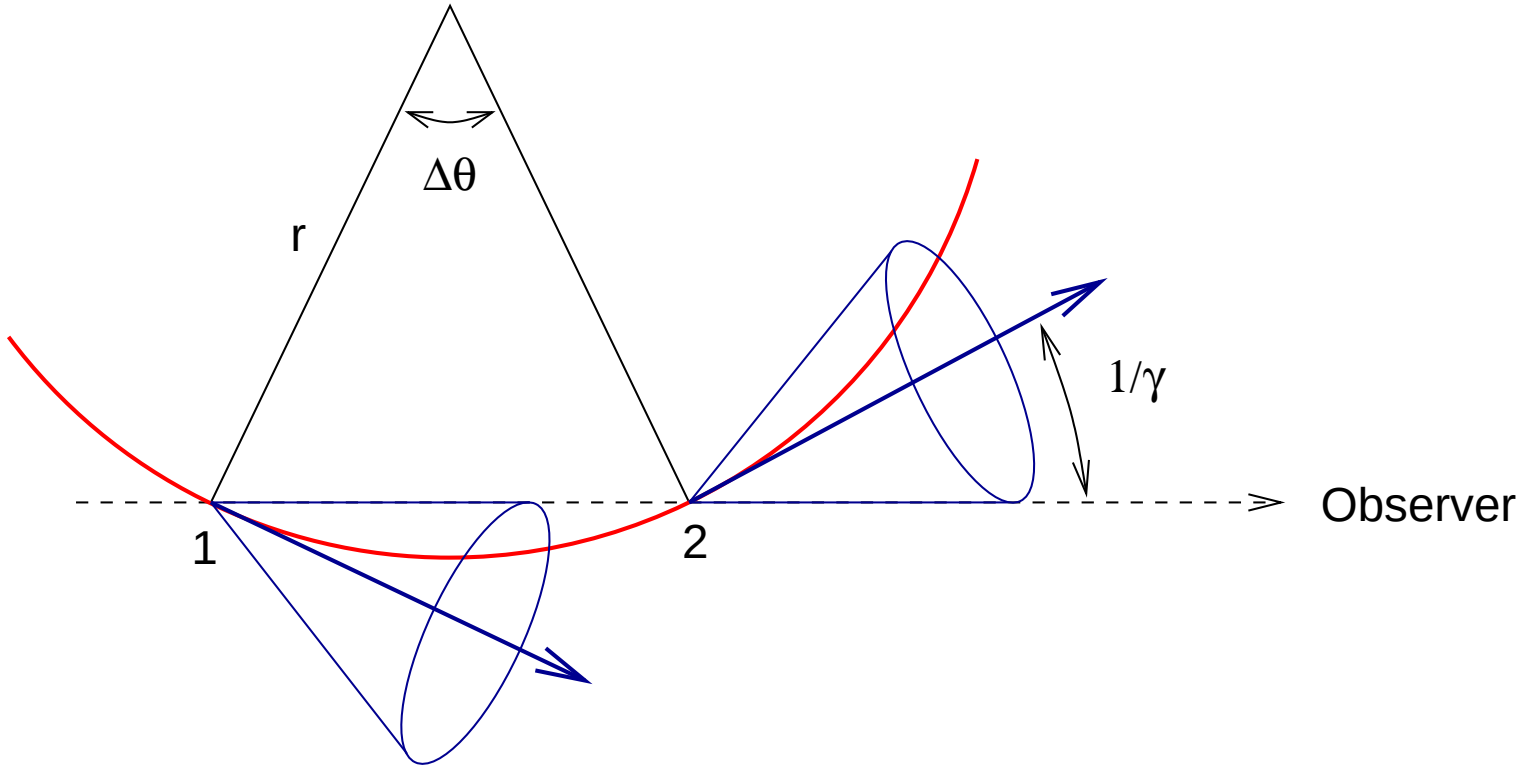

(after Fig. 6.2 of Rybicki & Lightman, 1979)

Observer frame: Doppler effect! (electron is closer to us at end of time interval)

$\Longrightarrow$ observed pulse duration:

$$\tau = \left(1 - \frac{v}{c}\right) \Delta t = (1 - \beta)\Delta t \qquad (6.12)$$

Radiated Energy

For $\gamma \gg 1$, i.e., $\beta = v/c \sim 1$

$$\frac{1}{\gamma^2} = 1 - \frac{v^2}{c^2} = (1+\beta)(1-\beta) \approx 2(1-\beta) \tag{6.13}$$

such that

$$\tau = (1-\beta)\Delta t = \frac{1}{2}\left(1 - \frac{v^2}{c^2}\right)\Delta t = \frac{1}{\gamma^2 \omega_\mathrm{L}} \tag{6.14}$$

Thus the characteristic frequency of the radiation is given by

$$\omega_\mathrm{c} = \gamma^2 \omega_\mathrm{L} = \frac{eB}{m_\mathrm{e} c}\left(\frac{E}{m_\mathrm{e} c^2}\right)^2 \tag{6.15}$$

Short gyration pulses $\Longrightarrow$ broad spectrum (Heisenberg: $\Delta\omega\Delta t > 1$) with the highest frequency in the regime of $\nu_\mathrm{c} = \omega_\mathrm{c}/2\pi$.

Nonthermal Synchrotron Radiation

For an electron distribution, $n(\gamma)$, the emitted spectrum is found by properly weighting contributions of electrons with different energies:

$$P_\nu = \int_1^\infty P_\nu(\gamma) n(\gamma) d\gamma \tag{6.16}$$

Most important case: nonthermal synchrotron radiation, where electrons have a power-law distribution

$$n(\gamma)d\gamma = n_0 \gamma^{-p} d\gamma \quad . \tag{6.17}$$

The spectral energy distribution P_ν of an electron with total energy $E = \gamma m_e c^2$ can be written as

$$P_\nu(\gamma) = \frac{4}{3}\beta^2\gamma^2 c\sigma_T U_B \phi_\nu(\gamma) \tag{6.18}$$

where the spectral shape is described by a function $\phi_\nu(\gamma)$ with

$$\int \phi_\nu(\gamma) \mathrm{d}\gamma = 1 \quad . \tag{6.19}$$

Nonthermal Synchrotron Radiation

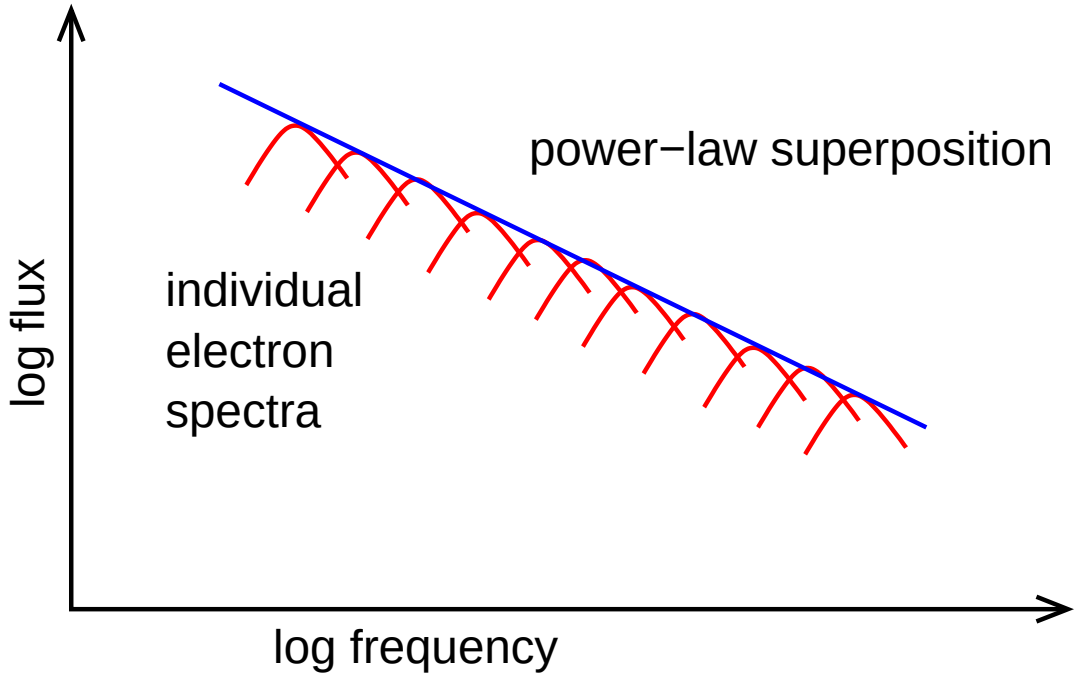

after (Shu, 1991, Fig. 18.4)

Assume that photons are only emitted at the characteristic frequency $\gamma^2\nu_\mathrm{L}$ (Eq. 6.15).

this is a good approximation since the spectrum emitted by an electron has a strong peak at that frequency

Therefore

$$\phi_\nu(\gamma) \sim \delta(\nu - \gamma^2\nu_\mathrm{L}) \qquad (6.20)$$

For a nonthermal electron distribution with $\propto \gamma^{-p}$, one can then show that

$$P_\nu = \frac{2}{3} c\sigma_\mathrm{T} n_0 \frac{U_\mathrm{B}}{\nu_\mathrm{L}} \left(\frac{\nu}{\nu_\mathrm{L}}\right)^{-\frac{p-1}{2}} \qquad (6.21)$$

The spectrum of an electron power-law distribution is a power-law!

Synchrotron Self-Absorption

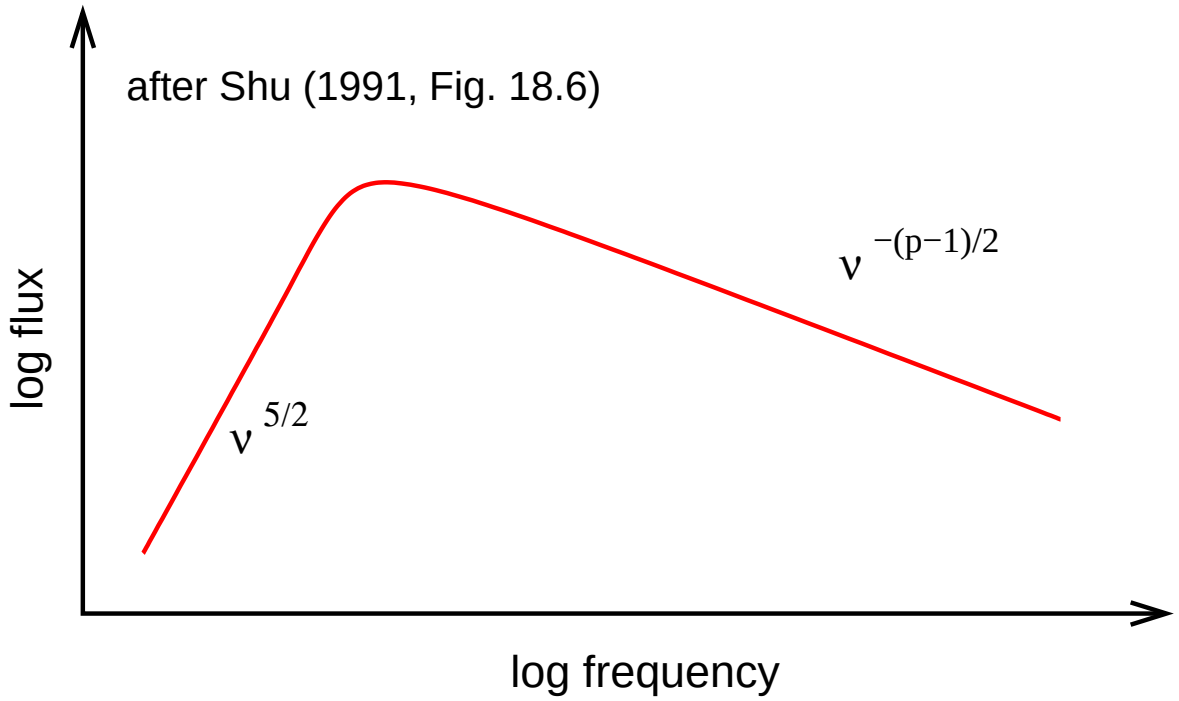

At low ν: synchrotron emitting electrons can absorb synchrotron photons:
synchrotron self-absorption.

For a power law electron distribution $\propto E^{-p}$, total spectral shape is:

For large frequencies: $P_\nu \propto \nu^{-(p-1)/2}$

For low frequencies: $P_\nu \propto B^{-1/2}\nu^{5/2}$ (independent of p!)

One often uses the terms optically thick/thin to describe the absorbed/unabsorbed part of a synchrotron spectrum. The turnover describes the $\tau = 1$ surface, e.g., of a jet. In general: $\tau \propto R$ (R: size of the emitting region). More compact regions are optically thick, more extended regions are optically thin.

Observations

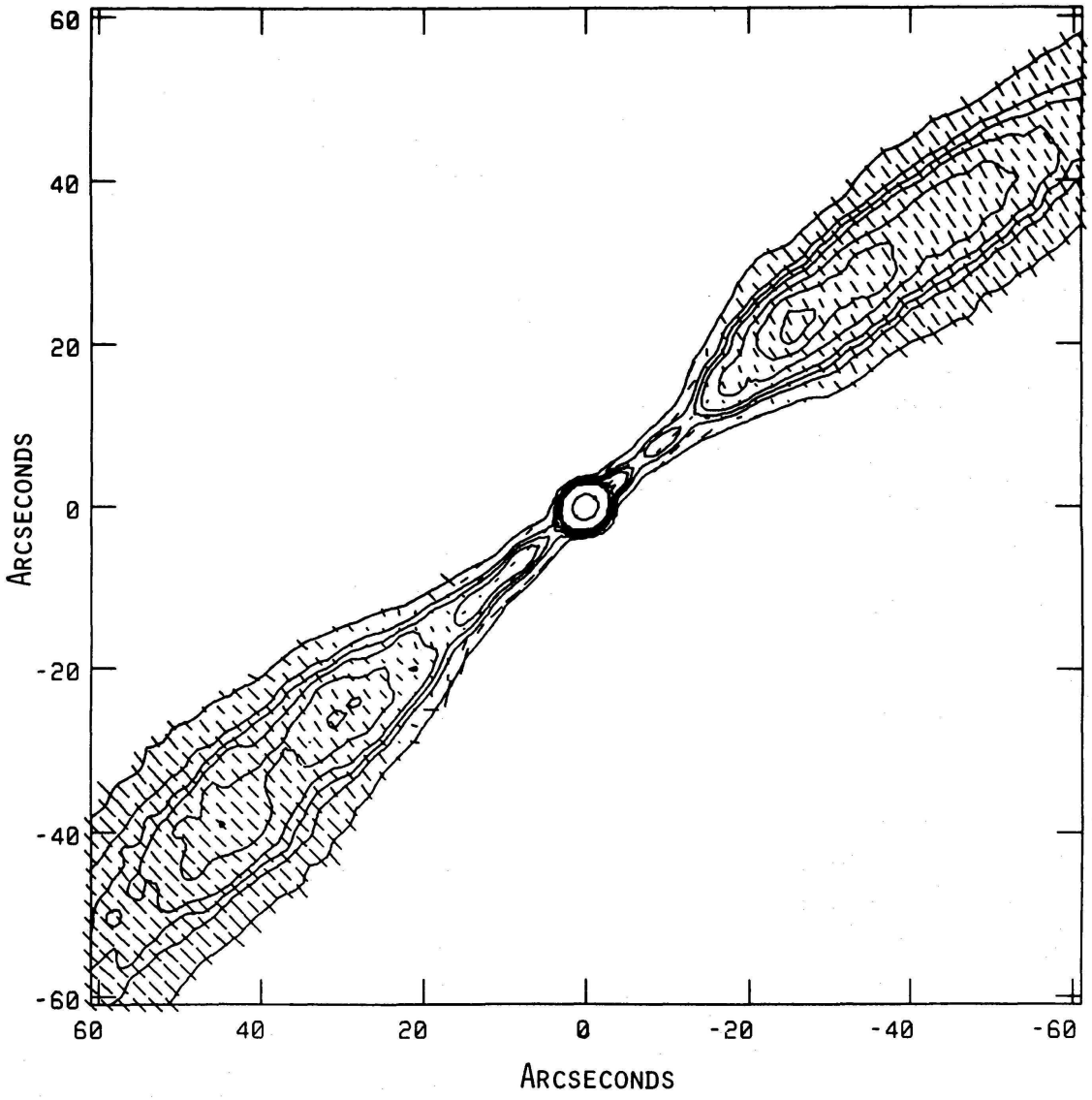

polarization in two-sided jet sources (FR 1): up to 40%

$\Rightarrow$ Synchrotron Radiation

B-field orientation:

- close to core: $B \parallel$ jet axis
- away from core ($\sim$10% jet length): $B \perp$ jet axis

B-field can change orientation again in knots

(B-field configuration in IC 4296; Killeen et al., 1986, Fig. 25b)

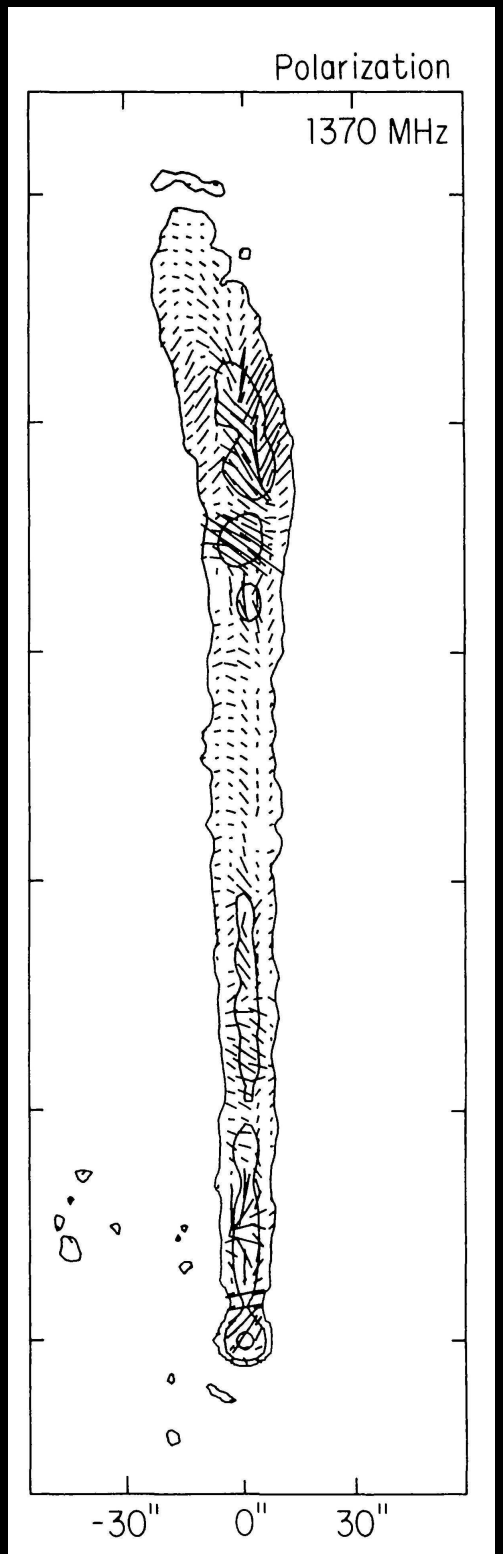

polarization in one-sided jet sources (FR 2): similar to FR 1, i.e., 40% and higher

B-field orientation in FR 2: parallel to jet axis throughout the jet

(E-field configuration in NGC 6251, note: B-field is perpendicular to E-field!; Perley et al., 1984, Fig. 17)

Multifrequency VLBI Observations

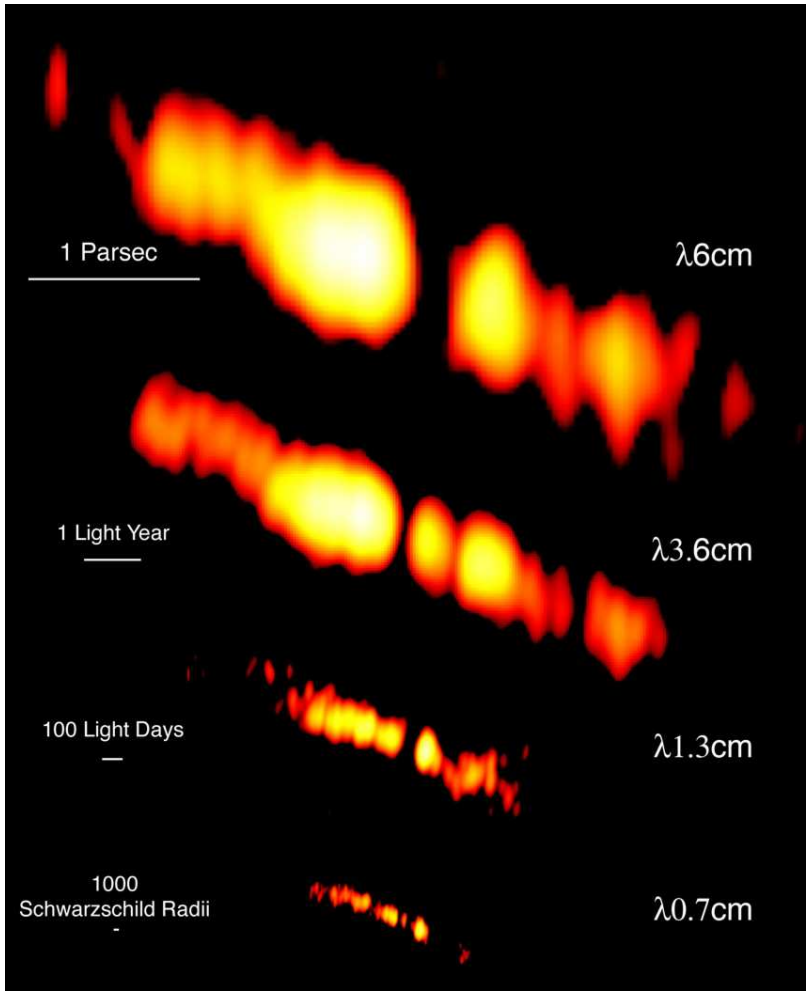

The Twin-Jet in NGC 1052 observed with the VLBA at 4 frequencies; Image: M. Kadler

At higher frequencies

1. the angular resolution improves
2. the structure changes: different parts of the jet dominate the emission at different frequencies (superposition to a flat spectrum)
3. emission shows up in the central emission gap; spectral index $\alpha > 2.5 \Rightarrow$ no self absorption
4. the absorption is caused by free-free absorption in the circumnuclear torus; at high frequencies, the torus becomes transparent

Kameno et al. (2001); Kadler et al. (2004)

Superluminal Motion

VLBI resolution 1 mas

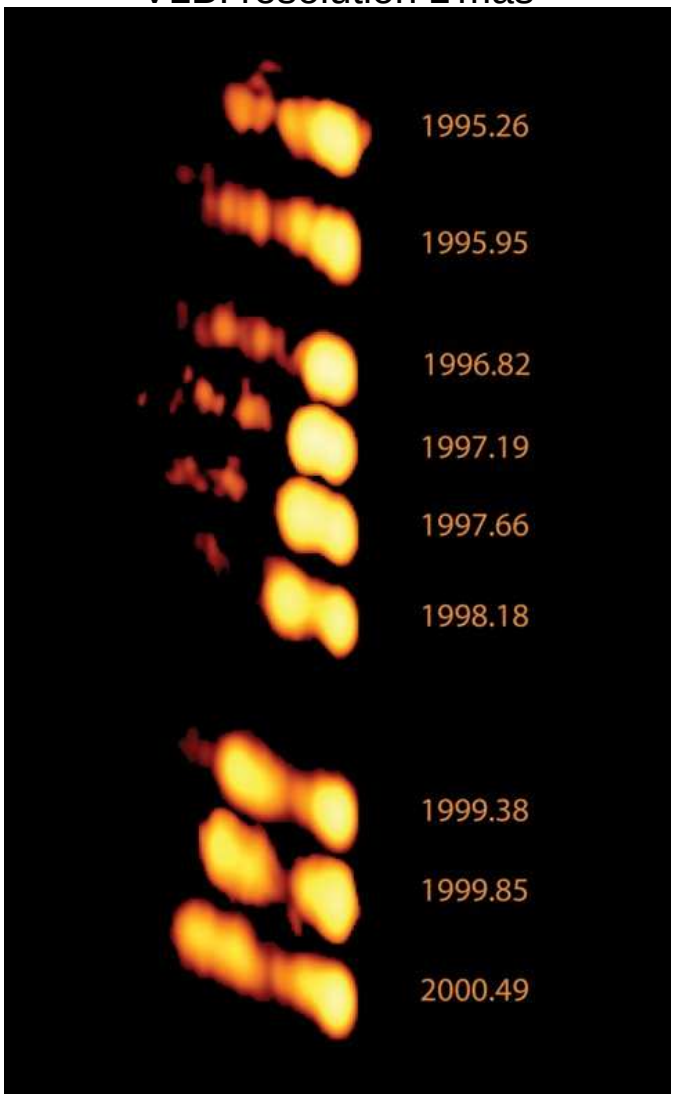

Kadler et al. (2008)

3C 111: Apparent speed of jet: $\sim 5c$

Superluminal motion: The apparent velocities of jet features ("blobs") measured in many AGN jets often exceed the speed of light.

First discovered in 1971 in 3C279
(Cohen et al., 1971; Whitney et al., 1971).

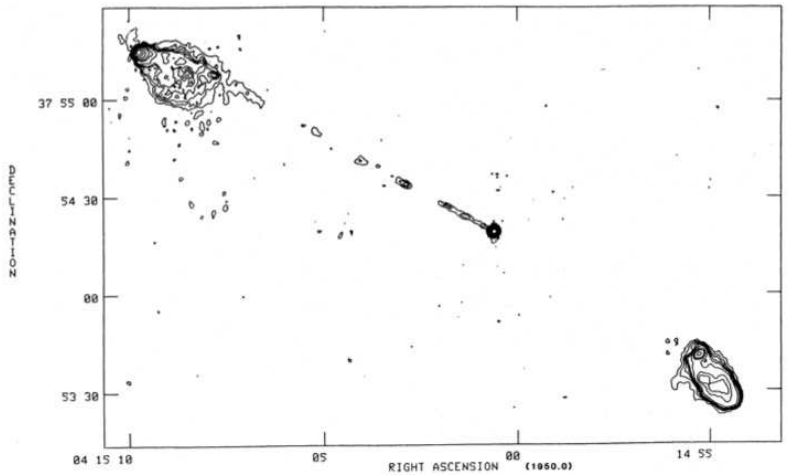

VLA resolution $\sim$ 1 arcsec

Superluminal Motion

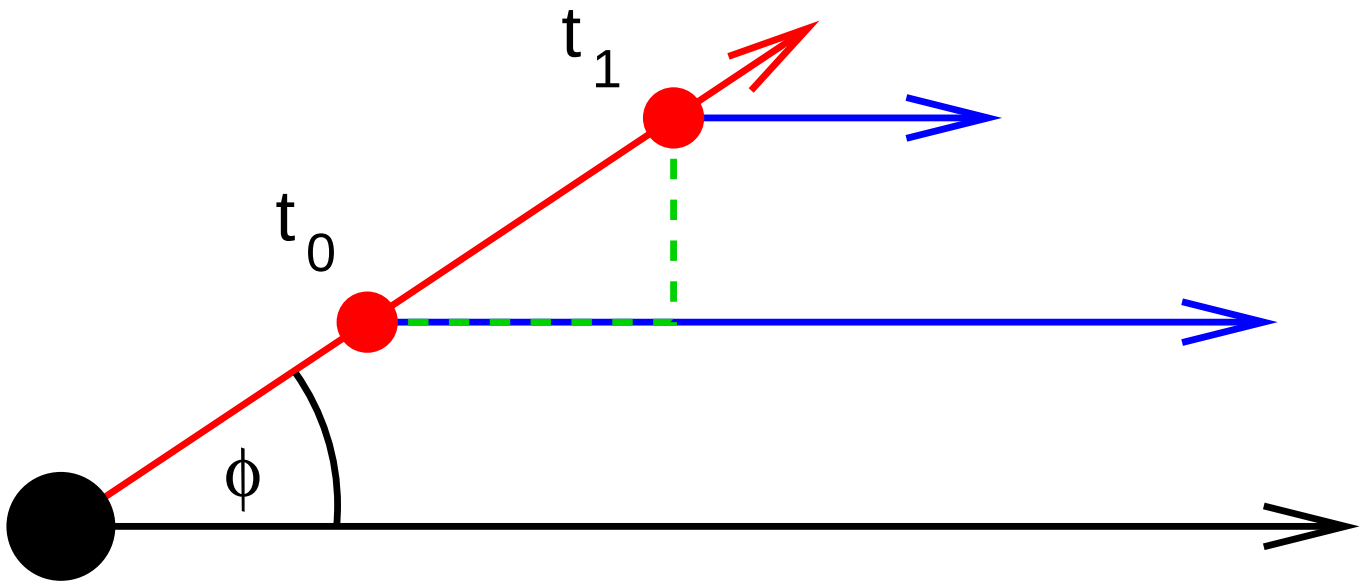

Consider blob moving towards us with speed v and angle ϕ with respect to line of sight, emitting light signals at t_0 and $t_1 = t_0 + \Delta t_e$

Light travel time: Observer sees signals separated by

$$\Delta t_o = \Delta t_e - \Delta t_e \frac{v}{c} \cos\phi = \left(1 - \frac{v}{c} \cos\phi\right) \Delta t_e \tag{6.22}$$

Observed distance traveled in plane of sky:

$$\Delta \ell_\perp = v \Delta t_e \sin\phi \tag{6.23}$$

Superluminal Motion

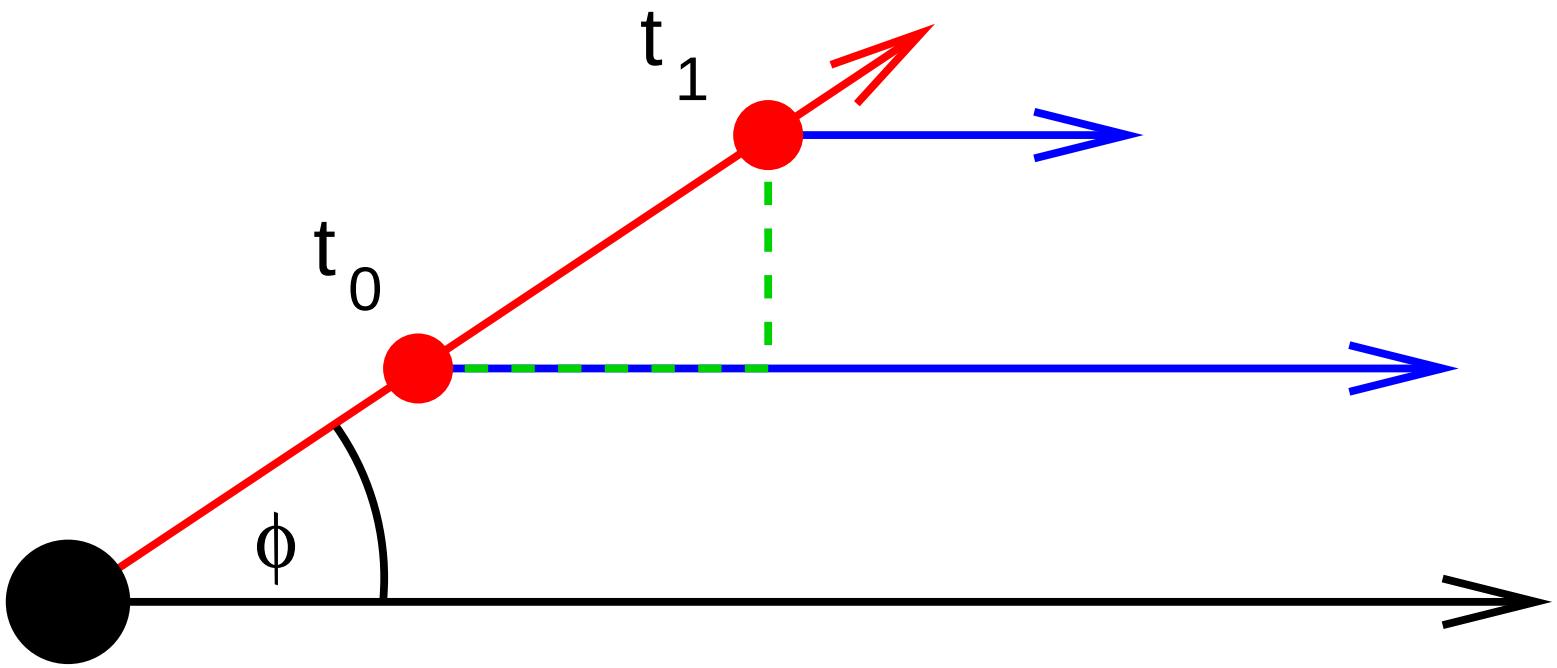

Apparent velocity deduced from observations:

$$v_{\text{app}} = \frac{\Delta \ell_\perp}{\Delta t_{\text{o}}} = \frac{v \Delta t_{\text{e}} \sin \phi}{\left(1 - \frac{v}{c} \cos \phi\right) \Delta t_{\text{e}}} = \frac{v \sin \phi}{\left(1 - \frac{v}{c} \cos \phi\right)} \tag{6.24}$$

$\Longrightarrow$ For v/c large and ϕ small: $v_{\text{app}} > c$

Superluminal Motion

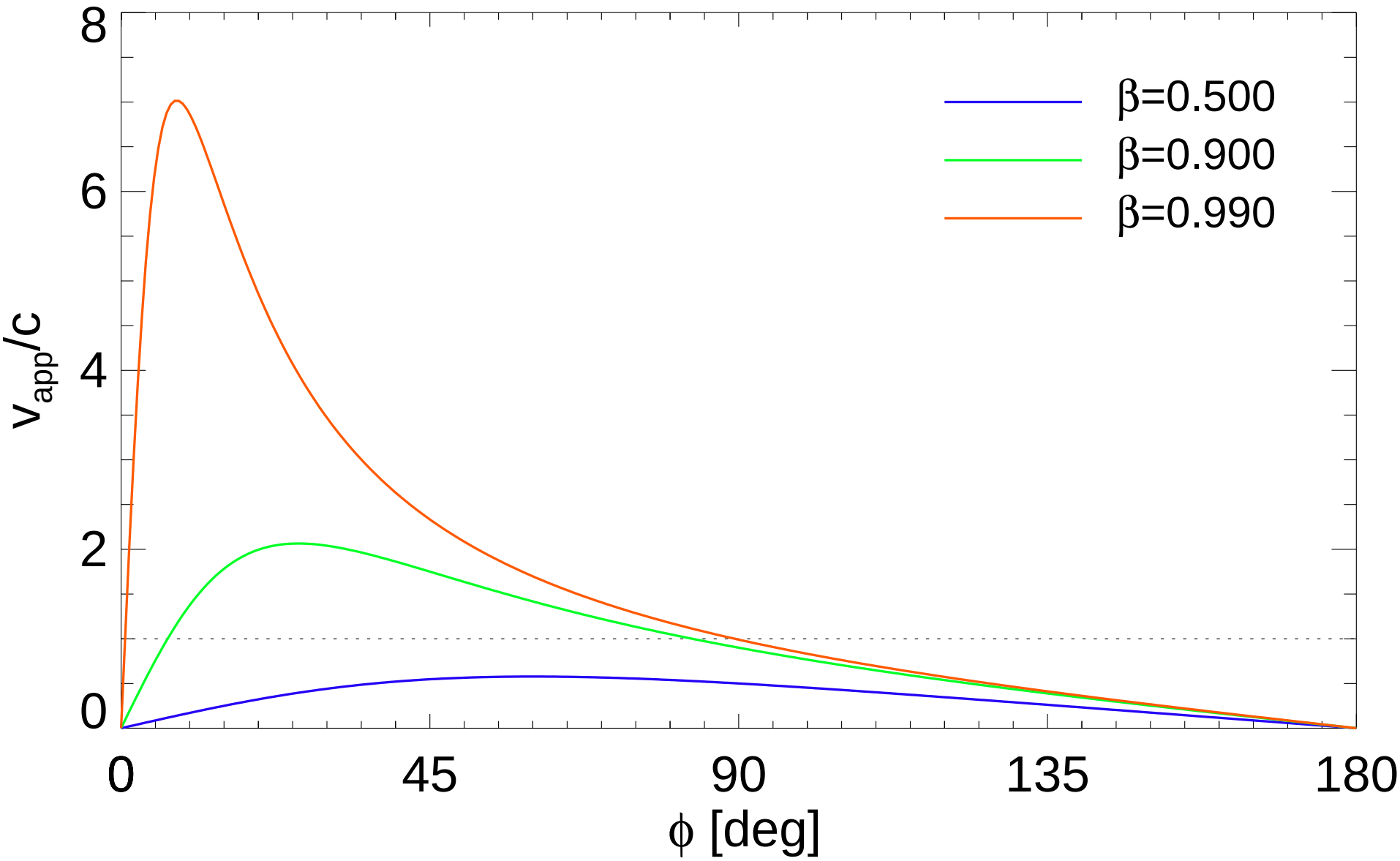

Relativistic Boosting

If jet plasma is moving at relativistic speeds, we have to consider also other relativistic effects.

Remember that

$$\nu_{\text{obs}} = \frac{1}{\Delta t_{\text{A}}} = \frac{\nu_{\text{em}}}{\gamma\left(1 - \frac{v}{c}\cos\theta\right)} \tag{6.25}$$

and

$$\gamma = \frac{1}{\sqrt{1 - \frac{v^2}{c^2}}} \quad . \tag{6.26}$$

This defines the relativistic Doppler factor

$$\mathcal{D} = \frac{\nu_{\text{obs}}}{\nu_{\text{em}}} = \frac{1}{\gamma\left(1 - \frac{v}{c}\cos\theta\right)} = \frac{\sqrt{1-\beta^2}}{1 - \beta\cos\theta} \tag{6.27}$$

(the difference to the classical Doppler factor is only the γ factor).

The Doppler factor is a strong function of the aspect angle and can become very large for $v \to c$.

Relativistic Boosting

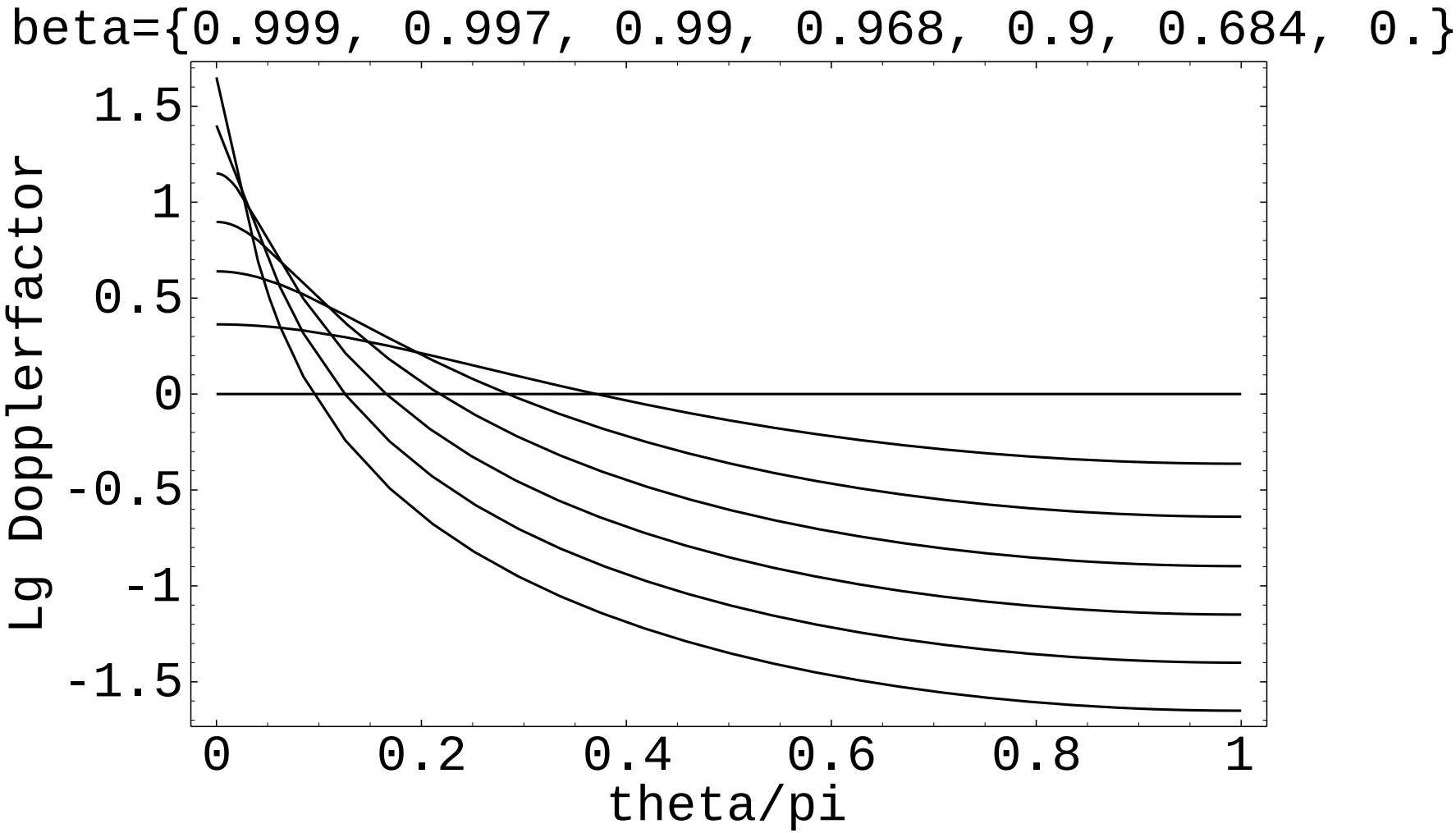

Within $\sim 1 - 2$ deg, the Doppler factor can approach values of 100 or higher.

Relativistic Boosting

One can show (i.e., Rybicki & Lightman, chap. 4.9) that S_ν/ν^3 is invariant under Lorentz transformation, where S_ν is the flux density.

Therefore, observed intensity of a moving blob:

$$\frac{S(\nu_{\rm obs})}{\nu_{\rm obs}^3} = \frac{S(\nu_{\rm em})}{\nu_{\rm em}^3} \tag{6.28}$$

and

$$S(\nu_{\rm obs}) = \frac{\nu_{\rm obs}^3}{\nu_{\rm em}^3} S(\nu_{\rm em}) = \mathcal{D}^3 S(\nu_{\rm em}) \tag{6.29}$$

Specifically, for a blob with a power law spectrum ($S(\nu) = A\nu^\alpha$):

$$S(\nu_{\rm obs}) = \mathcal{D}^3 A \nu_{\rm em}^\alpha = \mathcal{D}^3 A \mathcal{D}^{-\alpha} \nu_{\rm obs}^\alpha \tag{6.30}$$

$$S(\nu_{\rm obs}) = \mathcal{D}^{3-\alpha} S(\nu_{\rm em}) \quad . \tag{6.31}$$

Even for relatively modest relativistic velocities of $0.97c$ ($\gamma \simeq 4$), for example, the flux in the forward direction can be boosted by a factor 1000, while it is reduced by a factor 1000 in the backward direction!

Jet One-Sidedness

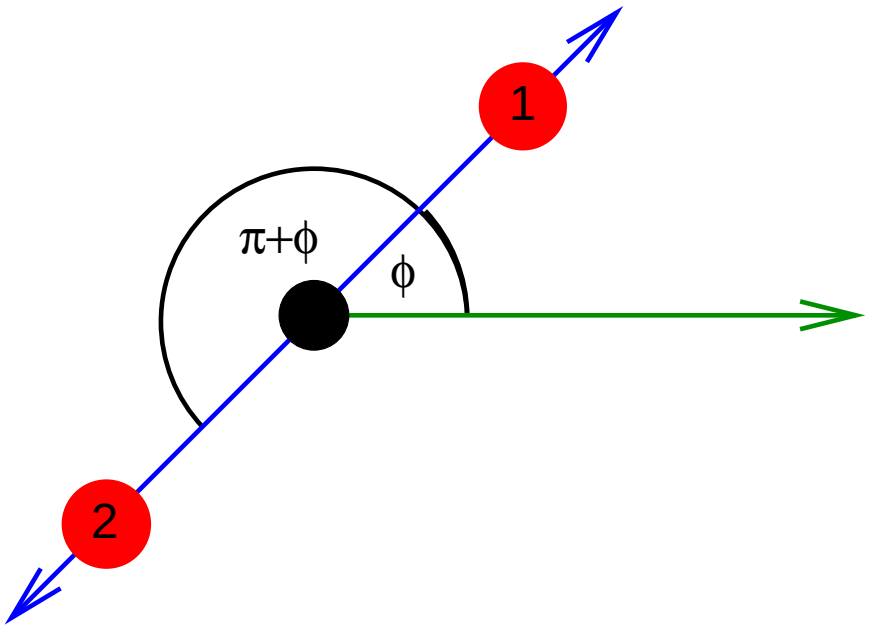

Now take a source emitting blobs symmetrically in two directions.

From Eq. (6.30) the ratio of fluxes from the blobs is

$$\frac{S_1}{S_2} = \left(\frac{1+\beta\cos\phi}{1-\beta\cos\phi}\right)^{3-\alpha} \qquad (6.32)$$

Even for mildly relativistic speeds and large angles, features on the approaching side are always significantly brighter than on the receding side.

Jet can be expressed as a series of blobs. But the number of blobs observed scales as the Doppler factor, such that for jets:

$$\frac{S_1}{S_2} = \left(\frac{1+\beta\cos\phi}{1-\beta\cos\phi}\right)^{2-\alpha} \qquad (6.33)$$

One sidedness of jets is a relativistic effect!

Jet One-Sidedness

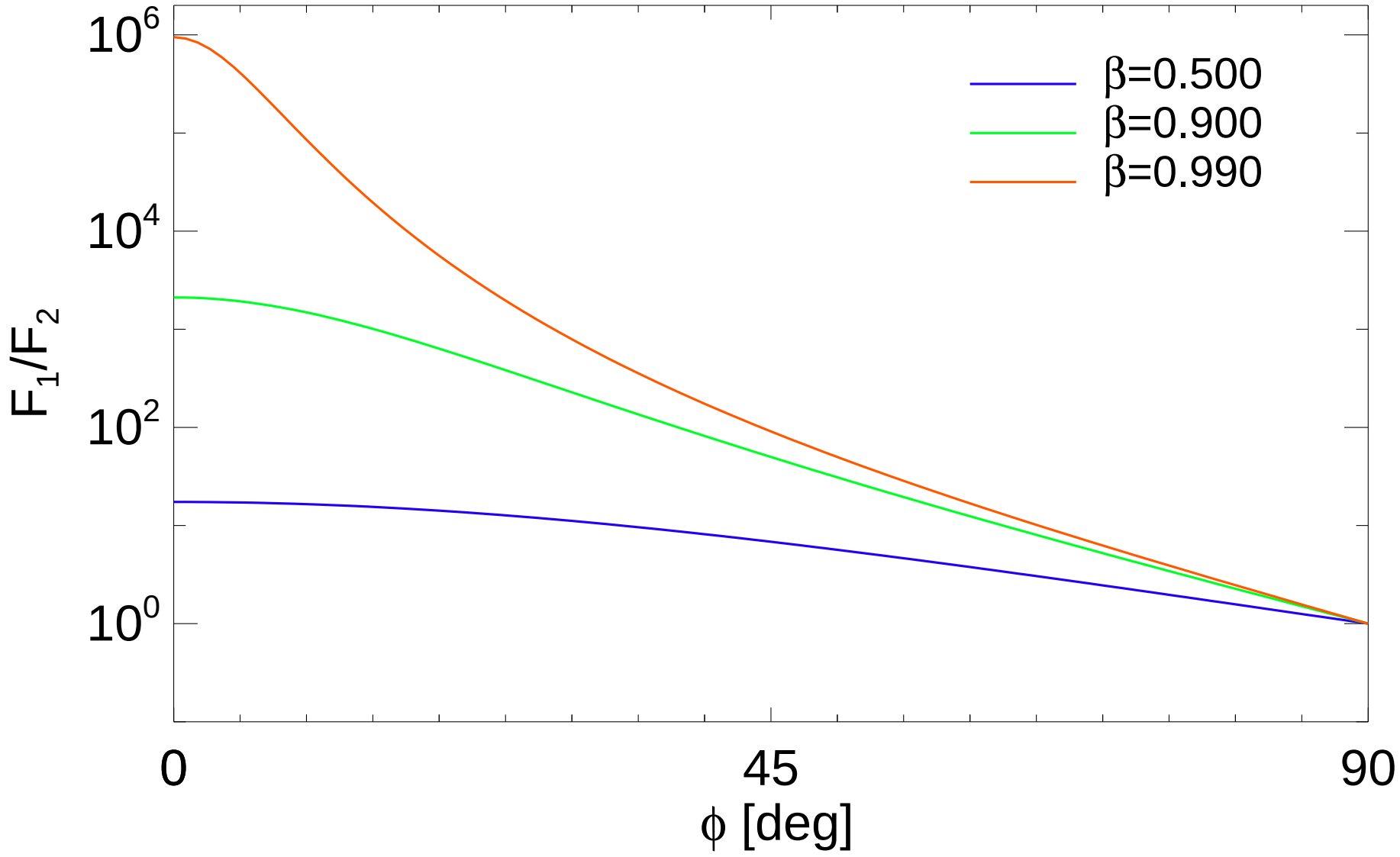

Flat-Spectrum Radio Sources: Blazars

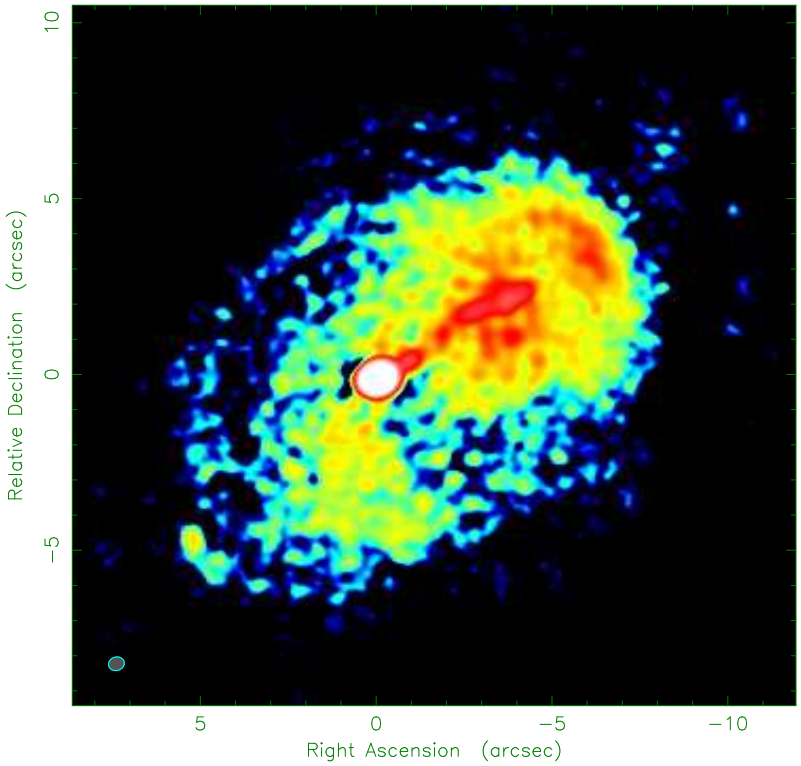

Image courtesy: U. Bach, MPIfR

0716+714, BL Lac object at redshift $z = 0.3$ (Nilsson et al., 2008)

Highly variable, core dominated object

“Fried-egg” morphology – really the end-on view of a radio lobe?

Almost all the flux density is concentrated within a few milliarcseconds-size compact jet!

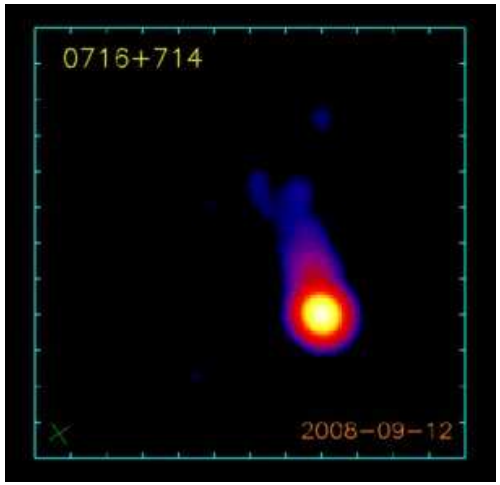

Image Courtesy: MOJAVE

“Roughly equal numbers of steep-spectrum extended double-lobed sources and flat-spectrum objects that are unresolved on arcsec scales.” (Zensus, 1997)

Broad band emission

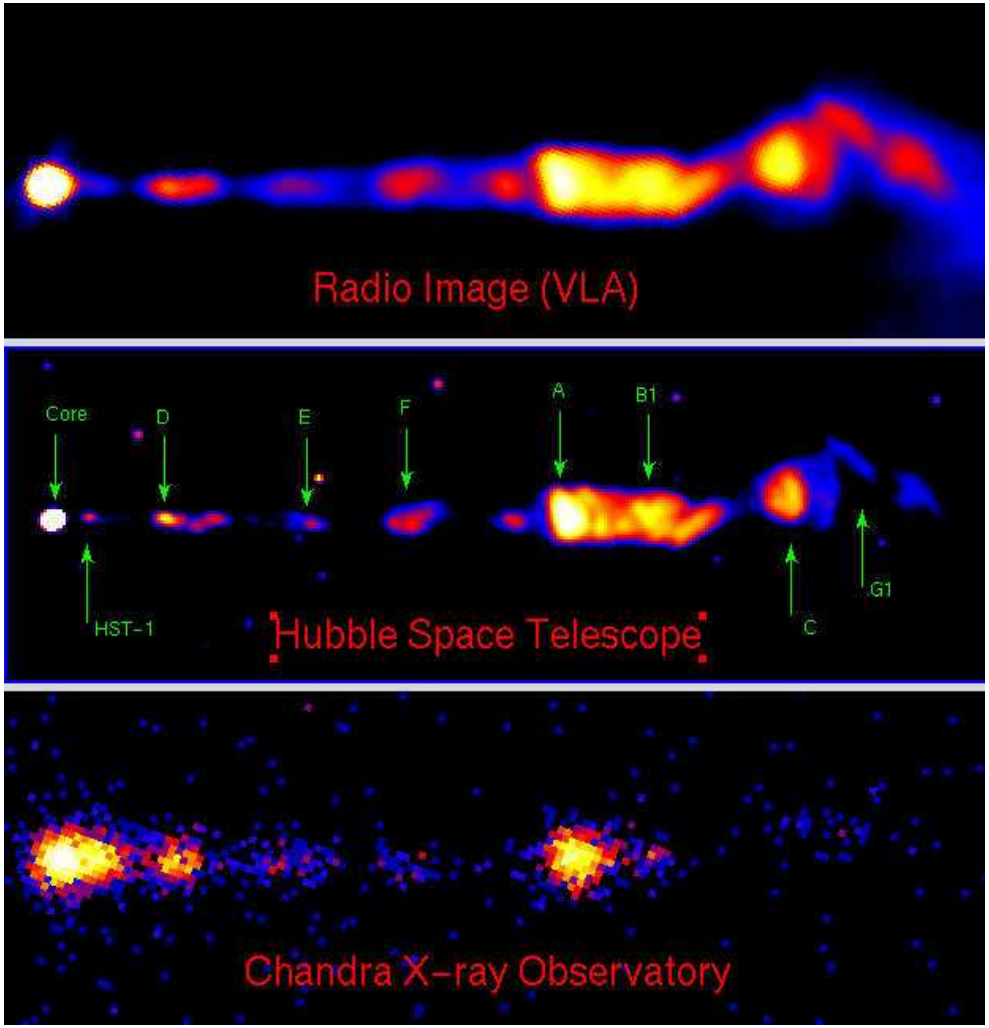

M 87 – Credit: X-ray: NASA/CXC/MIT/H.Marshall et al., Radio: F.Zhou, F.Owen (NRAO), J.Biretta (STScI), Optical: NASA/STScI/UMBC/E.Perlman et al.)

Synchrotron process dominates the broadband spectrum:

- Similar morphologies in the radio, optical, X-ray.
- X-ray spectral index α_X typically steeper than in the radio
- Correlated variability.

Electrons of energies in the range $\sim 10^7 \ldots 10^8$ are needed.

Common assumption:
Particle acceleration in relativistic shocks.

Broad band emission

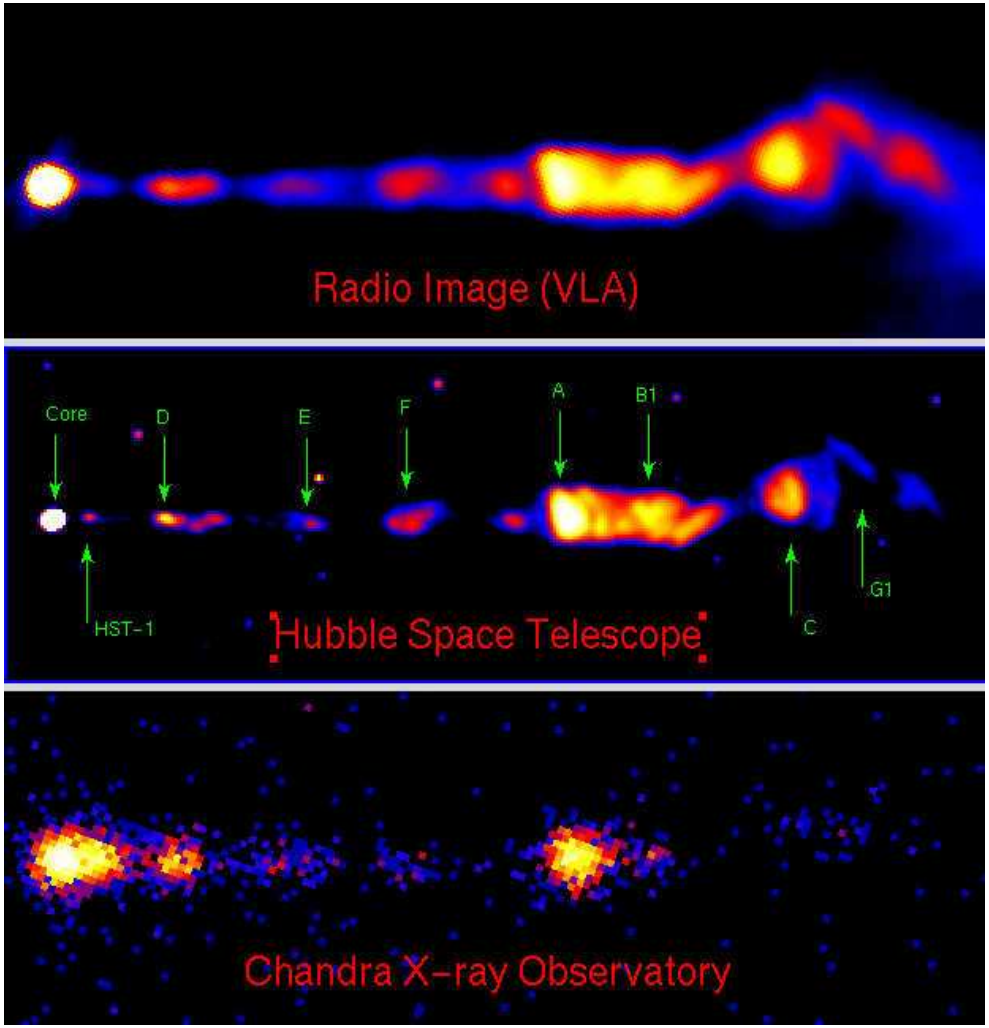

M 87 – Credit: X-ray: NASA/CXC/MIT/H.Marshall et al., Radio: F.Zhou, F.Owen (NRAO), J.Biretta (STScI), Optical: NASA/STScI/UMBC/E.Perlman et al.)

Life-time of e^- with energy E is

$$t_{1/2} \sim 1.6 \times 10^7 \text{ years} \left(\frac{B}{10^{-7}\,\mathrm{T}} \right)^{-2} \gamma^{-1} \tag{6.34}$$

X-ray synchrotron radiating electrons with $\gamma = 10^7$ cool on time scales of years.

$\Rightarrow$ Size of emission region $\sim$ acceleration regions.

Easy to fulfill for compact cores and even for jet knots, but continuous emission between the knots is problematic.

Electron acceleration must take place continuously, e.g., through turbulence in an outer shear layer (Stawarz & Ostrowski, 2002).

Introduction

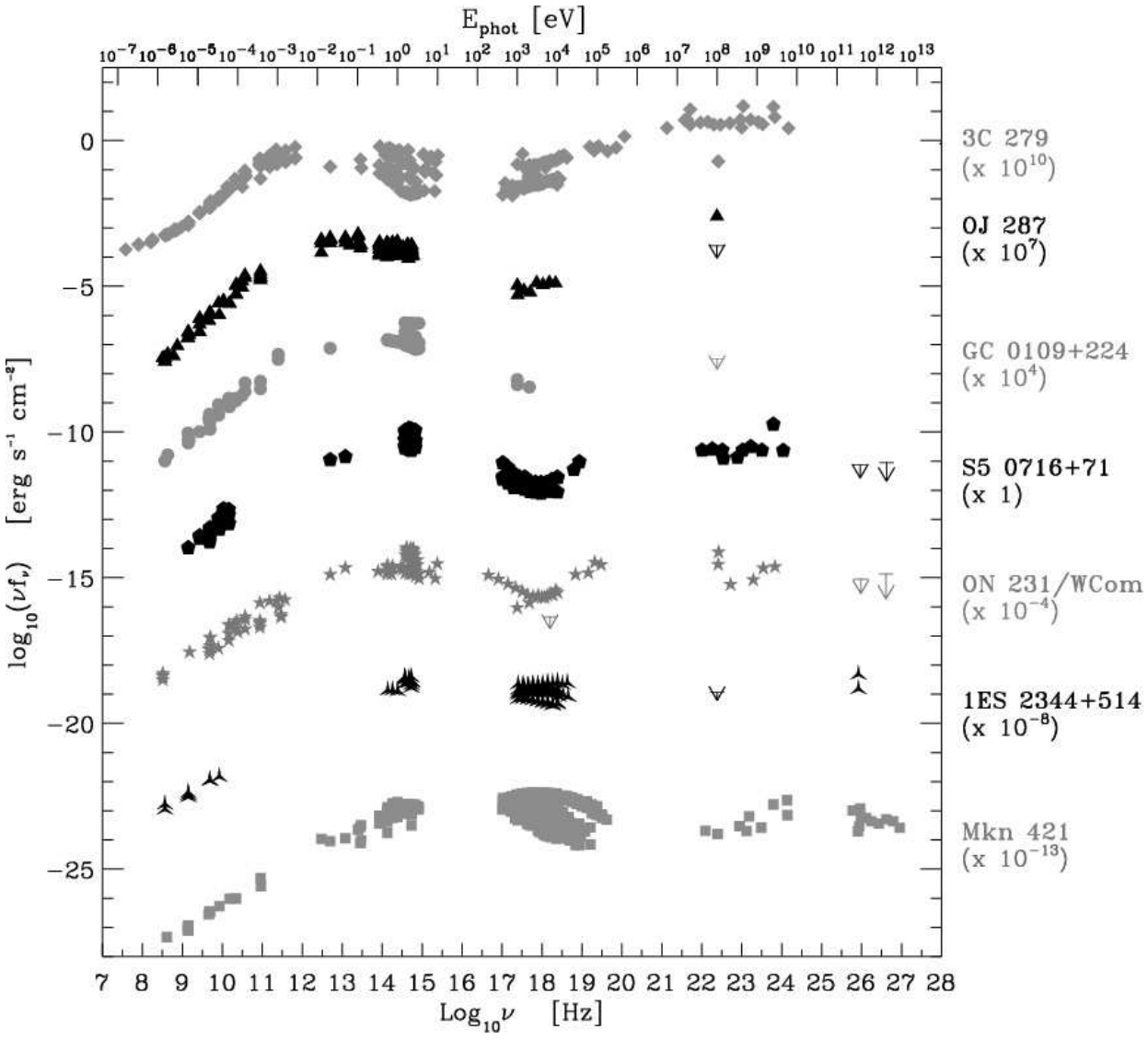

(Fiorucci et al., 2004)

Blazars emit across the whole electromagnetic spectrum!

We have seen broad-band emission from kpc-scale jets to be due to syn-chrotron and IC emission. Remember that blazars are compact (on kpc-scales).

Introduction

Blazars are broadband emitters and the most natural targets for multiwavelength astronomy!

The expression *Blazar* was first used in 1978 to express that optically violently variable quasars (OVVs) and BL Lac objects share their extreme variability characteristics.

Although been first detected in the optical and radio, a large portion of their total energy output is at high energies: hard X-rays, γ-rays, and up to the very high energy (VHE) regime.

γ-ray telescopes like *Fermi* find that blazars are the dominant population of extragalactic γ-ray sources.

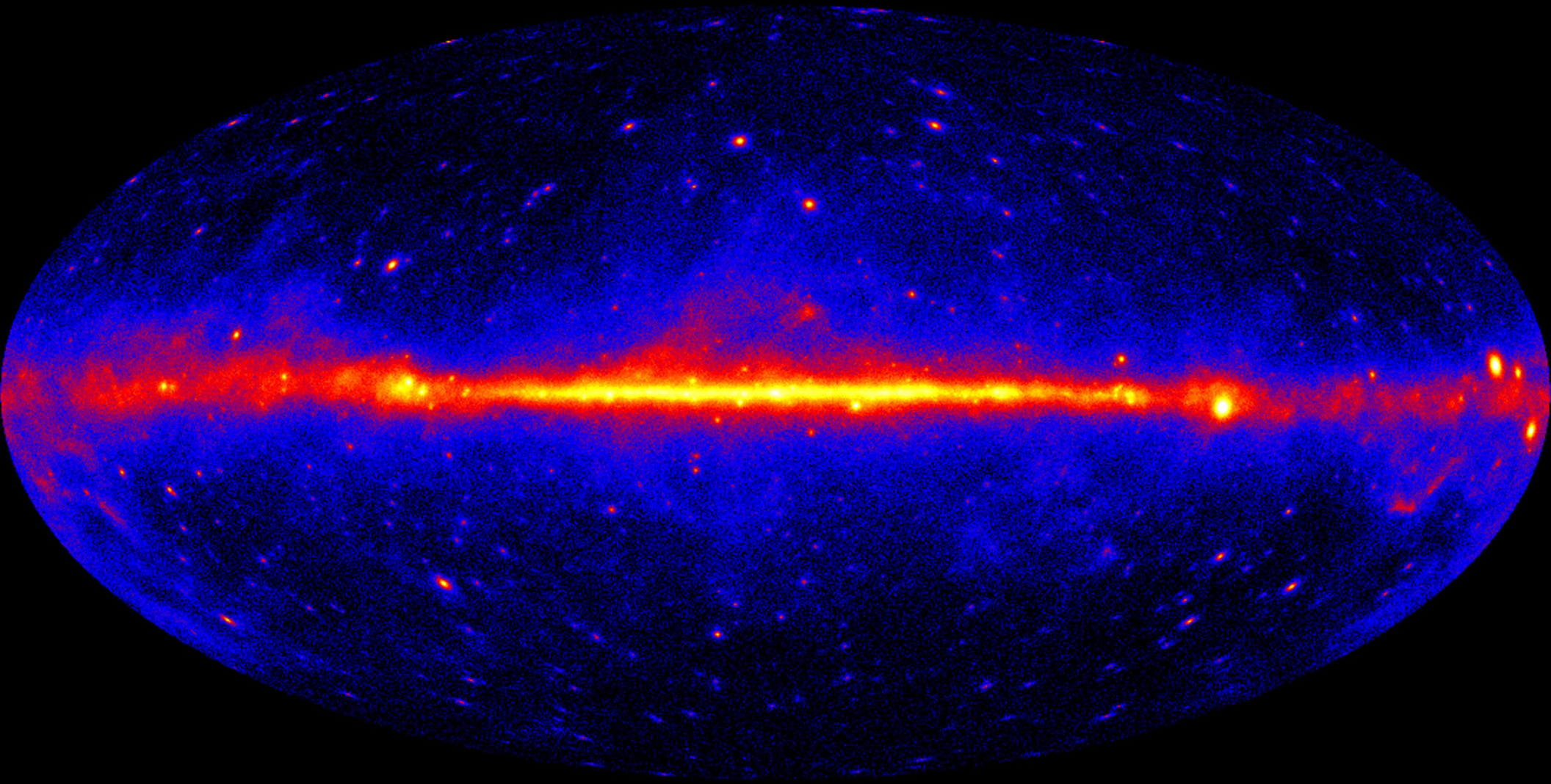

One-year all-sky image of the *Fermi* Gamma-ray Space Telescope (2008/09)

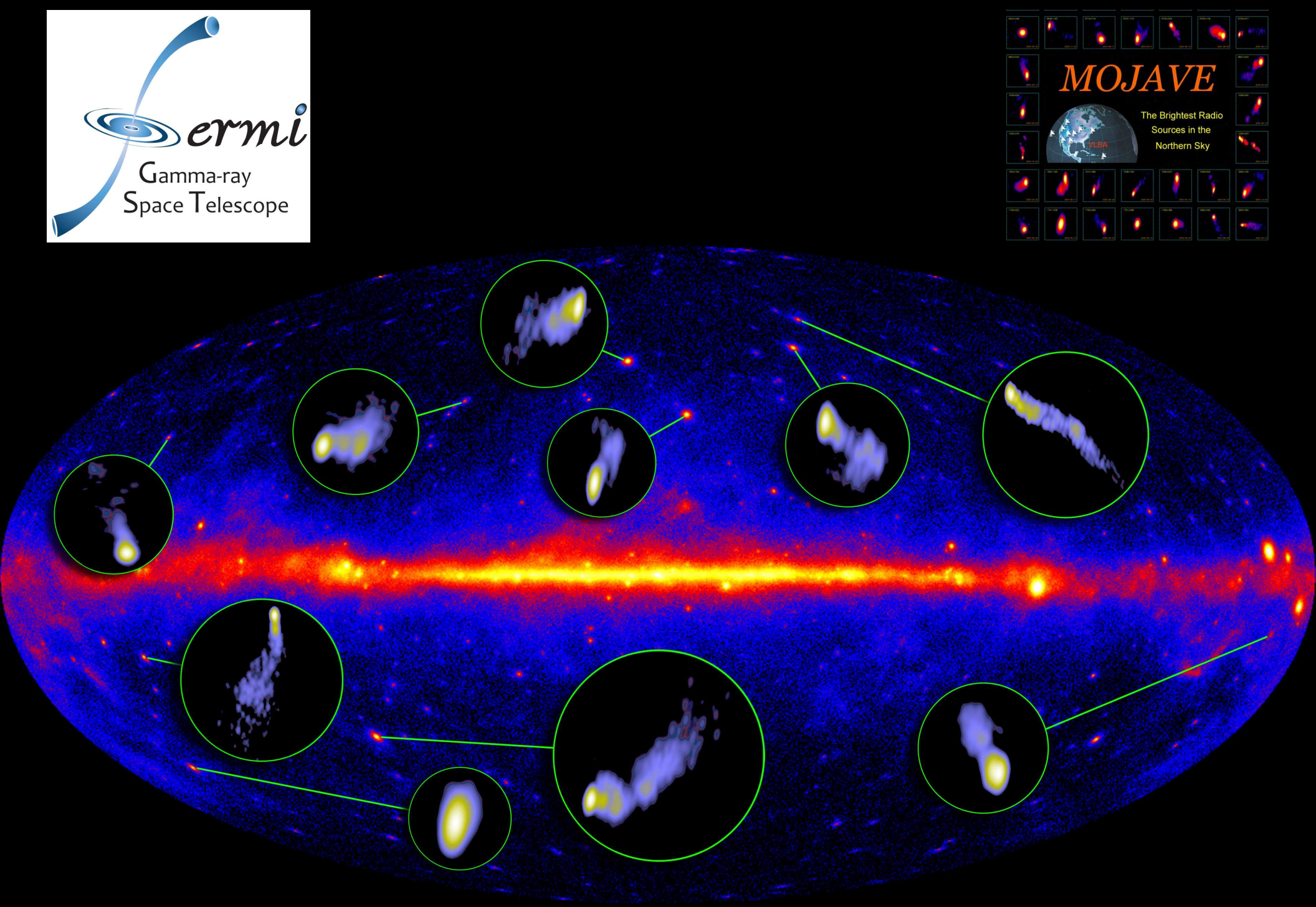

High galactic-latitude gamma-ray point sources are
flat-spectrum radio quasars and BL Lac objects

The Blazar Sequence

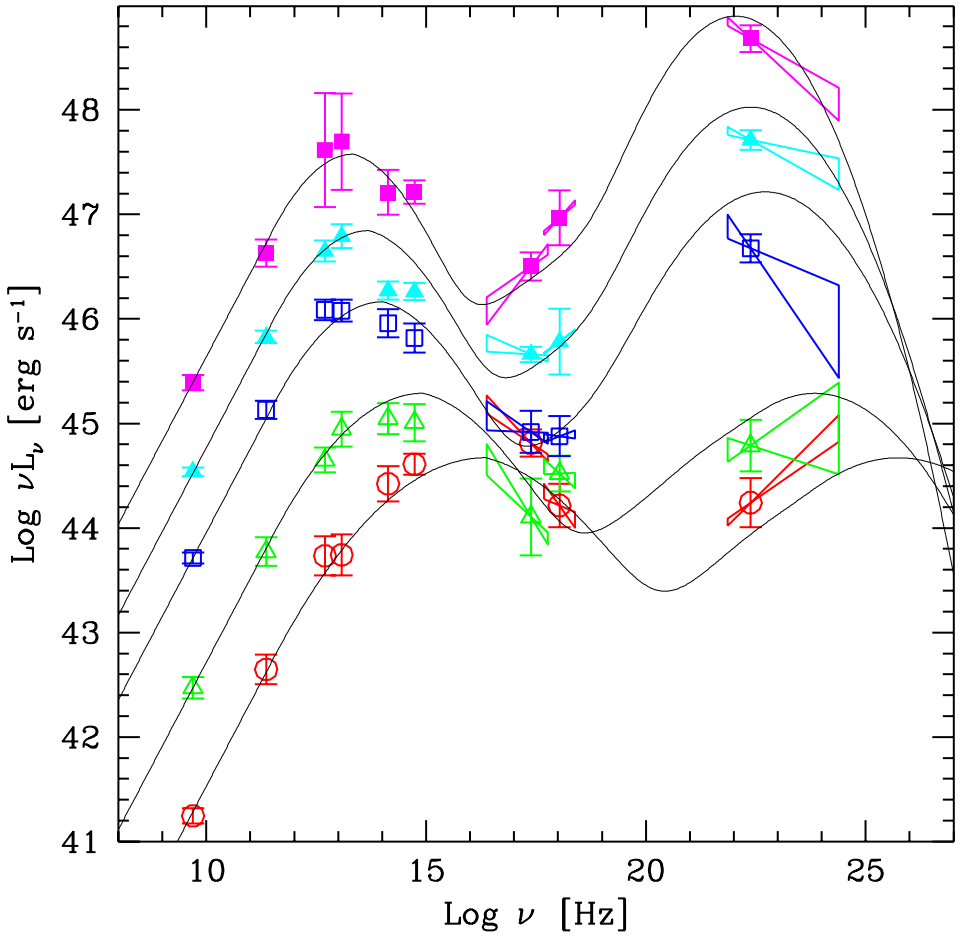

(Donato et al., 2001, based on Fossati et al. (1998))

Construction of average blazar spectral energy distributions (SEDs) binned according to radio luminosity (Fossati et al., 1998; Donato et al., 2001)

- For all luminosity classes, two broad peaks
- High-luminosity sources peak at lower frequencies (IR and MeV range): LBL objects
- Low-luminosity sources peak at higher frequencies (UV/X-rays and up to TeV energies): HBL objects

The Blazar Sequence

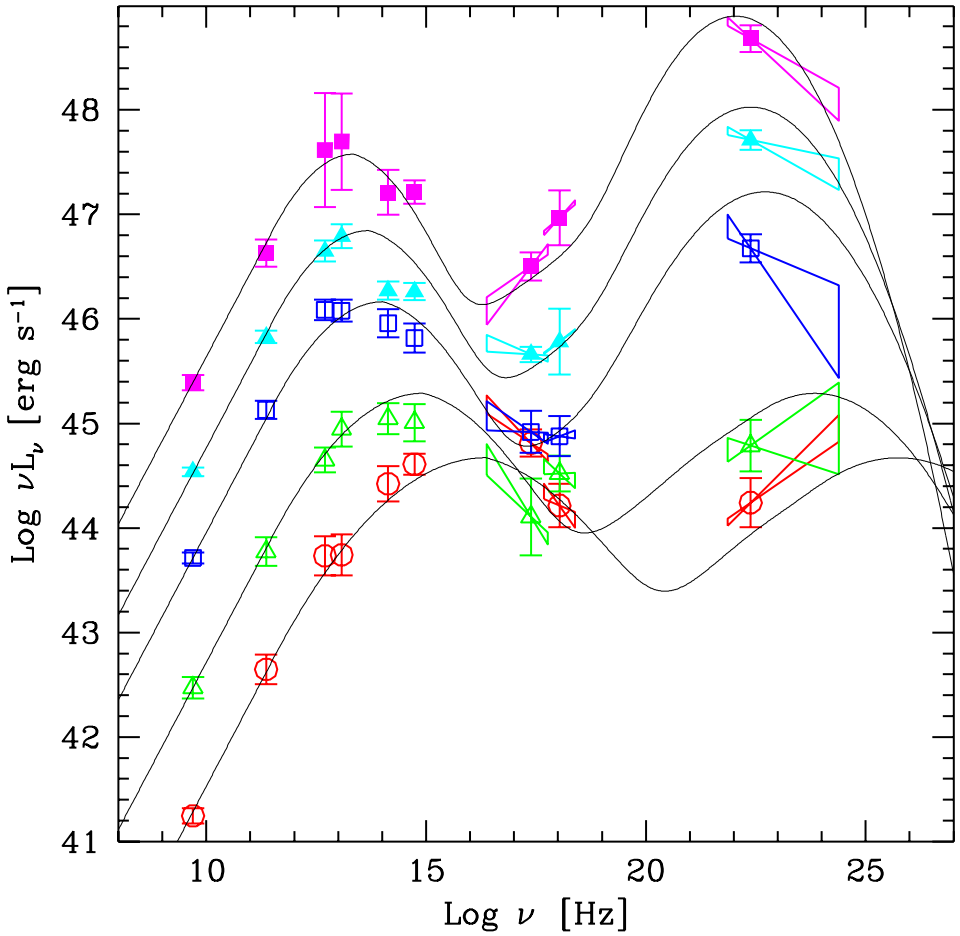

(Donato et al., 2001, based on Fossati et al. (1998))

Analytic parametrization:

- Peak frequencies are inversely proportional to luminosity
- Constant ratio of the two peak frequencies
- Strength of the second peak proportional to luminosity

Attention: EGRET detected preferentiall blazars during outbursts $\Rightarrow$ Bias in high-energy data.

Ongoing debate about the validity of the blazar sequence. A (small) number of sources do not fit in.

Prototypical Example: 3C 273 (SED Components)

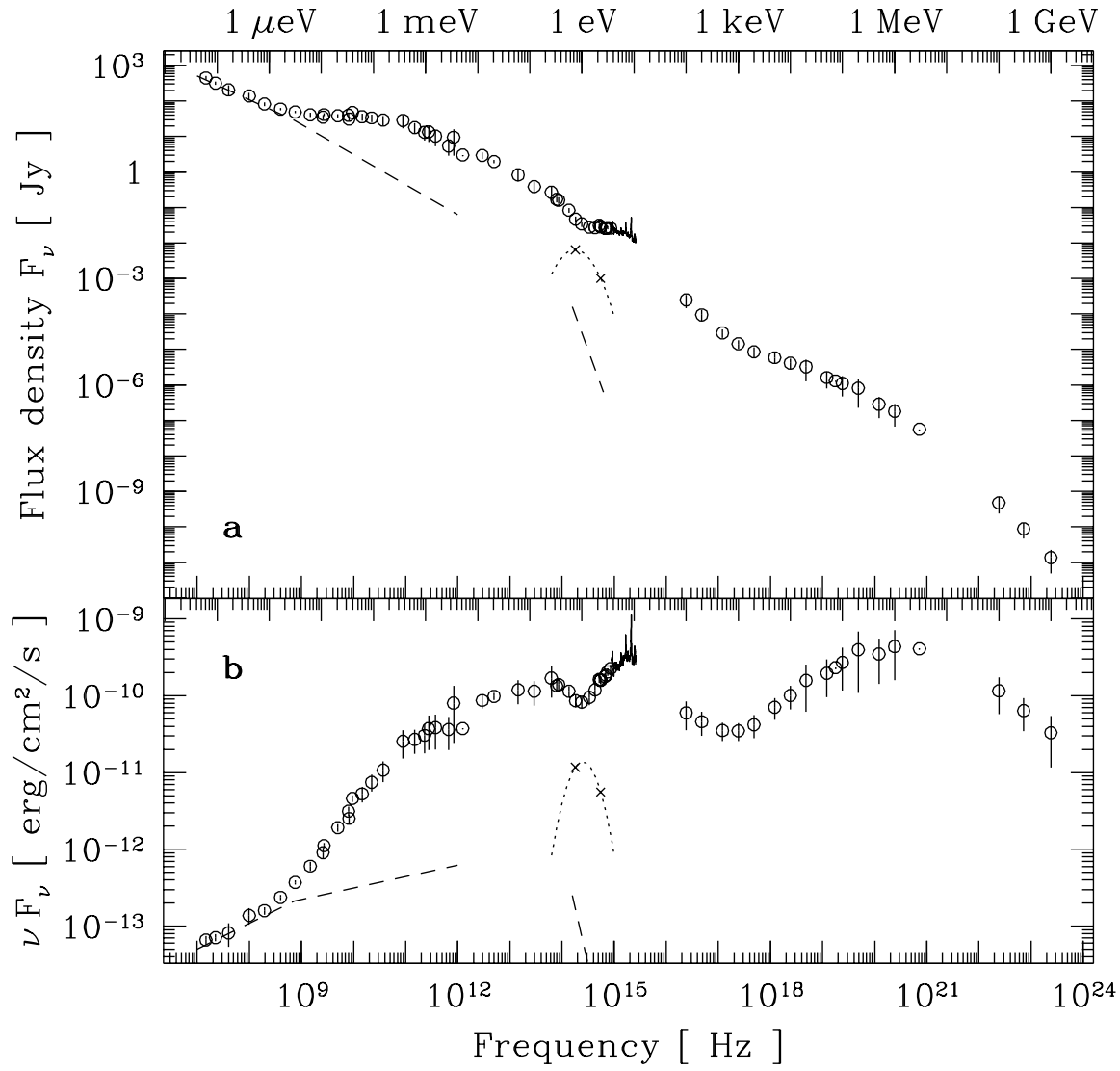

(Türler et al., 1999)

3C 273:

- First detected and brightest (and probably best studied) quasar
- Bright throughout the whole electromagnetic spectrum
- Prominent “big blue bump”
- Huge public database: Türler et al. (1999); Soldi et al. (2008)

Prototypical Example: 3C 273 (SED Components)

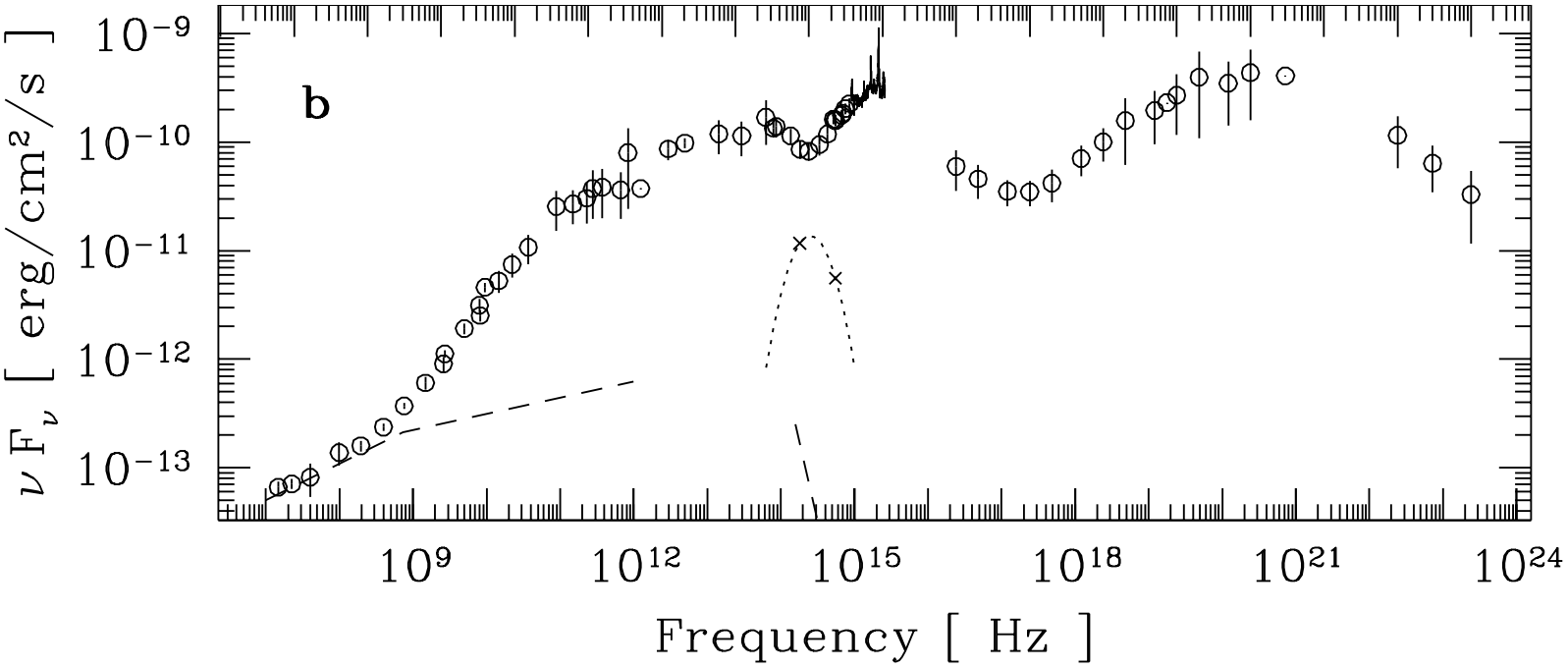

- Radio: low-frequency emission from large-scale jet; high-frequencies from compact jet (flat spectrum in F_ν)
- up to IR: synchrotron emission from compact jet (possibly plus dust component (dusty torus?))
- “big blue bump” in the optical: accretion disk (?)
- X-rays and up: inverse Compton emission (possibly from multiple seed photon fields)

Broadband Emission Models

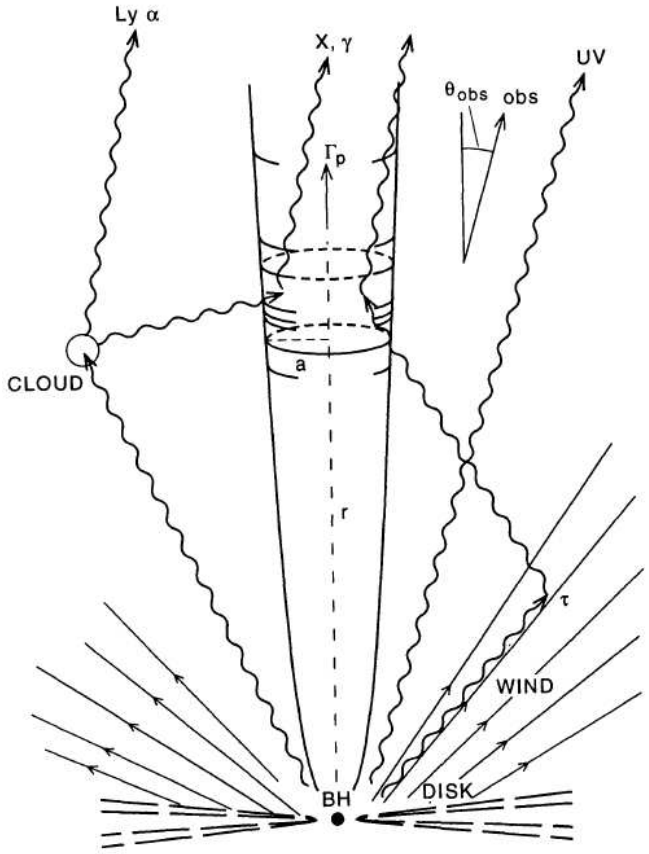

Geometry in leptonic models (Sikora et al., 1994)

General agreement that the low-energy component is jet-synchrotron emission.

High-energy photons are produced in

- Leptonic models: Compton scattering of soft seed photons by the same relativistic electrons responsible for the synchrotron emission. Seed photons are
  - the synchrotron photons (SSC, e.g. Tavecchio et al., 1998), or
  - external, e.g., from the accretion disk or the BLR (EC, e.g. Sikora et al., 1994)
- Hadronic models: reactions involving high-energy protons (hadron-hadron or photon-hadron collisions, pair production and subsequent e^+e^- cascades (e.g. Mannheim, 1993))

Hadronic models are attractive because they can explain the observed ultra-high energetic (UHE) cosmic rays but they have problems explaining the observed blazar X-ray spectra.

Broadband Emission Models

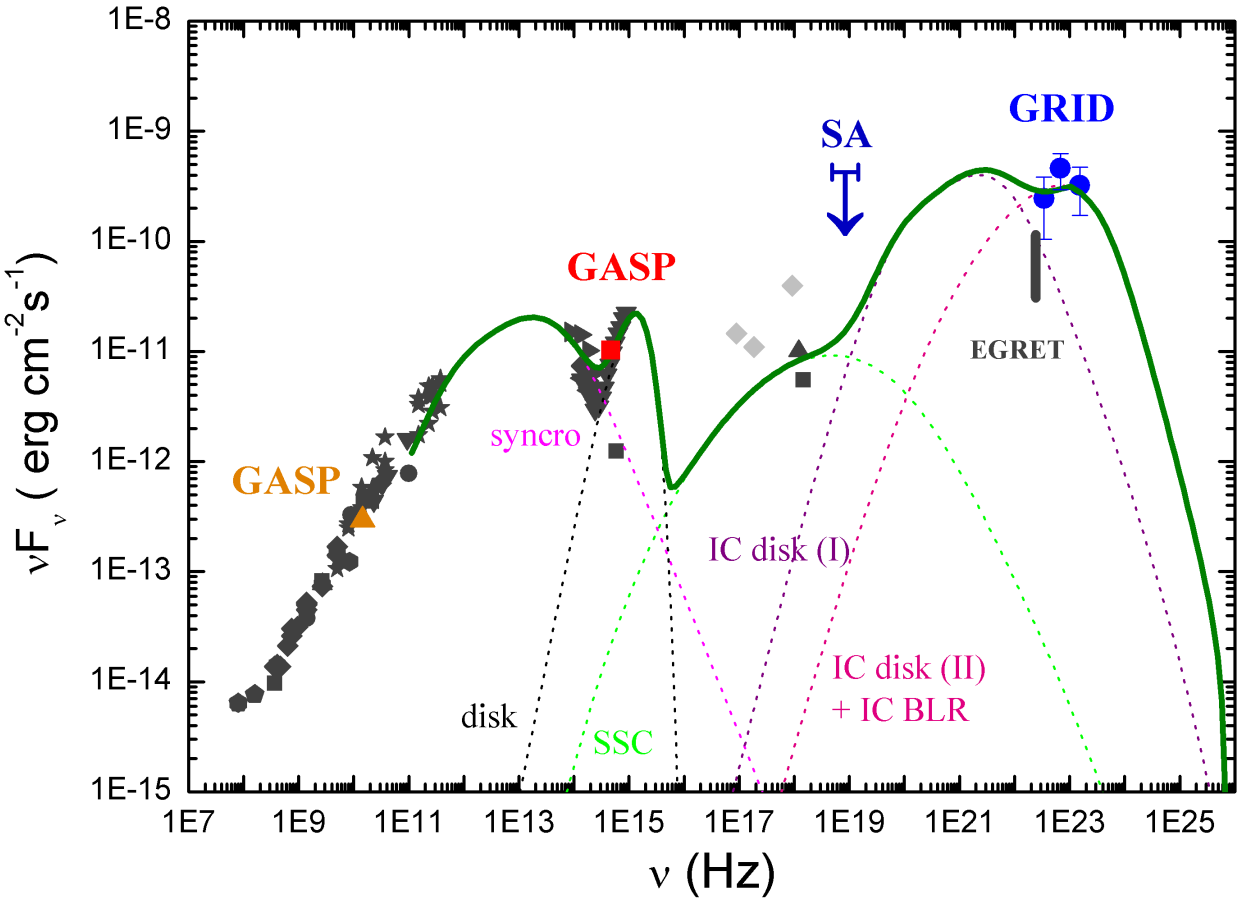

Pucella et al. (2008)

This is an SED of PKS B 1510-089; see below

Modeling the broad-band SED:

- Consider primary components: synchrotron, disk, scattered BLR emission
- Inverse-Compton components from SSC and EC (of the dominating external photon fields)

Broadband Emission Models

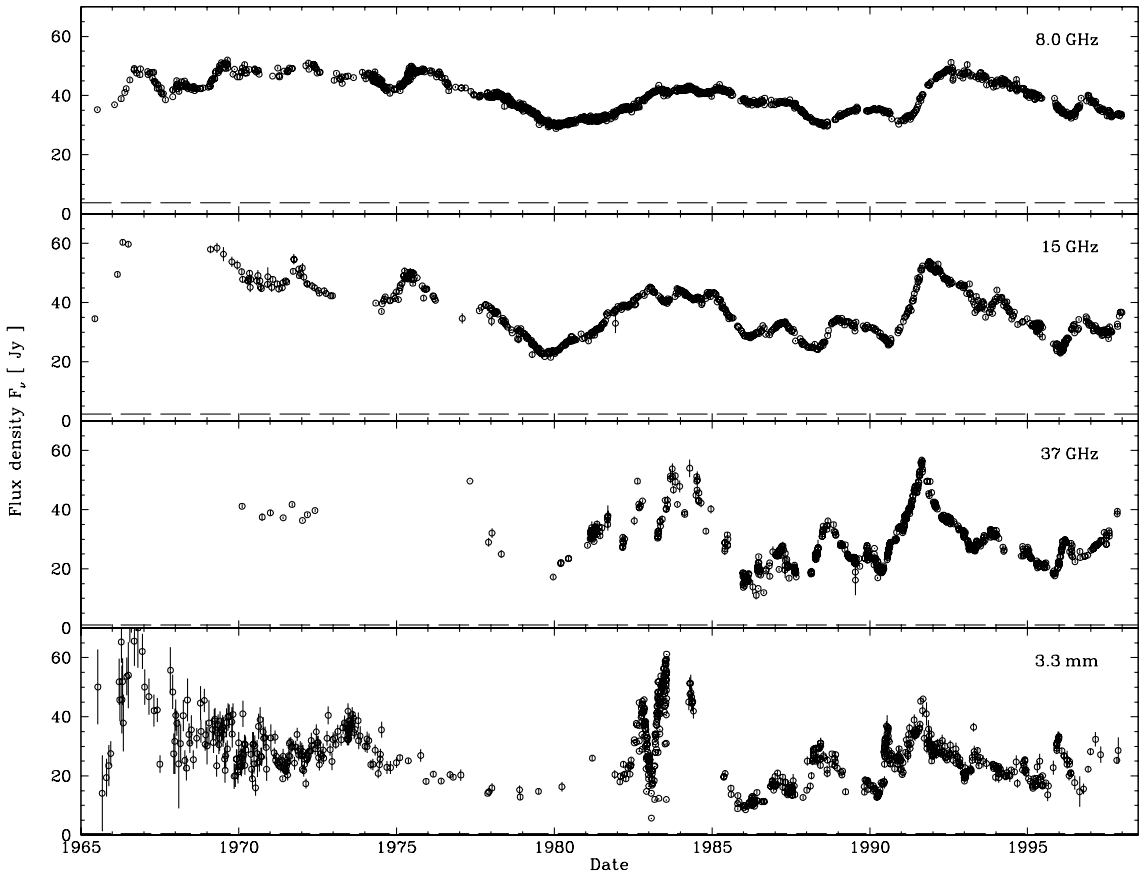

(Türler et al., 1999)

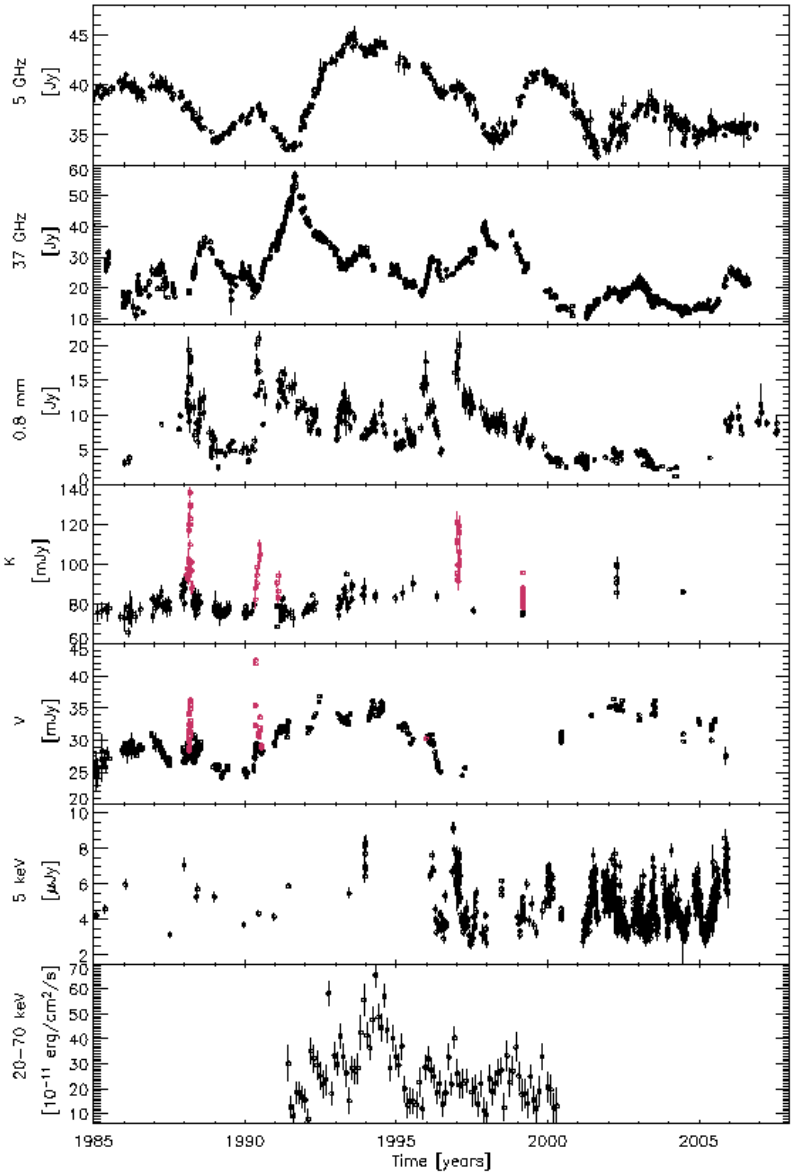

(Soldi et al., 2008)

Variability at all wavelengths but with different time scales and amplitudes ⇒ multiple emission components and/or mechanisms

Broadband Emission Models

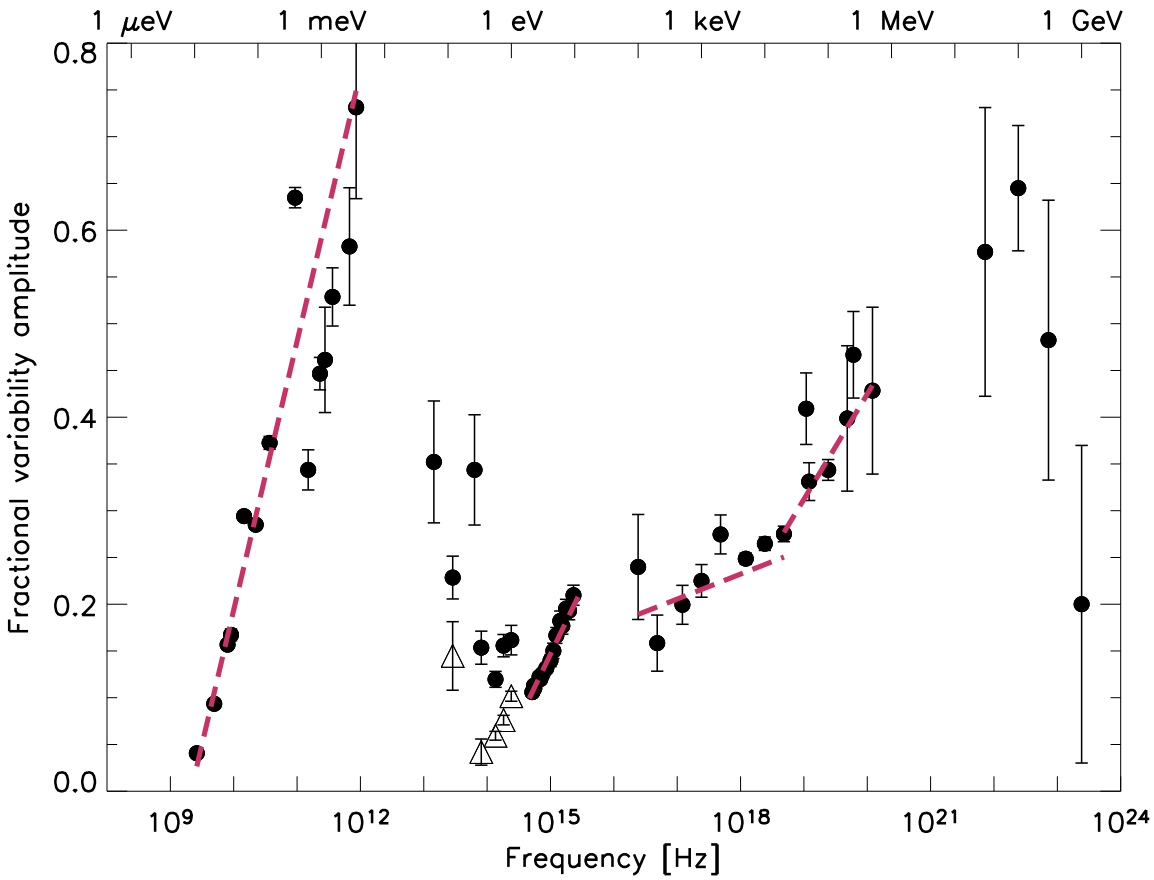

(Soldi et al., 2008)

Fractional variability amplitude:

$$F_{\mathrm{var}} = \sqrt{\frac{S^2 - \bar{\varepsilon^2}}{\bar{x}^2}} \qquad (6.35)$$

with the sample variance of the light curve S^2, the average flux $\bar{x}$, and the mean of the squared measurement uncertainties $\bar{\varepsilon^2} = \frac{1}{N}\sum_i \varepsilon_i^2$.

The fractional variability amplitude strongly depends on frequency, rising towards the high-energy end of the synchrotron and IC components. Less-variable IR emission (from dust?).

Blazar Variability at γ-Ray Energies

Blazars are extremely variable on time scales as short as days! $\Rightarrow$ Source dimensions $R \sim \mathcal{O}(10^{10}\,\mathrm{m})$

High photon density n_γ may enable pair production:

$$\gamma + \gamma \rightarrow e^- + e^+ \tag{6.36}$$

if $E_\gamma > \mathrm{m}_e c^2 = 511\,\mathrm{keV}$.

Optical depth for pair production:

$$\tau_{\gamma\gamma} = n_\gamma \sigma_{\gamma\gamma} R, \tag{6.37}$$

with $\sigma_{\gamma\gamma}$ the cross section for pair production (close to the Thomson cross section σ_T close to the energy threshold).

n_γ from energy density ($L_\gamma / 4\pi R^2 c$) divided by mean energy ($m_e c^2$). Therefore:

$$\tau_{\gamma\gamma} \sim \left(\frac{L_\gamma}{4\pi R^2 m_e c^3} \right) \sigma_\mathrm{T} R \sim 200 \left[\frac{L_\gamma}{10^{48}\,\mathrm{erg\,s^{-1}}} \right] \left[\frac{R}{10^{10}\,\mathrm{m}} \right], \tag{6.38}$$

i.e., photons cannot escape, unless L_γ is emitted non-isotropically.

Short time scales and high γ-ray luminosities provide and independent proof of relativistic beaming in blazar jets.

Blazars at Very High Energies

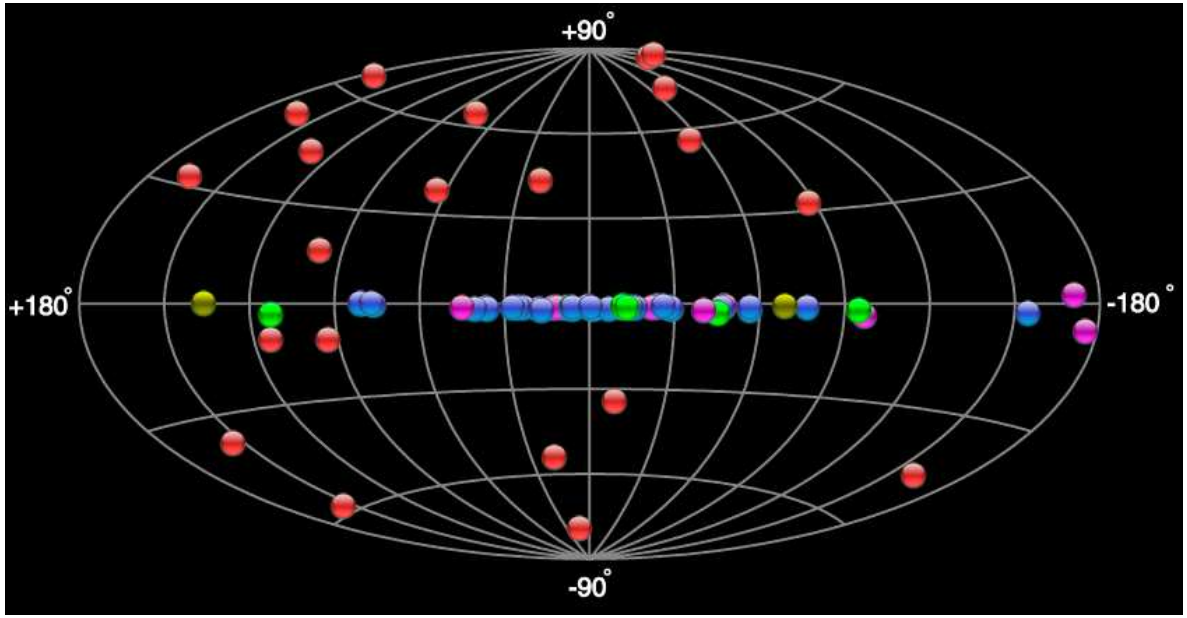

The blazar sequence predicts a dominance of HBL objects at very high energies. This is confirmed by recent blazar detections of TeV telescopes (H.E.S.S., MAGIC, VERITAS, CANGAROO):

- Currently 23 HBL objects detected and only five LBL objects (check `http://tevcat.uchicago.edu/` for updated lists)

Blazars at Very High Energies

TeV blazars are weak radio sources, because the cm-range is so far left of their synchrotron peak and because they are low-luminosity objects.Similarly, they are bright X-ray sources and relatively weak in the MeV/GeV range.

Despite their variability and SEDs require very high Doppler factors, VLBI measures slow jets (barely superluminal Piner et al., 2008, and references therein) $\Rightarrow$ 1) extremely small angles or 2) jet deceleration from the “blazar scale” to the “VLBI scale”, or 3) another sign of jet-stratification (spine-sheath structure).

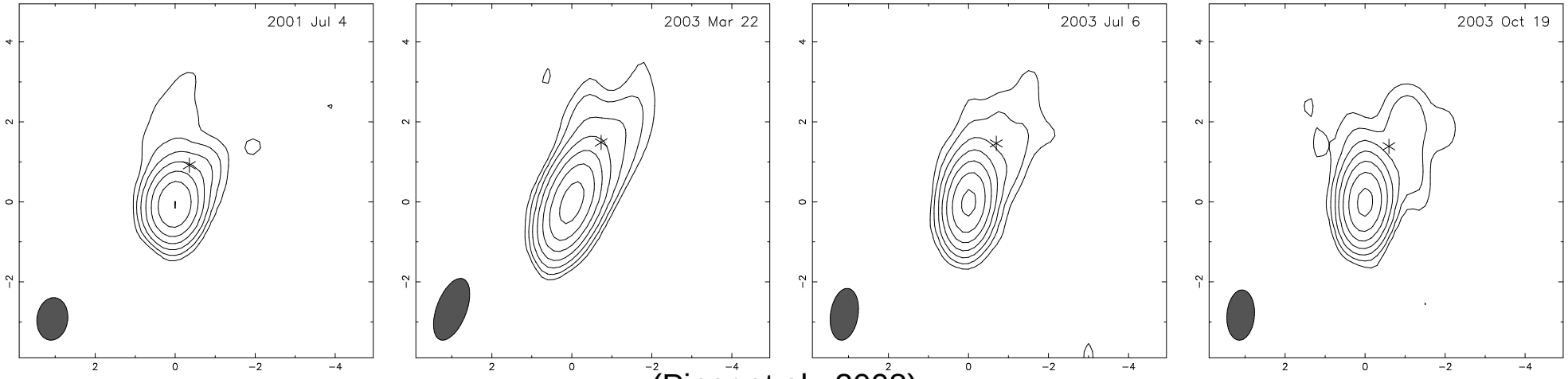

(Piner et al., 2008)

A TeV Galaxy: M 87

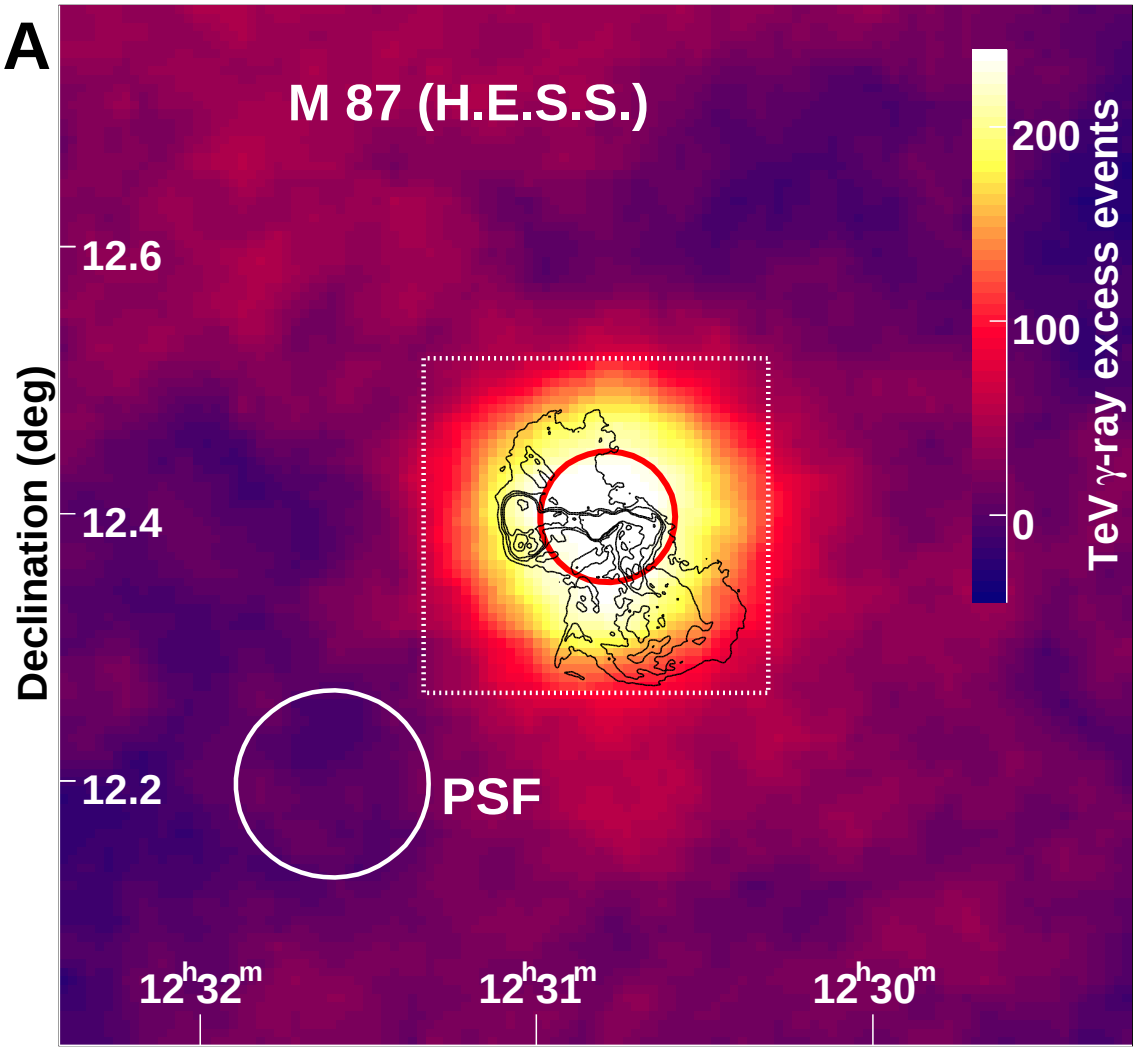

(Aharonian et al., 2006)

- M 87 established as a TeV source by H.E.S.S. (Aharonian et al., 2006)
- Previous 4-σ tentative detection by HEGRA; non-detection by Whipple
- Hard spectrum ($\Gamma \sim 2.2$) detected up to 20 TeV

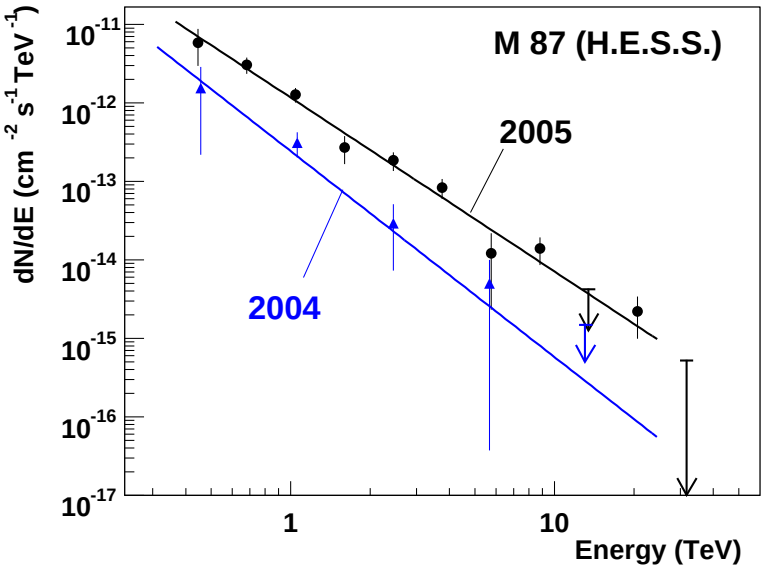

A TeV Galaxy: M 87

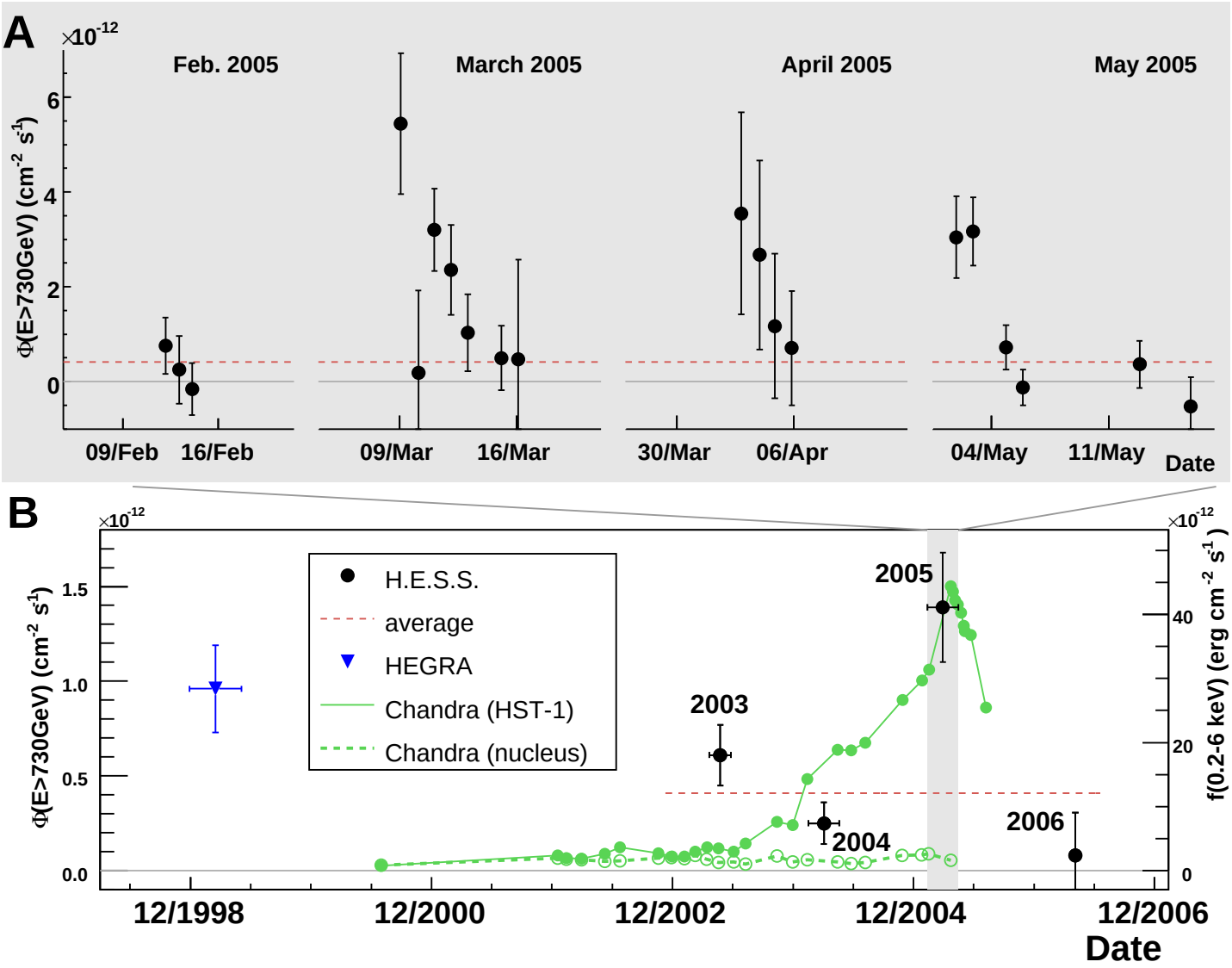

(Aharonian et al., 2006)

- TeV flux variable on time scales from years down to days
- Emission region must be compact
- Highest measured fluxes coincide with a flare of the HST-1 knot in the M 87 jet as measured by *Chandra* (Harris et al., 2006) (at this epoch brighter than the nucleus!)

A TeV Galaxy: M 87

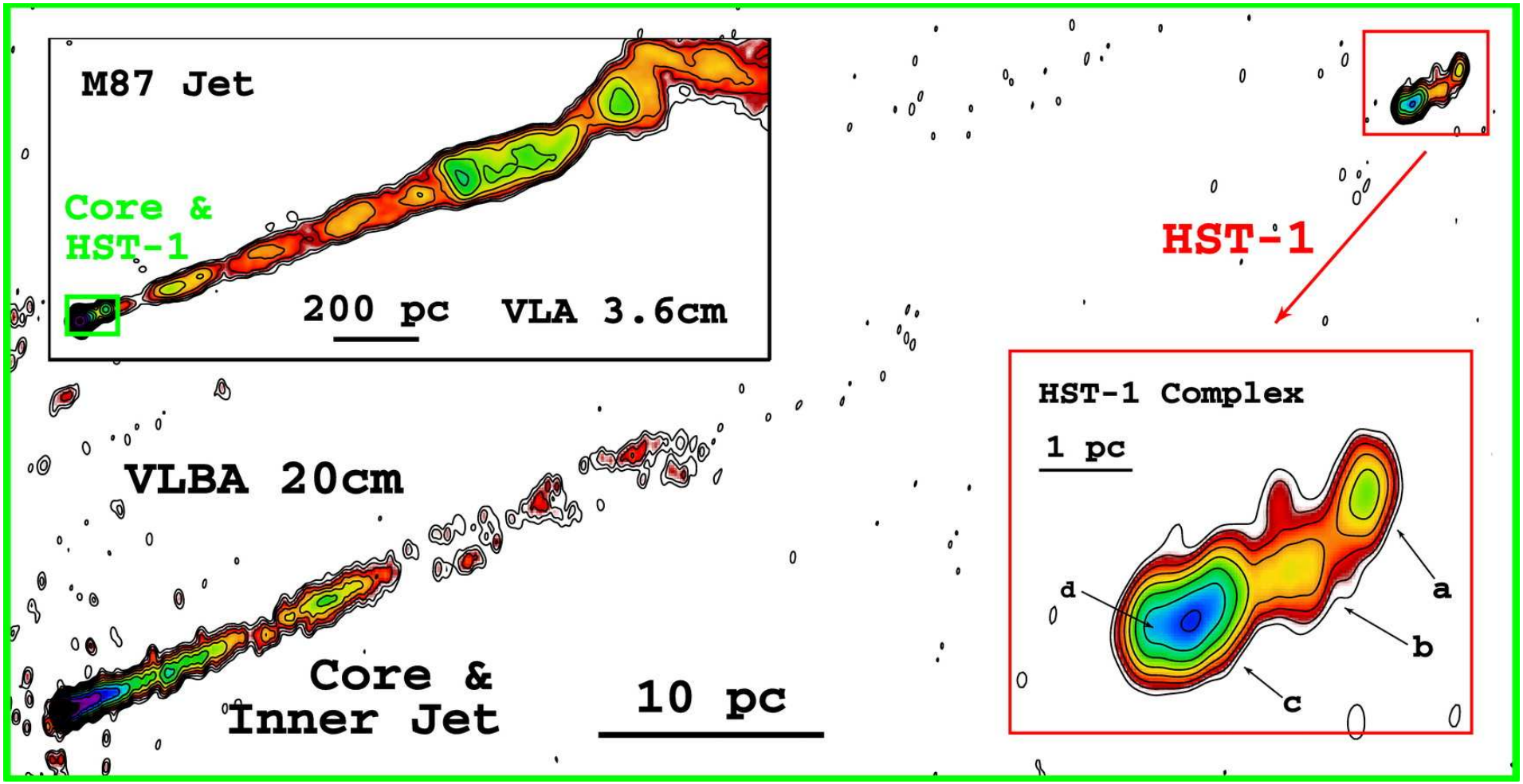

HST-1 resolved by VLBI, but still compact sub-structure (Cheung et al., 2007)

A TeV Galaxy: M 87

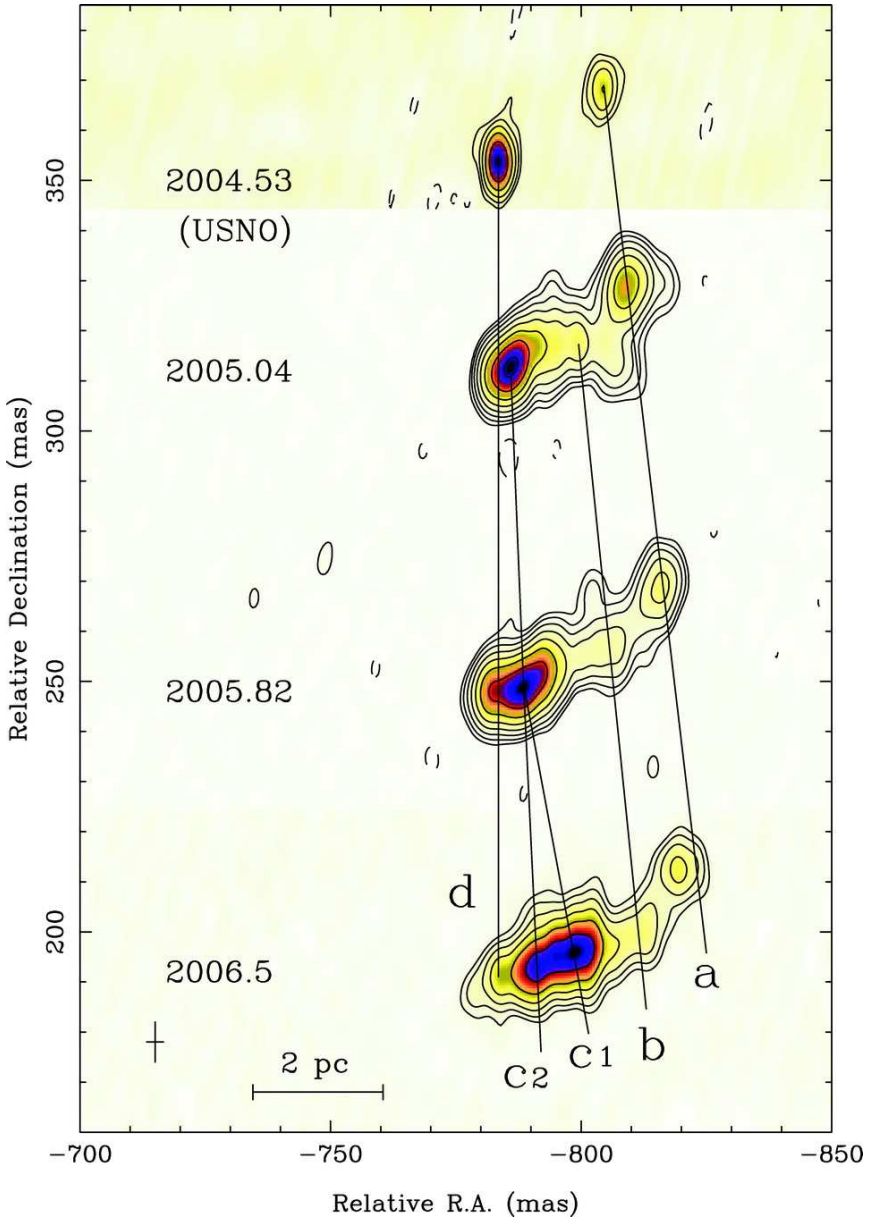

- HST-1 has moving sub-components with superluminal speeds up to $\sim 4c$ in agreement with optical measurements by Biretta et al. (1999).

$\Rightarrow$ Relativistic bulk motion $>$ 120 pc downstream from the central engine and coinciding with the flaring putative TeV emission region

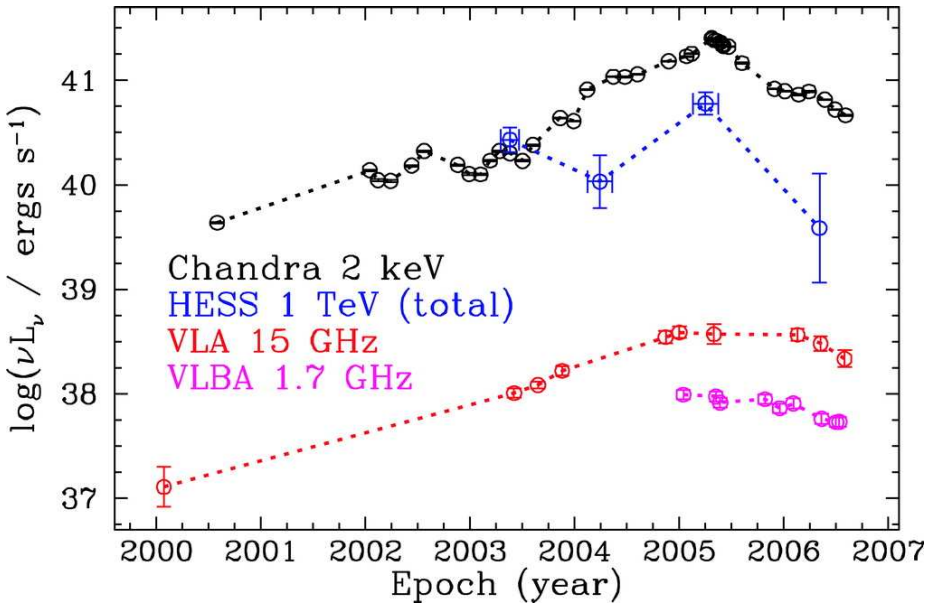

(Cheung et al., 2007)

Jet Formation

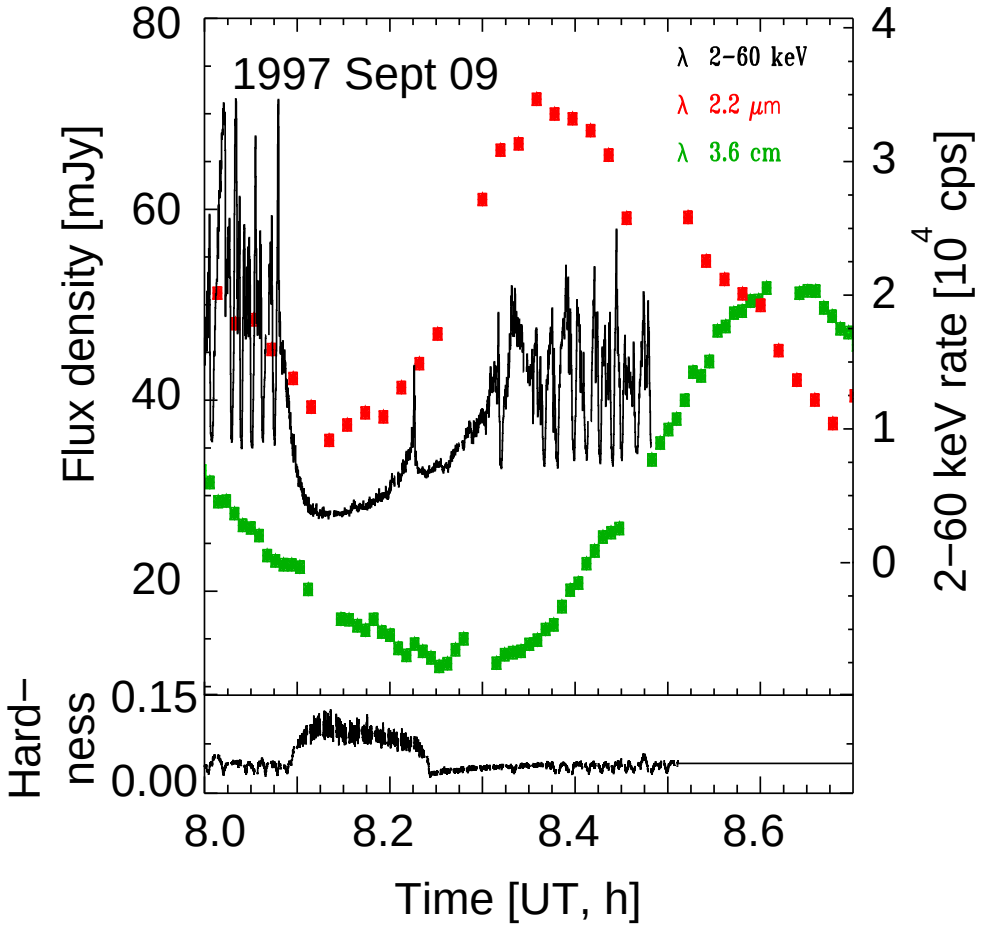

(GRS 1915+105; Mirabel et al., 1998)

Dynamics of jet formation are better studied in Galactic black holes with jets ("microquasars") because of shorter timescales.

Find clear X-ray–radio correlation (similar also seen in some AGN such as 3C120)

$\Longrightarrow$ "universal disk-jet-connection"

movie time: `jetmovies/agn_xray_020505_11_640x480_95pc`

Marscher et al. (2002): 3C120: X-ray dips followed by radio ejection events

$\Longrightarrow$ jets and accretion disk are related.

Jet Formation

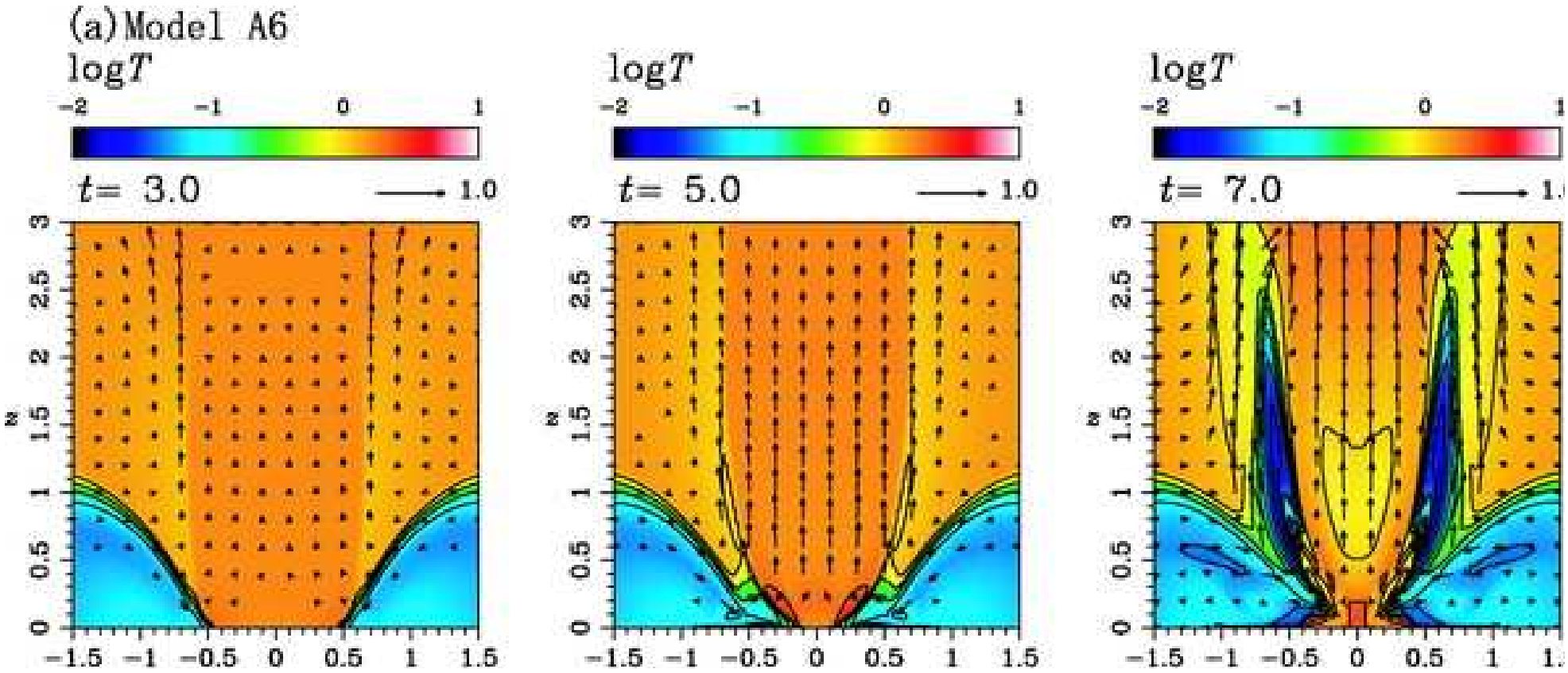

Evolution of a newly launched jet (Kigure & Shibata, 2005)

To study jet confinement and propagation: use magnetohydrodynamical simulations

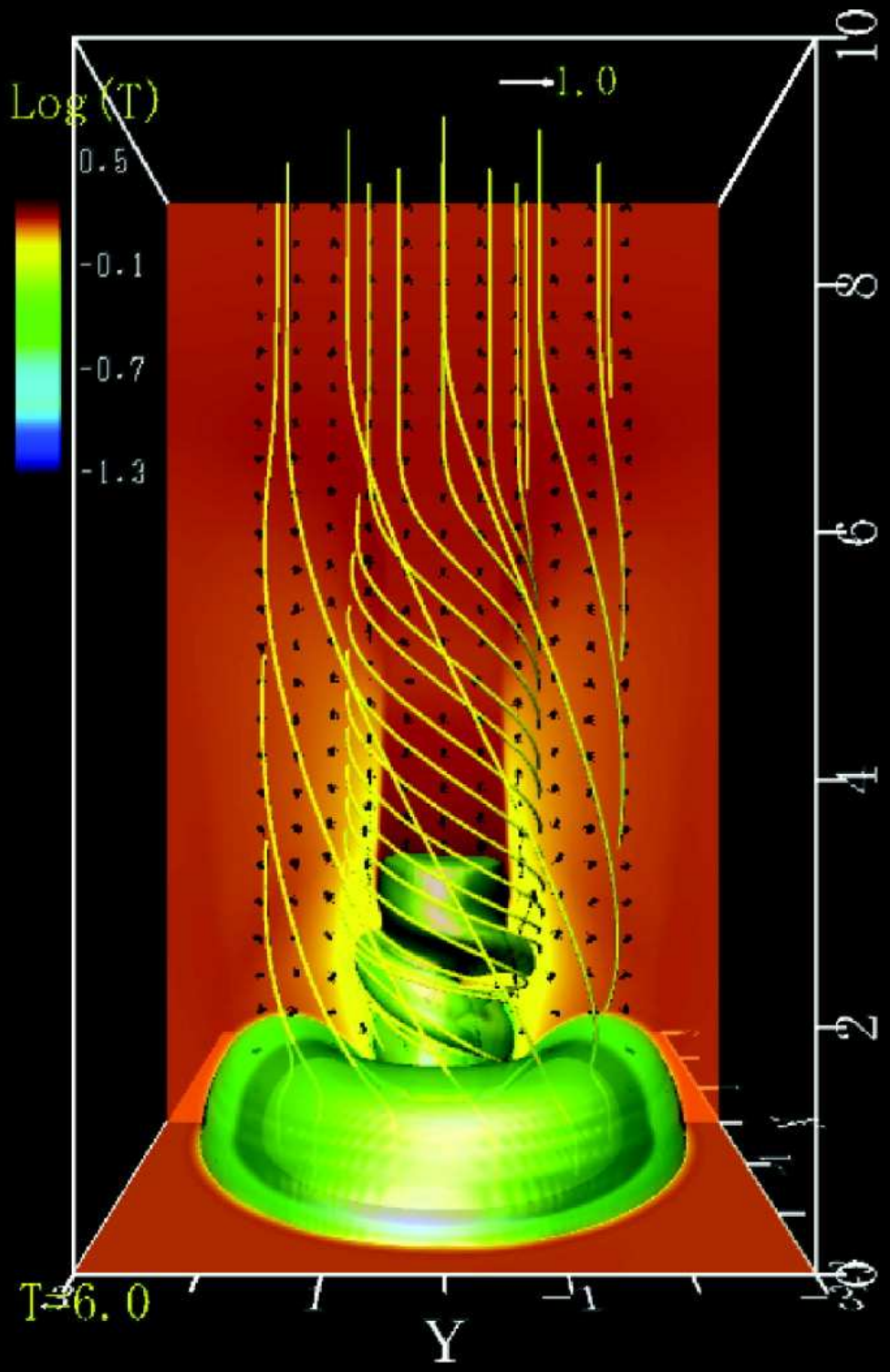

Temperature profile and B-field configuration of a MHD-jet

Movie: `jetmovies/d155mvj.avi`: Time evolution of B-field and density close to a BH (Matsumoto&Machida).

(Kigure & Shibata, 2005, Fig. 6)

Jet Formation

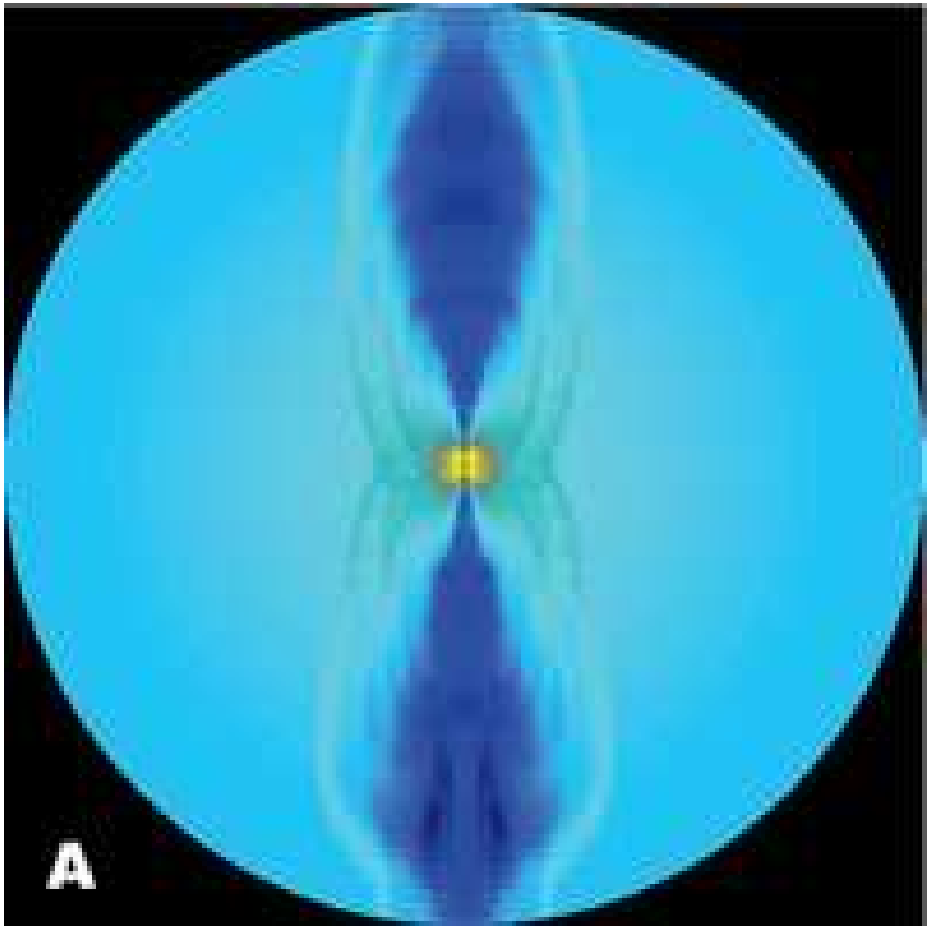

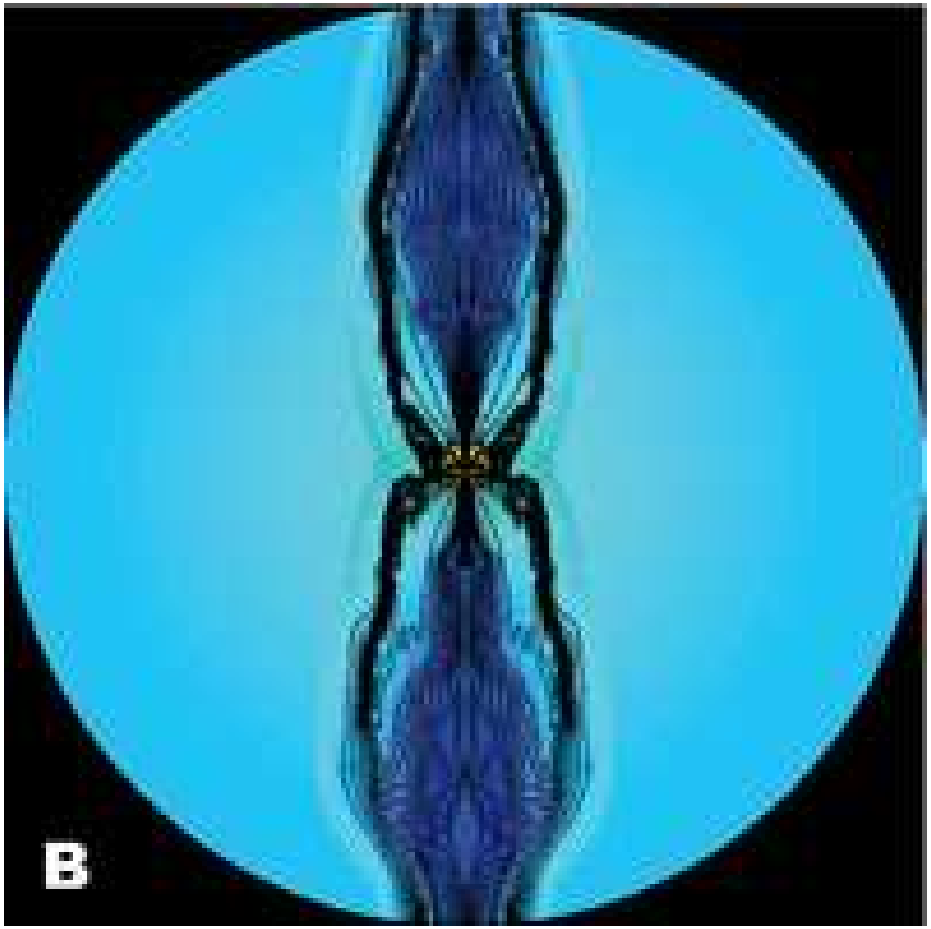

(McKinney, 2006, Fig. 1)

$\log \rho$ (left) and $\log \rho$ and B for a jet launched via a disk.

Outer radius is $10^4 GM/c^2$.

Aharonian, F., Akhperjanian, A. G., Bazer-Bachi, A. R., et al. 2006, Science, 314, 1424
Biretta, J. A., Sparks, W. B., & Macchetto, F. 1999, ApJ, 520, 621
Cheung, C. C., Harris, D. E., & Stawarz, Ł. 2007, Astrophys. J., Lett., 663, L65
Cohen, M. H., Cannon, W., Purcell, G. H., et al. 1971, ApJ, 170, 207
Donato, D., Ghisellini, G., Tagliaferri, G., & Fossati, G. 2001, A&A, 375, 739
Fiorucci, M., Ciprini, S., & Tosti, G. 2004, A&A, 419, 25
Fossati, G., Maraschi, L., Celotti, A., Comastri, A., & Ghisellini, G. 1998, MNRAS, 299, 433
Harris, D. E., Cheung, C. C., Biretta, J. A., et al. 2006, ApJ, 640, 211
Kadler, M., Ros, E., Lobanov, A. P., Falcke, H., & Zensus, J. A. 2004, A&AS, 426, 481
Kadler, M., Ros, E., Perucho, M., et al. 2008, ApJ, 680, 867
Kameno, S., Sawada-Satoh, S., Inoue, M., Shen, Z.-Q., & Wajima, K. 2001, PASJ, 53, 169
Kigure, H., & Shibata, K. 2005, ApJ, 634, 879
Killeen, N. E. B., Bicknell, G. V., & Ekers, R. D. 1986, ApJ, 302, 306
Mannheim, K., 1993, A&A, 269, 67
Marscher, A. P., Jorstad, S. G., Gómez, J.-L., et al. 2002, Nature, 417, 625
McKinney, J. C., 2006, MNRAS, 368, 1561
Mirabel, I. F., Dhawan, V., Chaty, S., et al. 1998, A&A, 330, L9
Nilsson, K., Pursimo, T., Sillanpää, A., Takalo, L. O., & Lindfors, E. 2008, A&A, 487, L29
Perley, R. A., Bridle, A. H., & Willis, A. G. 1984, ApJS, 54, 291
Perlman, E. S., Biretta, J. A., Sparks, W. B., Macchetto, F. D., & Leahy, J. P. 2002, New Astronomy Review, 46, 399
Piner, B. G., Pant, N., & Edwards, P. G. 2008, ApJ, 678, 64
Pucella, G., Vittorini, V., D'Ammando, F., et al. 2008, A&A, 491, L21
Rybicki, G. B., & Lightman, A. P. 1979, Radiative Processes in Astrophysics, (New York: Wiley)
Shu, F. H., 1991, The Physics of Astrophysics, Vol. I. Radiation, (Mill Valley, CA: University Science Books)
Sikora, M., Begelman, M. C., & Rees, M. J. 1994, ApJ, 421, 153
Soldi, S., Türler, M., Paltani, S., et al. 2008, A&A, 486, 411
Stawarz, Ł., & Ostrowski, M. 2002, ApJ, 578, 763
Tavecchio, F., Maraschi, L., & Ghisellini, G. 1998, ApJ, 509, 608
Türler, M., Paltani, S., Courvoisier, T. J.-L., et al. 1999, A&AS, 134, 89
Whitney, A. R., Shapiro, I. I., Rogers, A. E. E., et al. 1971, Science, 173, 225
Zensus, J. A., 1997, Ann. Rev. Astron. Astrophys., 35, 607